

# The regulation of the Hsp70 family molecular chaperone BiP via phosphorylation

Written by Gabriel Steven Grey

Submitted in accordance with the requirements for the degree of PhD.

The University of Leeds

Faculty of biological sciences

Examination – September 2023

I confirm that the work submitted is my own and that appropriate credit has been given where reference has been made to the work of others.

This copy has been supplied on the understanding that it is copyright material and that no quotation from the thesis may be published without proper acknowledgement.

The right of Gabriel Steven Grey to be identified as Author of this work has been asserted by Gabriel Steven Grey in accordance with the Copyright, Designs and Patents Act 1988.

## Contents

Abstract .....	6
Acknowledgements.....	7
Chapter 1: Introduction.....	8
1.1 The Hsp70 family, a group of ubiquitous molecular chaperones.....	8
1.1.1 Hsp70 is a highly conserved family. ....	8
1.1.2 The ER and its sole Hsp70, BiP .....	10
1.2 Hsp70 structure and allosteric cycle.....	11
1.2.1 Hsp70s are composed of two conserved domains. ....	11
1.2.2 Allosteric cycle of BiP .....	11
1.2.3 Allosteric Hotspots in Hsp70s .....	14
1.3 BiP is a key player of the protein quality control network.....	15
1.3.1 Conventional chaperone Hsp70 functions .....	15
1.3.2 Additional functions of BiP .....	15
1.3.3 BiP's role as a regulator of the unfolded protein response .....	16
1.4 Multiple level of regulation of Hsp70s .....	22
1.4.1. Regulation of Hsp70 gene expression .....	22
1.4.2 Evolution fine tuning of Hsp70s .....	23
1.4.3 Hsp70 regulation by its co-chaperones.....	24
1.4.4 The chaperone code.....	26
1.5 study aims. ....	30
Chapter 2 – 6: Results .....	31
Chapter 2: Identification of ER unique sequence conservation patterns .....	31
2.1 Classical vs non-classical Hsp70 displays significant structural and sequence differences.....	31

2.2 Sequence based identification of location specific subfamilies of Hsp70s.....	36
2.3 SBD $\beta$ and NBD domains are the most conserved parts of Hsp70s.....	41
2.4 ER unique conservation patterns in Hsp70s .....	45
2.5 Identification of ER unique phosphorylation sites .....	48
Chapter 3: Protein construct design and production.....	51
3.1 Protein constructs .....	51
3.2 All constructs were capable of being expressed and purified. ....	51
3.3 BiP construct optimization .....	54
Chapter 4: Characterization of BiP conformational landscape using methyl NMR. ...	57
4.1. NMR as a tool to characterize small changes in the BiP conformational ensemble.....	57
4.2 Characterization of substrate binding to BiP.....	63
Chapter 5: BiP interactions with the stress sensor IRE1 as a tool to monitor ER specific functions of BiP.....	68
5.1 Two IRE1-LD derived peptides interact with BiP as classical chaperone substrates.....	68
5.2 Perturbations in <sup>310</sup> GSTLPLL <sup>317</sup> and <sup>356</sup> RNYWLLI <sup>362</sup> sites of IRE1 affect IRE1 oligomerization. ....	72
Chapter 6: Regulation of BiP conformation and function through ER specific phosphorylation sites.....	76
6.1 T460D and Y570D substitutions significantly increase ATPase activity.....	76
6.2 T460D and Y570D substitutions perturb the conformational landscape of BiP. ....	77
6.3 Phosphomimetic mutants are capable of binding substrate. ....	82
6.4 Phosphomimetic mutations decrease BiP's ability to deoligomerize IRE1-LD..	84
Chapter 7: Discussion.....	87
7.1 Paralog specific conservation patterns as a tool to guide experimental design...	87
7.2 The allosteric fine tuning of BiP through phosphorylation .....	89

7.3 Functional importance of the T460 and Y570 sites .....	94
Chapter 8: Concluding remarks.....	97
Chapter 9: methods.....	99
9.1 Plasmid production and sequencing .....	99
9.2 Protein expression and purification .....	100
9.3 NMR labelled protein expression and purification .....	102
9.4 TEV cleavage.....	103
9.5 Peptide stock and addition to samples .....	104
9.6 Mass spectrometry analysis .....	105
9.7 NMR experiments and data analysis.....	105
9.8 Malachite Green ATPase assay.....	106
9.9 IRE1 oligomerization assay.....	106
9.10 Conservation of amino acids analysis .....	107
9.11 Source of reagents used throughout the study .....	112
References.....	114
Appendix figures .....	139
Appendix.1 Conservational analysis additional data .....	139
Appendix. 2 Additional NMR spectra .....	186
Appendix. 3 Additional IRE1-LD oligomerization gels .....	191

## Abstract

As the sole member of the Hsp70 family found within the endoplasmic reticulum, BiP plays a critical role in the protein homeostasis of the ER in order to prevent build-up of unfolded proteins which would lead to ER stress. Due to this critical function and a complex allosteric cycle associated with it, the chaperone requires a complex multi-layered system of regulation. It is one aspect of this regulation, the limitedly characterised phosphorylation of BiP, which this study aimed to generate a greater understand of the mechanism of.

In this regard, this study was able to identify and select two substrate binding domain located phosphorylation sites which were demonstrated to be only conserved within ER located Hsp70s (and non-conserved in Hsp70 located in other sub-cellular locations) based on conservational analysis of ER and cytoplasmic located Hsp70s. These sites were mutated to phosphomimetic mutations in order to simulate the effects of phosphorylation and characterise them. The study used a combination of methyl NMR to monitor changes in the conformational ensemble, biochemical assays to measure alterations to the rate of ATP hydrolysis and effects to the interactions with a known substrates IRE1 in the characterisation process.

This approach allowed the characterisation of a regulation mechanism of BiP, in which phosphomimetic mutants and potentially phosphorylation caused a disruption of the domain undocked conformation whilst stabilising both the domain docked and intermediate transient conformation which results in the fine-tuning of BiP functions. These functions include increased ATPase activity as well as a reduced ability to deoligomerize IRE1. Additionally, the study was successful in the identification of the BiP binding site of IRE1-LD.

## Acknowledgements

I would like to express my deepest appreciation to Dr Anastasia Zhuravleva, without her constant support and guidance there is no chance that this endeavour would have been possible. Thanks to her as my supervisor, I have not only been able to produce a thesis in which I can be proud of but also improved myself as a researcher.

I would also like to thank Dr Bob Schiffrin, he was a valued member of research team who advice on my bioinformatic analysis was critical in overcoming numerous issues and help with coding and software choices which allowed for a far better project.

I would also like to thank Dr Arnout Kalverda and the NMR department here at University of Leeds, their help with not only with the running of the machines but the training and support I received to complete my data collection. This has formed a core part of my project and without their help, there would have been no way this project would have been able to make any progress in characterising the mutants or locating the BiP binding site of IRE1.

Additionally, I would like to thank Dr Iain Manfield and his team. The training and access to a wide range of equipment pretty much covered every experiment I have completed that wasn't NMR based. Their help has been invaluable over the last four years.

Finally, I would like to thank Dr James Ault for training in Mass spectrometry. Without the verification of the constructs spotting an error in the construct design, the data would likely have been false. I am very grateful that mass spec helped me avoid that mistake.

## Chapter 1: Introduction

### 1.1 The Hsp70 family, a group of ubiquitous molecular chaperones

#### 1.1.1 Hsp70 is a highly conserved family.

The 70 kDa heat shock protein (Hsp70) family is a family of proteins composed of ubiquitous molecular chaperones (1). This family of proteins functions as “cellular housekeepers” in order to maintain protein homeostasis through a wide range of functions (1,2). Various Hsp70s are expressed across multiple subcellular locations within in all eukaryotes and prokaryotes, performing functions which are shared between all Hsp70s, as well as subcellular specific roles (3). The expressed Hsp70s exist alongside a wide range of co-chaperones that aid the functions of the molecular chaperone family, moreover together the chaperone and co-chaperones constitute up to 3 % of the total protein mass of unstressed cells (4).

The members of the Hsp70 family are the most abundant molecular chaperones within a cell, and they are located within the cytoplasm, the endoplasmic reticulum (ER), mitochondria and chloroplasts, with functions to protect proteins from synthesis to degradation (1,3,5). In the early stages of a protein life, the Hsp70 serves to aid in the *de novo* folding of polypeptides as they emerge from ribosomes to protect them from aggregation by protecting aggregation prone subunits as they fold correctly (6). From here the cytoplasmic Hsp70 can aid in the translocation of proteins into the mitochondria, chloroplast and the ER, with an alternative Hsp70 within the organelle acting to aid the transport via a directional pulling mechanism (7). In the final stages of the protein life cycle, Hsp70 plays a role in targeting degradation by the proteasome or the autophagic system (8,9). As you can see there is a wide range of functions, which shall be discussed in more detail in chapter 1.3.

Hsp70s are highly conserved in all organisms (1), to the point that even the evolutionarily distanced bacteria DnaKs are about 45 % identical and 60 % similar to human cytoplasmic located HspA1A and the ER located BiP (10,11). This includes a shared structure and conformational landscape which will be discussed in more detail in chapter 1.2. Humans are known to possess at least 13 Hsp70s located in all subcellular locations (table 1).

**Table 1: Human Hsp70s.** A table summarizing the 13 human Hsp70 displaying all names of the protein and gene, subcellular locations, and length of sequence (number of amino acids) (3,11).

<b>Protein</b>	<b>Other names</b>	<b>Gene names</b>	<b>Subcellular location</b>	<b>Length</b>
HspA1A	Hsp70-1, Hsp72, HspA1, Hsp70-1A, Hsp70i	<i>HSPA1A</i>	Cytoplasm, nucleus cytoskeleton, microtubule organizing centre, centrosome	641
HspA1B	Hsp70-2, Hsp70-1B	<i>HSPA1B</i>	Cytoplasm, nucleus, extracellular exosomes, blood microparticle	641
HspA1L	Hsp70-1L, Hsp70-hom, Hsp70-1t, Hum70t	<i>HSPA1L</i>	Cytoplasm, nucleus	641
HspA2	Heat shock 70kD protein 2, Hsp70.2	<i>HSPA2</i>	Cytoplasm, nucleus, cell membrane, extracellular exosomes	639
BiP	Hsp70-5, HspA5, Grp78, Mif-2	<i>HSPA5</i>	ER, extracellular exosomes	654
HspA6	Hsp70-6, Hsp70B'	<i>HSPA6</i>	Cytoplasm, extracellular exosomes	643
HspA7	Hsp70-7, Hsp70B	<i>HSPA7</i>	Blood microparticles, extracellular exosomes	367
HspA8	Hsp70-8, Hsc70, Hsc71, Hsp71, Hsp73	<i>HSPA8</i>	Cytoplasm, nucleus, cell membrane, extracellular exosomes	646
Grp75	Hsp70-9, HspA9, HspA9B, MOT, MOT2, PBP74, mot-2, mtHsp70, mortalin	<i>HSPA9</i>	Mitochondria, nucleus	679
HspA12A	Hsp70-12A, FLJ13874, KIAA0417	<i>HSPA9</i>	Intracellular, extracellular exosomes	675
HspA12B	Hsp70-12B, RP23-32L15.1, 2700081N06Rik	<i>HSPA12B</i>	Endothelial cells, intracellular, blood plasma	686
HspA13	Hsp70-13, Stch	<i>HSPA13</i>	extracellular exosomes, microsomes	471
HspA14	Hsp70-14, Hsp70L1	<i>HSPA14</i>	Cytoplasm, membrane	509

### 1.1.2 The ER and its sole Hsp70, BiP

The ER is the largest membrane bound organelle within eukaryotic cells, with over 30% of the total proteome within the ER at a given time (12–14). The ER serves multiple critical roles; the most often considered is its role in protein synthesis and folding (15). In terms of protein synthesis, secretory or integral membrane protein translation occurs in the cytoplasm. The mRNA containing ribosomes are recruited to the ER membrane based on the recognition of signal sequence within the amino terminus of the nascent polypeptide by signal recognition particle (SRP) (16,17). The mRNA, ribosome, nascent polypeptide and SRP are docked to the ER as a set, allow translation into the ER for the emerging polypeptide through the translocon (18–20).

After synthesis or translation, the protein can undergo proper folding and modifications (N-linked glycosylation, disulfide bond formation and oligomerization) within the ER (21). This is in addition to other functions such as lipid biogenesis (22) and acting as a major store of intracellular calcium (with the ER lumen  $\text{Ca}^{2+}$  concentration is 100–800  $\mu\text{M}$ , and the extracellular  $\text{Ca}^{2+}$  concentration is  $\sim 2$  mM compared to the cytoplasmic  $\sim 100$  nM) (23,24).

In order to successfully fulfil the task of protein folding, there has to be balance between the ER protein load and the folding capacity (25). Disruption to this balance can occur due to multiple reasons; such as Physiologic stresses (e.g., increased secretory load) or pathological stresses (e.g. presence of mutant proteins), which results in the capacity of the ER to fold proteins becoming saturated (26). As ER stress is associated with multiple disease, such as Diabetes mellitus, Neurodegeneration disease (such as Parkinson's disease) and cancer (26,27), a mechanism to regulate the protein homeostasis and counteract the negative effects of ER stress is vital.

In order to combat this ER stress, the organelle possess a complex series of chaperone and co-chaperones which includes a single member of the Hsp70 family. BiP (the Binding immunoglobulin protein) is a critical component in the ER, where it fulfils all the previously mentioned roles of the Hsp70 family with a few ER specific ones such as within the ERAD system and the unfolded protein response (UPR) (28–30). It is this member of the Hsp70 family which this project will focus on.

## 1.2 Hsp70 structure and allosteric cycle

### 1.2.1 Hsp70s are composed of two conserved domains.

The Hsp70 family possesses a highly conserved structure with key features being shared across the entire family of proteins. Similar to the majority Hsp70s, the ER located Hsp70 BiP consists of a 45 kDa nucleotide binding domain (NBD) and a 25 kDa substrate binding domain (SBD) connected by an interdomain linker (IDL) (Figure 1) (31–33). The NBD can be further subdivided into four subdomains (IA, IB, IIA and IIB) arranged into two lobes with a cleft in between (32,34) and the SBD is divided into two sub-domains; the “binding pocket” (SBD $\beta$ ) and the “lid” (SBD $\alpha$ ) (Figure 1). The SBD $\beta$  is composed of an eight-stranded  $\beta$ -sandwich, housing a substrate binding cavity with a central hydrophobic pocket (31,35–37).

The two domains have distinct functions for the protein with the NBD responsible for the binding and hydrolysis of ATP whereas the SBD is responsible for the binding of unfolded protein substrates (1,29). The IDL has a role in connecting the two domains as well as interaction with the NBD that triggers domain rearrangements in Hsp70 during the allosteric cycle (1,38,39).

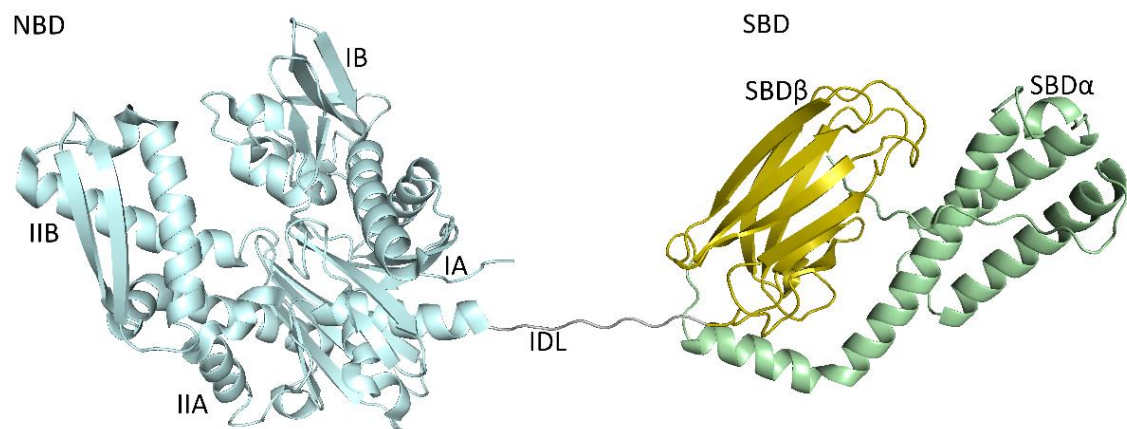


**Figure 1: Domain structural organization of the ER located Hsp70 BiP.** Cartoon representing the crystal structures of NBD (blue, PDB code ID 5e85) and SBD (6HA7) of BiP in domain undocked conformation coloured coded with NBD (blue), SBD $\beta$  in (yellow) and SBD $\alpha$  in (green), connected by interdomain linker (IDL). Structure is labelled to display subdomains names.

### 1.2.2 Allosteric cycle of BiP

Similar to bacterial Hsp70 DnaK (2,40–42) and cytoplasmic Hsp70s (43), BiP co-exists in two end point conformations, the domain docked and the domain undocked conformation. In the domain undocked conformation, the two domains do not interact with the IDL. The IDL is instead exposed to solvents and the SBD $\alpha$  is docked onto the SBD $\beta$  to fully enclose the substrate binding cavity (Figure 2, bottom) (42,44–46). Whereas in the domain docked conformation the IDL interacts with the NBD, which

triggers the SBD $\alpha$  dissociation from the SBD $\beta$ . The SBD $\alpha$  and SBD $\beta$  are instead both docked onto the NBD (Figure 2, top) (31,42,47,48). Hsp70s transitions through these two end point conformations during its allosteric cycle, which is driven by the binding of both substrates and nucleotides.

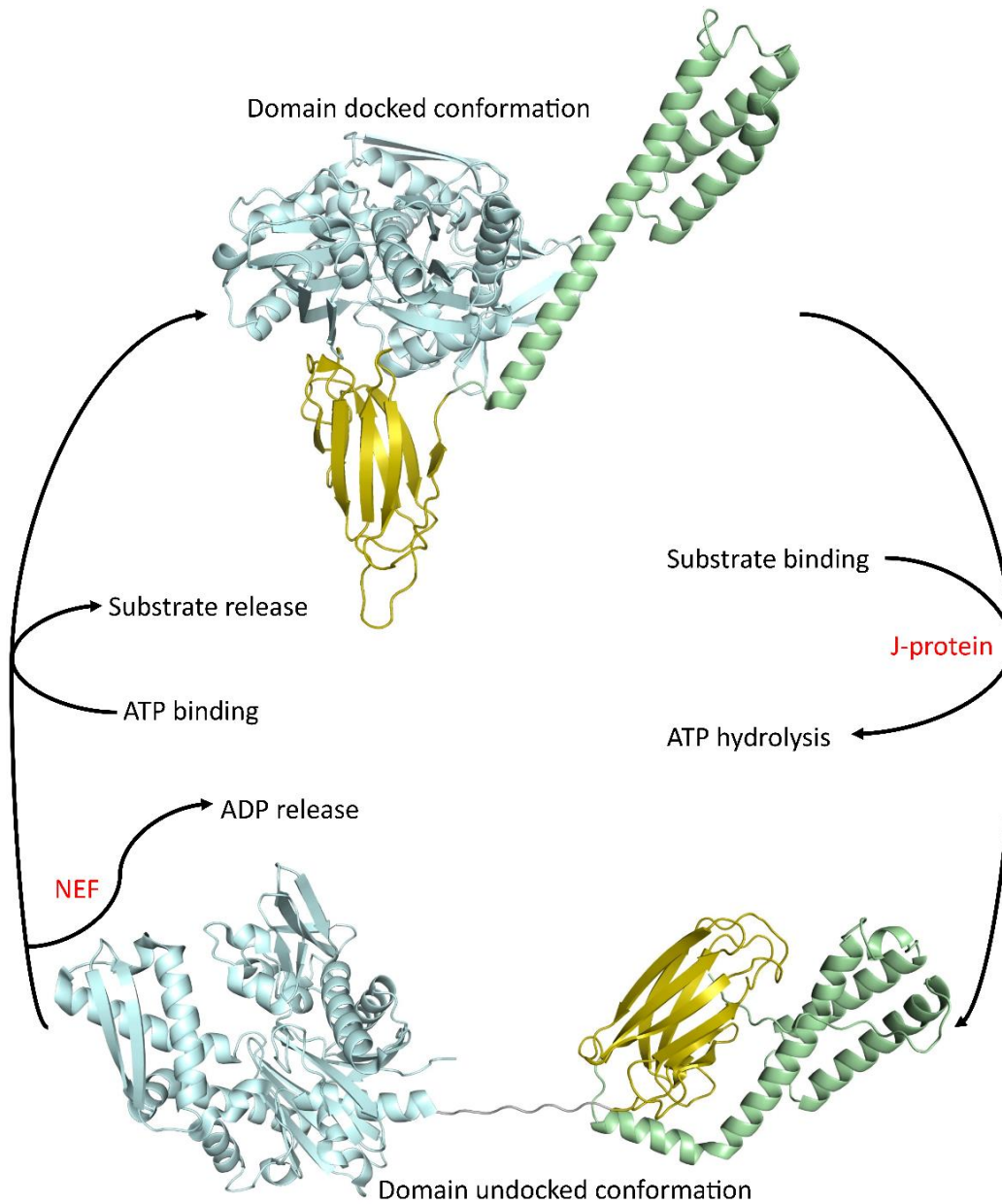


**Figure 2: allosteric cycle of BiP.** A cartoon depicting the allosteric cycle of BiP, where it transitions between the two end point conformations; domain docked (PDB code 5e84) and domain undocked (PDB code 5e85 and 6HA7) conformation. Cycle driven through the binding of substrate and ATP co-chaperones involved displayed in red.

BiP like all Hsp70s, transitions through these two end point conformations during its allosteric cycle. The shifting of BiP through these two conformations is vital for the functions of BiP, due to the varying properties within the two conformations. An often-cited example is the difference in affinity for substrate, with the domain undocked conformation having the substrate binding affinity several magnitudes higher than the affinity in the domain docked conformation. Moreover, SBD $\alpha$  bindings to SBD $\beta$  in the domain undocked conformation results in a far slower association dissociation rate compared to the domain docked conformation (31,44,47–49). For example for DnaK, the  $k_d$  for a substrate is  $0.078 \pm 0.007 \mu\text{M}$  with a  $k_{\text{off}} / k_{\text{on}}^1$  of  $9.1 \pm 0.2 \text{ s}^{-1} \times 10^{-4}$  and  $1.17 \text{ M}^{-1} \text{ s}^{-1}$  in the presence of ADP vs the  $k_d$  for a substrate is  $1.8 \pm 0.3 \mu\text{M}$  with a  $k_{\text{off}} / k_{\text{on}}^1$  of  $2.31 \pm 0.03 \text{ s}^{-1} \times 10^{-4}$  and  $1.28 \text{ M}^{-1} \text{ s}^{-1}$  in the presence of ATP (50). This displays the significance of the conformation and the ability of BiP to transition between them on its characteristic and functions. As a result, transitions between the domain docked and undocked conformations is vital for the functions of Hsp70s, allowing controllable substrate binding and release during its allosteric cycle.

ATP binding and hydrolysis enables the precise control of the thermodynamic equilibrium between domain docked and undocked conformations (Figure 2) (1,29). This is allosteric regulation, where the binding of a ligand to a site topographically distinct from the site of the protein associated with a function regulates the function (51). This allosteric cycle is shared amongst the Hsp70 family, with most understanding derived from bacterial DnaK (1,29). ATP binding favours the IDL binding to the NBD and consequently for the SBD to dock onto the NBD. However, the SBD $\alpha$  docking to NBD leaves the NBD catalytic residues in a conformation not suitable for efficient ATP hydrolysis, locking the chaperone without bound substrate in an ATP bound domain docked conformation. The binding of substrate into the pocket of the SBD $\beta$  favours the interactions of SBD $\beta$  and SBD $\alpha$ , causing a shift in the conformational equilibrium towards the domain undocked conformation. The binding of substrate is aided by the group of co-chaperones, known as the J-domain (red in Figure 2). This undocking of the SBD from the NBD in the presence of ATP does not result in the IDL dissociation from the NBD, enabling the IDL induced rotation of the NBD lobes to a position that is significantly more efficient for ATP hydrolysis (42,52,53). The consequence of ATP hydrolysis is the IDL dissociation from the NBD, which shifts the NBD out of optimal ATP hydrolysis positioning and leaves it with the ADP bound domain undocked conformation (Figure 2) (1,38,39).

Nucleotide exchange factors (NEF), a co-chaperone of Hsp70s (red in Figure 2), initiate the return to domain docked conformation, through the co-chaperone aiding in the release of bound ADP (54,55). This allows fresh ATP to bind, and this triggers SBD $\alpha$  and SBD $\beta$  to separate via an unclear conformational event. SBD $\beta$  binds the NBD again, opening the substrate binding pocket releasing the bound substrate and returning BiP to the domain docked conformation (56,57) (Figure 2). This restarts the allosteric cycle.

### 1.2.3 Allosteric Hotspots in Hsp70s

There is a close link between the conformational landscape of Hsp70s and the thermodynamic and kinetics of its allosteric cycle. It has been previously demonstrated that specific regulatory regions in Hsp70s structure, also known as “allosteric hotspots”, enable an additional level of regulation for the Hsp70 allosteric cycle and functions (46). Particularly, even subtle changes near the domain interfaces in bacterial DnaK has been used to display perturbations, which include amino acids substitutions and ligand binding, which can affect both the conformational cycle and chaperone activity of Hsp70s (36,42).

Similarly, in BiP, several allosteric hotspots have been identified within the regions where the SBD and NBD or the SBD $\alpha$  and SBD $\beta$  interact (42). This includes, V461 (located near the substrate binding site), I526 (located at the central hub for the  $\beta$ SBD allosteric network, I437 (located near the  $\beta$ SBD-NBD interface) and I538 (located at the  $\beta$ SBD  $\alpha$ Lid and  $\alpha$ Lid NBD interfaces). “Soft” substitution (also known as a conservative replacement) where an amino acid is exchanged for another that has similar properties within these sites has been demonstrated to shift the conformational equilibrium. Particularly V461F and I526V favour domain docked conformation and I437V and I538V favour domain undocked conformation (46). Intriguingly, “soft” perturbations in the allosteric hotspots can even ‘mimic’ the effect of ATP binding, resulting in the domain docked conformation in the absence of ATP in both BiP and DnaK (36,46). The V461F mutant is of particular interest due to it having been an often-used mutant in BiP study due to it severely reduced substrate binding ability (58).

Consequently, evolutionally conserved regions, and post-translational perturbations in allosteric hotspots that lead to changes in the Hsp70 allosteric cycle are important factors that affect Hsp70 activity and functions. This is a complex system, where small variation to any one of these factors can drastically alter the protein.

## 1.3 BiP is a key player of the protein quality control network.

### 1.3.1 Conventional chaperone Hsp70 functions

As a member of the Hsp70 family, the most prominent function of BiP is assisting protein folding and preventing misfolding. Similar to other Hsp70s, BiP is capable of interacting promiscuously with an incredibly large range of protein substrates in their different conformations, which includes nascent unfolded polypeptides emerging from the ribosome, misfolded protein, and folding intermediates. The binding and release of unfolded protein substrate from Hsp70s serve to protect these protein substrates from aggregation and to allow either the protein to be folded correctly or targeted for degradation (1,29).

The Hsp70 SBD $\beta$  is formed of a two layered twisted  $\beta$ -sandwich that contains a hydrophilic cleft onto which substrate bind. This has been identified in DnaK as the residues 404M, 427S, 429A, 433Q and 437T (39,47). These residues bind to solvent exposed five residue hydrophobic regions of protein substrate. Binding can be further stabilized if positively charged residues are following the hydrophobic region. This type of motif is abundantly found in most globular proteins, although mostly within the hydrophobic core of native folded proteins, which means they are only predominantly accessible to Hsp70s when its protein substrates are unfolded or misfolded (41,59). Screening using 4360 cellulose-bound peptides scanning the sequences of 37 biologically relevant proteins revealed that these motifs occur on average every 30–40 residues in the majority of proteins (59).

As the same hydrophobic motifs are responsible for protein aggregation, their binding to Hsp70s protect these proteins from the potential of misfolding. The substrate interacts with the small hydrophobic pocket of the SBD $\beta$  and the helical lid of the SBD $\alpha$  through a series of hydrogen bonding and hydrophobic interactions (60–64). The fact that Hsp70s can promiscuously bind to almost all unfolded and misfolded proteins allows it to fulfil this classical chaperone function for situations or substrates which may arise in normal cellular or stress conditions.

### 1.3.2 Additional functions of BiP

BiP, like most Hsp70s, is far more complex than just being a single function protein (29). It is directly involved in a wide variety of functions, typically linked with protein homeostasis in some capacity. As mentioned during its classical chaperone role, BiP is capable of targeting the misfolded protein for destruction via the ER associated protein degradation (ERAD) pathway (29,30). BiP recognises the hydrophobic regions of the misfolded protein and can target it for degradation through interactions with J-domain co-chaperone (ERdj4 and ERdj5) and with other ERAD components (29,53). This is coupled with BiP serving to solubilize proteins it targets for degradation. This was

displayed to be a vital role of BiP during the ERAD process with mutants that reduces BiP's ability to solubilize, causing impaired degradation of misfolded proteins (65–67).

In addition, BiP also plays a role in calcium regulation. The ER  $\text{Ca}^{2+}$  concentration is several orders of magnitude higher than the cytoplasm, at 100 to 800  $\mu\text{M}$  (24). BiP is capable of acting as a high capacity  $\text{Ca}^{2+}$  binding protein in order to store around 25 % of the ER calcium concentration (68). This is a key function as deregulation of calcium levels within the ER has been associated with multiple disease states (69).

Surprisingly, BiP has a function which is carried out not within the ER, but instead can be expressed on cell surfaces. Here, BiP exists as a peripheral protein on the plasma membrane via interactions with other cell surface proteins, including glycosylphosphatidylinositol (GPI) anchored proteins (70–72) and serves to promote either cell survival or apoptosis based on the interactions with other proteins (73–75).

### 1.3.3 BiP's role as a regulator of the unfolded protein response

ER stress is a condition where the ability of the ER to fold protein is overloaded by the demand for protein folding, typically due to increased secretory load, or pathological stresses (26). ER stress can be incredibly harmful, being linked to diseases such as neurodegenerative disease (e.g., Parkinson's disease) (76), metabolic disorders (e.g., diabetes) (77) and cancer (78). The unfolded protein response (UPR) serves as a mechanism which serves to counteract build-up of unfolded or misfolded proteins within the ER composed of a network of signal transduction pathways that are capable of altering gene transcription, mRNA translation, triggering ERAD pathways and altering protein modifications (78).

The UPR pathway in mammals consists of three signalling cascades, which can be initiated by one of the transmembrane protein sensors: Inositol-requiring enzyme 1 (IRE1), protein kinase RNA like endoplasmic reticulum kinase (PERK) and activating transcription factor 6 (ATF6) (79). These signal transducing proteins contain ER luminal domains capable of sensing unfolding proteins as well as cytosolic regions responsible for interacting with signalling molecules or translational and transcriptional apparatus (79,80) (Figure 3). This occurs through activation of signalling cascades of the UPR system associated with each of these proteins (81).

ATF6 mediates a transcriptional response to promote folding and the ERAD pathways (82). It moves into the Golgi apparatus in order to be cleaved by site specific proteases S1P and S2P and this results in the release of the cytosolic portion, ATF6I (a bZIP transcription factor). This factor is capable of migrating into the nucleus to upregulate the expression of UPR related genes (Figure 3 right) (28,83,84).

The other two activator proteins are different. The luminal domains (LD) of both IRE1 and PERK share structural similarities (85,86), and both cytosolic portions contain a kinase domain that auto phosphorylates to activate the pathway (87–90). For PERK, the kinase activation leads to phosphorylation of eukaryotic translation initiation factor-2 $\alpha$  (eIF2 $\alpha$ ), which results in the ribosome inhibition and brief reduction of global cell translation in order to reduce the demands of protein folding machinery. Although, it does reduce the general protein synthesis, of a cell, it does cause the upregulation of the UPR genes such as activation transcription factor 4 (ATF4) (Figure 3 middle) (89,91).

For IRE1 though, when it is phosphorylated, it activates endoribonuclease in order to splice mRNA of XBP1 to form a potent transcriptional activator, in order to upregulated UPR genes (Figure 3 left) (87–90,92,93). The upregulated genes serve to increase the capacity for protein folding as well as increase the amount of protein degradation and transport to reduce the total amount of misfolded protein within the ER (28,94). It is this activator that the project will focus on, in terms of its interaction with BiP

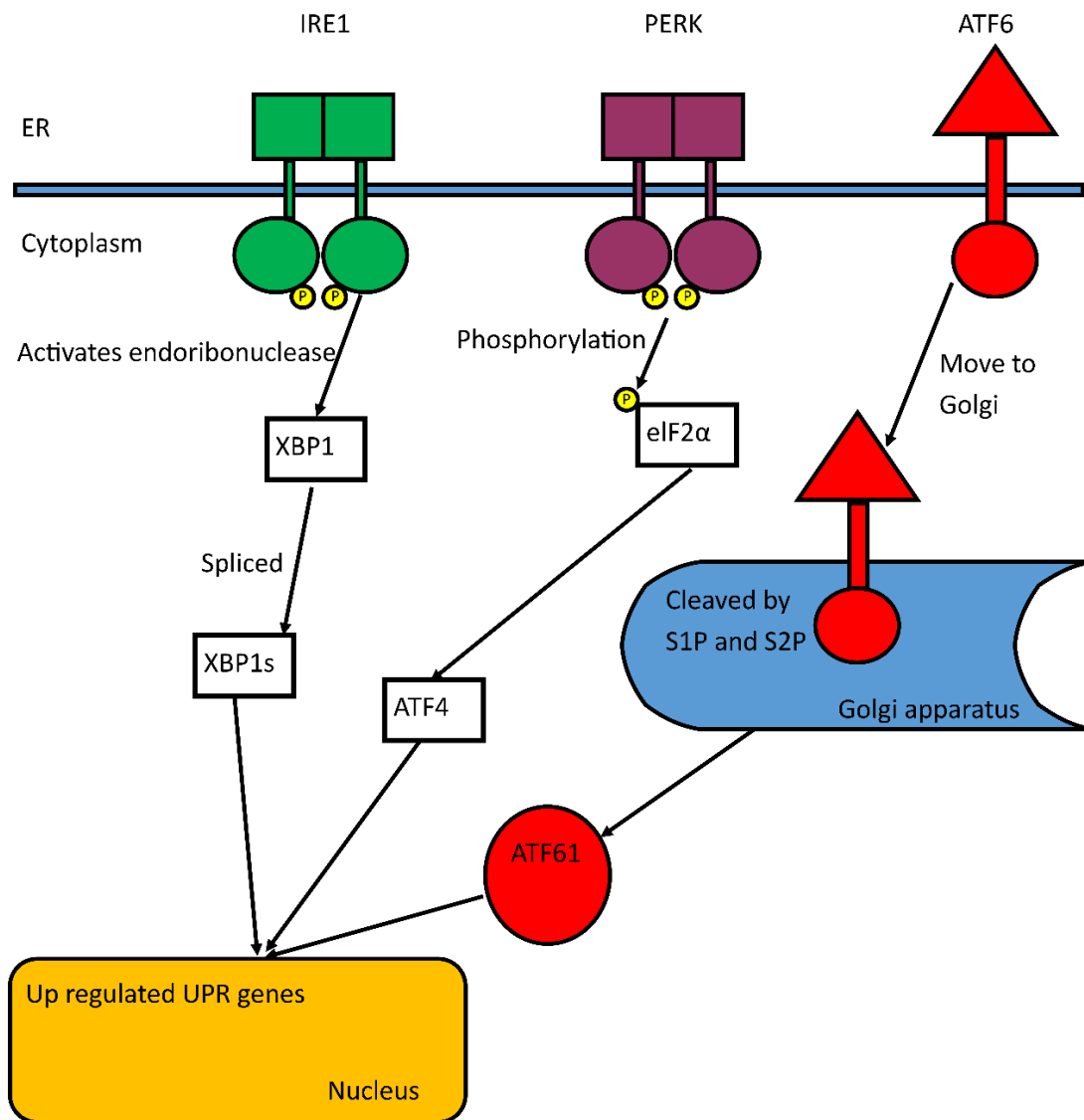


**Figure 3: the UPR signalling pathway summary.** A cartoon depicting the overview of the three UPR pathways associated with transmembrane protein sensor, with the general signal cascade which serves to activate the expression of the UPR related genes. It displays the three activator proteins: IRE1, PERK, and ATF6 and the cascades associated (95).

BiP is known to be the key regulator of the complex pathway though its interactions with all three stress sensors remain elusive. While the exact mechanism of how BiP controls UPR activation is still unknown, the IRE1 branch is currently the best characterised and understood out of the three models of how BiP and ER stress (the accumulation of unfolded proteins) control IRE1 activation. These models are the “direct association” model, the “allosteric” model, and BiP “competition” model (95).

The direct association model (Figure 4A) postulates that the IRE-LD binds directly to an unfolded or misfolded protein, resulting in conformational changes, its oligomerization and activation (96–100). The crystal structure of yeast IRE1-LD reveals that dimerization of IRE1-LD results in formation of a peptide binding groove (100) with IRE1-LD directly

interacting with hydrophobic peptides within these peptide binding groves (98,101). It has been suggested that peptide binding induces the conformational changes in the IRE1-LD dimer that favours the formation of the oligomers (98,101) and therefore the activation of the UPR (28,101,102). In this model, BiP does not play a key role in UPR activation but can fine tune this process by interacting with the same unfolded protein substrates that interact with IRE1-LD, preventing their interactions with IRE1-LD, and thus affecting IRE1 activation (28).

The competition model (Figure 4B) proposes that BiP is actively involved in the IRE1 activation process through chaperone type interactions with the IRE1-LD. In the absence of stress (accumulation of unfolded protein substrate), IRE1-LD binds to BiP as a chaperone substrate via the BiP SBD. These interactions suppress IRE1-LD dimerization and its activation. Because these interactions are closely reminiscent of BiP binding to its unfolded protein substrate, a key regulator of the BiP chaperone cycle, co-chaperone ERdj4 plays an important role in the process. ERdj4 binding to IRE1-LD mediates the IRE1 BiP interactions as well as triggering ATPase activity of BiP. The accumulation of unfolded protein substrates that compete with IRE1-LD for BiP binding, in turn, results in BiP dissociation from IRE1-LD, promoting IRE1-LD oligomerization and IRE1 activation (103–108). For this theory to be correct, it requires that BiP binds through only the SBD, requiring the ERdj4 J-domain protein in order to act like substrate-chaperone type interaction (28), however it has been demonstrated to bind via NBD as well, binding between IRE1-LD and BiP without ERdj4 (109–111). This suggests that this theory is less likely to be accurate.

In the allosteric model (Figure 4C), IRE1-LD directly interacts with BiP NBD, in a non-conventional nucleotide independent manner (111–113). Similar to the competition model (Figure 4B), this model suggests that the accumulation of unfolded proteins upon ER stress results in BiP dissociation from IRE1-LD and its consequent oligomerization and activation. While similar to the competition model, the allosteric model suggests that protein substrate binding to BiP results in as yet unknown, ATP independent conformational changes in the chaperone that allosterically prevent BiP NBD binding to IRE1-LD. This results in the oligomerisation of IRE1 and therefore in the activation of the UPR (28,111).

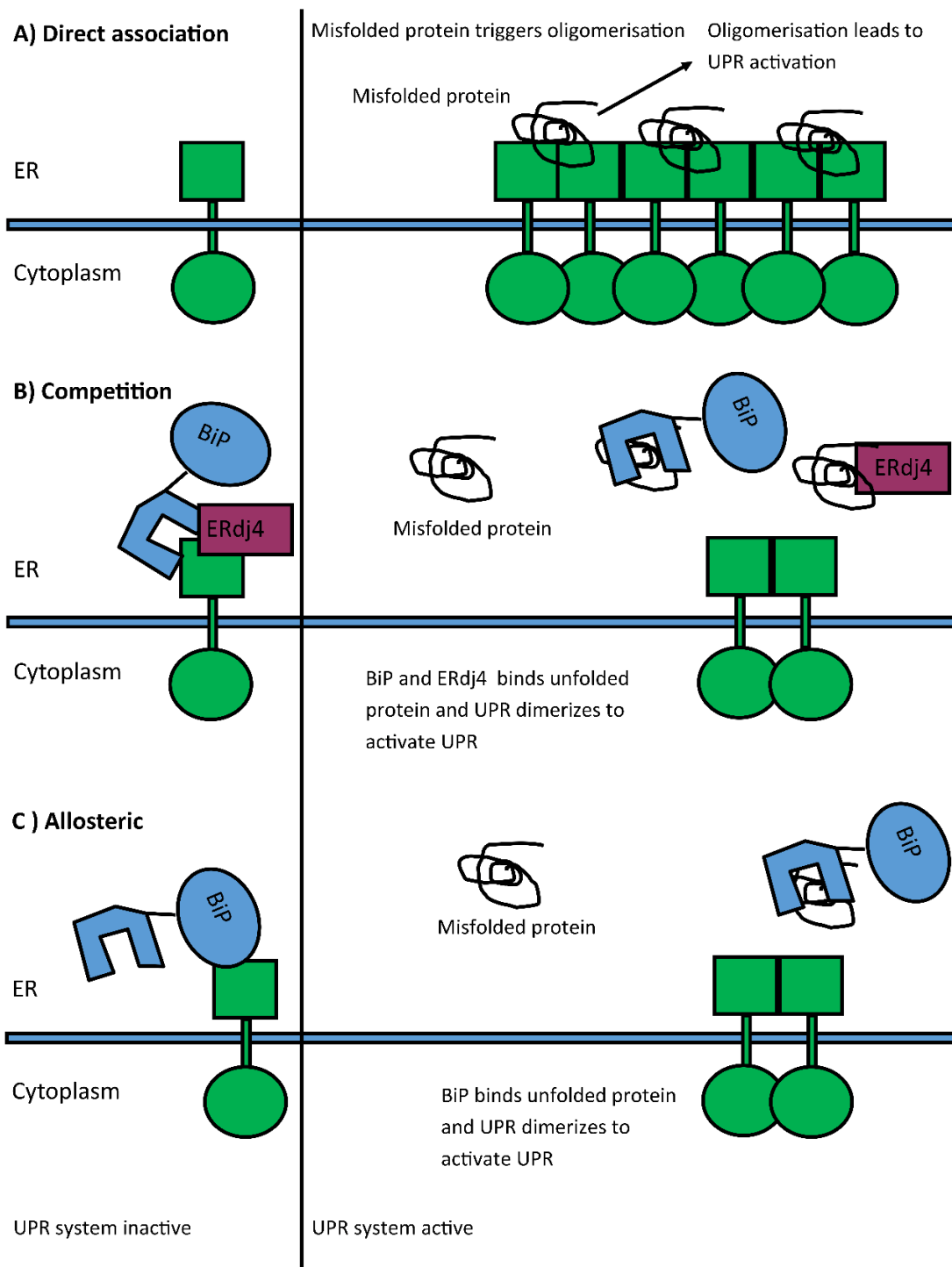


**Figure 4: Potential IRE1-LD models of IRE1 activation.** Cartoons of the three literature models: direct association in which misfolded protein directly associated with IRE1 to form oligomers (A), competition in which BiP aided by ERdj4 repress IRE1 through chaperone like activity to prevent formation of oligomers (B) and allosteric where BiP NBD interacts with IRE1 to prevent formation of oligomers (C) and summarizes how BiP and IRE1 may interact with unfolded protein to regulate the UPR (28).

Growing evidence suggests that both unfolded protein substrates and BiP can directly bind and control IRE1-LD oligomerization (111,114,115). This study will address this possibility of interaction by characterization of interactions between IRE1-LD, BiP and unfolded protein substrates as an aspect of the research. It will also elucidate how post-translational fine tuning of BiP activity effects these interactions.

## 1.4 Multiple level of regulation of Hsp70s

BiP possesses a complex allosteric cycle (discussed in chapter 1.2.2), essential for its wide range of vital functions (chapter 1.3) that are critical for ER protein homeostasis. To be able to respond and adapt to the constantly changing ER environment and pathological and physiological stresses to efficiently perform its diverse functions, BiP activity requires translational and post-translational regulation. Growing evidence suggests that similar to other Hsp70s, BiP regulation is not just a simple 'on and off' switch of its activity (46,53,116). It is instead a far more complex fine tuning of its specific functions, comprised of multiple levels of different regulation. In this section, the basic principles of BiP regulation are discussed (Figure 5).

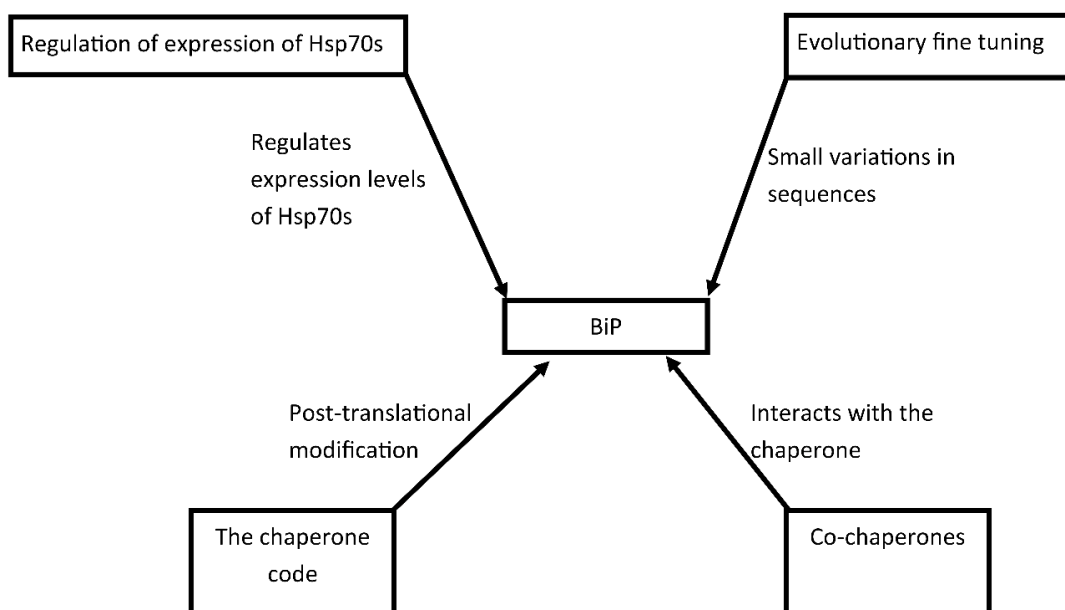


**Figure 5: regulation of BiP and other Hsp70s.** A cartoon summarizing some of the components of Hsp70 regulation and how they interact with Hsp70s in order to regulate the protein, with all four parts acting together to regulate the chaperone.

### 1.4.1. Regulation of Hsp70 gene expression

The first level of regulation for the Hsp70 is the control of where and at what levels the Hsp70s are expressed. This regulation of expression of the survival gene is vital for mounting a response to severe cellular stress such as elevated temperature, reactive oxygen species generation, hypoxia, and lowered pH (117). Under stress conditions such as heat, both heat shock factor 1 (HSF1) (and HSF2 in a less well characterised manner) are activated. Under normal non stress conditions, HSF1 is sequestered in monomeric form by constitutive chaperones Hsp70 and Hsp90 in the cytoplasm. Under stress conditions, such as heat shock, a build up of misfolded proteins trigger Hsp70 and Hsp90 to be sequestered to counteract the stress and restore protein homeostasis. This allows HSF1 to trimerize and translocate to the nucleus, binding to the heat shock element

(HSE) in order to activate transcription of Hsp70 (118–120). More Hsp70s allows not only misfolded proteins to be bound and either folded correctly or targeted for degradation by Hsp70 (such as through the ERAD system as in BiP (chapter 1.3.2)) but also for HSF1 to be bound by Hsp70 to switch off the gene transcription (118). This is similar to how BiP regulates the previously discussed UPR (chapter 1.3.3) in which BiP interacts with the three stress sensors to prevent UPR activation and under stress conditions allows the activation of the response. With BiP being one of the upregulated genes of the UPR response which serves to expressed increased levels of BiP in order to counteract the ER stress (101). Through controlling the expression of Hsp70 genes, it is possible for cells to regulate the functions of the Hsp70 by simply up and down regulating the protein expression in response to stress or non-stress conditions.

#### 1.4.2 Evolution fine tuning of Hsp70s

The essential nature of Hsp70 means that the family is highly conserved with only a small amount of sequence variations found within each member of the family. However, these small variations in different Hsp70 isoforms are essential to fulfil specific chaperone functions in different and often rapidly changing environments (121). As a result, within the Hsp70 sequences small but functionally vital variations exist even in highly conserved critical regions of the protein.

A well studied example of these variations is found within BiP's substrate binding site. The ability to bind unfolded protein substrate efficiently and controllably is essential for the majority, if not every one of the Hsp70 functions (1,29). The substrate binding site of Hsp70 is one of the most conserved parts of the chaperone, enabling promiscuous binding to unfolded or misfolded proteins (60). The access to the substrate binding site and thus kinetics of substrate binding and release is under the control of two flexible SBD loops, forming the hydrophobic contacts (arch) that control the substrate access to the cleft (31,32,39). This region is not fully conserved (31), with sequence variations in this region have been shown to control kinetics and specificity of substrate binding.

ER-located Hsp70 BiP is known to have a slower substrate binding kinetics than bacterial Hsp70 DnaK. Intriguingly, the only sequence difference in the substrate binding site between these two Hsp70s is valine 429 in BiP, corresponding to residue 404 in DnaK that is substituted by methionine. Strikingly, a single point V429M substitution in BiP is sufficient to eliminate these differences in substrate binding kinetics between these two Hsp70 family members (122). It has been suggested that in BiP Y570 and R492 form an SBD $\alpha$  SBD $\beta$  contact (Figure 6) that slows down the substrate entrance to the substrate binding cleft (31). In BiP, the valine side chain in the position 429 is too short to disrupt these SBD $\alpha$  SBD $\beta$  interactions resulting in relatively slow substrate binding kinetics. However, a large methionine side chain in this position disturbs the Y579 R492 contact, thus resulting in faster substrate binding and release (31,123). Variations in the specificity for substrates have been demonstrated with some studies displaying that

cytosolic Hsp70s preferably binds leucine enriched peptide motifs whereas BiP prefers motifs with aromatic residues (60). This is a beautiful illustration of how a subtle amino acid substitution in the Hsp70 sequence can drastically alter its functions, allowing nature to fine tune Hsp70 activity without significant changes in chaperone structure and allosteric mechanisms.

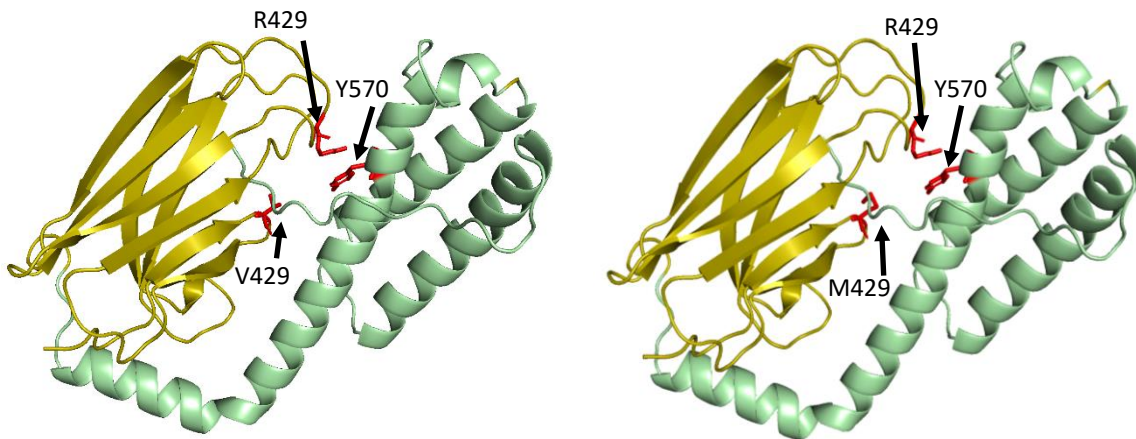


**Figure 6: methionine size disturbs Y570 and V492 interactions.** Cartoon representing the crystal structures of SBD (6HA7; 5e85) in yellow and SBD $\alpha$  in green with the R429 and Y570 displayed in red. In addition, the structures contain either the smaller V429 (left) not blocking the substrate binding cleft or the larger V429M (right) mutation.

#### 1.4.3 Hsp70 regulation by its co-chaperones

The next layer of Hsp70 regulation is co-chaperones that orchestrate the Hsp70 chaperone cycle as well as provide substrate selectively (53,55,124). Similar to other Hsp70s, BiP has two main groups of co-chaperones: ER localized DnaJ family members (ERdjs) (DnaJ, also known as Hsp40s, is the name of the entire co-chaperone family) and nucleotide exchange factors (NEFs) (53,55,124).

There are seven known ERdjs within humans, called ERdjs 1-7 (Table 2). There are three types of DnaJ family co-chaperones, classified based on how similar they are to *E. coli* DnaJ. Type I (including ER located ERdj3) J domain proteins have an N-terminal J domain, a flexible Gly/Phe-rich region linker, often include a cysteine-rich zinc-binding domain, and a C-terminal dimerization domain. Type II J-domain proteins (including ER-located ERdj4,) have similar organization but possess no cysteine rich zinc binding domain. Type III only have the J-domain in common with the *E. coli* DnaJ (53).

*Table 2: ERdjs summary. Table displaying the seven known human ERdjs with their classes, functions, and any distinct structural features. Data sourced from review (53).*

<b>ERdj</b>	<b>Class</b>	<b>Function</b>	<b>Structural feature</b>
ERdj1	3	Binds to exit site on the 80S ribosome	integral membrane DnaJ
ERdj2	3	Binds translocon complex	integral membrane DnaJ
ERdj3	1	Binds to misfolded proteins	Same structure as <i>E. coli</i> DnaJ
ERdj4	2	Binds to misfolded proteins	Same structure as <i>E. coli</i> DnaJ without the cysteine rich zinc binding domain
ERdj5	3	Responsible for efficient folding and section of disulphide-containing proteins	Has a six thioredoxin (Trx) domains
ERdj6	3	interaction with proteins by a redox mechanism	Ha a nine tandemly arranged tetratricopeptide repeat (TPR) motifs
ERdj7	3	Unknown	

J-domain proteins play key roles in substrate and functional specificity of Hsp70s (53) including BiP (same table as above). ERdj1 and ERdj2, integral membrane DnaJ family members which bind to the tunnel exit site on the 80S ribosome (ERdj1) or translocon complex (ERdj2), that are responsible for the regulation of translation in a BiP dependent manner and engage BiP to the nascent polypeptide as they enter the ER (125–128). ERdj3 is a soluble co-chaperone that is expressed at the highest levels of an ERdjs in normal conditions; it directly binds to misfolded proteins in the ER and deliveries them to BiP (129–131). ERdj4 is another soluble co-chaperone that, on the other hand, is expressed at low levels during normal conditions but is overly expressed under conditions of ER stress (132,133). ERdj4 selects terminally misfolded protein to be delivered to the ERAD machinery (53,134). ERdj4 has also been suggested to facilitate interactions between IRE1 and BiP that control the UPR (chapter 1.3.3) (105). ERdj5, in turn, is responsible for efficient folding and selection of disulphide containing proteins. It has six thioredoxin (Trx) domains, two of which are enzymatically inactive, which is critical for their interaction with proteins by a redox mechanism (135–137) . ERdj6 contains the nine tandemly arranged tetratricopeptide repeat (TPR) motifs aiding in the recruitment of translated polypeptides (53,58,138). Finally, ERdj7 is a widely expressed integral membrane protein and is conserved across kingdoms but roles remain a mystery (53,139,140).

Another class of Hsp70 co-chaperone is nuclear exchange factors (NEFs) aiding in the removal of bound ADP from Hsp70s to allow the binding of fresh ATP. There are two NEFs for BiP: glucose-regulated protein of 170 kDa (Grp170) and Sil1 (55). SIL1 binds to BiP NBD at the cleft at the top surface of the IB and IIB subdomains of the NBD and separates the IIB and IB sub domains to release the ADP (141,142). Grp170 has a different mechanism of action: the C-terminal  $\alpha$ -helical and nucleotide binding domains of Grp170 embraces the NBD of BiP and destabilizes it, enabling ADP release (55,124). While Sil1 is structurally unrelated to the Hsp70 family, Grp170 belongs to the Hsp110 family that share many structural features of conventional Hsp70s. Interestingly, Grp170 possesses chaperone functions itself, and its roles in the ER proteostasis is yet to be understood (143).

#### 1.4.4 The chaperone code

With the consideration that BiP and other Hsp70 can be regulated by even subtle local perturbations such as amino acid substitutions, post-translational modifications (PTM) provide another level of regulation of BiP activity or its specific functions (144,145). There is a wide range of different PTMs (including phosphorylation, acetylation, methylation, SUMOylation, and ubiquitination (table 3)), all occur at a variety of sites and fulfil a multitude of respective roles, which modify molecular chaperones and co-chaperones. This collection of chaperone and co-chaperone specific PTMs are referred to as the chaperone code (144).

*Table 3: the chaperone code. A table summary of known post-translation modification of BiP, estimation on the reported number of sites and known effects to the chaperone (145–156).*

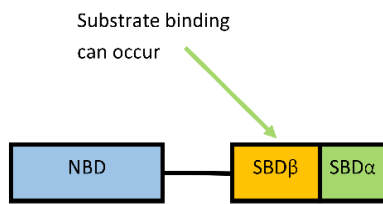
PTM	Modification	Number of sites for BiP	Effect on BiP
Phosphorylation	The addition of a phosphoryl group	~ 50	Transitions BiP into inactive oligomer
Acetylation	The addition of an acetyl group	~ 25	Alters interaction with known co-chaperones
Methylation	The addition of a methyl group	~ 10	Remains poorly understood – suggested role in gene regulation
SUMOylation	SUMO proteins covalently attached	~ 2	Unknown
AMPylation	Adenosine monophosphate molecule covalently attached	Unknown	On off switch – traps protein in domain docked conformation
Ubiquitination	Ubiquitin is attached	~ 20	Target protein for degradation
ADP ribosylation	Transfer of an ADP ribose from NADH onto a target protein	Unknown	Temporary off switch – decreases in time of high protein burden

A good example of the effectiveness of PTMs in the regulation of BiP can be found in the AMPylation of the residue T518. This mechanism is viewed as an on off switch of the protein where AMPylation levels decrease in inverse proportion to unfolded protein levels (149). T518 AMPylation results in the stabilization of the domain docked conformation even in the absence of ATP, locking the protein in the ATPase and substrate binding inactive state (148,154,155). As this does not prevent ATP binding nor the recruitment of J-type co-chaperones, it is thought to trap BiP in the inactive conformation with the protein being able to resume the chaperone activity immediately following its de-AMPylation (149). This is beautiful example of how a simple modification can alter BiP function, with just the addition of an Adenosine monophosphate molecule acting as an on off switch for the chaperone. This is beneficial in BiP regulation because it allows the inactivation of BiP in times of excess of BiP in comparison to client proteins, which can counteract the overacting chaperone activity which can lead to low substrate release that is detrimental to ER function or excess degradation of clients (157–159).

The chaperone code is a critical component of BiP regulation but currently only an estimated 5 % of the identified PTM sites have been characterised (144). As there is undeniable evidence that PTMs play a vital role in the regulation of Hsp70s and BiP, it is critical to boost the understanding of this field in order to greater understand the regulation of the vital chaperone. Currently, 51 phosphomimetic sites have been identified typically through high output proteomic discovery mass spectrometry (160–163), with only a few being confirmed with other techniques. This includes T37 and T229 which were suggested by immunoprecipitation phosphorylation assay combined with mutations of theorised phosphorylation sites (164). This study aims to help elucidate this through characterisation of one type of PTMs, phosphorylation, which have been identified within BiP.

Within BiP, it has been suggested that phosphorylation (no precise site of phosphorylation was identified for this effect) triggers BiP to transition into an inactive oligomer state and reduce substrate binding capabilities (147). Due to the hydrophobic nature of the BiP interdomain linker (IDL), the SBD of one BiP molecule can bind to IDL of another BiP molecule, locking the chaperone in the inactive conformation the (Figure 7), reducing binding to its unfolded protein substrates and, thus, resulting in the decrease of BiP activity (165). The oligomer form BiP adopts was elucidated through bacterial protease (SubA). This is an enzyme which cleaves the IDL of BiP. As the oligomer form displays less cleavage in the presence of ADP (where it would adopt the domain undocked conformation with an exposed cleavable IDL), it implies that the IDL is not exposed. Therefore, it is assumed that the IDL is covered by the binding of a second BiP protein (165).

### Active monomer BiP



### Inactive monomer BiP

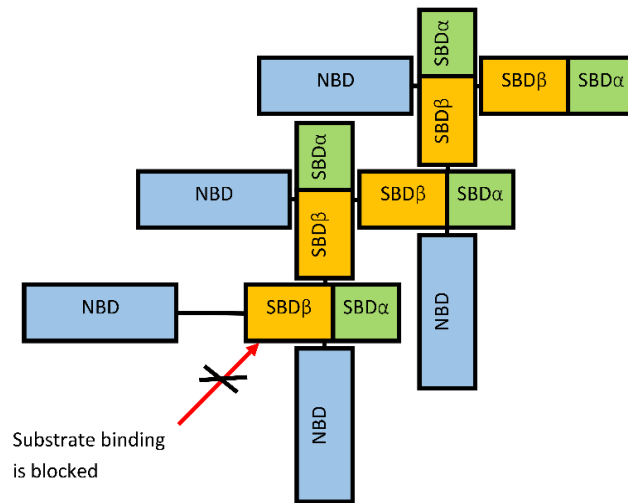


**Figure 7: Deactivation of BiP by oligomerization.** Cartoon depicting the literature theorised oligomer form of BiP (right) (165), which displays the SBD of one BiP molecule bound to the IDL of a second BiP molecule. This process is repeated to form a long chain of BiP. This is alongside the active monomer form of BiP (left) with an SBD that remains free to binding unfolded protein substrate.

While ADP bound WT BiP can form oligomers in the absence of protein substrate, no oligomerization has been observed in the presence ATP (at the normal cell conditions). The fact that phosphorylation of BiP results in its oligomerization in the cellular environment could suggest that phosphorylation results in a shift in the conformation equilibrium toward the domain undocked conformation that has a higher ability to interact with BiP substrates and thus, binding to IDL. However, the exact mechanism is yet to be elucidated.

Interestingly, BiP phosphorylation has also been shown to decrease in the presence of tunicamycin, an antibiotic that triggers ER stress via inhibiting glycosylation of newly synthesis proteins. These findings clearly demonstrate that, in addition to the translational regulation of the BiP expression level (chapter 1.4.1), reversible phosphorylation of BiP plays an important buffering role, triggering BiP to be more inactive in the absence of ER stress and more active in the presence of stress (147,166). Reversible dephosphorylation of BiP provides a quick, real-time response to the ER stress by shifting the BiP pool from its inactive oligomers into the active monomer form.

Another critical role in which PTMs (particularly phosphorylation) regulate Hsp70 activity is via altering how Hsp70s interact with other proteins, particularly co-chaperones and other members of the quality control network (145). For example, the EEVD motif located at the C-terminal of the cytoplasmic Hsp70 interacts with the co-chaperones Hop and CHIP, enabling substrate transfer from Hsp70 to Hsp90. Phosphorylation of Hsp70

T636 and S631 residues located in this region significantly affect HOP and CHIP interactions, interfering with this process (167,168).

The modulation of BiP interactions with other proteins due to phosphorylation has also been demonstrated to be vital in cell cycle progression. The vital control of cellular growth and division in response to signals (e.g. nutrient availability and genome integrity) in control complex interlinked signal transduction pathways (145). For example, Ydj1 regulates the entry of the Cln3 G<sub>1</sub> cyclin into the nucleus (169) through the two proteins competing for the binding by the yeast Hsp70 Ssa1. Ydj1 is favoured by Ssa1 but if Hsp70s T36 is phosphorylated then the chaperone favours the recruitment of Cln3. It is thought that in times of nutrient scarcity, Ssa1 is phosphorylated in order to target Cln3 for destruction and this leads to cell cycle arrest (145).

Both the phosphorylation of Hsp70s in order to effect the HOP/CHIP or the Ydj1/Cln3 interactions demonstrates how phosphorylation can play an important role in the regulation of Hsp70s interactions with client proteins as well as how this alteration can effect the wider molecular pathways associated with these proteins.

## 1.5 study aims.

Growing evidence suggests that Hsp70 phosphorylation events are capable of fine tuning the Hsp70 allosteric cycle as well as altering interactions with co-chaperones and other client proteins. As there is undeniable evidence that PTMs play a vital role in the regulation of Hsp70s and BiP, it is critical to boost the understanding of this field in order to greater understand the how individual PTMs or their combinations (chaperone code) control and fine tune overall BiP chaperone activity and its ER specific functions.

The phosphorylation of BiP is a less well characterised modification than other modifications, with limited knowledge of the potential role or mechanism of phosphorylation being unknown in BiP. Phosphorylation was chosen to be the focus of this study due to the significant role it plays in the regulation of key functions of Hsp70s (discussed in chapter 1.4.4), suggesting that similar to other Hsp70 phosphorylation is likely significant in the regulation of BiP. This study aims to help elucidate the role of ER specific phosphorylation events in BiP on its conformation, allosteric cycle, and functions through a combination of NMR, biophysical and biochemical assessments driven by bioinformatic guided selection of ER specific phosphorylation sites.

1. Using bioinformatic approaches, to identify phosphorylation sites that are unique for the ER specific functions of BiP.
2. Using methyl NMR and biochemistry / biophysical approach, to elucidate how ER specific phosphorylation events affect the BiP's allosteric cycle and its ATPase activity.
3. Using biophysical approaches, to investigate how ER specific phosphorylation events affect BiP's ability to control activation of the ER stress sensor IRE1.

## Chapter 2 – 6: Results

### Chapter 2: Identification of ER unique sequence conservation patterns

The Hsp70 family is a highly conserved family of proteins which shares a highly conserved sequence and displays very similar structure and functions (introduction chapter 1.1, 1.2.1). Despite the similarities, the proteins each are responsible for functions that are specific to their subcellular environment in addition to functions shared between the entire family (1,3,29). Phosphorylation is a well-known mechanism for the regulation of the functions and allosteric cycle of Hsp70s; the understanding of how location specific phosphorylation events fine tune Hsp70 functions could provide long awaited insights into how different Hsp70s are regulated in different conditions.

The initial aim of this study was the development of a bioinformatics driven approach to identify PTM sites in the ER Hsp70 BiP that are responsible for the specific functions or are important for the ER environment. There are around fifty phosphorylation sites that have been identified in BiP (160), with no individual residues being previously characterised to possess functional importance *in vivo* or *in vitro*, the study decided to adopt a comparative amino acids conservation analysis as an approach for the identification of ER specific phosphorylation sites. This approach is based on the assumption that residues that are conserved in all Hsp70s are likely to be vital for functions, structure, or interactions for the entire Hsp70 family and therefore residues that are only conserved in ER located Hsp70s are likely to be important for Hsp70 ER specific functions. This study developed a bioinformatic approach to generate two sequence sets, ER located Hsp70 (Hsp70<sup>ER</sup>) and cytoplasmic located Hsp70s (Hsp70<sup>CT</sup>) and by comparing amino acid conservation patterns of these sets, select phosphorylation sites that are conserved only in ER located Hsp70s.

2.1 Classical vs non-classical Hsp70 displays significant structural and sequence differences.

Hsp70s are highly conserved in all organisms (1), to the point that even the evolutionary distanced bacteria DnaK are about 45 % identical and 60 % similar to human cytoplasmic located HspA1A and the ER located BiP (10,11). Humans possess 13 known Hsp70s (3). The analysis of the human Hsp70s phylogenetic tree (Figure 8) reveals key evolutionary relationships between the human paralogs. There are five closely related cytoplasmic Hsp70 (Figure 8 red), as well as mitochondrial HspA9 (Figure 8 orange) and ER HspA5 (Figure 8 Green) are significantly more distant from this first group but also from each other. Surprisingly, there are four (Figure 8 black) Hsp70s which are distantly related to all other human Hsp70s.

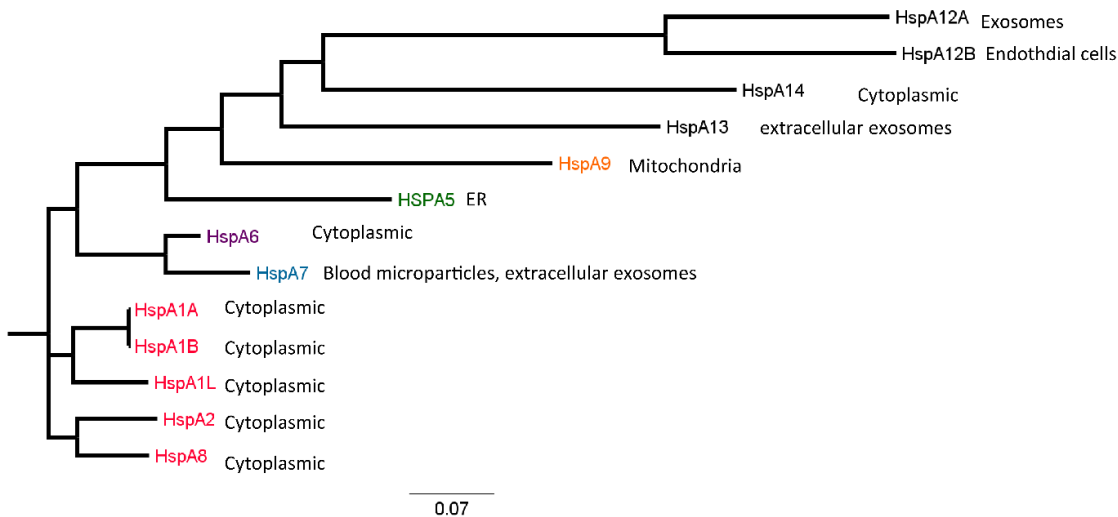


**Figure 8: Human Hsp70 phylogenetic tree.** Phylogenetic tree analysis of 13 Human Hsp70s, sourced from uniprot, carried out with clustal omega online servers (10). The subcellular location of each Hsp70 listed next to gene name. Groups of closely related cytoplasmic (red), a pair of closely related cytoplasmic (purple) / blood particle (blue) Hsp70, ER Hsp70 (green), mitochondrial Hsp70 (orange) and distantly four related Hsp70 (black).

As described in Chapter 1.2.1, the typical Hsp70 consists of a nucleotide binding domain (NBD) connected via an interdomain linker to a substrate binding domain (SBD) which is divided into the SBD $\beta$  (that contains the substrate binding pocket) and SBD $\alpha$  (lid) (Chapter 1.2.1 Figure 1) (1,29). Remarkably, only 8 of the 13 human Hsp70s possess the expected structural layout (Figure 9), with the remaining 5 human Hsp70s (HspA7, HspA13, HspA14, HspA12A and HspA12B) displaying significantly different structural organization. Particularly, whilst all of them have typical NBD structures, only three of them has the SBD $\beta$  and none possess the SBD $\alpha$ . Viewing the overlaid structure of the 8 “classical” Hsp70s displays just how identical the structures are, with NBD and SBD $\beta$  displaying almost no differences between the 8 chaperones. The only significant difference that is visible is located with the SBD $\alpha$ , which despite a similar structure and sequence, do not overlay with each other (Figure 10). This suggests that the SBD is less conserved amongst Hsp70 family members. This alignment of structures displays an RMSD value on average of 3.941 when comparing BiP with the other 7 “classical Hsp70s”, which suggest incredibly similar structures (170).

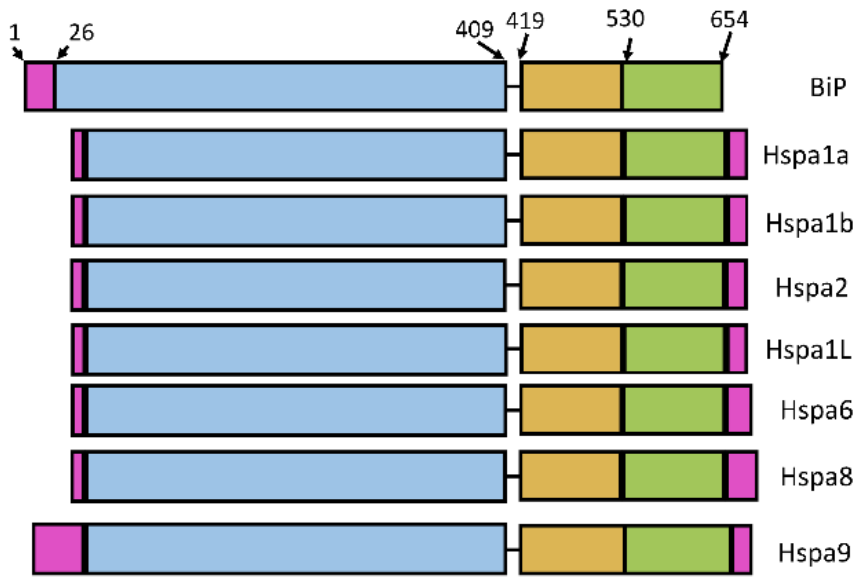
Consequently, the 5 other Hsp70s can be considered as “non-classical Hsp70s” as they share less than 40% sequence identical to other human Hsp70s and have different organization (Figure 9 and 11). As both SBD $\beta$  and SBD $\alpha$  are critical for the Hsp70 cycle and functions (1,29), these five Hsp70s are likely to have very different functions to other ‘classical’ Hsp70s. Four out of the five of the non-classical Hsp70 were the identified distantly related Hsp70s (Figure 8 black). Interestingly despite the identified NBD of these Non-classical being identified as NBDs, when compared to the NBD of BiP only Hspa7 is more than 50 % (55.0 %) identical to BiP NBD. The remaining four are significantly less identical to BiP NBD (Hspa12a - 16.6 %, Hspa12b - 18.1 %, Hspa13 – 34.9

% and Hspa14 – 32.7 %). These low levels of identity between classical and non-classical Hsp70 in the one shared domain further suggests that these are separate protein groups.

There are other examples of non-classical Hsp70s, which includes large Hsp70s such as human nucleotide exchange factors (NEFs) Grp170 and other Hsp110s (54,124). These proteins have an NBD that are similar to other Hsp70s, but their SBD is significantly larger than in the classical Hsp70s (54,55,124). Interestingly, the proteins play an important but distinct role in the chaperone cycle (allosteric cycle and role of NEFs discussed in chapter 1.2.2), where they serve to remove bound ADP from other Hsp70s to allow the fresh binding of ATP. It is possible that these five “non-classical” Hsp70s are similar to NEFs in this regard.

As the study aims to analyse the conservation of classical Hsp70s, the non-classical Hsp70s were removed from the further analysis. The sequence identity for the remaining 8 classical Hsp70s, is more than 50%. It is of note that the sequence identity for all classical cytoplasmic Hsp70s is about 70%, whilst the sequence similarity between non-classical cytoplasmic Hsp70s and either mitochondrial or ER Hsp70s is significantly lower. These findings suggest that organelle specific (cytoplasmic, ER or mitochondrial) Hsp70s are likely to have distinct evolutionary rates, conservation patterns and other sequence features. Full detail of Hsp70s organism, uniprot code and sub-cellular location can be found in chapter 9.10 in table 10.

### Classical Hsp70



### Non-Classical Hsp70

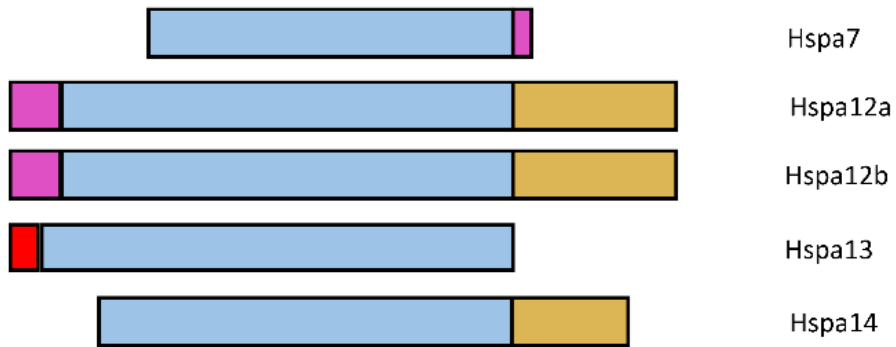


**Figure 9: Domain structures of human Hsp70s.** The domain arrangements of sequences of each of the known human Hsp70 proteins. The arrangement is coloured with NBD (blue), SBD $\beta$  (yellow), SBD $\alpha$  (green),  $\alpha$ -helix red) and unstructured terminal regions (purple). Size of each domain is proportional to size of box representing the domain. The 13 human Hsp70s have been divided into the 8 "classical" and 5 "non-classical" Hsp70s.

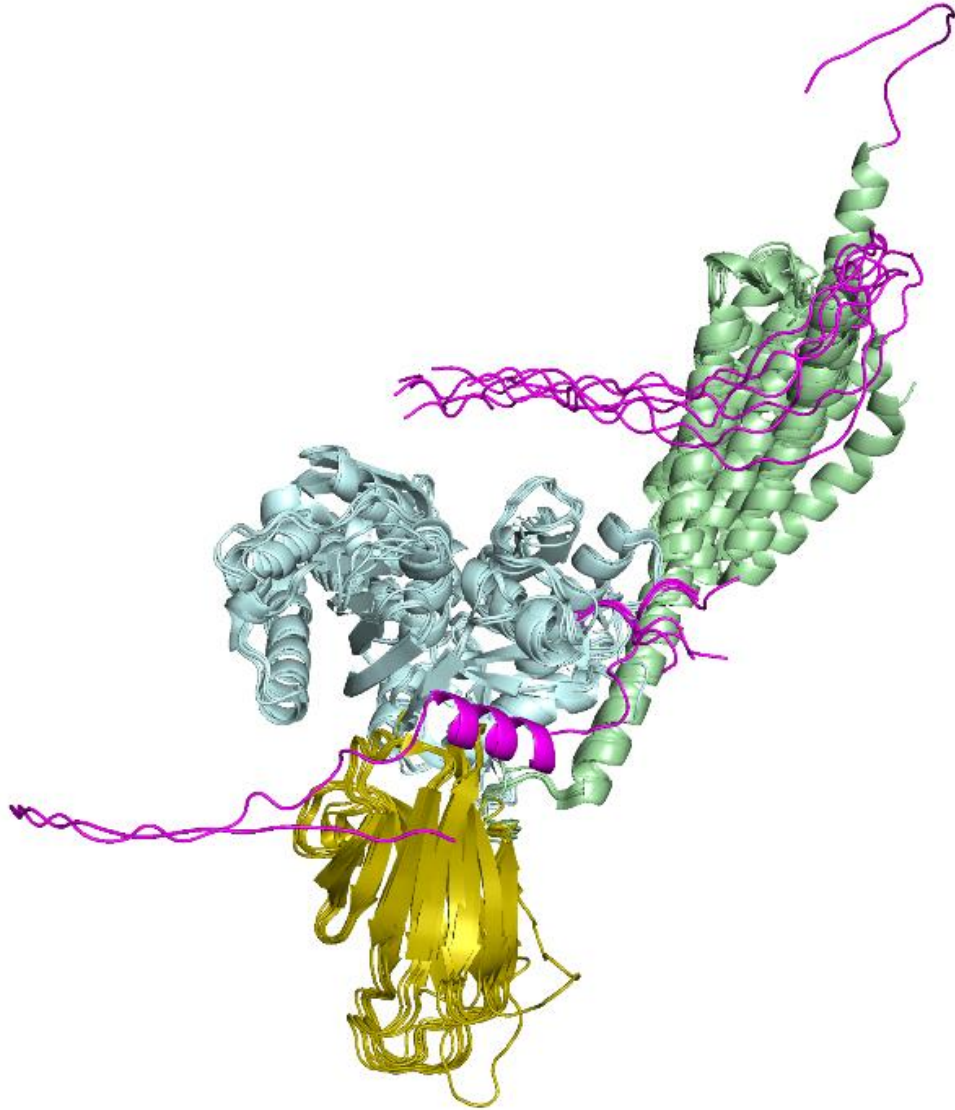


**Figure 10: Shared conformation of classical Hsp70s.** Cartoon overlay of either the crystal structures or alpha fold predicted structures of the 8 classical Hsp70 displaying their near identical structure and conformation. Crystal structures RCSB PDB codes are BiP (5e84), and alpha fold DB code are HspA9 (AF-P38646-F1), HspA1A (AF-P0DMV8-F1), HspA1B (AF-P0DMV9-F1), HspA1L (AF-P34931-F1), HspA2 (AF-P54652-F1), HspA6 (AF-P17066-F1) and HspA8 (AF-P11142-F1). Colour codes for each domain and subdomain are NBD (blue), SBD $\beta$  (yellow), SBD $\alpha$  (green), and unstructured terminal regions (purple).

	ER		Cytoplasmic					Mit		Non-classical				
	A	B	C	D	E	F	G	H	I	J	K	L	M	
A	Green	Orange	Orange	Orange	Orange	Orange	Orange	Orange	Red	Red	Red	Red	Red	
B		Green	Green	Green	Green	Green	Green	Orange	Red	Red	Red	Red	Red	
C			Green	Green	Green	Green	Green	Orange	Red	Red	Red	Red	Red	
D				Green	Green	Green	Green	Orange	Red	Red	Red	Red	Red	
E					Green	Green	Green	Orange	Red	Red	Red	Red	Red	
F						Green	Green	Orange	Red	Red	Red	Red	Red	
G							Green	Orange	Red	Red	Red	Red	Red	
H								Green	Red	Red	Red	Red	Red	
I									Green	Orange	Red	Red	Red	
J										Green	Red	Red	Red	
K											Green	Red	Red	
L												Green	Red	
M													Green	

A = HspA5 B = HspA1A C = HspA1B D = HspA1L E = HspA2 F = HspA8 G = HspA6  
H = HspA9 I = HspA12A J = HspA12B K = HspA13 L = HspA14 M = HspA7

100—70 % identity    70—40 % identity    40—0 % identity

**Figure 11: Human Hsp70 subcellular groups sorted by sequence identity.** A table depicting the level of identity of each human Hsp70 with other human Hsp70s coloured according to key. Sequence identity calculated using stretcher (10). Subcellular location of the sequence displayed above the letter code, mit standing for mitochondria.

## 2.2 Sequence based identification of location specific subfamilies of Hsp70s.

To examine whether it's possible to separate Hsp70 paralogues from orthologues using sequence identity information only; the *Drosophila melanogaster*, *Arabidopsis thaliana*, *Caenorhabditis elegans*, *Saccharomyces cerevisiae* and *Dictyostelium discoideum* Hsp70s were compared to Hsp70 within the same organisms similar to method used for the human Hsp70s (as described in chapter 2.1). As discussed above, any sequence of less than 40 % identity to other Hsp70s were considered to be “non-classical” and thus removed from any future analysis (Figure 12). In all analysed organisms, the high level of conservation was observed between Hsp70s located in the same subcellular location (Figure 12). The majority of the non-classical Hsp70s are located within the cytoplasm except for *Saccharomyces cerevisiae* LHS1 and *Arabidopsis thaliana* Hsp70-17 which are both ER located. Full detail of Hsp70s organism, uniprot code and sub-cellular location can be found in chapter 9.10 in table 10.



***Drosophila melanogaster***

	Cyt						ER	Mit
	A	B	C	D	E	F	G	H
A	Green	Green	Green	Green	Green	Green	Orange	Orange
B	White	Green	Green	Green	Green	Green	Orange	Orange
C	White	White	Green	Green	Green	Green	Orange	Orange
D	White	White	White	Green	Green	Green	Orange	Orange
E	White	White	White	White	Green	Green	Orange	Orange
F	White	White	White	White	White	Green	Orange	Orange
G	White	White	White	White	White	White	Green	Orange
H	White	Green						

- A = Heat shock 70 kDa protein cognate 1      D = Major heat shock 70 kDa protein Ba      G = BiP  
 B = Heat shock 70 kDa protein cognate 2      E = Major heat shock 70 kDa protein Bbb      H = Heat shock 70 kDa protein cognate 5  
 C = Major heat shock 70 kDa protein Aa      F = Heat shock 70 kDa protein cognate 4

***Arabidopsis thaliana***

	ER			Cyt							Chl		Mit		Non		
	A	B	C	D	E	F	G	H	I	J	K	L	M	N	O	P	
A	Green	Green	Green	Orange													
B	Green	Green	Green	Orange													
C	White	Green	Green	Orange													
D	White	White	White	Green													
E	White	White	White	White	Green												
F	White	White	White	White	White	Green											
G	White	White	White	White	White	White	Green										
H	White	White	White	White	White	White	White	Green									
I	White	White	White	White	White	White	White	White	Green								
J	White	White	White	White	White	White	White	White	White	Green							
K	White	White	White	White	White	White	White	White	White	White	Green						
L	White	White	White	White	White	White	White	White	White	White	White	Green	Green	Green	Green	Green	Green
M	White	White	White	White	White	White	White	White	White	White	White	White	Green	Green	Green	Green	Green
N	White	White	White	White	White	White	White	White	White	White	White	White	White	White	Green	Green	Green
O	White	White	White	White	White	White	White	White	White	White	White	White	White	White	White	White	Green
P	White	White	White	White	White	White	White	White	White	White	White	White	White	White	White	White	White

- A = BiP-1      G = Hsp70-4      M = Hsp70-10  
 B = BiP-2      H = Hsp70-5      N = Hsp70-15  
 C = BiP-3      I = Hsp70-18      O = Hsp70-17  
 D = Hsp70-1      J = Hsp70-6      P = Hsp70-8  
 E = Hsp70-2      K = Hsp70-7  
 F = Hsp70-3      L = Hsp70-9

100—70 % identity    70—40 % identity    40—0 % identity

**Figure 12: additional organism Hsp70 subcellular groups sorted by sequence identity.** A table depicting the level of identity of each Hsp70 with other Hsp70s of the same organism coloured according to key. Subcellular location of the sequence displayed above the letter code, mit standing for mitochondria, cyt for cytoplasmic, non for non-classical and chl for chloroplast. Sequence identity calculated using stretcher (10).

Next, the average identity percentage of cytoplasmic vs ER Hsp70s of the same organism, ER vs cytoplasmic Hsp70 of the same organism and all ER vs ER Hsp70, were plotted to identify the paralogue/orthologue cut-off point. This displayed that ER located Hsp70s are around 67 % identical to each other but only around 58 % identical to cytoplasmic Hsp70s on average across all organisms analysed (Figure 13). This was calculated by determining the highest average sequence identity in which the ER and cytoplasmic were identical. In this case, Human Hsp70 was the most identical (on average 58 % identically between ER located BiP and the cytoplasmic Hsp70). Consequently, the 65% paralogue/orthologue cut-off was chosen for the following analysis to enable sequence-based separation between the ER and cytoplasm located Hsp70s.

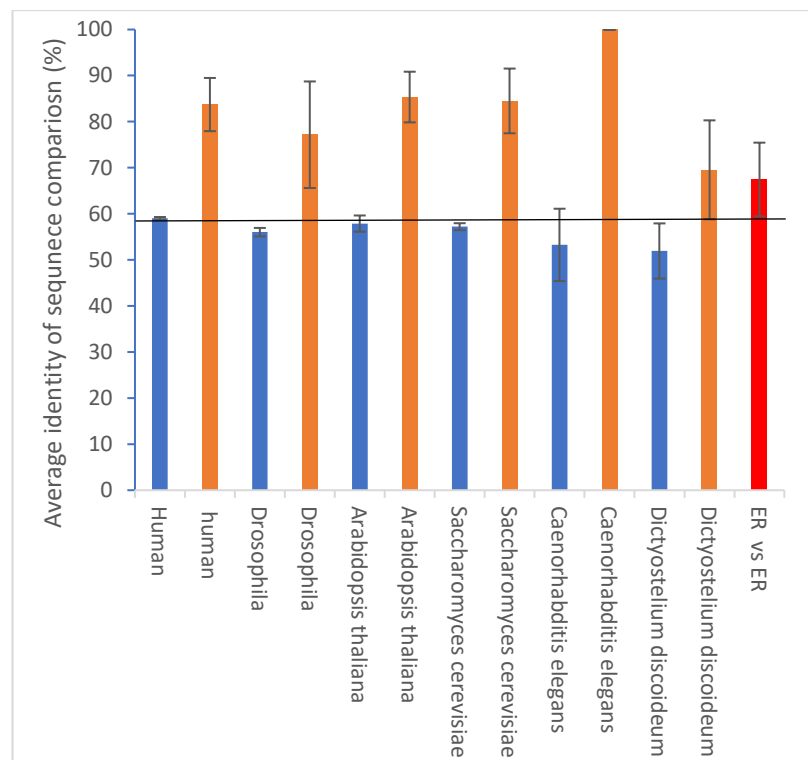


**Figure 13: average shared identity of Hsp70 sequences.** A bar chart depicting the average identity between Hsp70s located in different sub-cellular locations for all organisms studied. This includes average identity between all cytoplasmic located hsp70s (orange), average identity between the ER located Hsp70s within an organism vs the cytoplasmic located Hsp70s within an organism (blue) and the average identity between all classical ER located Hsp70s. Sequence identity calculated using stretcher by comparing 2 hsp70s at a time, then a mean average of every pair within a group being calculated.

Using this cut-off point, two sets of sets of Hsp70<sup>ER</sup> and Hsp70<sup>Cyt</sup> were selected by the ConSurf server (171–173) that selected homologue sequences. The identified orthologue/paralogue cut-off of 65% was used as the minimum identity percentage to generate two sets of Hsp70 homologous sequences: Hsp70<sup>ER</sup> and Hsp70<sup>Cyt</sup> (details of sequences selection in methods 9.10). Selected sequences were then manually checked using information available on the UniProt website (11), serving to remove sequences which were known to be of the incorrect subcellular location or either 20 % larger or

smaller than the average Hsp70 (in total, 12 sequences out of the 268 of the Hsp70<sup>ER</sup> and 25 of the 572 of the Hsp70<sup>Cyt</sup> were removed at this step). The final Hsp70<sup>ER</sup> and Hsp70<sup>Cyt</sup> sets contain 256 and 547 homologous sequences, respectively, with the relative proportions of Hsp70 members from the Animal, Plant and Protista kingdoms being similar in Hsp70<sup>ER</sup> and Hsp70<sup>Cyt</sup> sets (Figure 14). There is a relative smaller proportion of fungus Hsp70s in the cytoplasmic set compared to the ER set, which is likely due to a smaller number of Hsp70 cytoplasmic paralogs for fungus compared to other kingdoms.

Additionally, as the Hsp70 from closely related organisms were shown to be evolutionary closer to each other than from Hsp70 from organism more distantly related, it can be assumed that these proteins are all of the same family. Furthermore, a random selection of Hsp70s from both sets were compared to either BiP (HSP70<sup>ER</sup>) or HspA1A (HSP70<sup>ER</sup>) and shown to be at least as identical as the expected homologue/paralogue cut-off (Figure 14).

Consequently, these results clearly demonstrated that this approach that was based on different, organelle specific evolutionary rates in the Hsp70 family, was able to separate Hsp70 paralogues from orthologues using sequence identity information only and successfully generate two sets of sequences of Hsp70s, ER located Hsp70s (Hsp70<sup>ER</sup>) and cytoplasmic located Hsp70s (Hsp70<sup>Cyt</sup>) enabling analysis of conservation of residues through ConSurf and Weblogo (171–174).

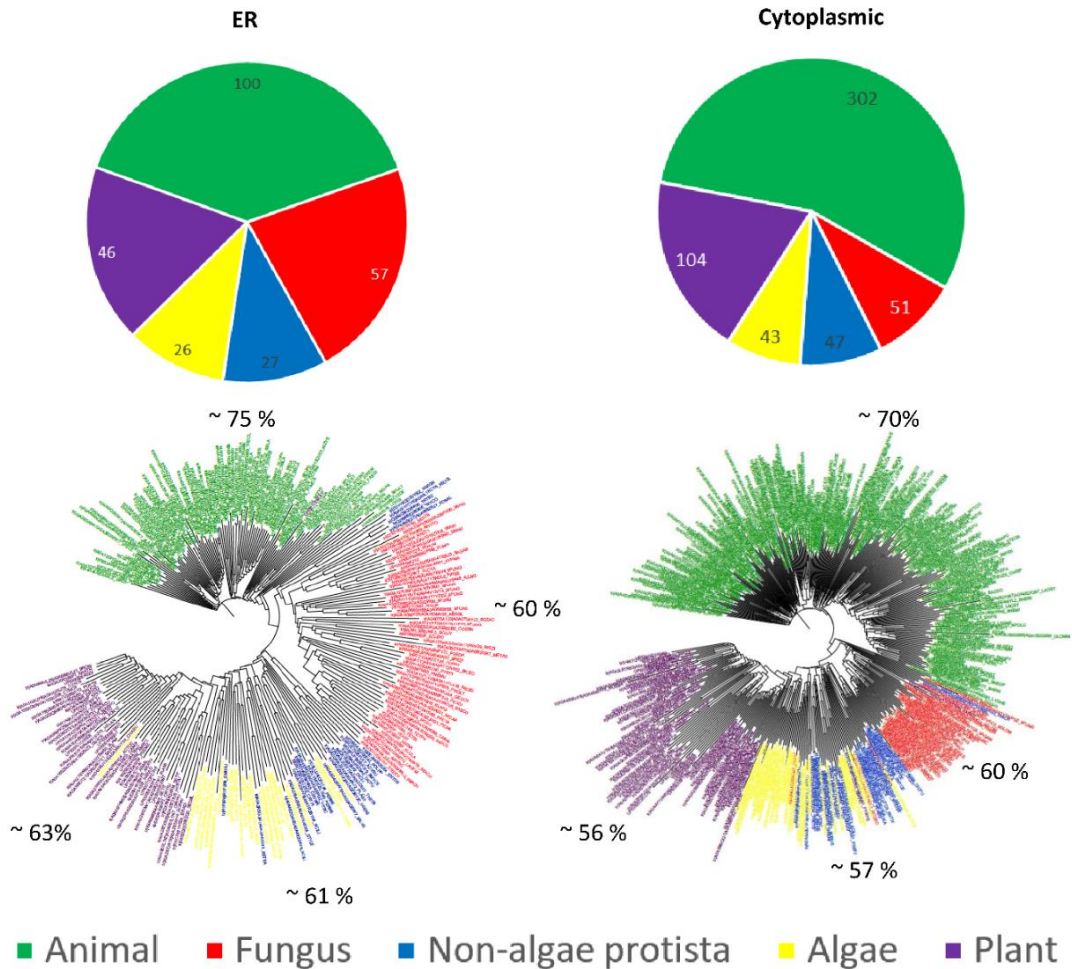


**Figure 14: Summary of sequences in each sequence set.** Pie chart depicting the number of sequences in each organism group for both ER and cytoplasmic Hsp70 sequence sets. Corresponding Phylogenetic trees for each sequence set generated using clustal omega (10) displayed below each chart with matching colour scheme. Random sequences from each set were selected and sequence identity to either BiP (ER) and HspA1A (cytoplasmic) were calculated to ensure the sequences were in the range of the paralogue/orthologue cut-off point. identity values displayed around the phylogenetic trees.

### 2.3 SBD $\beta$ and NBD domains are the most conserved parts of Hsp70s.

In agreement with previous observations (40), our analysis revealed that the NBD is significantly more conserved than the SBD in both Hsp70<sup>ER</sup> and Hsp<sup>cyt</sup> sets (Figure 15). As expected, the majority of conserved residues are located in the central part of NBD near the nucleotide binding site, responsible for nucleotide binding and ATP hydrolysis (figure 16). Key regions that are associated with key functions of the family are likely to be highly conserved within the protein family.

When the SBD $\beta$  and SBD $\alpha$  were considered separately, the analysis reveals that these two subdomains have drastically different conservation. Surprisingly, the SBD $\beta$  has even a higher level of conservation than the NBD, whilst the SBD $\alpha$  has a significantly lower conservation than the NBD and SBD $\beta$  (Figure 15). This highlights the key role of SBD $\beta$  for

Hsp70 function (particularly, substrate binding) and allosteric communication with NBD (39,42). In SBD $\alpha$  the majority of conserved residues located near the SBD $\beta$  SBD $\alpha$  contact interface which are observed in the domain undocked conformation highlighting the importance of this interface for Hsp70 function and conformation (Figure 16). Indeed, the conservation for these residues is likely due to their roles in the regulation of substrate binding and communication with SBD $\beta$  (175,176)

Fascinatingly, while the majority of conserved residues overlap between Hsp70<sup>ER</sup> and Hsp70<sup>cyt</sup> sets, there are some unique conservation sites in each set (shown in red and green colours in Figure 15). This suggests that the overall conservation patterns of the cytoplasmic and ER Hsp70s are similar due to the shared chaperone functions, structure, and conformations of the family. This is further shown with the limited number of residues where different amino acids are highly conserved in both sequences sets (figure 15 coloured orange). However, some conserved sites are location specific, suggesting their roles in organelle specific functions or environmental features of either Hsp70<sup>ER</sup> or Hsp70<sup>cyt</sup>. In the next chapter, these location specific conservation patterns will be discussed in detail.

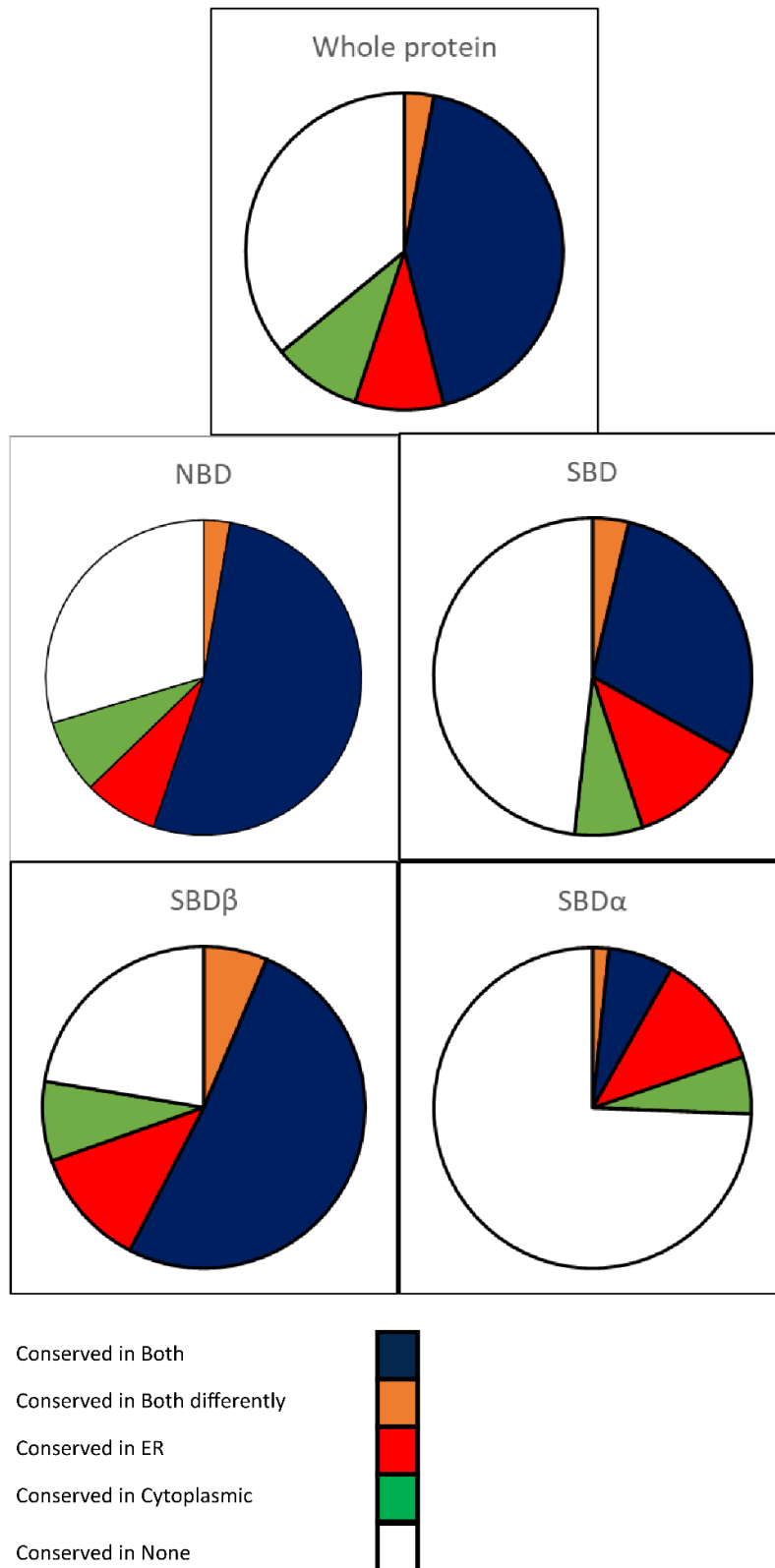


**Figure 15: Hsp70 and ER Hsp70 unique conservation of BiP proportions.** Pie chart depicting the portion of residues of BiP that are either conserved in all Hsp70s (blue), ER Hsp70s (red), cytoplasmic Hsp70 (green), conserved in both but with different amino acids (orange) or not conserved (white) for the entire protein or domains/subdomains.

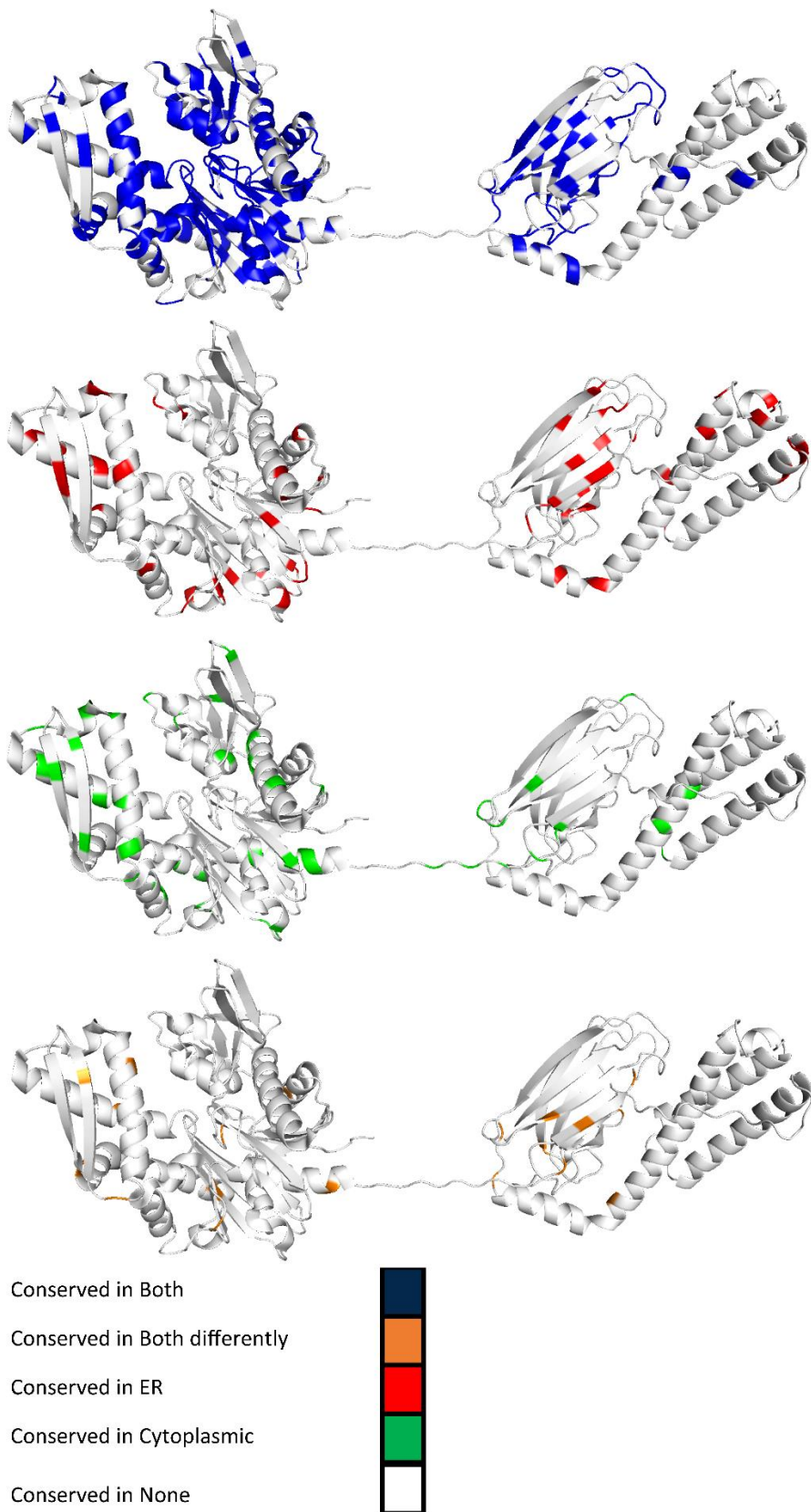


**Figure 16: Hsp70 and ER Hsp70 unique conservation of BiP on structure.** Cartoon showing the domain undocked BiP structure (PBD codes used are 58E5, 6HA7) coloured either to highlight Hsp70 conservation (Blue), ER unique conservation (red), conserved in both but with different amino acids (orange) or cytoplasmic unique conservation (green).

## 2.4 ER unique conservation patterns in Hsp70s

By comparing the conservation patterns of Hsp70<sup>ER</sup> and Hsp70<sup>cyt</sup> sets, the study identified residues that have ER unique and cytoplasmic unique conservation. Importantly, at least some of these organelle specific conservation regions (discussed below) overlap with previously characterized functional and allosteric sites of BiP.

One such region is located near the substrate binding site in the SBD. The substrate binding site comprises the residues that are directly involved in interaction with substrate (defined as 425-434) and residues that facilitate substrate binding and release. The last group includes those which have been suggested to form hydrophobic contacts with bound substrates (R492 and Y570) and residues that are important for interactions between SBD $\beta$  and SBD $\alpha$  and provide access to the substrate binding cleft (Figure 6, chapter 1.4.2) (31,58). This region is vital for the majority of Hsp70s functions, and therefore not surprisingly, the entire region is highly conserved in all Hsp70s. However, there are four residues located in this region that are uniquely conserved in the Hsp70<sup>ER</sup> set (Table 4 and Figure 17). Two of these residues (I426 and S452) have only minor variations between the ER and cytoplasmic sets (I426 is substituted by L and S452 by T in the majority of cytoplasmic Hsp70s), suggesting their minimal significance. The remaining two variations of V429 to A and Y570 to F are likely to have more significantly different effects on chaperone conformation and function. This is speculated to be due to V429 variations already from the M in DnaK that are already known to alter substrate binding affinity (31,123) (chapter 1.4.2), and therefore it is likely the substantial change of Y570 is likely to alter key BiP functions as well.

Intriguingly, the majority of ER Hsp70s (except fungus Hsp70<sup>ER</sup>) have valine in position 229; fungus Hsp70<sup>ER</sup> has threonine and the majority of Hsp70s<sup>cyt</sup> has alanine. This is a previously identified site uniquely conserved in ER Hsp70 with functional significance in substrate binding kinetics (chapter 1.4.2). The fact that our analysis has successfully identified this region based on sequence information alone provides a proof of principles for the bioinformatic approach, demonstrating that it enables the identification of ER unique amino acid positions in the chaperones that are responsible for ER related functions and environment. This increased the confidence of the accuracy of the prediction of the non-characterised sites identified. Full ConSurf analysis displayed in appendix (appendix Figure 1 and 2).

**Table 4: conservation of substrate binding site.** Table depicting the residues of BiP for key regions of the substrate binding interface with corresponding residue cytoplasmic Hsp70 HspA1A and Consurf score (171–173) (out of 9) for each residue with a score of 7 or higher being considered conserved.

Residue number in BiP	ER residue	Consurf score ER	Cytoplasmic residue	Consurf score cytoplasmic	Conservation class
425	G	9	G	9	BOTH
426	I	9	L	6	ER
427	E	9	E	9	BOTH
428	T	9	T	9	BOTH
429	V	7	A	7	Different
430	G	9	G	9	BOTH
431	G	9	G	8	BOTH
432	V	9	V	7	BOTH
433	M	9	M	9	BOTH
434	T	8	T	7	BOTH
461	V	9	V	8	BOTH
463	I	9	I	8	BOTH
451	F	9	F	9	BOTH
452	S	8	T	7	Different
492	R	9	R	9	BOTH
570	Y	7	F	3	ER

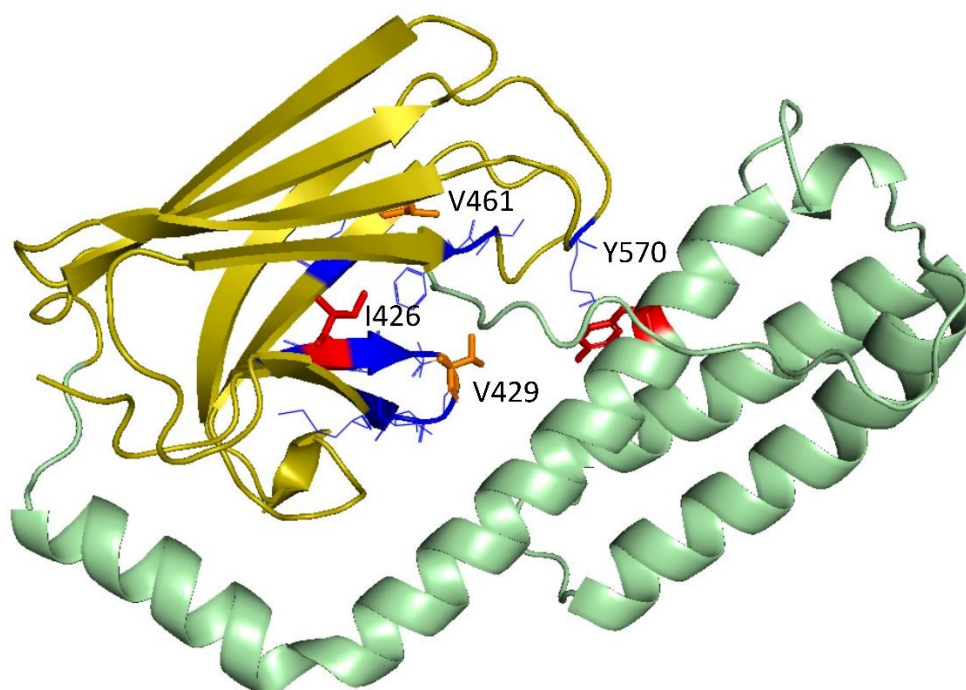


**Figure 17: conservation of substrate binding site.** Crystal structure (PDB code 58E5) of BiP SBD colour coded with SBDβ (yellow) and SBDα (green). The conservation of substrate binding regions is colour coded based on conservation, with residues conserved in either all Hsp70 (blue), both differently (orange) or ER located Hsp70 (Red).

Another region with the ER unique conservation pattern is located near the nucleotide binding site. The analysis of five previously identified ATP contact points (G36-T39, K96, G227-T229 and G364-R367) (177), displayed that residues were conserved in all Hsp70s, highlighting the importance of this region for Hsp70 functions. However, the conservation rates of K294 (R in cytoplasmic set) and the non-conserved A298 (conserved T in cytoplasmic) varied between the ER and cytoplasmic Hsp70 sets (table 5 and Figure 18). Interestingly, both residues are located in the  $\alpha$ -helix that forms an interface between lobe I and lobe II of the NBD (Figure 1) that controls conformational changes in NBD. The nucleotide is known to bind to the bottom of the interface between subdomains IB and IIB (section of lobe 1 and 2), it has been suggested that nucleotide-dependent conformational changes due to subdomain reorientations are crucial to NBD functions (178), and therefore this variation may alter the reorientation. Consequently, location specific variations in this region can be used to fine tune the chaperone allosteric cycle for location specific activities. Full Consurf analysis displayed in appendix (appendix Figure 1 and 2).

*Table 5: conservation of nucleotide binding site. Table depicting the residues of BiP for key regions of the nucleotide binding interface with corresponding residue cytoplasmic Hsp70 HspA1A and Consurf score (out of 9) for each residue with 7 or higher being considered conserved.*

Residue number in BiP	ER residue	Consurf score ER	Cytoplasmic residue	Consurf score cytoplasmic	Conservation class
36	G	9	G	9	BOTH
37	T	9	T	9	BOTH
38	T	9	T	9	BOTH
39	Y	9	Y	8	BOTH
96	K	9	K	9	BOTH
227	G	9	G	9	BOTH
228	G	9	G	9	BOTH
229	T	9	T	9	BOTH
293	E	9	E	9	BOTH
294	K	8	R	8	Different
295	A	9	A	9	BOTH
296	K	9	K	9	BOTH
297	R	9	R	9	BOTH
298	A	4	T	7	CYTO
299	L	9	L	9	BOTH
300	S	9	S	9	BOTH

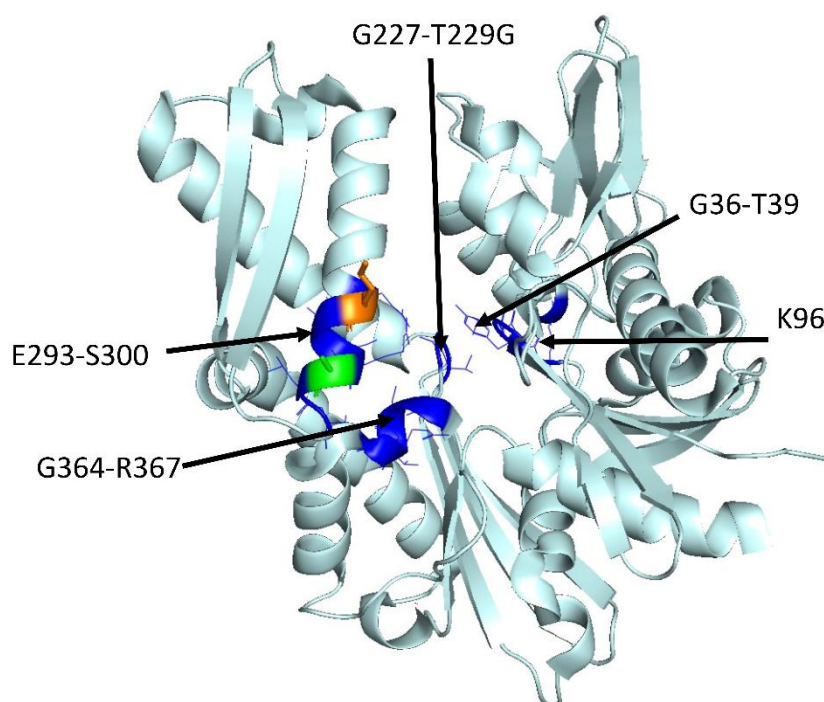


**Figure 18: conservation of nucleotide binding site.** Crystal structure (PDB code 6HA7) of BiP NBD. The conservation of nucleotide binding regions is colour coded based on conservation calculated by ConSurf (171–173) with residues conserved in either all Hsp70 (blue), cytoplasmic located Hsp70 (green) (A298) or conserved in both but differently conserved between ER and cytoplasmic located Hsp70s (E293) (orange).

Taken together, our analysis revealed ER unique conservation sites (table 4, 5 and Figure 17, 18) and thus, can potentially guide experimental research that would lead to better understanding of how specific Hsp70 functions can be regulated by evolution but also by posttranslational perturbations in these uniquely conserved regions. This project focused on the characterization of ER unique phosphorylation sites to elucidate their importance for BiP functions and activity.

## 2.5 Identification of ER unique phosphorylation sites

There are 51 and 37 potential phosphorylation sites in BiP and HspA1A respectively, with more NBD sites being located within the NBD than the SBD (28/51 and 24/37 in NBD for BiP and HspA1A) (Figure 19) (160). Based on the conservation analysis of Hsp70<sup>cyt</sup> and Hsp70<sup>ER</sup> sets 51 % (26 sites) of these phosphorylation sites are conserved in both cytoplasmic and ER sets, no conservation in either set was found for 39% (20 sites) of sites, 2% (1 site) is only conserved in cytoplasmic Hsp70s and 8% (4 sites) is only conserved in ER Hsp70s (Table 6). Particularly, the ER unique sites are the NBD located T69 and S319 and the SBD located T460 and Y570 as well as the single cytoplasmic unique S567 (table 6 and Figure 20). Full phosphorylation analysis displayed in appendix (appendix Figure 5) with complete Weblogo analysis (appendix Figure 3 and 4).

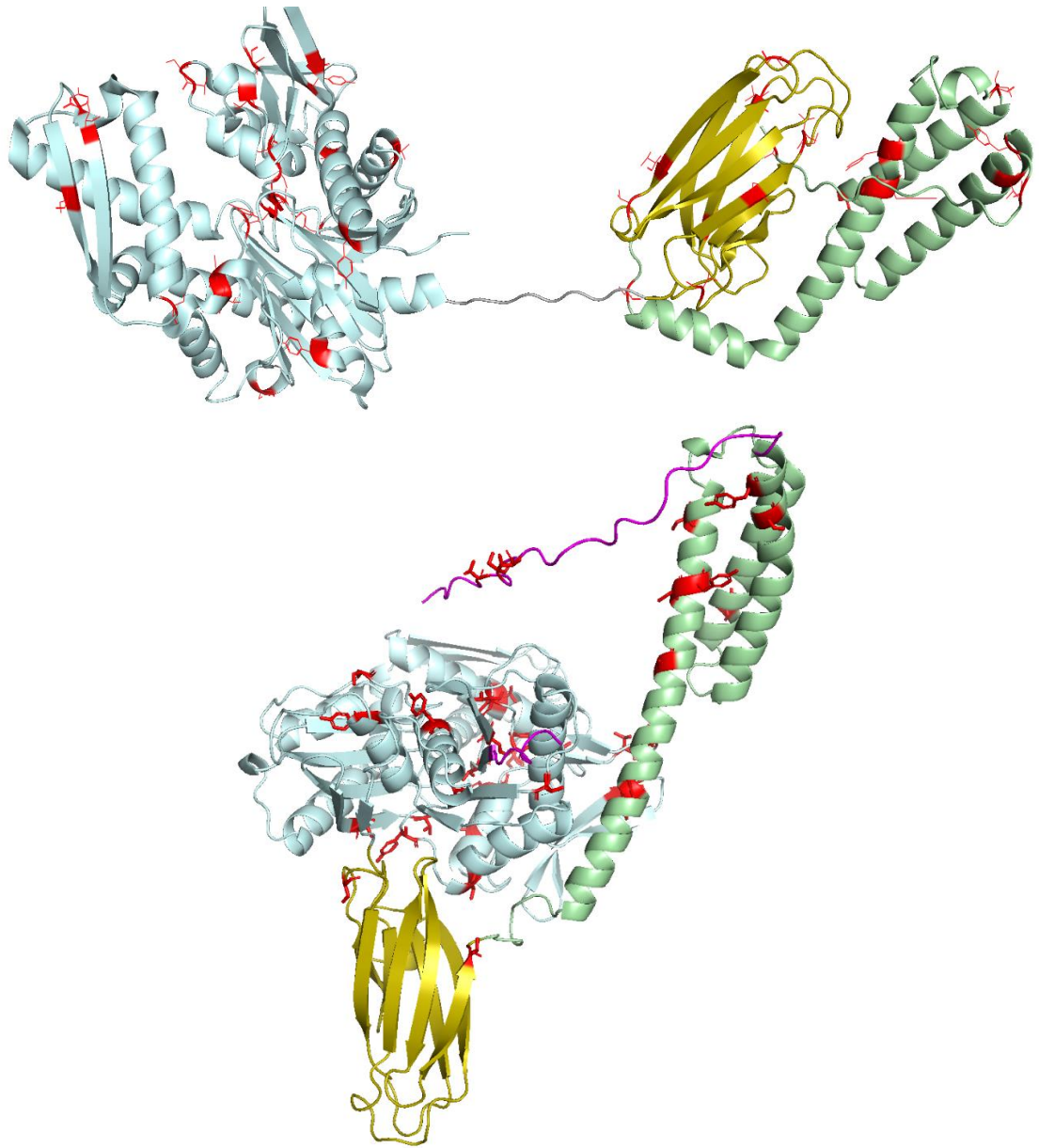


**Figure 19: location of known phosphorylation sites.** Top - Crystal structure of BiP in the presence of ADP (PDB codes are 58E5, 6HA7). Bottom - alpha fold predicted structures of HspA1A (alpha fold DB code is AF-PODMV8-F1). Colour codes for each domain and subdomain are NBD (blue), SBD $\beta$  (yellow), SBD $\alpha$  (green), displaying the proteins and unstructured terminal regions (purple). Phosphorylation sites are shown as red lines.

**Table 6: conservation of phosphorylation site.** Table depicting the residues of BiP for key regions of the phosphorylation sites with corresponding residue cytoplasmic Hsp70 HspA1A and Weblago score (174)(out of 4) score for each residue with 2.5 being considered conserved. Red highlighted signifies conserved residues.

	ER metazoa	ER fungus	ER viridiplantae	ER SAR	Cyt metazoa	Cyt fungus	Cyt viridiplantae	Cyt SAR
<b>T65</b>	T 3.5	T 3	T 4	T 1	T 3	T 2	T 2	T 2
<b>S319</b>	S 3.5	S 3.5	S 4	S 2.5	S 1.5	S 4	T 1.5	T 1
<b>T460</b>	T 3.5	T 2.5	T 3	A 1	G 2	G 3.5	G 1	G 3.5
<b>Y570</b>	Y 3.5	Y 1.5	Y 3.5	Y 1.5	F 3	Y 2	Y 2.5	F 1

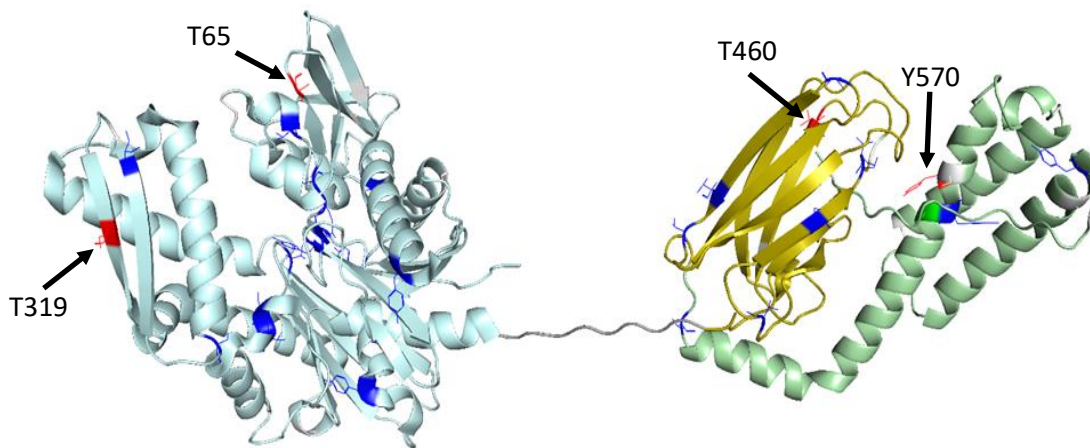


**Figure 20: conservation of potential phosphorylation sites.** Cartoon representing the crystal structure (PDB code 5e85 and 6HA7) of BiP in domain undocked conformation coloured coded with NBD (blue) SBDβ (yellow) and SBDα (green). The conservation of phosphorylation sites is colour coded based on conservation, with residues conserved in either all Hsp70 (blue, cytoplasmic located Hsp70 (green) or ER located Hsp70 (Red) or none (white).

The next step of this study was focused on the experimental characterization of two ER unique PTM sites located in SBD, T460 and Y570. These two residues were mutated into aspartic acid to introduce a phosphomimetic substitution that mimics the charge and size of the phosphate group, allowing characterization of how phosphorylation in these positions affect the chaperone function and conformation. To perform this analysis, the recombinant proteins were expressed and purified from bacterial cells (methods 9.2 and 9.3), followed by characterization of their conformational landscape using methyl NMR (methods 9.7) and functions such as ATPase hydrolysis (methods 9.8) and ability to deoligomerize BiP natural substrate IRE1 (methods 9.9).

## Chapter 3: Protein construct design and production

### 3.1 Protein constructs

The study used three variants of human BiP wildtype (WT), T460D and Y570D. An N-terminal His-Tag followed by TEV cleavage sites was used to enhance protein purification (full details in method section 9.2, 9.3 and 9.4). In addition to the wildtype and mutants, an ATP deficient variant of all BiP constructs containing a T229G mutation will be produced. This substitution serves to limit the chaperones ATP hydrolysis activity, slowing its transition through the allosteric cycle and therefore “trapping” the protein in the ATP bound state without altering the conformational landscape of BiP (46). This allows BiP to be analysed in its ATP bound state without transitioning to the ADP bound state during NMR measurements (discussed in chapter 4, 5 and 6) where the ATP needs to be stable for ~3 hours.

To characterize BiP, interactions with the ER stress sensor IRE1, N-terminal His-Tagged IRE1 luminal domain (IRE1-LD) (full details in method section 9.2) and its two variants, <sup>315</sup>LL<sup>316</sup> to DA and <sup>359</sup>WLLI<sup>362</sup> to GSSG were used (mutants discussed in chapter 5.2).

### 3.2 All constructs were capable of being expressed and purified.

The initial stage was to verify the ability to express the new human BiP constructs. Small scale expression assessment was used to assess the ability of the constructs to be expressed. All constructed were capable of being expressed and were soluble, which was shown by the large bands in the induced and soluble fractions at the predicted 70 kDa size (Figure 21). This confirms that the constructs designed were suitable to be produced within the laboratory for characterisation.

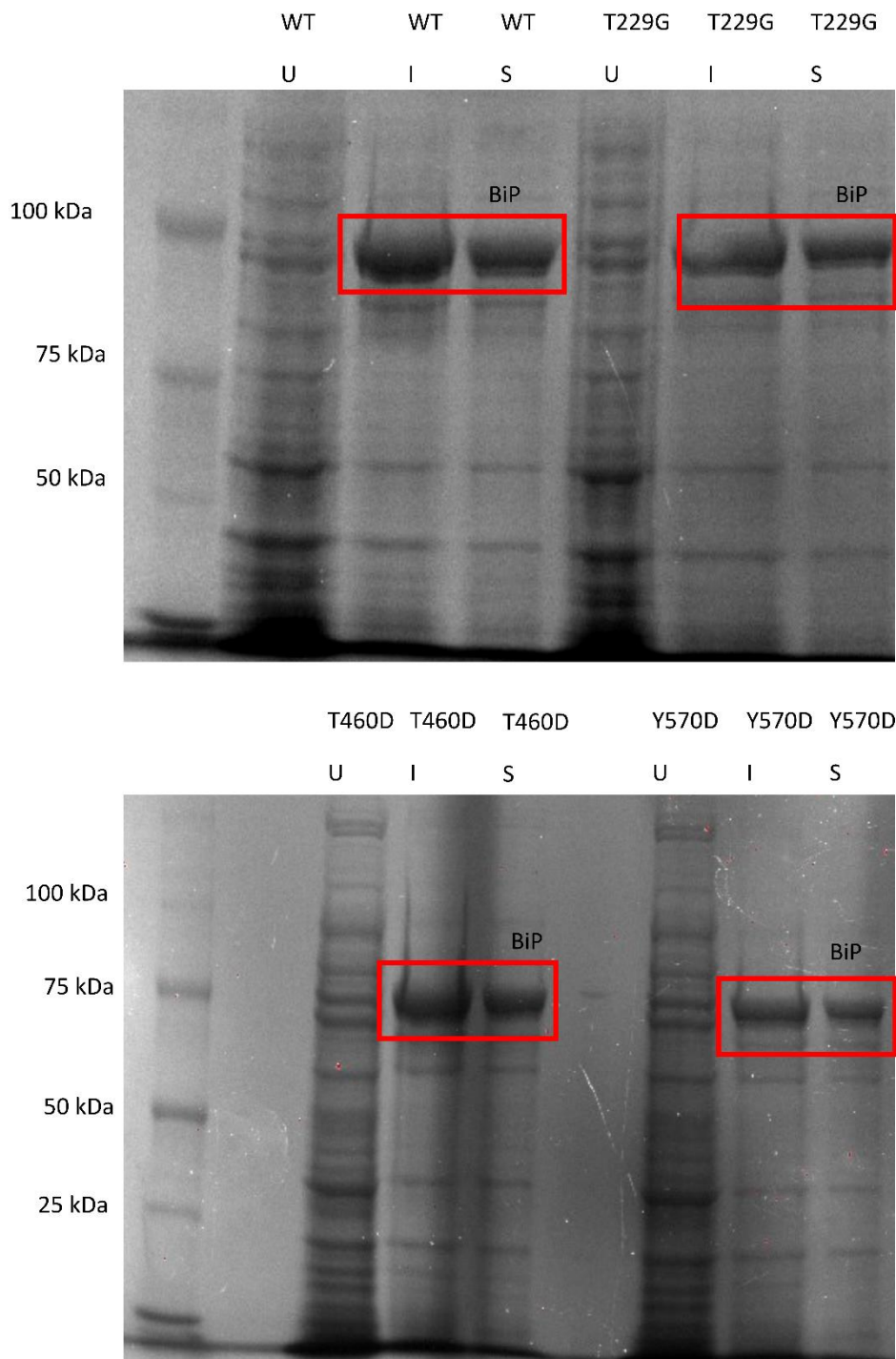


**Figure 21: Small scale expression of BiP constructs.** SDS-PAGE gels depicting the small-scale expression fractions of the uninduced cells (U), the induced cells (I) and the soluble protein (S) of each cell for the BiP WT, T229G, T460D and Y570D constructs. All gels were run on a 7.5 % SDS-PAGE gel and stained with Coomassie blue stains.

All proteins were successfully expressed at a large scale and purified by a single step immobilized metal affinity chromatograph (IMAC) (see methods 9.2) (Figure 22) as previously described in a previous study (46), producing an average of 40 - 80 mg of protein per litre of culture for BiP constructs and 20 - 30 mg per litre of culture for IRE1-

LD constructs. IRE1-LD is expected to be 49.62 kDa but will appear to be larger on the gel due to the globular structure of the protein (179) affecting how the protein runs on the gel by causing it to run more slowly (180). SDS-PAGE analysis was used to determine that the BiP and IRE1 were ~ 80-90 % pure (Figure 23), which is sufficient for all NMR and biochemical assays performed here.

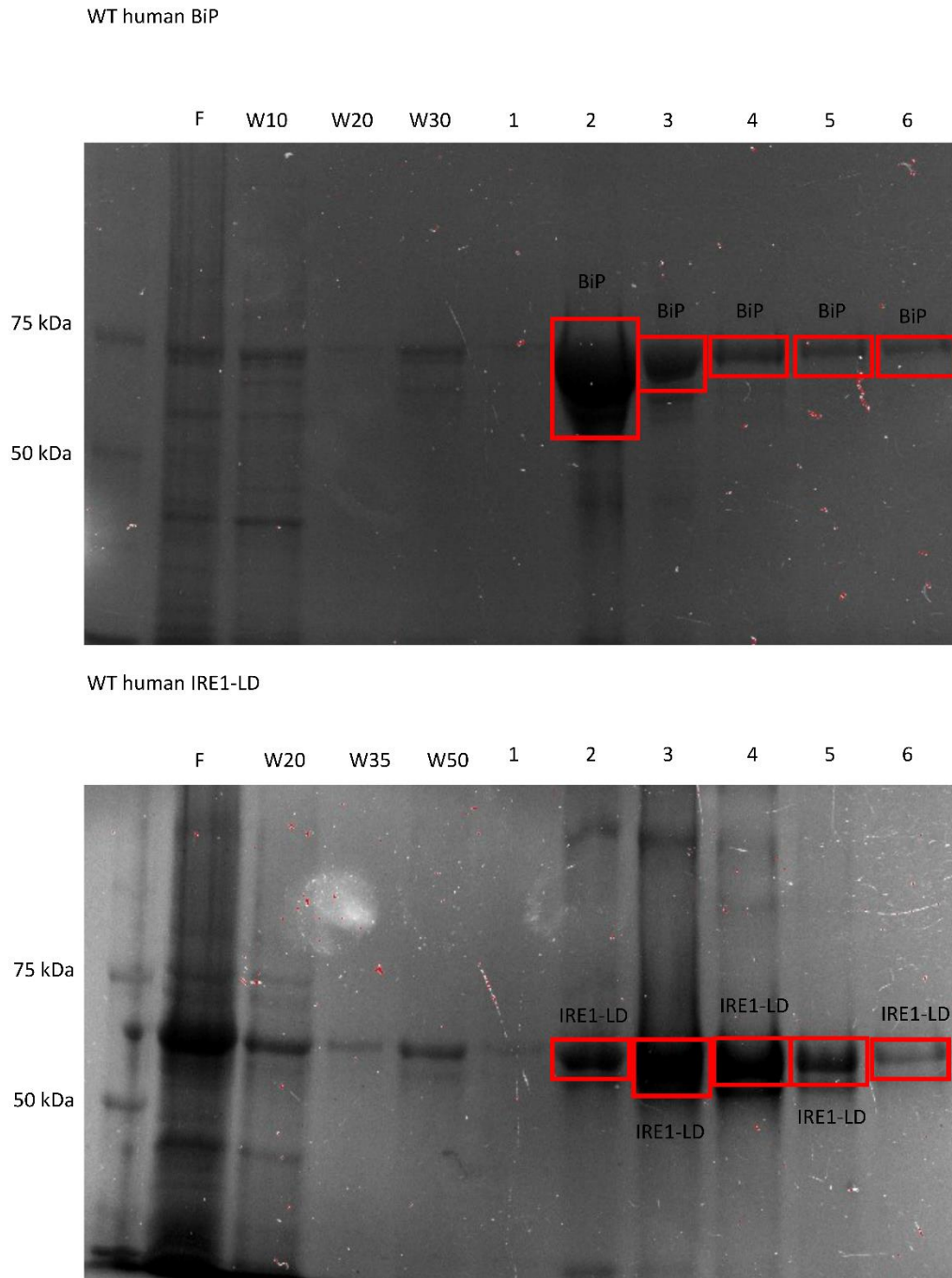


**Figure 22: Purification of BiP and IRE1.** SDS-PAGE gels displaying the purification of the BiP WT (Top) and IRE1-LD WT (bottom). Sample consisting of; flow through (F), 3 imidazole washes at 10, 20 (W10, W20 and W30) and 30 mM or 20-, 35- and 50-mM concentrations (W20, W35 and W50) and 6 elution fractions (1,2,3,4,5 and 6) (500 mM imidazole), were run on a 7.5 % SDS-PAGE gel and stained with Coomassie blue stains.

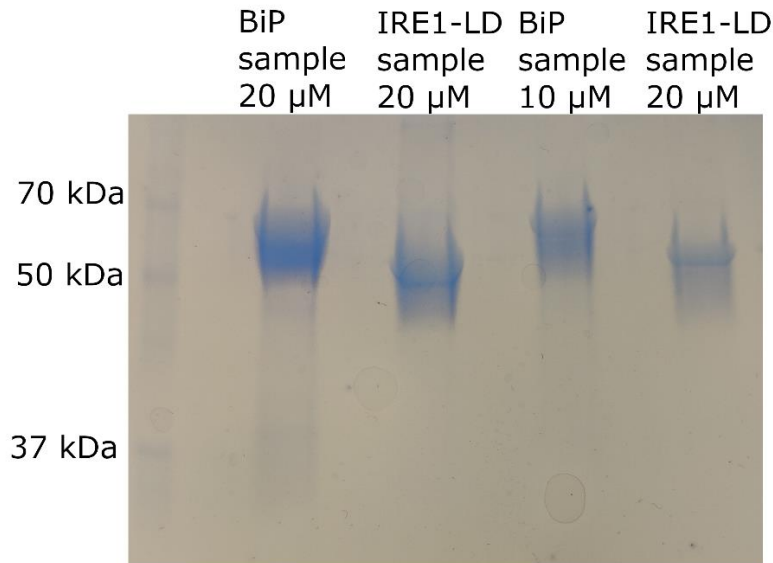


**Figure 23: Purity of BiP and IRE1.** SDS-PAGE gel depicting the pure sample of BiP WT and IRE1-LD WT at either 20 or 10  $\mu$ M protein concentrations. All gels were run on a 7.5 % SDS-page gel and stained with Coomassie blue stains.

### 3.3 BiP construct optimization

To remove the His-Tag that can potentially interfere with BiP conformation and function, the TEV cleavage was achieved by incubating BiP with TEV at a 10:1 ratio for 18 hours at 4°C, resulting in nearly 100% cleavage as confirmed by SDS-PAGE. TEV and any uncleaved BiP were then removed by an additional IMAC step (see Methods chapter 9.2). It is expected that BiP uncleaved will be 71.62 kDa and cleaved BiP is expected to be 69.52 kDa, which is what was displayed by the mass spec data, confirming the successful cleavage of the his-tag (figure 24).

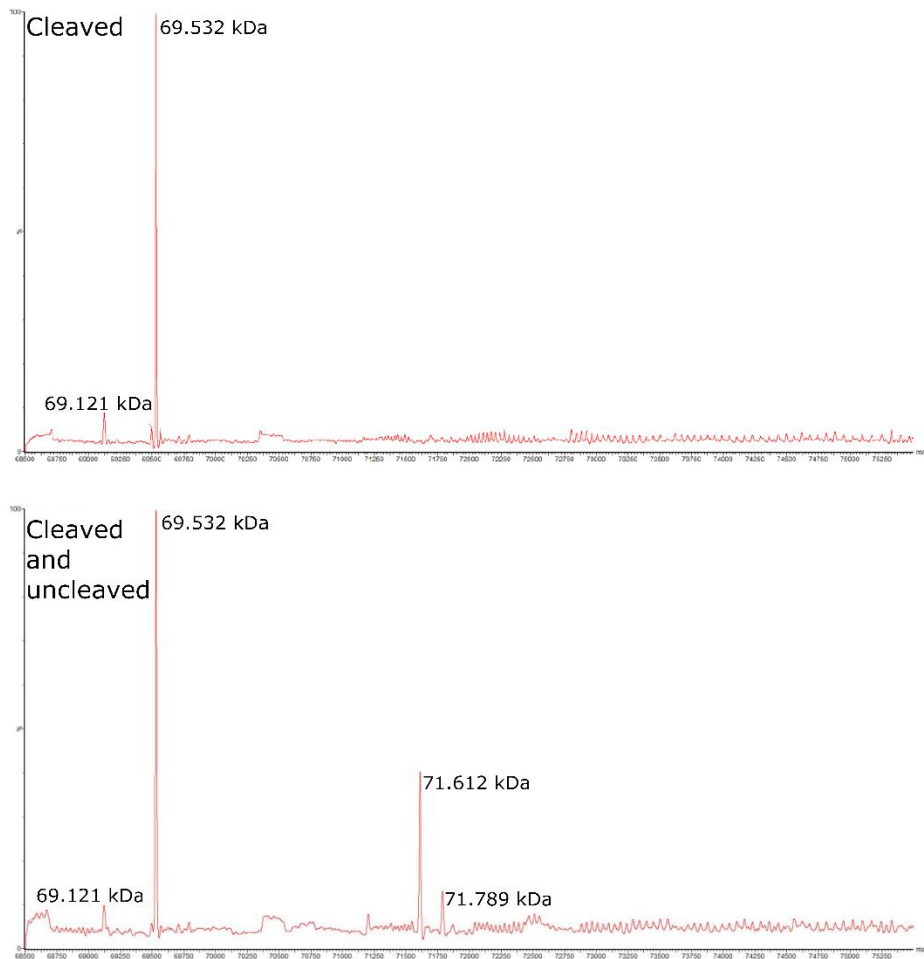


**Figure 24: conformation of TEV cleavage.** Results of intact protein mass spectrometry using a Liquid chromatography mass spectrometry (LC-MS) system of either His-tag cleaved BiP human WT or a mixture of his-tag cleaved and uncleaved BiP human WT sample.

To test whether the His-Tag affects BiP function, the malachite green ATPase assay was performed for the cleaved and uncleaved protein as ATP hydrolysis has been directly linked to Hsp70 chaperone activity (29,181). Remarkably, the presence of His-Tag significantly reduces BiP ATPase activity (Figure 25). Consequently, all BiP samples used with in this study had the His-Tag cleaved to ensure full functionality. Additionally, when compared to previous studies, this study data displayed 369.57 nmol (Phosphate)·h<sup>-1</sup>·mg<sup>-1</sup> compared to 290 nmol (Phosphate)·h<sup>-1</sup>·mg<sup>-1</sup> previously displayed (182). As these are in the same magnitude, any variation can be due to difference in constructs and the proteins can be assumed to be equivalent.

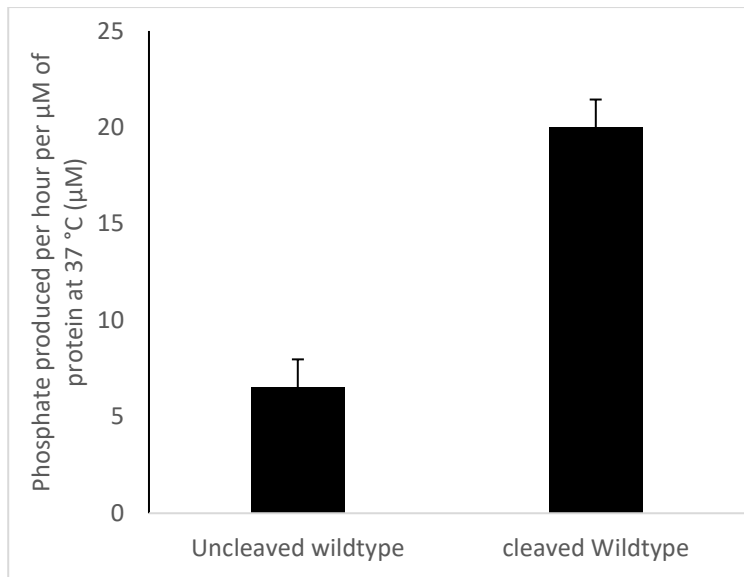


**Figure 25: His-Tag effect on BiP ATPase activity.** Bar chart depicting ATPase activity of wildtype human BiP with the His-Tag either uncleaved or cleaved. ATPase rate determined based on free phosphate groups measured with a malachite green assay.

## Chapter 4: Characterization of BiP conformational landscape using methyl NMR.

### 4.1. NMR as a tool to characterize small changes in the BiP conformational ensemble.

The allosteric cycle of BiP entails the chaperone transition between two end point conformations, where the protein adopts distinct arrangements between the NBD, SBD $\alpha$  and SBD $\beta$  (chapter 1.2.2, Figure 2) (2,41). The study employed methyl NMR to monitor changes in the conformation landscape of BiP, which allowed the observation of phosphorylation induced and substrate binding induced alterations. This chapter discusses the wildtype (WT) BiP conformation in varying conditions to provide the base for analysis of the modifications effect on the protein.

To prevent ATP hydrolysis during the NMR experiments, the study employed the T229G ATPase deficient mutant (46), which possesses reduced ATPase activity without altering the conformation. As the variant protein is unable to hydrolysis the nucleotide, it is unable to transition through the allosteric cycle and therefore the mutation traps the protein in the ATP bound state for the duration of the experiment. This allows an ATP bound BiP spectra to be able to be recorded by the NMR spectrometer.

As characterised in previous studies (46), isoleucine methyl NMR is capable of monitoring the conformational landscape of BiP under different ligand binding states. This includes ATP bound and ADP bound states in the presence and absence of unfolded and substrates. Similar to the previous results from the laboratory, in the presence of ADP, BiP adopts a single, ADP domain undocked (ADP.U) conformation. As it has been demonstrated previously (46), in this conformation, the NBD and SBD are undocked and mostly independent of each other (Figure 26).

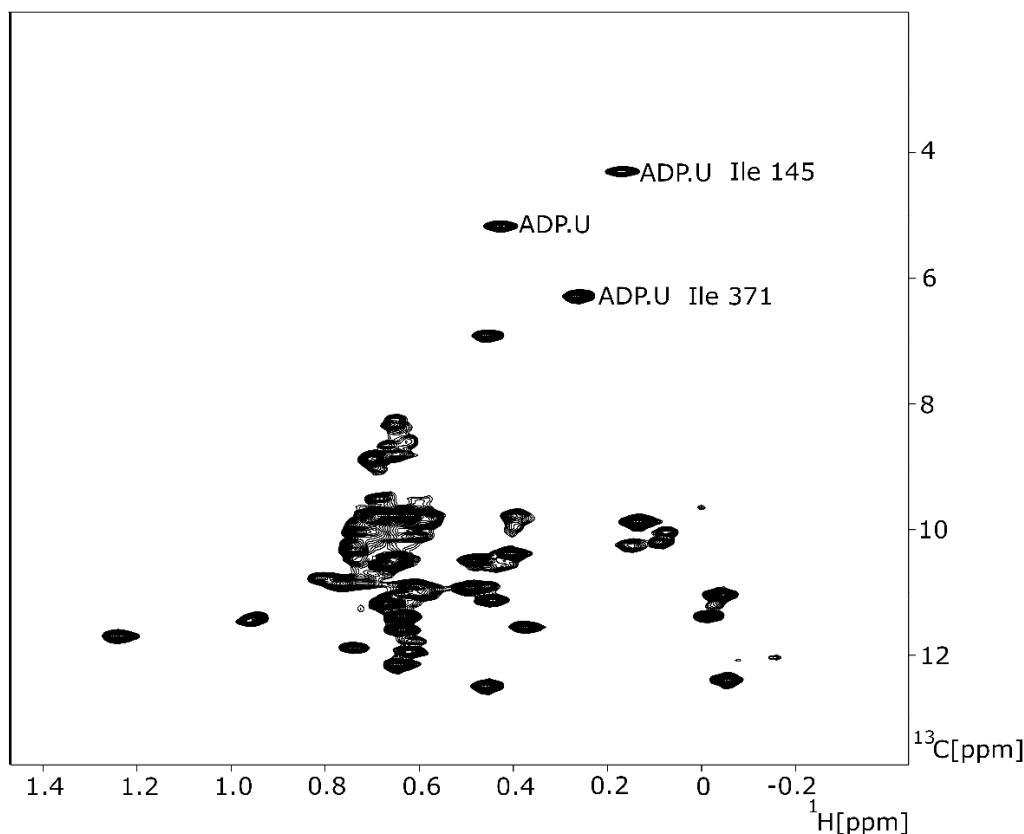


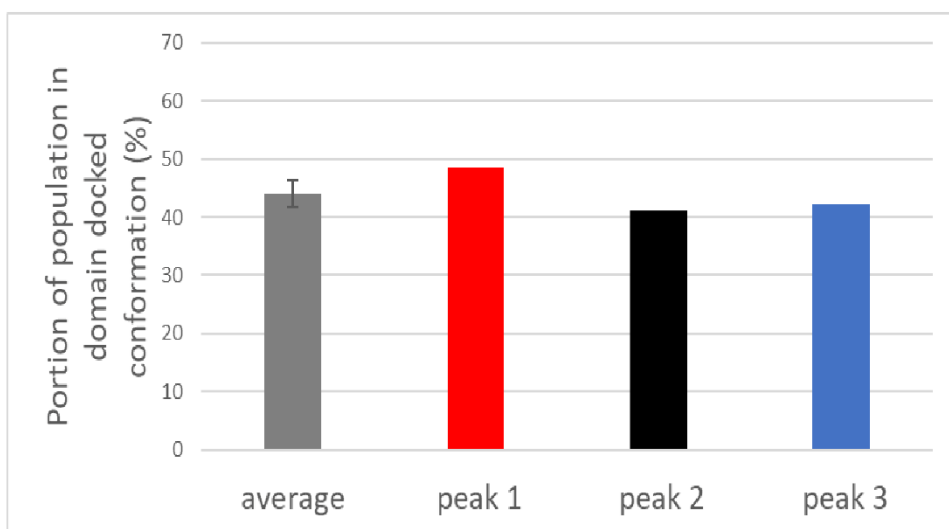
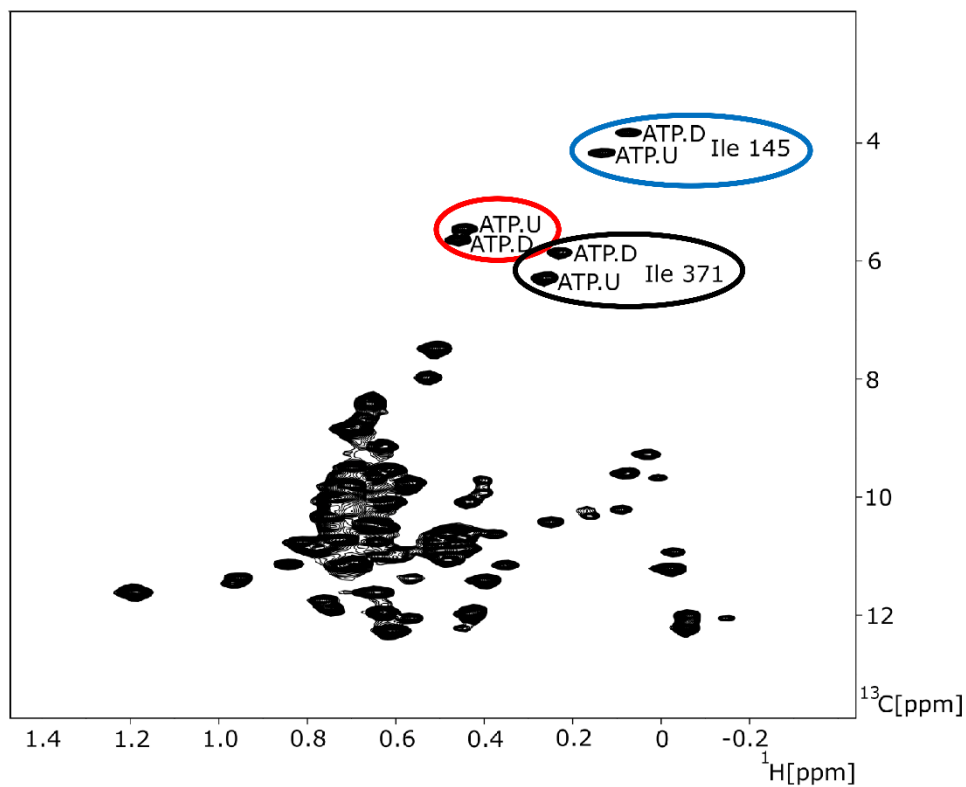
*Figure 26: BiP conformational landscape in the presence of ADP. The isoleucine region of methyl-TROSY spectra of full length human BiP T229G in the presence of 5 mM ADP recorded at 25 °C on a 750 MHz Bruker spectrometer.*

This is different from BiP in the presence of ATP, where it adopts two interconverting conformations ATP bound domain undocked (ATP.U) and ATP bound, domain docked (ATP.D) (Figure 27). The domain undocked conformations ATP.U and ADP.U are nearly identical structurally but do possess slight differences around the nucleotide binding site, which results in a difference in peaks corresponding to the residues near the nucleotide binding site on the spectra. The domain docked (ATP.D) conformation is drastically different structurally and functionally (46). It has been shown previously, that in this conformation NBD and SBD $\beta$  interact with each other, while SBD $\beta$  dissociates from SBD $\alpha$ . These significant structural changes between ATP.U and ATP.D result in distinct functional properties of these conformations. Particularly, the domain undocked conformation has a significantly higher affinity for substrates but have slower rates of substrate binding and release; in turn, ATP.D has higher ATPase activity (36,42,46).

As BiP co-exists as ATP.U and ATP.D in the presence of ATP, for this reason there are more than 42 peaks (the number isoleucine within BiP sequence). This is because the same residue will have multiple corresponding peaks if it exists in different local environments within the same sample. In the case of BiP in the presence of ATP, the NMR spectrum contains two sets of peaks with each doublet corresponding to ATP.U and ATP.D conformations of the same methyl group (Figure 27) (46). The relative intensity of each

peak of the doublet is proportional to the relative population of ATP.U and ATP.D. The study used three representative, non-overlapping peak doublets to calculate the relative population in different conditions and for different BiP constructs. These three peak doublets have been selected due to their previous assignments to either the ATP.U or ATP.D conformation, ensuring that the calculation for proportion the population in each conformation is correct (not any errors in the calculation due to peaks in each doublet being assigned to incorrect conformational state).

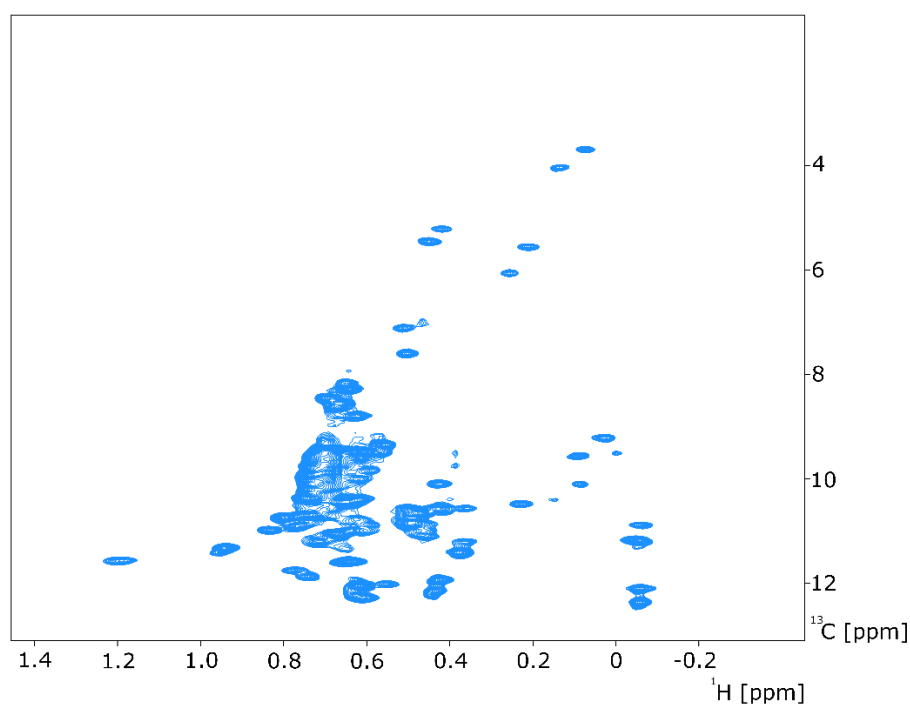
The analysis of BiP T229G revealed that in the presence of ATP, 44 %  $\pm$  2.4 % domain docked conformation is present (figure 27), which agrees with the results of previous studies (46). This approach was then used to determine if the alterations to conditions or mutations alter the conformational equilibrium of BiP.



**Figure 27: BiP conformational landscape in the presence of ATP.** The isoleucine region of methyl-TROSY spectra of full length human BiP T229G in the presence of 40 mM ATP recorded at 25 °C on a 750 MHz Bruker spectrometer. Bar chart depicting percentage of domain docked conformation for the three doublet peaks calculated based on relative intensity of the peak. Standard error based on average peak intensity is used for error bars.

BiP is known to be a very dynamic protein (42,46–48), with its conformational landscape being not only affected by ligand binding but also by a range of factors including pH and temperature. When comparing the spectra of BiP in the presence of ATP at three different temperatures (5, 25 and 37°C), all peak experience near identical temperature coefficient (changes in peak position as a function of temperature change) (Figure 28), suggesting that temperature has minimal or no effect on either conformation. Temperature coefficient refers to the by the notion that heating of a sample causes increases in thermal motion in the protein (183), which means that there will be some expected shift in peak position between the temperatures, though as it is minimal shift it can be assumed that it has no effect on conformation.

However, temperature variations alter the equilibrium between ATP.U and ATP.D with the lower temperature favouring the domain docked conformation and higher temperatures favouring the domain undocked conformation (Figure 29). With 5 °C displaying 54.83 % ± 3.24, 25 °C displaying 44.06 % ± 2.34 and 37 °C displaying 37.31 % ± 4.29. This example demonstrates that NMR enables precise monitoring of even relatively small (~ 10 %) shifts in the Hsp70 conformational equilibrium.



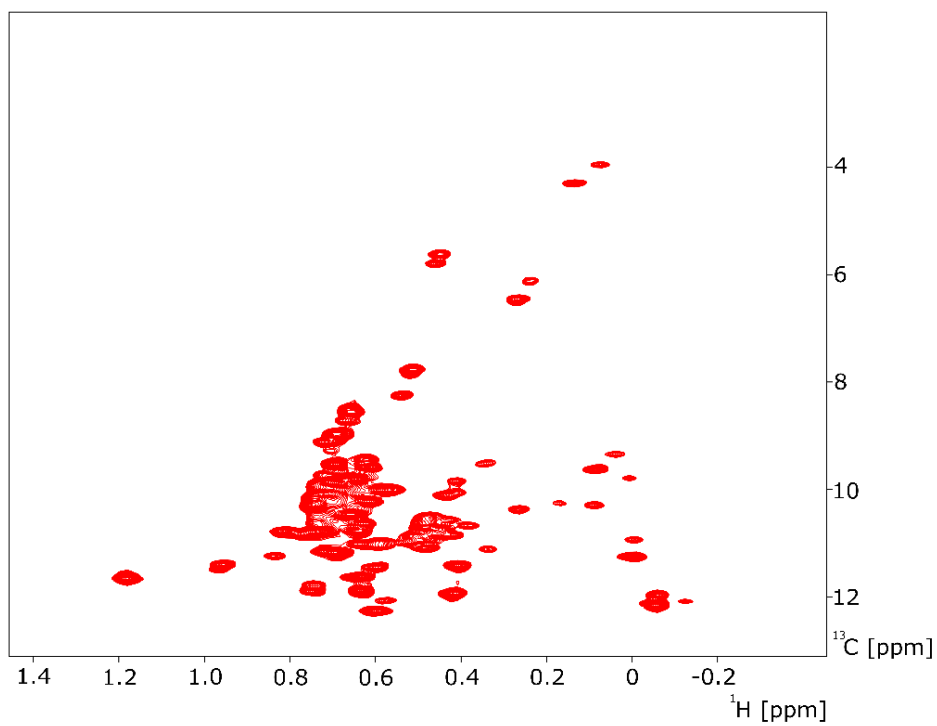
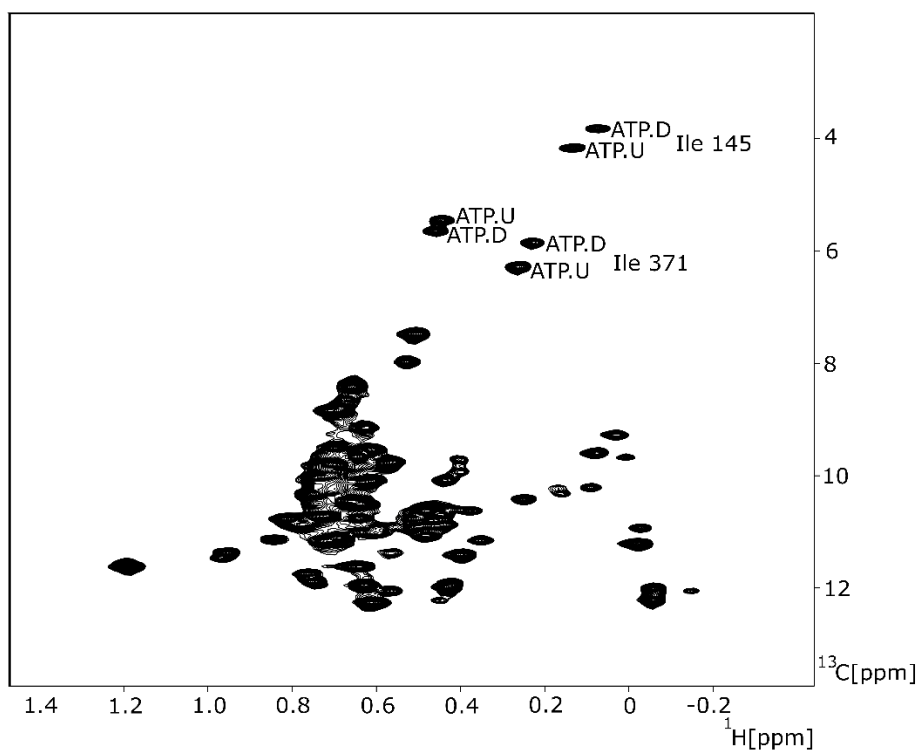


**Figure 28: BiP spectra display minimal variations at varying temperatures.** The isoleucine region of methyl-TROSY spectra of full length human BiP T229G in the presence of 40 mM ATP recorded at either 5 °C (blue), 25 °C (black) or 37 °C (red) on a 750 MHz Bruker spectrometer.

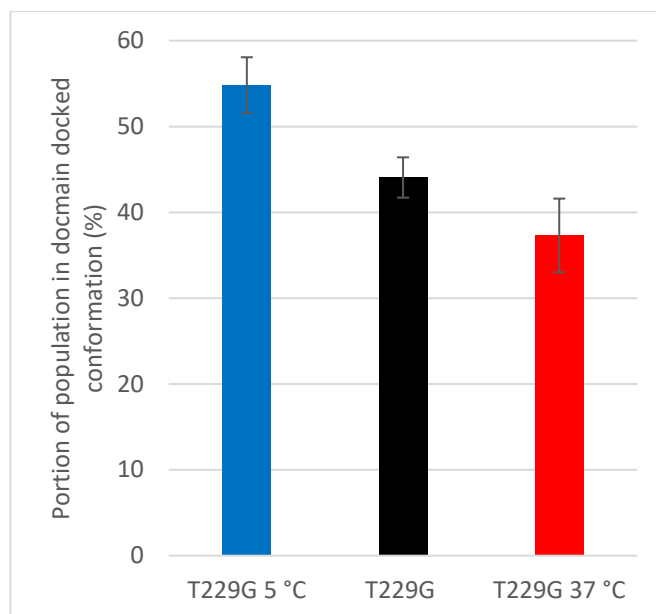


**Figure 29: BiP conformational equilibrium shift at varying temperatures.** Bar chart depicting percentage of domain docked conformation for the three doublet peaks calculated based on relative intensity of the peak at three different temperatures: 5 °C.(blue), 25 °C.(black) and 37 °C (red). Standard error based on average peak intensity is used for error bars.

#### 4.2 Characterization of substrate binding to BiP

Other than changes in temperature, different factors can trigger perturbations in the Hsp70s conformational ensemble such as Hsp70 binding to a model unfolded protein substrate (36). The study used a previously characterised peptide called peptide 2 (CP2) (sequence HTFPAVL) which has been shown to bind to the SBD ( $K_d = 11.6 \pm 0.6 \mu\text{M}$ ) (123) and results in the stabilization of the undocked conformation (36). This alteration to the conformational equilibrium allows the binding of substrate to be characterised by methyl NMR.

In the presence of ADP, the addition of 1 mM CP2 results in only minor changes in the NMR spectra, particularly the appearance of additional six low intensity peaks (Figure 30). These results suggest that in the presence of ADP substrate binding has only a local effect (near the substrate binding site) on BiP, resulting in no conformational changes in the protein conformation.

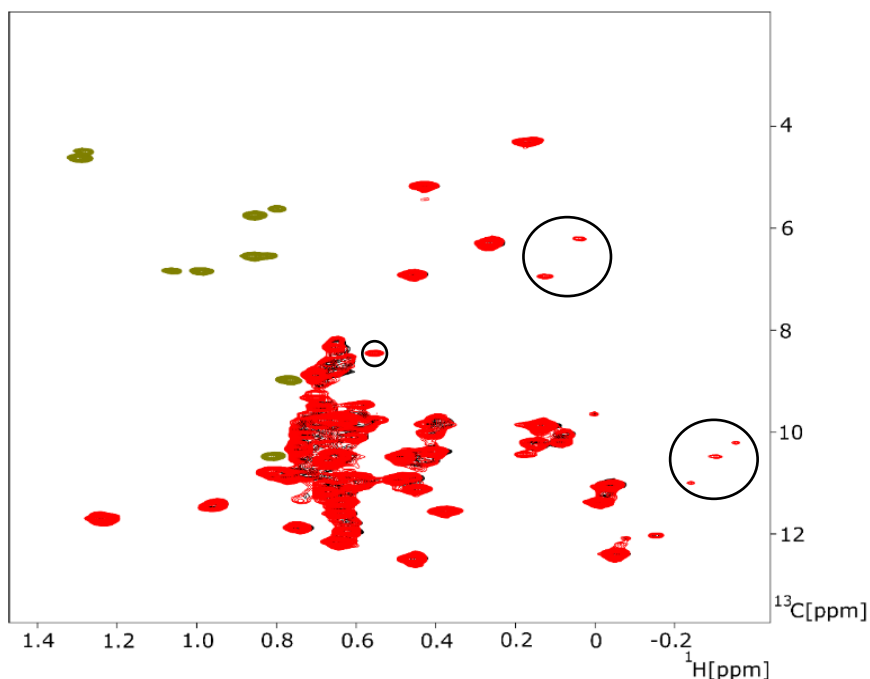


**Figure 30: Minor perturbation of ADP bound BiP spectra due to substrate binding.** Overlay of the isoleucine region of methyl-TROSY spectra of full length human BiP T229G in the presence of 5 mM ADP (Black) and full length human BiP T229G in the presence of 5 mM ADP and 1 mM CP2 (Red) recorded at 25 °C on a 750 MHz Bruker spectrometer. Additional peaks of substrate bound spectra highlighted within black circles.

In contrast, the addition of 1 mM CP2 in the presence of ATP produces very significant changes in the NMR spectra. Whilst the peaks positions remain mostly unperturbed, there are distinct changes in relative peak intensities between the ATP.D and ATP.U conformations induced by substrate binding. As expected from previous results (42,52), the addition of substrate triggers the protein to transition from ATP.D to ATP.U conformations from 44% docked in the absence of substrate to 19% in the presence of substrate (Figure 31). This shift in conformational equilibrium can be seen throughout the spectra with a decreased intensity of multiple peaks that are likely linked to the domain docked conformation. Full image of the overlay of BiP + ATP and BiP + ATP + CP2 peptide spectra displayed in appendix figure 14.

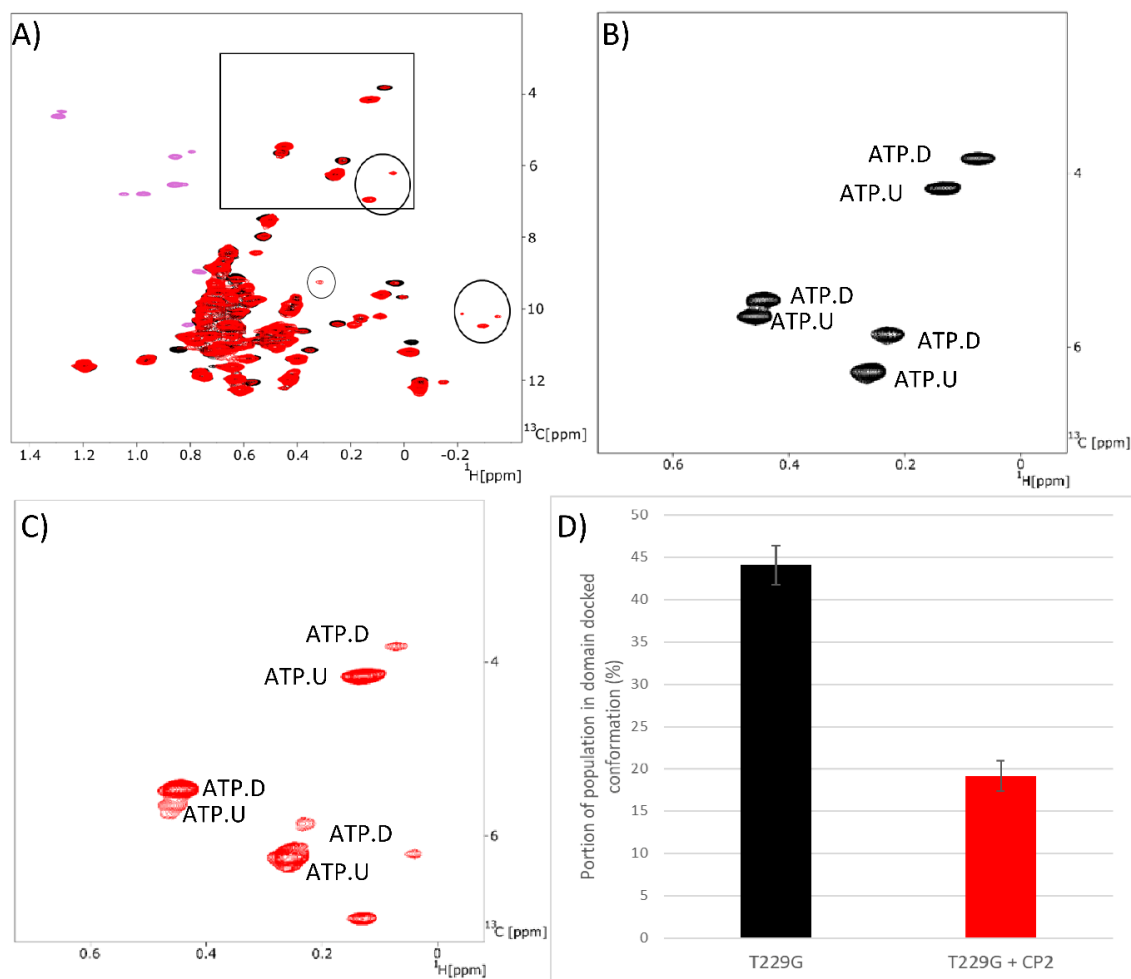


**Figure 31: Conformational equilibrium shifts of ATP bound BiP spectra due to substrate binding.** A) Overlay of the isoleucine region of methyl-TROSY spectra of full length human BiP T229G in the presence of 40 mM ATP (Black) and full length human BiP T229G in the presence of 40 mM ATP and 1 mM CP2 (Red) recorded at 25 °C on a 750 MHz Bruker spectrometer. Blowup of the representative region of methyl-TROSY spectra of ATP-bound T229G BiP in the presence of 40 mM ATP (B) or 40 mM ATP and 1 mM CP2 (C). D) Bar chart depicting percentage of domain docked conformation for the three doublet peaks calculated based on relative intensity of the peak. Standard error based on average peak intensity is used for error bars.

Additionally, in the presence of ATP and substrate there were the six low intensity peaks similar to the ones displayed in ADP spectra (25). The overlay of the spectra of the ATP and ADP BiP in the presence of 1 mM CP2 revealed that five of these additional six peaks fully overlap (Figure 32), suggesting that these peaks are likely to correspond to the CP2 bound SBD located methyl groups of the domain undocked conformation. Further experimentation is required to identify the location of the corresponding residues and without would be impossible to confirm the cause of the additional 6 peaks.

Additionally, both spectra show additional peaks as either green (BiP in the presence of ADP (figure 30 and 32) or pink (BiP in the presence of ATP (figure 30 and 32). These peaks are not related to BiP but instead are due to the presence of the peptide (peptide in the

sample which is not interacting with BiP) within the solution. For this reason, these peptide peaks can be ignored.

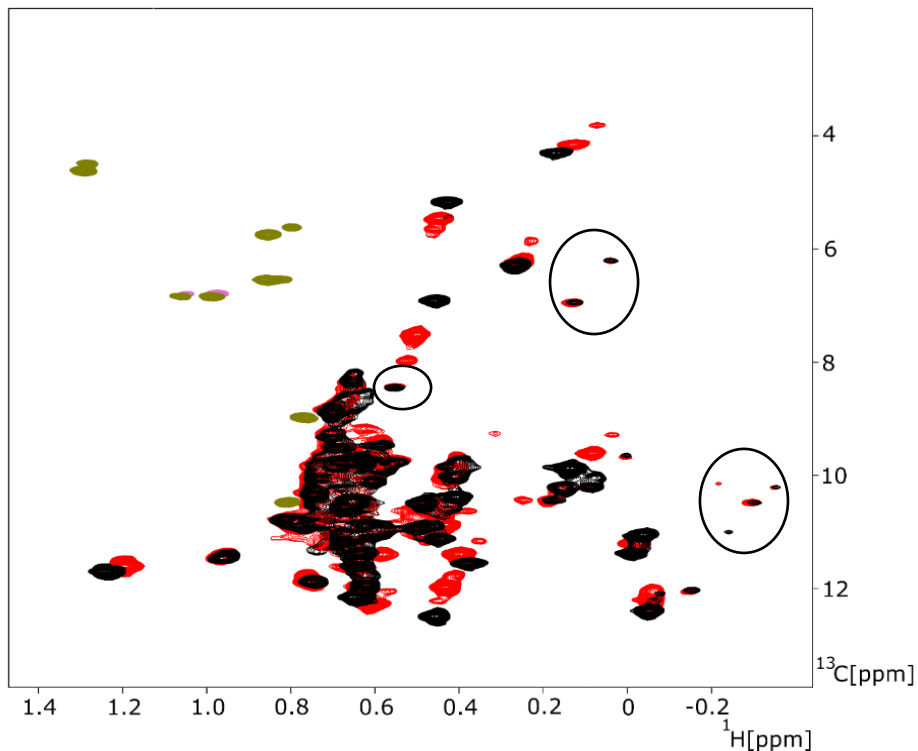


**Figure 32: Shared peaks of substrate bound BiP in the presence of ATP and ADP.** Overlay of the isoleucine region of methyl-TROSY spectra of full length human BiP T229G in the presence of 5 mM ADP and 1 mM CP2 (Black) and full length human BiP T229G in the presence of 40 mM ATP and 1 mM CP2 (Red) recorded at 25 °C on a 750 MHz Bruker spectrometer.

This binding of substrate can be verified with the use of a malachite green ATPase assay. It is known that the level of activation in ATPase activity is increased in the presence of substrate, due to substrate binding triggering ATPase activity in Hsp70s (1). This means comparison of BiP ATPase levels in the presence and the absence of substrate can be used to confirm substrate binding. For example, there is a significant increase in ATPase activity in the presence of CP2 (Figure 33), which confirms the binding displayed in the methyl NMR data.

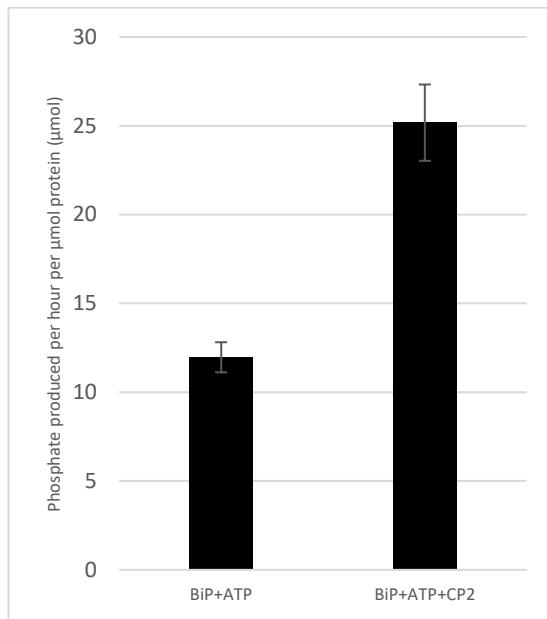


**Figure 33: Substrate binding increase of ATPase hydrolysis.** Malachite green ATPase assay displaying increased levels of ATP hydrolysis due to the addition of 1mM CP2 to wildtype BiP compared to the wildtype BiP in the absence of peptide.

## Chapter 5: BiP interactions with the stress sensor IRE1 as a tool to monitor ER specific functions of BiP.

### 5.1 Two IRE1-LD derived peptides interact with BiP as classical chaperone substrates.

As discussed in chapter 1.3.3, BiP is capable of controlling IRE1 activation through the prevention of its oligomerization through binding to an undetermined binding site or sites of IRE1-LD. The previous bioinformatic analysis in the laboratory (personal communication) identified six potential BiP binding sites that are located in the C-terminal disordered part of IRE1-LD and have high propensity to bind BiP as determined by the BiPPred algorithm (184) (table 7). This is software that predicts 7 amino acids sequences on BiP that have a high chance of being binding sites. The binding of these peptides to BiP were assessed using the methyl NMR and ATPase assays described in chapter 3 and 4.

**Table 7: IRE1-LD sequence-based peptides.** Table listing the six IRE1-LD sequences and the section of sequence on which the peptide is based.

Peptide	Sequence
P1 <sup>IRE1</sup>	305AVVPRGS <sup>311</sup>
P2 <sup>IRE1</sup>	310GSTLPLL <sup>317</sup>
P3 <sup>IRE1</sup>	356RNYWLLI <sup>362</sup>
P4 <sup>IRE1</sup>	385KHRENV <sup>391</sup>
P5 <sup>IRE1</sup>	388ENVIPADS <sup>395</sup>
P6 <sup>IRE1</sup>	442KDMATIIL <sup>449</sup>

Methyl NMR spectra of ATP bound T229G BiP in the presence of either one of these six peptides or model CP2 were recorded to obtain the relative population of ATP.D and ATP.U conformations calculated as described in chapter 4. Four of the six peptides; P1<sup>IRE1</sup>, P4<sup>IRE1</sup>, P5<sup>IRE1</sup> and P6<sup>IRE1</sup> display no changes in NMR spectra up to 1 mM concentration, indicative of no binding occurring in this concentration range (Figure 34). The full spectra for each conditions are displayed in appendix (appendix Figure 6, 9, 10 and 11).

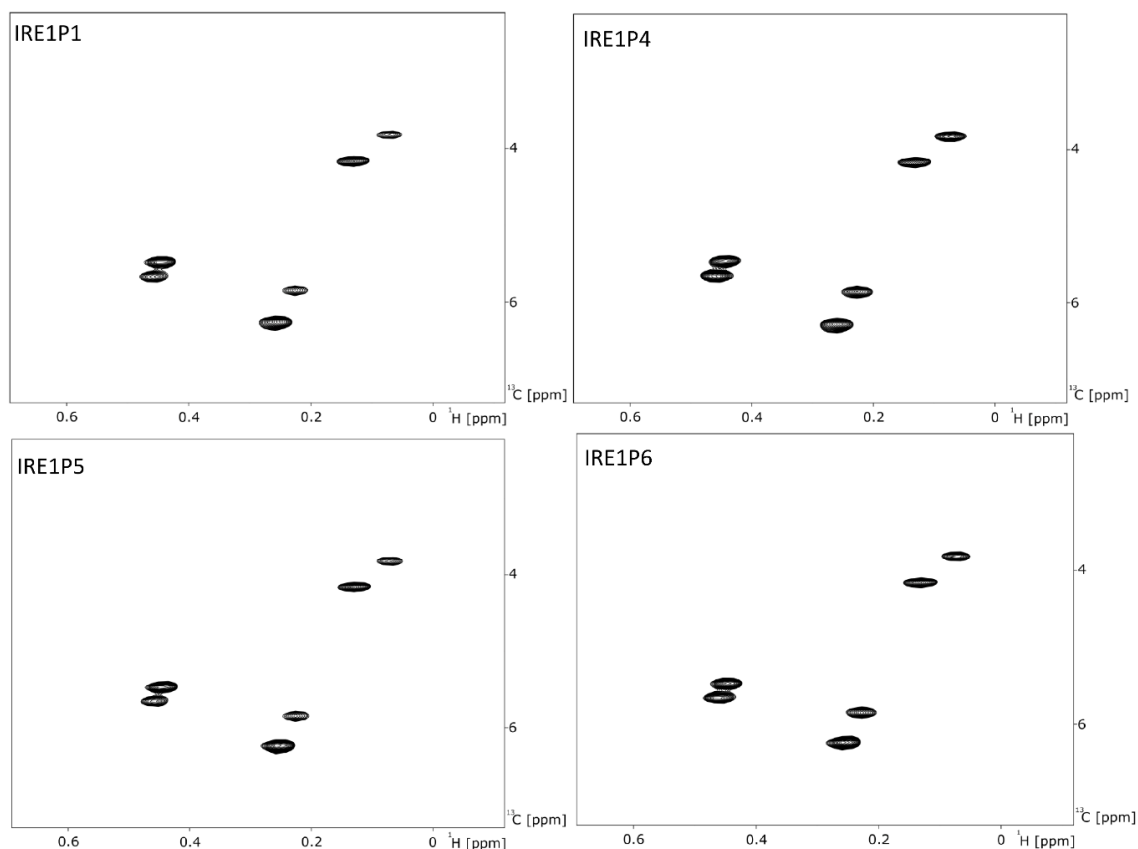


**Figure 34:** Four IRE1 peptide displaying no signs of binding by BiP. Blowup of the representative region of isoleucine region of methyl-TROSY spectra of full length human BiP T229G in the presence of 40 mM ATP and either 1 mM IRE1P1, 1mM IRE1P4, 1 mM IRE1P5 and 1mM IRE1P6.

Due to limited peptide solubility, the experiments for P2<sup>IRE1</sup> and P3<sup>IRE1</sup> peptides were performed at 50  $\mu$ M peptide concentrations. Surprisingly, both P2<sup>IRE1</sup> and P3<sup>IRE1</sup> displayed signs of binding at this concentration (Figure 35), with the addition of these peptides resulting in the characteristic 25 % shift in equilibrium to favour the ATP.U conformation (Figure 36). Remarkably, the addition of the model peptide CP2 at such low concentration results in no obvious changes in the NMR spectra, suggesting not only that P2<sup>IRE1</sup> and P3<sup>IRE1</sup> binds to BiP but also their affinity is significantly higher than a model substrate CP2 (Figure 35 and 36). The full spectrum for each condition is displayed in appendix (appendix Figure 7,8 and 12).

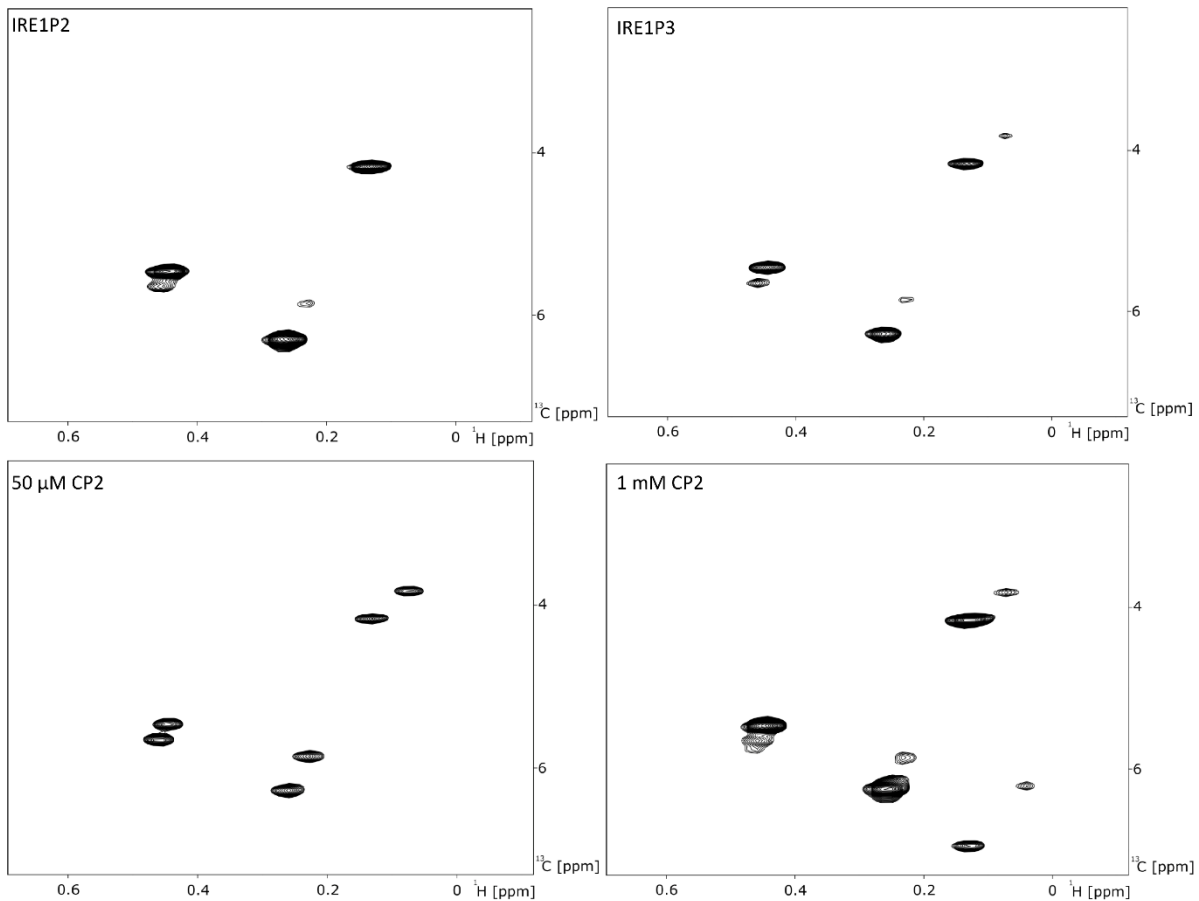


**Figure 35: T20 IRE1 peptide and CP2 at varying concentrations displaying either signs or no signs of binding by BiP.** Blowup of the representative region of isoleucine region of methyl-TROSY spectra of full length human BiP T229G in the presence of 40 mM ATP and either 50 μM IRE1P2, 50 μM IRE1P3, 50 μM CP2 and 1 mM CP2.

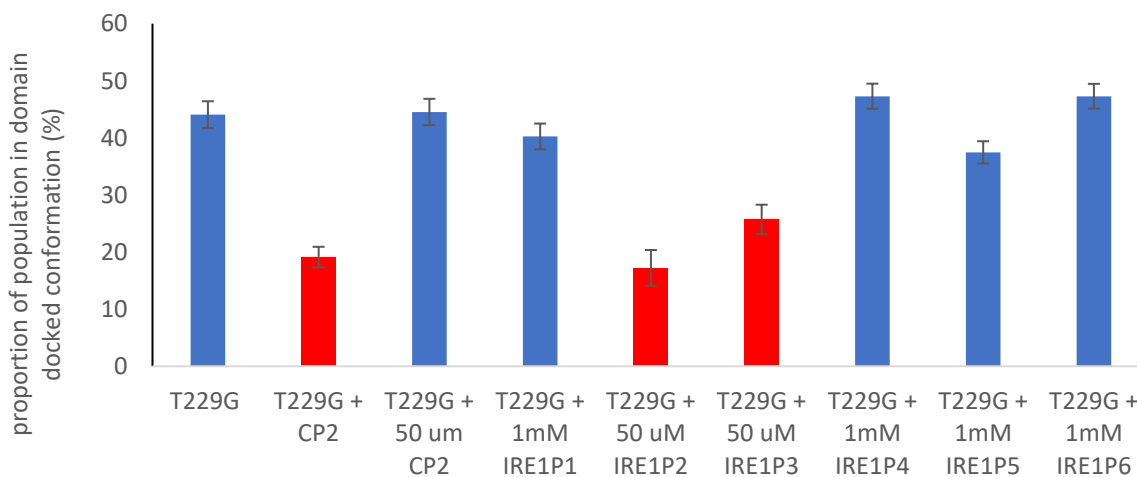


**Figure 36: Percentage of population of BiP in domain docked conformation.** Bar chart depicting percentage of domain docked conformation for the three doublet peaks calculated based on relative intensity of the peak. BiP is in the presence of varying peptides at either 50 μM or 1 mM concentration. Spectra that displayed significant signs of binding displayed in red and the remaining peaks displayed in blue. Standard error based on average peak intensity is used for error bars.

To further verify that P2<sup>IRE1</sup> and P3<sup>IRE1</sup> are 'classical' BiP substrates, a malachite green ATPase assay was employed to monitor how binding affected the ATPase activity of BiP. It is known that the binding of substrate to BiP SBD triggers ATP hydrolysis in NBD (1), therefore the addition of a model peptide such as CP2 will consequently trigger an increase in ATPase activity. In full agreement with the NMR results, the addition of either P2<sup>IRE1</sup> or P3<sup>IRE1</sup> results in a significant increase in ATPase activity, comparable with the effect of the model CP2 substrate (Figure 37).

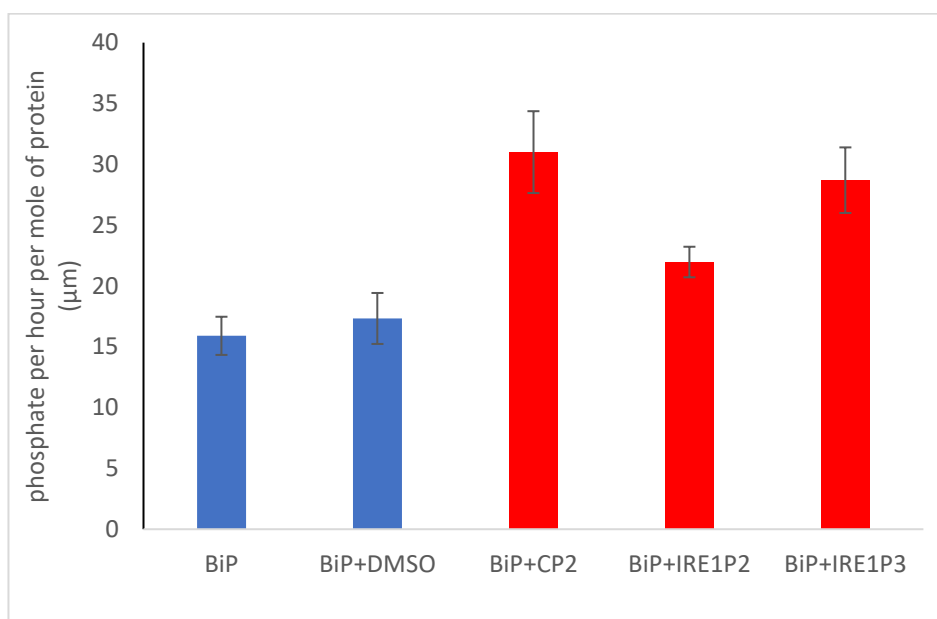


**Figure 37: peptide binding induced increases in ATP hydrolysis of BiP.** Malachite green ATPase assay displaying increases in ATPase activity induced by the addition of 1 mM of IRE1P2, IRE1P3 or CP2 with a DMSO control being included to ensure that the DMSO that the peptides are stored in has no effect on the protein.

Taken together, these experiments have identified two IRE1 derived peptides, P2<sup>IRE1</sup> and P3<sup>IRE1</sup>, derived from IRE1-LD that interact with BiP as 'classical' substrates, i.e., they interact with the BiP SBD resulting in conformational changes in the chaperone and stimulating its ATPase activity.

5.2 Perturbations in <sup>310</sup>GSTLPLL<sup>317</sup> and <sup>356</sup>RNYWLLI<sup>362</sup> sites of IRE1 affect IRE1 oligomerization.

Mutations in the <sup>310</sup>GSTLPLL<sup>317</sup> and <sup>356</sup>RNYWLLI<sup>362</sup> regions (corresponding to P2<sup>IRE1</sup> and P3<sup>IRE1</sup>, respectively) were introduced in order to test whether perturbations in these regions affect interactions with BiP to produce the IRE1-LD <sup>315</sup>DA<sup>316</sup> and <sup>359</sup>GSSG<sup>362</sup> variants. Both substitutions are expected to significantly affect BiP binding as it requires hydrophobic residues for interactions.

The assay to assess the interactions of IRE1-LD with BiP has been previously developed in the lab (Methods, chapter 9.9). IRE1-LD is known to form insoluble higher order oligomer in the presence of a model peptide dESP (MKKHKRILALCFLGLLQSSYSAAKKKK (98)). The assay adds 100, 200 or 400  $\mu$ M dESP concentrations to IRE1-LD in order to form these insoluble oligomers, which can be separated from soluble oligomer of IRE1-LD through centrifugation. The amount of soluble lower order oligomer and dimers within the supernatant and insoluble higher order oligomers within the pellet can be assessed through comparison of band intensity on a SDS-PAGE gel after the two fractions are separated through centrifugation (figure 38).

IRE1-LD wildtype will mostly be in the insoluble fraction in the presence of dESP peptide and this is also the case if BiP is added. However, if BiP is added with ATP, BiP is capable of deoligomerizing the higher order IRE1-LD oligomers into soluble lower order IRE1-LD oligomers. This will cause the majority of IRE1-LD to be in the soluble fraction only in the presence of ATP and BiP, otherwise it will be in the insoluble fraction (figure 38).

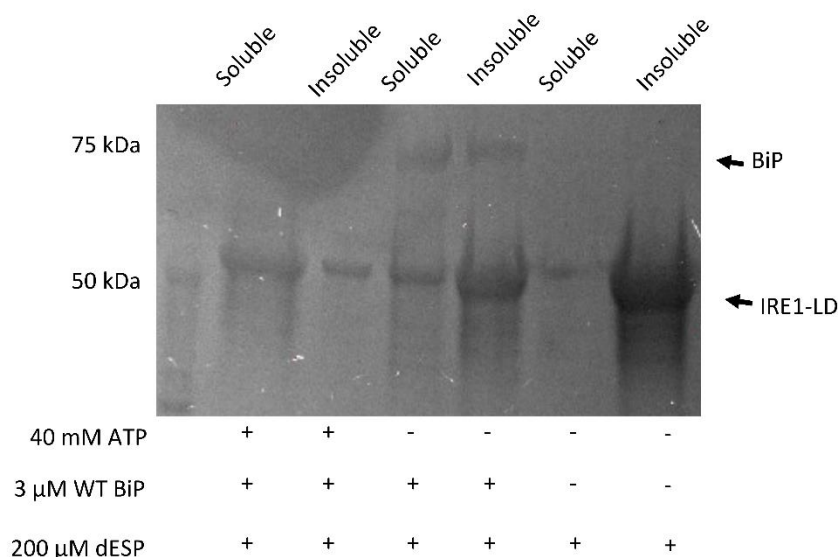
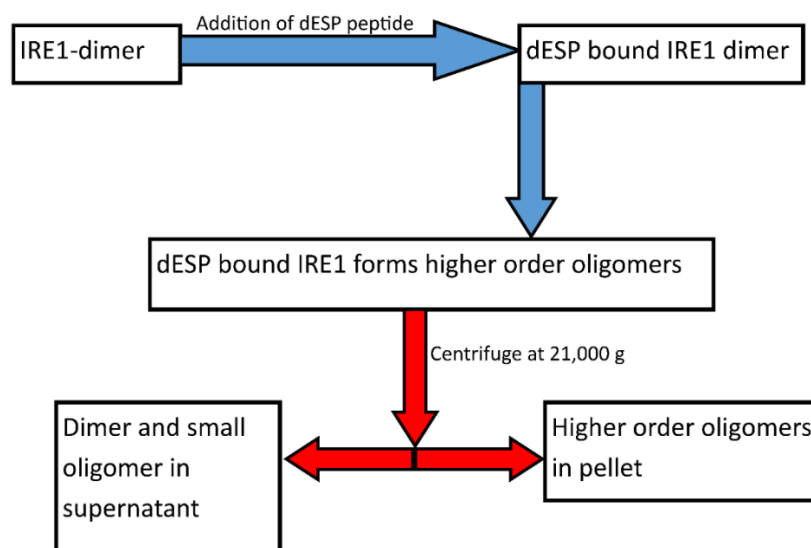


**Figure 38: IRE1 deoligomerization by wildtype BiP.** Cartoon depicting the formation of higher order IRE1-LD domain oligomers after the addition of ESPs peptide and the method to separate dimers and small order oligomers from higher order oligomers. SDS-PAGE gels depicting the soluble dimer fraction (soluble) and the high order oligomers (insoluble) for the WT IRE1-LD construct in the presence of either 40 mM ATP + 3 μM BiP + 200 μM ESPs peptide, 3 μM BiP + 200 μM ESPs peptide or 200 μM ESPs peptide.

IRE1-LD oligomerization was also shown to vary based on the concentration of dESP, with 47.30 % ± 3.2 in the soluble fraction at 100 μM and this value decreasing to 13.34 % ± 9.2 and 2.75 % ± 1.95 for 200 μM and 400 μM. Additionally, there is a decrease in the percentage of soluble IRE1-LD in the presence of BiP at 400 μM dESP concentration (figure 39). This displays that the concentration of the dESP peptide alters the oligomerization of the IRE1-LD protein. Full gels of deoligomerization can be found in the appendix (appendix Figure 15, 16, 17 and 18).

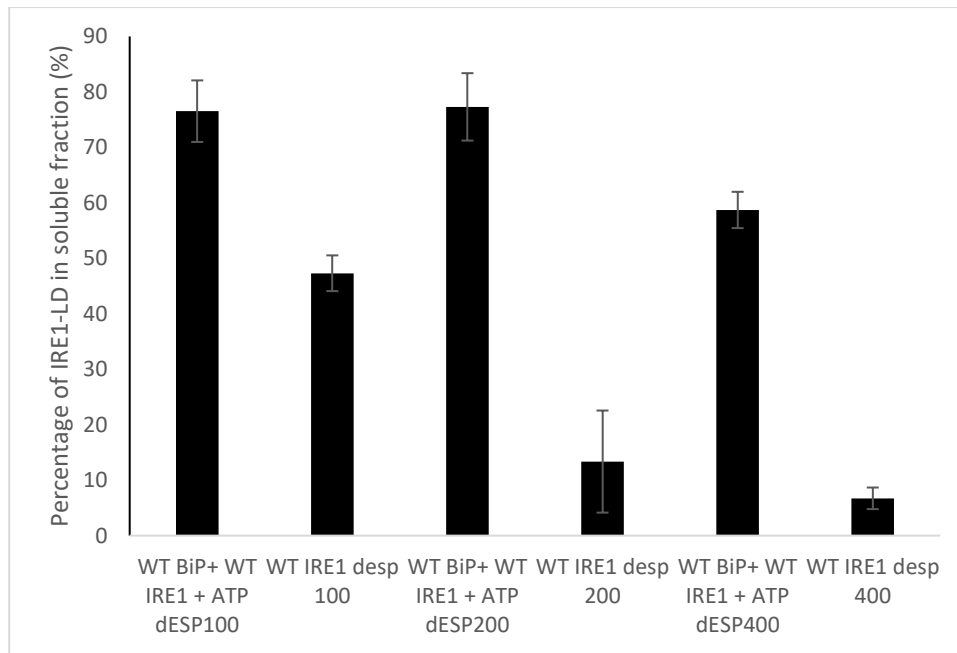


Figure 39: Bar charts displaying the proportion of Wildtype IRE1-LD population in the soluble lower order oligomers population in the presence of 100  $\mu$ M, 200  $\mu$ M or 400  $\mu$ M dESP and either no or 40  $\mu$ M ATP.

This assay was performed for WT IRE1-LD and its <sup>315</sup>DA<sup>316</sup> and <sup>359</sup>GSSG<sup>362</sup> variants to test whether these substitutions affect BiP's ability to deoligomerize IRE1-LD. As it has been demonstrated recently that both regions are important for IRE1-LD oligomerization and clustering (102,185), first it was examined whether the mutations affect IRE1-LDs ability to form insoluble oligomers.

Consistent with previous observations, both mutants displayed decreased ability to form higher order oligomers, with <sup>315</sup>DA<sup>316</sup> and <sup>359</sup>GSSG<sup>362</sup> only having 41 % and 43 % of the population in the insoluble form at 100  $\mu$ M dESP respectively compared to the WT ~ 80 % at both concentrations. The addition of higher 400  $\mu$ M concentration of dESP, both mutants displayed similar levels of oligomerization as the WT IRE1-LD, with > 90% insoluble oligomers for all constructs (Figure 40). All together, these results suggest that either substitution is sufficient to significantly disturb peptide-inducible IRE1-LD oligomerization, but insufficient to completely prevent the oligomerization process.

The addition of BiP and ATP to IRE1-LDs insoluble oligomers, formed in the presence of 400  $\mu$ M dESP, results in their solubilization (from > 90% to <50% of insoluble form in the absence and in the presence BiP, respectively) for either WT IRE1-LD or its <sup>315</sup>DA<sup>316</sup> and <sup>359</sup>GSSG<sup>362</sup> variants (Figure 40 Bottom). Furthermore, the addition of ATP and BiP at the lower concentration of 100  $\mu$ M dESP, displayed no significant effect on the portion of the insoluble oligomers (Figure 40 top) for the <sup>315</sup>DA<sup>316</sup> and <sup>359</sup>GSSG<sup>362</sup> variants, but displayed significant solubilization for the WT IRE1-LD (Figure 40 black). These results suggest that the <sup>310</sup>GSTLPLL<sup>316</sup> or <sup>356</sup>RNYWLLI<sup>362</sup> regions are important for BiP interactions with IRE1-

LD; however, there is no single BiP binding site that is fully responsible for IRE1-LD interactions with BiP. Additionally, these results clearly demonstrate that the BiP induced IRE1-LD deoligomerization assay can be used to monitor ER specific function of BiP in the WT chaperone and its variants (chapter 6). Full gels of deoligomerization can be found in appendix (appendix Figure 21, 22, 23, 24, 25 and 26).

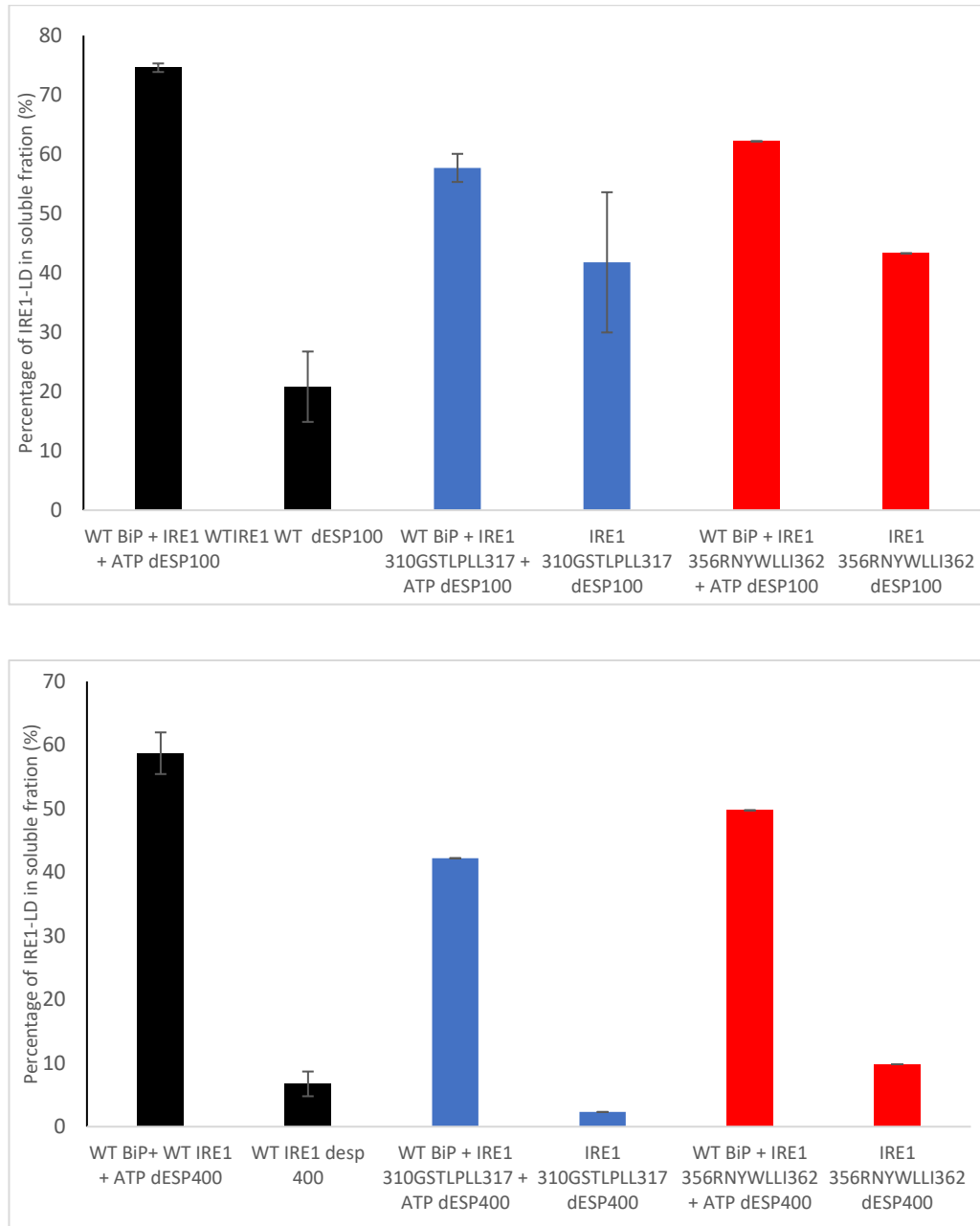


**Figure 40: deoligomerization of IRE-LD constructs.** Bar charts displaying the proportion of IRE1-LD population in the soluble lower order oligomers population for WT, <sup>15</sup>DA<sup>316</sup>, <sup>359</sup>GSSG<sup>362</sup> constructs in the presence of 100  $\mu$ M or 400  $\mu$ M dESP and either no or 40  $\mu$ M ATP.

## Chapter 6: Regulation of BiP conformation and function through ER specific phosphorylation sites

As described in chapter 2.4, the study identified four ER uniquely conserved phosphorylation sites and selected study the two SBD located sites. To mimic the phosphorylation modification, aspartic acid substitutions were introduced to either the T460 or Y570 positions (Figure 41). Both of these mutation sites are located near the interface of the SBD $\beta$  and SBD $\alpha$  (31) and therefore one possible effect of these substitutions could be changes in ability to substrate bind. Moreover, the location of the mutations near the SBD $\beta$  and SBD $\alpha$  interface may trigger complex effects to the BiP conformational landscape as been previously observed for other Hsp70 allosteric “hotspots”(46) and therefore could affect the BiP conformational ensemble and NBD activity. The study employed a combination of methyl NMR (described in chapter 4), ATPase assay (described in chapter 3) and IRE1 oligomerization assay (described in chapter 5) to elucidate whether phosphomimic substitutions in these sites affect BiP functions or conformations.

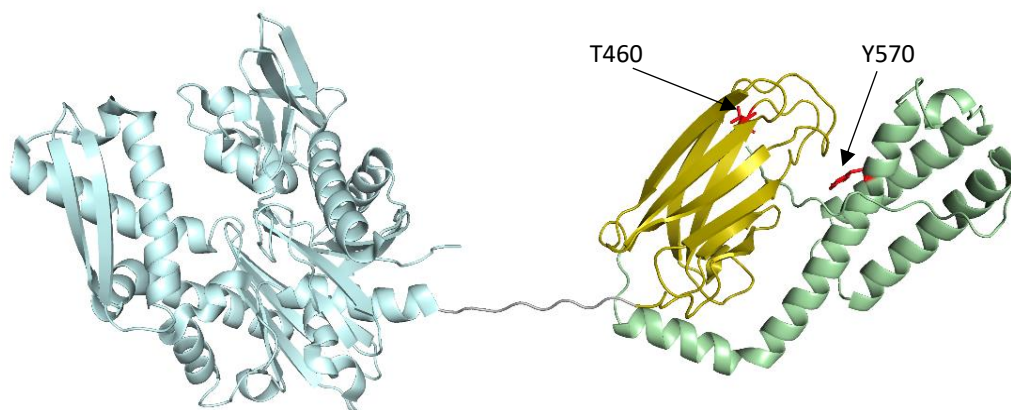


**Figure 41: phosphomimetic mutation location.** Cartoon representing the crystal structure (PDB code 5e85 and 6HA7) of BiP in domain undocked conformation colour coded with NBD (blue) SBD $\beta$  (yellow) and SBD $\alpha$  (green). Selected phosphorylation sites of the SBD $\beta$  T460 and SBD $\alpha$  Y570 displayed as red lines.

### 6.1 T460D and Y570D substitutions significantly increase ATPase activity.

Changes in ATPase activities are usually linked with either direct perturbations in the nucleotide binding site or mutation induced long range conformational changes affecting ATPase activity (42,178). Additionally, the level of activation in ATPase activity upon addition of BiP substrate provides information about whether the mutation affects substrate binding (chapter 4.2).

Due to the location of the mutation sites in the SBD, it was expected that the mutants were likely to alter substrate binding without necessarily affecting ATPase activity. In this case, one should expect that the mutants would have the same ATPase activity as the

WT BiP but a different level of ATPase stimulation in the presence of substrate. Surprisingly, the two phosphomimetic mutations in SBD showed the opposite effect, where the mutations result in significant increase in ATPase activity in the absence of peptide, with T460D possessing four times the ATPase activity of the wildtype and Y570D possessing two times the activity (Figure 42).

Furthermore, the addition of the CP2 model peptide further increases ATPase activity, suggesting that both variants bind the substrate (Figure 42). While this result does not exclude the possibility that the mutation induces small variations in substrate binding affinity, it indicates that perturbations in these SBD sites do not significantly perturb substrate binding to SBD but instead affect ATPase activity of the NBD. This suggests that the T460 and Y570 sites are likely to control chaperone functions through long range conformational changes in BiP rather than local effects in the SBD.

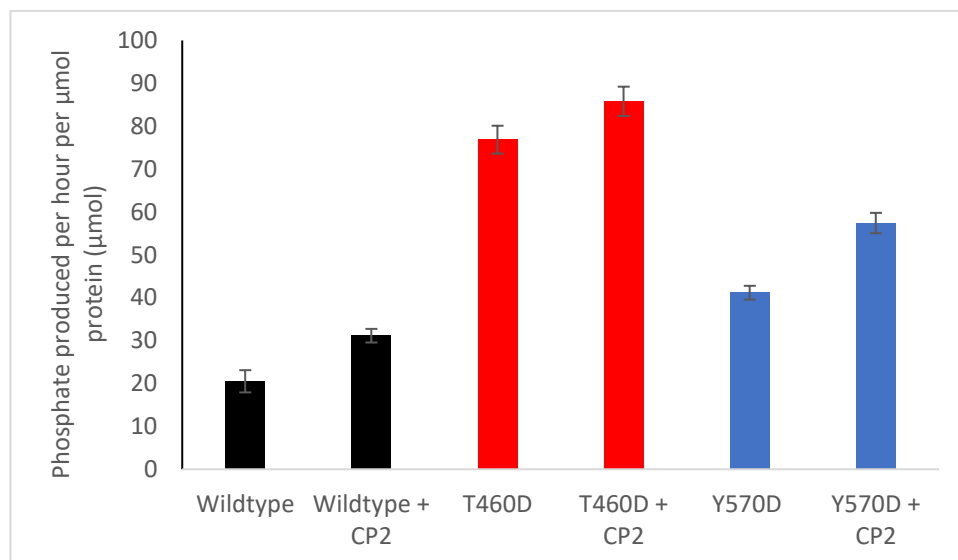


**Figure 42: phosphomimetic mutation increases BiP ATPase activity.** Malachite green ATPase assay displaying increased levels of ATP hydrolysis of phosphomimetic mutation compared to the wildtype BiP. Additionally, each mutant is shown in the presence and absence of 1 mM CP2.

## 6.2 T460D and Y570D substitutions perturb the conformational landscape of BiP.

As discussed in chapter 1.2.2, the BiP functions rely on transitions between two end point conformations driven by the binding of substrate and ATP hydrolysis. While ATPase activity directly controls the kinetics of this allosteric cycle, any perturbations in chaperone landscape, either by changing the equilibrium between the end point conformations or affecting structure of these conformations, can affect BiP functions. As the T460D and Y570D mutations may alter BiP functions through alterations to the conformation landscape of the chaperone, the study used the methyl NMR approach discussed in chapter 4.

First, the local (short range) effects of the mutations on the NMR spectra were investigated because peak position in an NMR spectra depends on the local magnetic field, which in turn is determined by the local chemical environment. This means an amino acid substitution alters the local chemical environment, resulting in changes in their peak position and intensity (186,187). As a result of mutation altering the local environment, all atoms located around the mutation site should be affected even if there are no long-range changes in protein structure and conformation induced by the perturbation. Indeed, there are 3 Ile methyl groups around (within 10 Å from) the T460D site in the domain undocked conformation and 4 Ile methyl groups in the domain docked conformation. Additionally, there are 3 Ile methyl groups and 2 Ile methyl groups around the Y570D site in either docked or undocked conformation respectively (Figure 43). Consequently, in the presence of ADP there are 3 and 2 peaks of the methyl NMR spectra that should be affected due to the local effects of the mutations for T460D and Y570D respectively. In the presence of ATP, due to the co-population of the two conformations, there are 7 and 4 peaks of the methyl NMR spectra should be affected due to the local effects of the mutations for T460D and Y570D respectively.

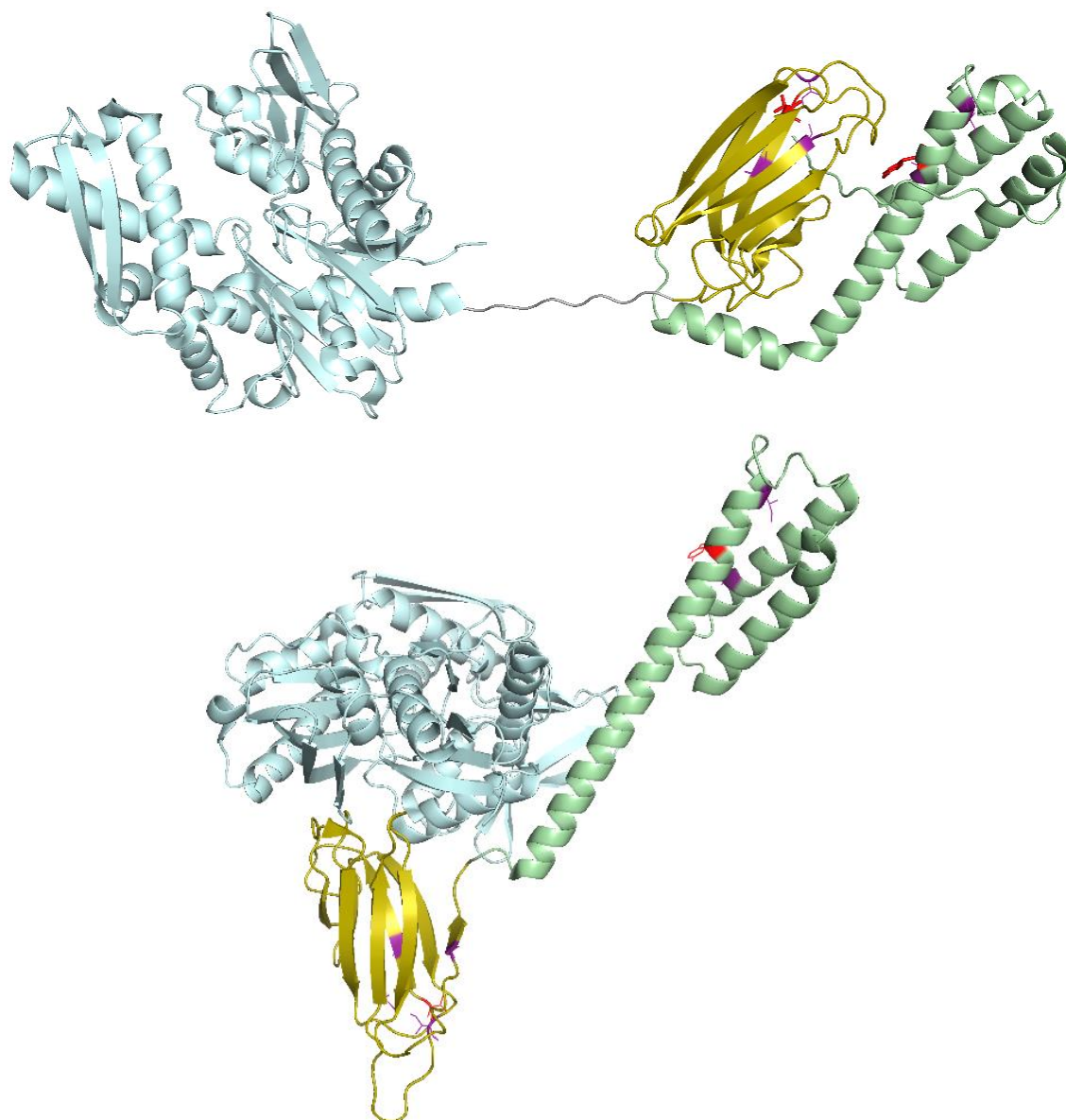


**Figure 43: Isoleucine residues in local environment of mutation sites.** A cartoon depicting the domain docked (PBD code 5e84) and domain undocked (PBD code 5e85 and 6HA7) conformation, with red displaying mutation location and purple displaying isoleucine within 10 Å of the phosphomimetic locations.

Overlaying the spectra recorded for either of the phosphomimetic mutants with the spectrum of WT BiP revealed changes in peak positions and peak intensities. Mutation resulted in only few peaks that were shifted, suggesting only local changes around the mutation site (Figure 44, 45). This displays the mutations do not alter the conformations that the proteins adopt.

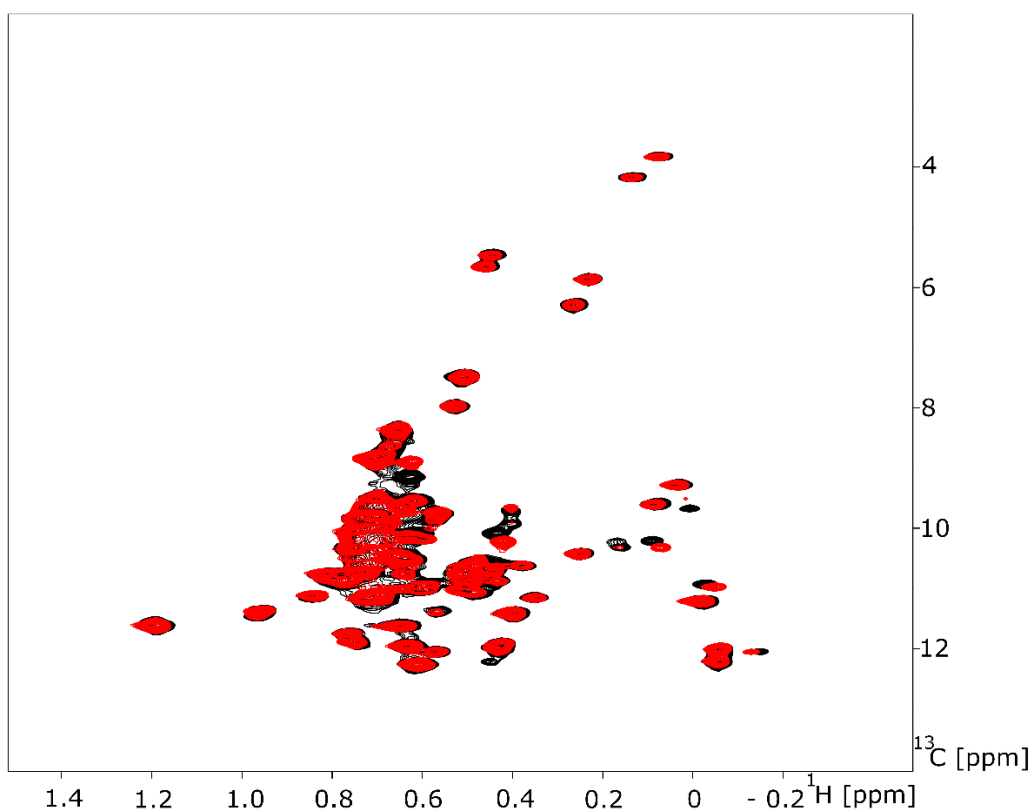
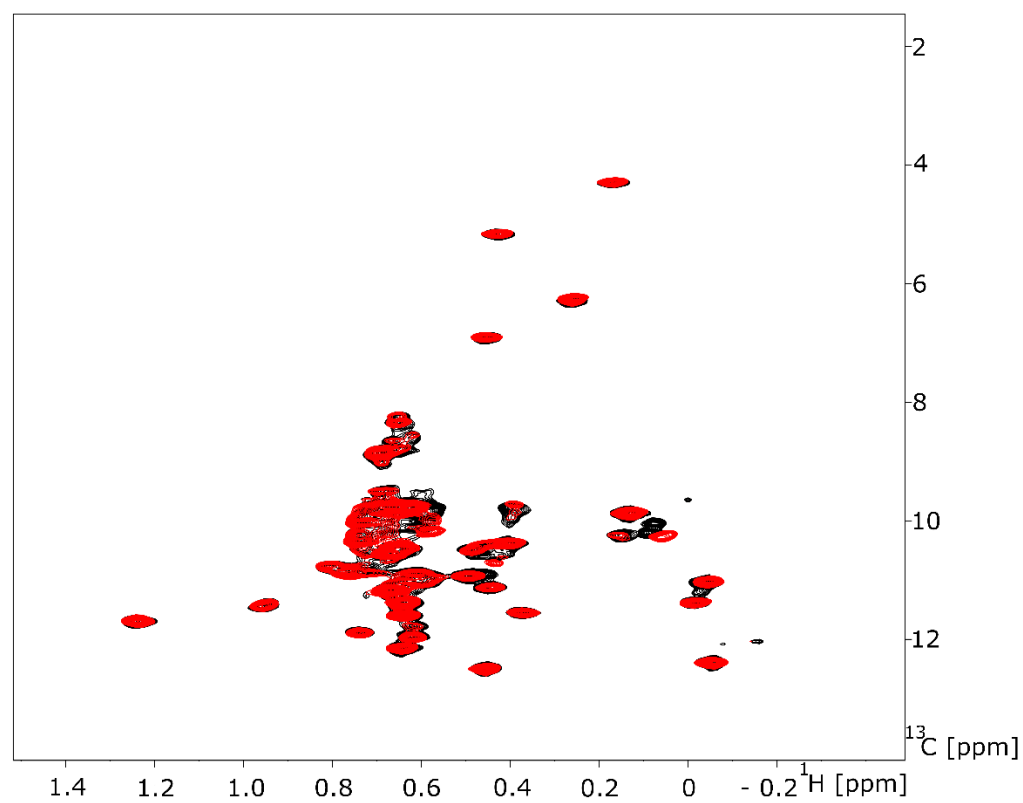


**Figure 44: Local effects of the T460D phosphomimetic mutations.** Overlay of the isoleucine region of methyl-TROSY spectra of full length human BiP T229G (black) and T460D T229G (Red) in the presence of either 5 mM ADP (top) or 40 mM ATP (bottom) recorded at 25 °C on a 750 MHz Bruker spectrometer.

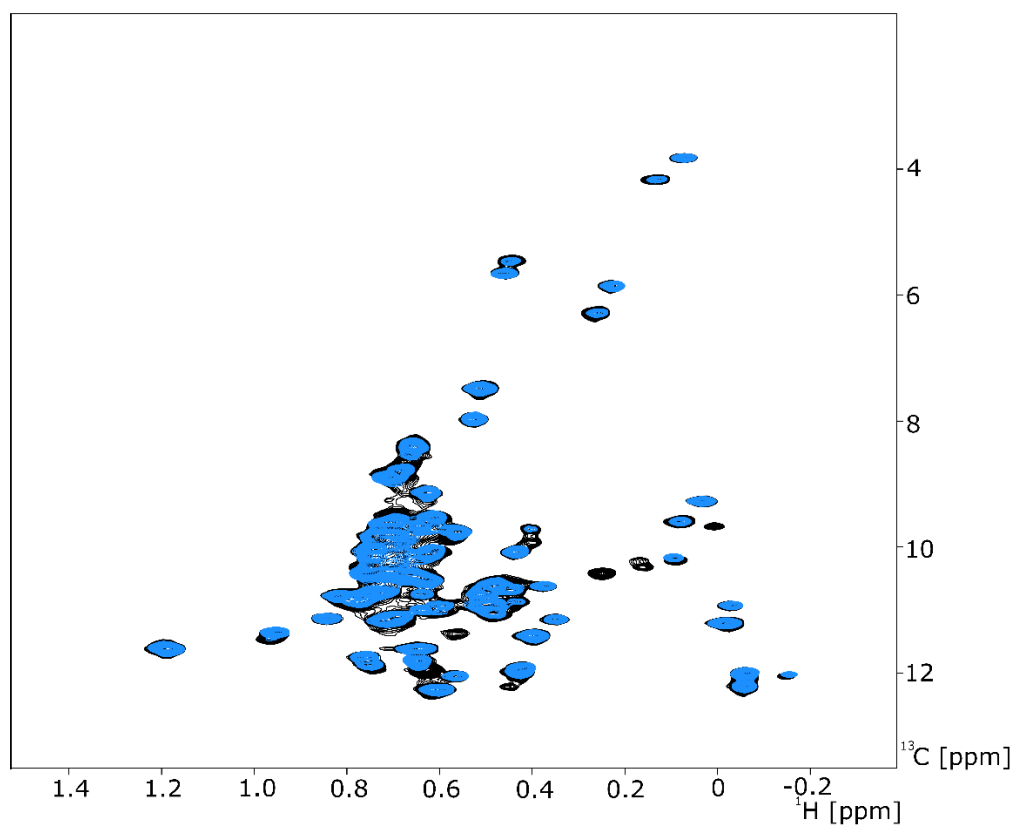
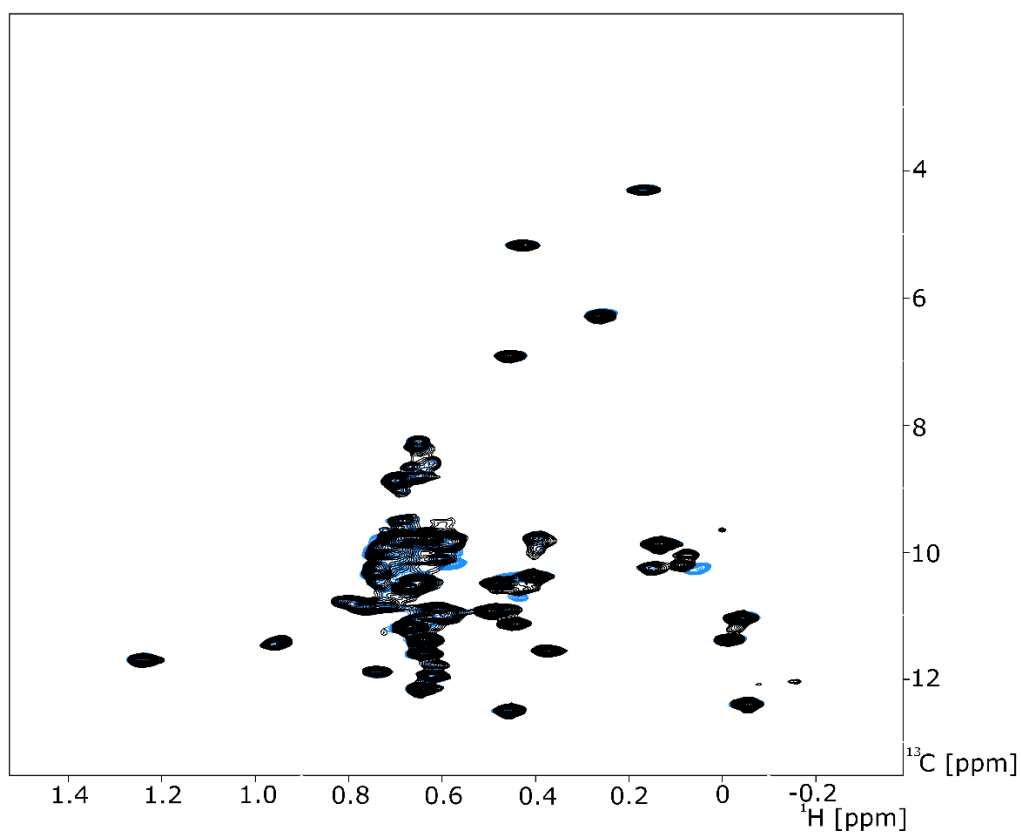


**Figure 45: Local effects of the Y570D phosphomimetic mutations.** Overlay of the isoleucine region of methyl-TROSY spectra of full length human BiP T229G (black) and Y570D T229G (Blue) in the presence of either 5 mM ADP (top) or 40 mM ATP (bottom) recorded at 25 °C on a 750 MHz Bruker spectrometer.

While the spectra showed minimal peak shifting, the peak intensities for the majority of peaks were significantly affected by either mutation. There was a significant (~ 10%) increase in intensities of peaks corresponding to the domain docked conformations (Figure 46), suggesting that both mutations favour domain docking. Moreover, for both mutations, the conformational shift toward the domain docked state occurs at the same extent (~ 10%) at 25 and 5°C (Figure 46), confirming that the T460 and Y570 sites control the population in the BiP conformational ensemble without significantly affecting structure of either conformation.

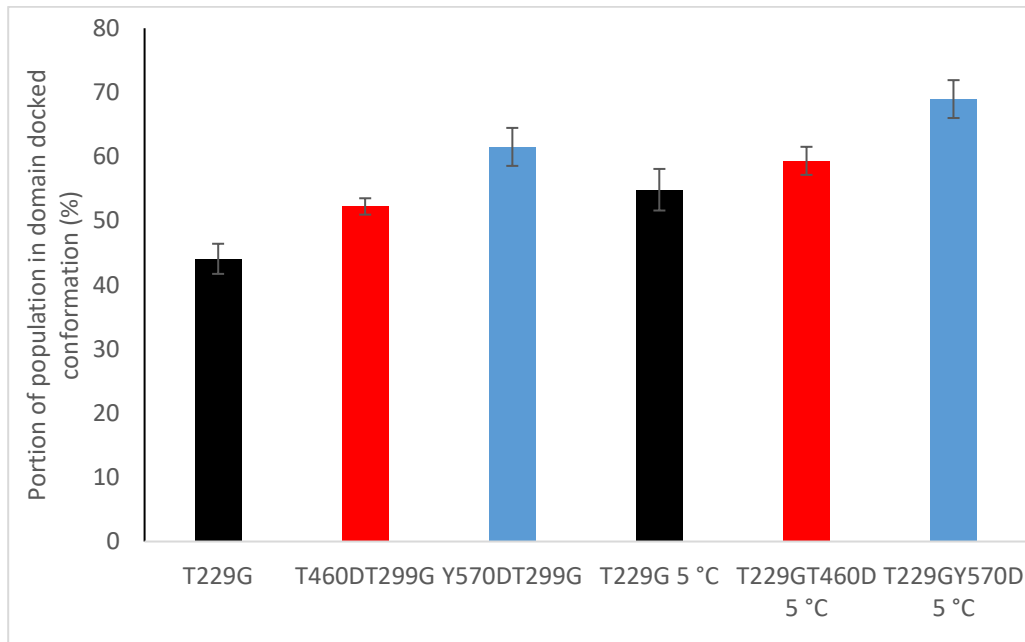
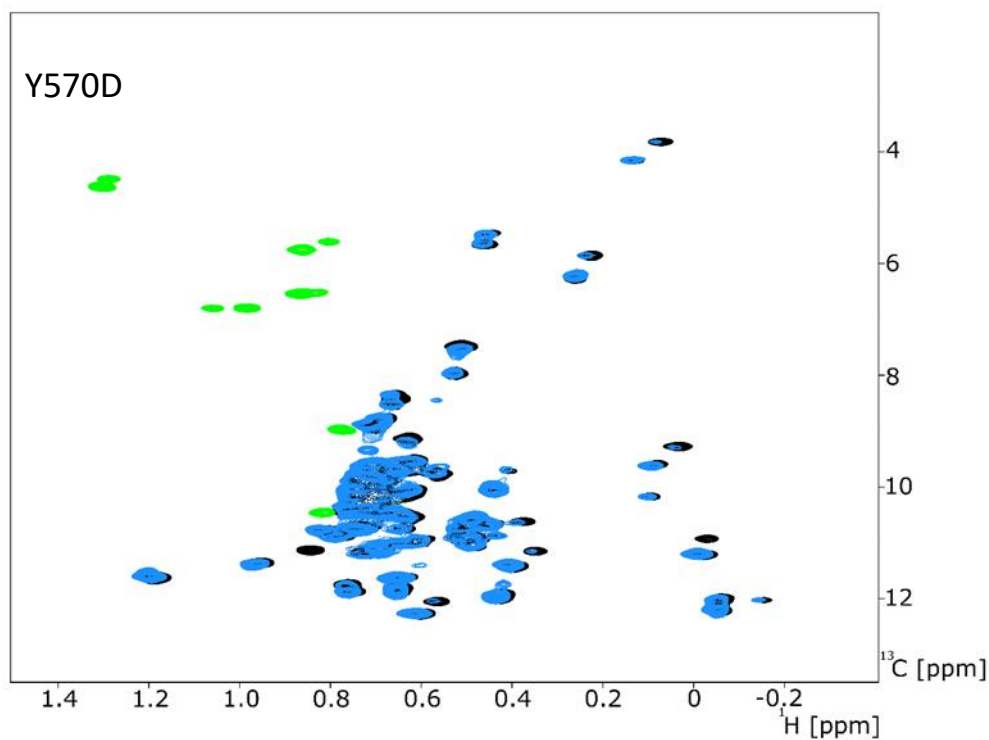
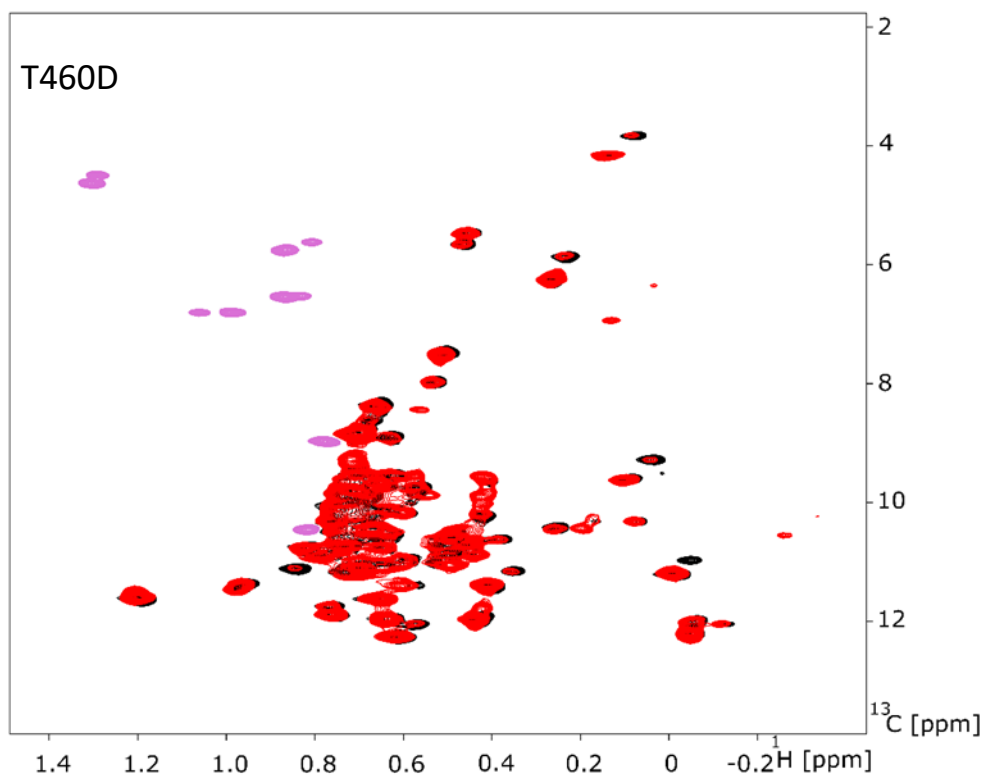


**Figure 46: Phosphomimetic mutations favour domain docked conformation.** Bar chart depicting percentage of domain docked conformation for the three doublet peaks calculated based on relative intensity of the peak of either T229G, T460D T229G or Y570D T229G mutant full length BiP at 25 °C or 5 °C. Standard error based on average peak intensity is used for error bars.

### 6.3 Phosphomimetic mutants are capable of binding substrate.

The ATPase data presented in chapter 6 suggested that the ATPases activity of the phosphomimetic mutants significantly increases in the presence of the model substrate, indicative of substrate binding. In order to validate these results, the study employed methyl NMR to monitor the substrate binding induced conformational changes in the phosphomimetic variants. Addition of the model peptide CP2 to the ATP bound T460D and Y570D variants resulted in stabilization of domain undocked conformation; the effect (25 % shift towards the domain undocked conformation) was comparable with the effect of CP2 binding to WT BiP (Figure 47,48). This combined with the previous ATPase data suggests that the phosphomimetic mutants are able to bind substrate and transmit the allosteric signal between domains like the wildtype chaperone.



Black = phosphomimetic mutant in presence of peptide  
 Red or Blue = phosphomimetic mutants

**Figure 47: Phosphomimetic mutations display signs of binding.** Overlay of the isoleucine region of methyl-TROSY spectra of full length human BiP T460D T229G in the presence of 40 mM ATP (red) with full length human BiP T460D T229G in the presence of 40 mM ATP and 1 mM CP2 (black) recorded at 25 °C on a 750 MHz Bruker spectrometer. Overlay of the isoleucine region of methyl-TROSY spectra of full length human BiP Y570D T229G in the presence of 40 mM ATP (blue) with full length human BiP Y570D T229G in the presence of 40 mM ATP and 1 mM CP2 (black) recorded at 25 °C on a 750 MHz Bruker spectrometer.

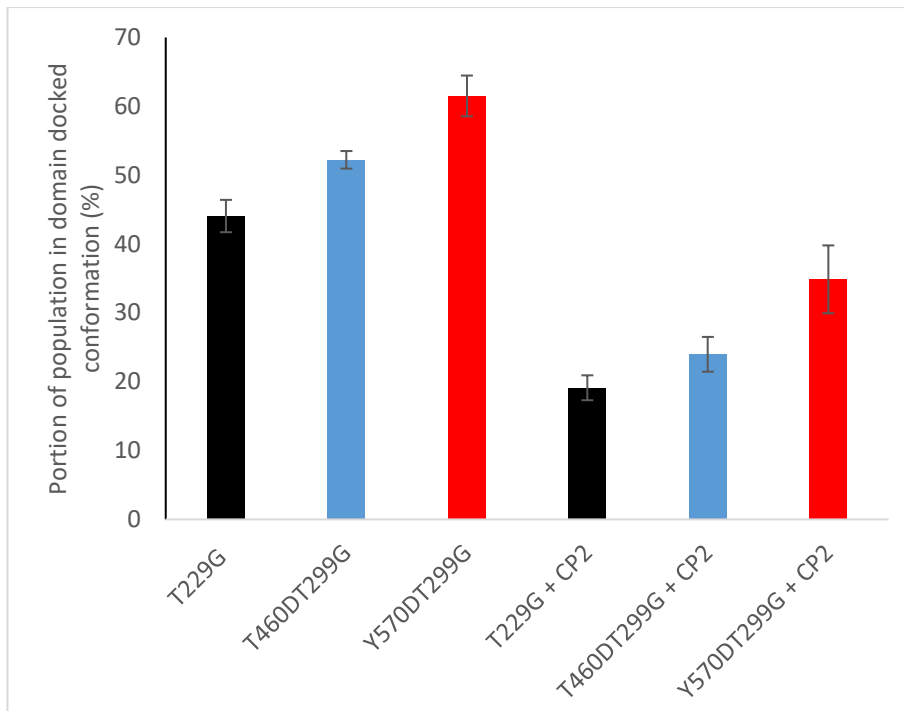


**Figure 48: Phosphomimetic mutations display signs of binding.** Bar chart depicting percentage of domain docked conformation for the three doublet peaks calculated based on relative intensity of the peak.

#### 6.4 Phosphomimetic mutations decrease BiP's ability to deoligomerize IRE1-LD

To further assess the effects of the phosphomimetic mutations on BiP functions, the study employed the IRE1-LD deoligomerization assay described in chapter 5. It is important to note that it has been demonstrated previously that ATPase activity and substrate binding is essential for BiP driven IRE1-LD deoligomerization (unpublished, personal communication), with the ATP deficient T229G mutant and the V461F mutant that is deficient for substrate binding displaying no ability to deoligomerize IRE1-LD (114,188).

As described previously (Chapter 5), in the presence of ATP, wildtype BiP results in solubilization of the majority (> 80%) of IRE1-LD oligomers that formed upon addition of 200  $\mu$ M of the model dESP peptide. While T460D and Y570D BiP variants result in IRE1-LD deoligomerization, the effect is significantly (~ 30-35 %) smaller compared to the wildtype (Figure 49). This suggests that perturbations in these sites fine-tune BiP ER specific activity, such as its ability to deoligomerize the stress induced IRE1-LD oligomers. Gels displaying deoligomerization of IRE1 are in appendix (appendix Figure 19, 20 and 17).

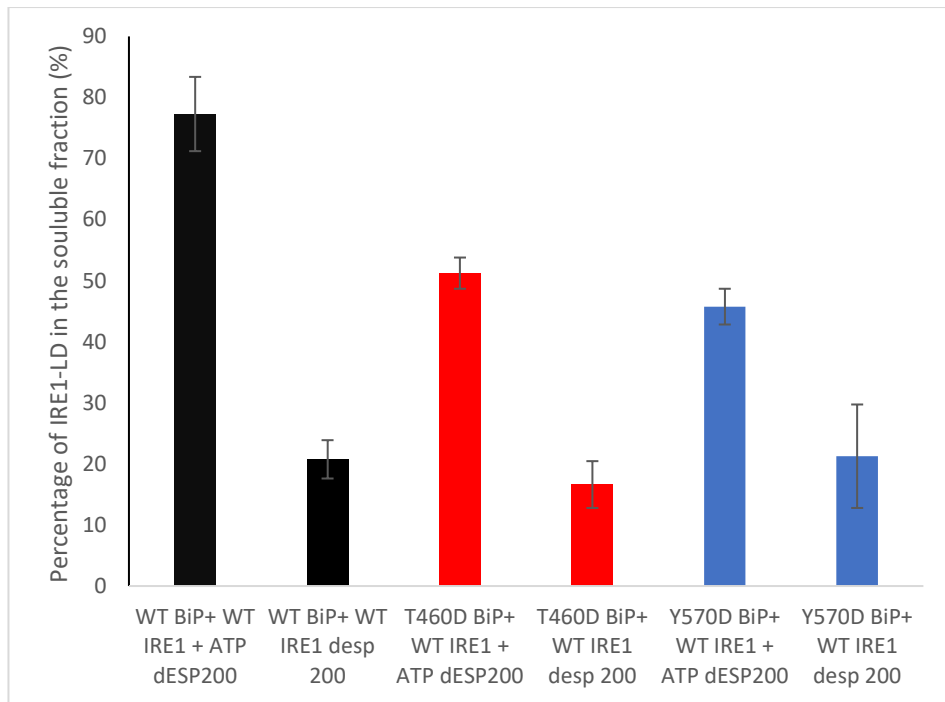


**Figure 49: Phosphomimetic mutations display a decreased ability to deoligomerize IRE1-LD.**

A bar chart depicting the percentage of either wildtype IRE1-LD sample in the presence of 200  $\mu\text{M}$  and the addition of 2  $\mu\text{M}$  BiP, 2  $\mu\text{M}$  BiP plus 40 mM ATP. Three forms of BiP (wildtype, T460D and Y570D) were used during this assay to assess their ability to deoligomerize the IRE1-LD

To test whether this decrease in portion of IRE1-LD in the soluble fraction is due to alteration in the chaperone deoligomerization ability and not due to a reduction in their ability to bind IRE1-LD, the study employed the methyl NMR binding approach (discussed in chapter 4) to determine if Y570D BiP is capable of binding the IRE1 derived peptide P3<sup>IRE1</sup> (discussed in chapter 5). Similarly, to the WT BiP, the addition of P3<sup>IRE1</sup> to ATP bound Y570D BiP results in 25 % shift in conformational equilibrium towards the domain undocked conformation (Figure 50), suggesting that the Y570D mutation doesn't affect BiP's ability to bind IRE1-LD. Full spectra of Binding displayed in appendix (appendix Figure 13).

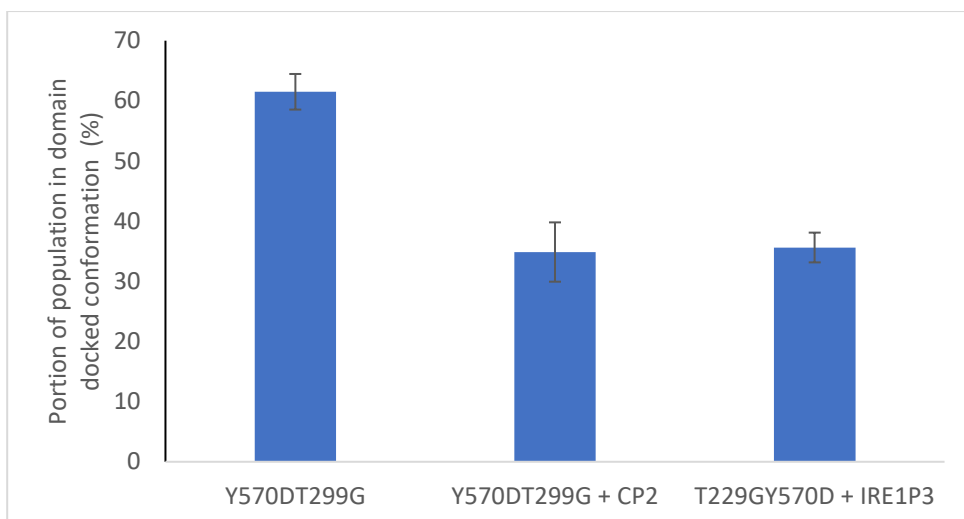


**Figure 50: binding assessment through methyl NMR of Y570D ability to bind IRE1.** A bar chart depicting average proportion of population of doublets in domain docked conformation for the Y570D BiP in the presence and absence of 1 mM CP2 or 50  $\mu$ M IRE1P3. Standard error based on average peak intensity is used for error bars.

The two T460D and Y570D phosphomimetic mutations have both displayed consistent effects: increasing its ATPase activity, favouring domain docking, as well as fine tuning BiP's ability to deoligomerization of the ER stress sensor IRE1. Importantly, perturbations in these sites do not switch the chaperone off, but rather gently adjust its functions through adjusting kinetics (via changes in ATPase activity) and thermodynamics (via affecting the conformational equilibrium) of the BiP allosteric cycle.

## Chapter 7: Discussion

### 7.1 Paralog specific conservation patterns as a tool to guide experimental design.

The study was able to generate organelle specific sets of Hsp70 sequences, which were then used to produce conservation patterns for ER and cytoplasmic located Hsp70s. This analysis allowed identification of the regions in the Hsp70 sequence that have unique, organelle specific conservation patterns and evolutionary rates. This information was further used to select and experimentally characterise phosphorylation sites that are unique for the ER located Hsp70s. Particularly, two ER unique phosphorylation sites, T460 and Y570, were identified from 51 previously reported BiP phosphorylation sites (160), enabling the detailed experimental characterization of how these perturbations fine tune Hsp70s conformation and functions.

This was a vital tool in the selection of phosphorylation sites, but this was not the sole information provided by this data set. Through the analysis of subdomains and known key functional regions, the study was able to draw multiple conclusions that increased the understanding of ER specific conservation in the ER family. For example, the current notion of the NBD being more conserved than the SBD within Hsp70 (189,190), was displayed to be accurate, although not entirely true with the SBD $\beta$  being more conserved than the NBD. This is of note as the increased number of ER uniquely conserved residues is likely linked to known ER unique specificity for substrates or ER unique functions linked to the SBD $\beta$  (60). This notion is further confirmed by the identification of four ER unique residues within the regions that interact with substrate (3 new and 1 previously identified).

Despite the use of the data to select phosphorylation sites for further study and identification of key regions of conservation, the study has only scratched the surface of the true potential of this data set as a tool to guide experimental design. The most promising potential application of the conservation analysis is undoubtedly as a tool to aid the study of Hsp70s as a target for drugs. Hsp70s have emerged as a target for drugs over the last couple of decades in particular (191–193), as Hsp70s have been linked to multiple disease states due to its critical functions in protein homeostasis (1,29). This has led to a large amount of research into drugs targeting Hsp70s and related co-chaperones, typically as inhibitors of Hsp70 functions, for conditions including cancer (194,195), liver fibrosis (196) and haematological diseases (197).

Interestingly, in recently years subcellular specific Hsp70 targets have emerged as a potential route for improving the effectiveness of any theoretical treatments. Due to Hsp70 role in stabilizing cancer cells, Hsp70 inhibitors have emerged as a target for cancer treatments (198). The variation of which Hsp70s inhibitors are administered alongside cancer treatments have been suggested to improve cancer treatment

effectiveness when the inhibitor is selected to target specific Hsp70s. It has been demonstrated that calibrating Hsp70 inhibitors for individual cancers and combination therapies in response to the variations in Hsp70 (e.g., between Hsp70, hsc70, Grp78) has been suggested to improved the patient's prognosis of cancer treatments. This is thought to be due to variations in subcellular localization, co-chaperones, and affinity for binding substrates as well as other factors, resulting in altered interactions for different Hsp70 inhibitors (199). This displays the potential in targeting specific Hsp70s, theoretically based on subcellular location, to improve the effectiveness of Hsp70 based drug treatment. This is in addition to how relatively minor differences in analogues of Hsp70 inhibitors drastically effect subcellular localization (200), displaying the possibility to target specific Hsp70 via sub-cellular localization target drug design. This suggests that subcellular specific Hsp70 treatment targeting is a potential avenue for research going forward.

Currently, new research is suggesting there is great potential of using sequence-based drug design (201) over traditional structural based drug design (202), and it is this subcellular specific Hsp70 treatment targeting research in which the conservational analysis could best be applied. Current research has been developing approaches to analyse sequences and conservation in order to aid drug designs (201,203), such as the DeepTarget an end-to-end DL model ((204) , ECOdrug (205) or TransformerCPI2.0 (201). These are all sequence analysis-based drug design-based tools which serve to predict binding pockets, including orthosteric sites or allosteric sites allowing drug design to be targeted the predicted significant sites (201). The addition of conservation analysis alongside this sequence analysis could provide an the could provide an additional layer of data to this avenue of research, allowing the targeting of regions based not only on software sequence prediction but also on the family conservation patterns that this study generated. From here it is thought targeting drugs to highly conserved predicted binding pockets or allosteric sites would be possible.

The bioinformatic analysis in this study has already located sites which could potentially be uniquely druggable for ER or cytoplasmic Hsp70s. For example, the study was able to identify four variations in the binding pocket (chapter 2.4), that were uniquely conserved within the ER. If one designed drug based on these unique features, it would potentially allow a drug to precisely target either cytoplasmic or ER Hsp70s. This could lead to better responses to treatment as shown in previous cancer treatments (199). This is a possible avenue of drug design as it is known that single amino acid variation can alter BiP interactions with antigens (206), ligands (207) and even known drugs (208).

There is also the potential to expand the analysis to include a mitochondrial Hsp70 set or apply the data to Hsp70 co-chaperones and the Hsp90 family, to expand the understanding of the Hsp70 quality control network. This would be a simple addition to the data set that would provide greater insights into Hsp70s by analysing more of Hsp70

or transitioning the analysis to focus on a second family of proteins (Hsp90, ERdjs, NEF) which is known to interact with Hsp70 (209).

This data set provided the study with an effective method of selecting phosphorylation sites which was invaluable for this research. As discussed, this is only scratching the surface of the true potential of this data set, with uses in drug design as well as in BiP research. The analysis of ER and cytoplasmic Hsp70 conservation is simply a versatile tool that can serve to aid in a huge amount of potential research of the molecular chaperone family as it did for this study.

## 7.2 The allosteric fine tuning of BiP through phosphorylation

This study provides detailed characterization of how phosphorylation in two ER unique sites, T460 and Y570, affect the BiP allosteric cycle and its functions, including its ability to deoligomerize the stress sensor IRE1. Despite both of these phosphorylation sites being located within the SBD, neither of the two result in significant perturbations in substrate binding. The variations in BiP instead result in the allosterically controlled alterations to ATPase activity (associated with the NBD) as well as favouring the domain docked conformations. Not surprisingly, this alteration of ATPase activity that controls the kinetics of the chaperone cycle and shifting the conformational equilibrium in the chaperone landscape, affects BiP ER specific activity, fine tuning the ability of BiP to deoligomerize the stress sensor IRE1-LD.

Several examples of how PTM can control Hsp70 activity have been reported to date. It has been previously suggested that the phosphorylation of BiP results in the transition of the protein to an inactive oligomeric form (147), likely due to favouring its domain undocked conformation (chapter 1.2.2). Similarly, phosphorylation of T66 allosterically disrupts domain docking and favours the domain undocked conformation, even in the presence ATP (210). This is opposite to the effect of AMPylation of T518 which causes BiP to favour the domain docked conformation even in the presence of ATP (157). These two examples display the potential for PTMs to reversibly switch the chaperone off by predominantly stabilizing either the domain docked or the domain undocked conformation regardless of which nucleotide bound state the chaperone has adopted and thus uncoupling ATP binding from the conformational transitions.

Perturbations in T460 and Y570 due to the introduction of the phosphomimetic mutations, however, have significantly more subtle effect than these other PTMs. Instead of a drastic on off effect, these sites enable fine tuning of BiP activity through altering both kinetics and thermodynamics of its chaperone cycle, providing an additional level of regulation, that is similar to interactions with co-chaperones and evolutionary fine tuning (discussed in chapter 1.4.2 and 1.4.3). This is in keeping with previous studies' observations which has demonstrated that the chaperone cycle and

activity of BiP and other Hsp70s can be gradually fine tuned by perturbations in its allosteric hotspots located at the interdomain interfaces (36,42,43,46). This leads to the question on how the perturbation to the SBD due to the amino acid substitution trigger this fine tuning of the chaperone, with the cause of this effect likely being different between the two sites due to their location but resulting in the same mechanism of regulation.

The T460D mutant is located in the SBD $\beta$  near the residues V461 and T518 (Figure 51). Interestingly, the residue V461 located in the same region has been previously shown to be a key residue in the SBD $\beta$  that regulates substrate affinity (58). The V461F substitution (Figure 51) is known to drastically decrease protein substrate affinity in the higher affinity ADP bound state of the chaperone (58). The V461F substitution in BiP and its equivalent in bacterial Hsp70 DnaK V436 results a drastic decrease in substrate affinity that can be potentially explained by blocking the central hydrophobic pocket of the substrate binding cavity by phenylalanine group (39,58,211). The larger amino acids R group blocking the substrate binding pocket is not thought to result in domain rearrangements, this allosteric effect of V461F is reminiscent to the effect of AMPylation of T518 (157). Both the AMPylation of T518 and V461F substitution 'trap' the chaperone in the domain docking conformation regardless of its ligand binding state (46,148,157). This leads to the decrease in substrate binding affinity upon the V461F substitution, and AMPylation is due to the predominance of the domain docked conformation that has drastically lower substrate binding affinity than the domain undocked state (with the undocked state being normally populated in the absence of ATP). This is in addition to the same SBD $\beta$  region that has been previously suggested be important in bacterial Hsp70 DnaK for allosteric signal transition from the substrate binding cleft to SBD $\beta$  NBD interdomain interface (36), suggesting this part of Hsp70 SBD is a key 'allosteric' hotspot that regulates domain docking through fine tuning SBD $\beta$  conformation. This is in full agreement with the fact that the effect of the T460D substitution is relatively subtle, as it results in relatively gentle adjustments in the allosteric cycle but does not completely deactivate BiP, enabling its regulation by ATP and substrate binding. This hotspot contains all discussed residues, T460, V461 and T518 (Figure 51) suggesting a significance of the region for BiP regulation.

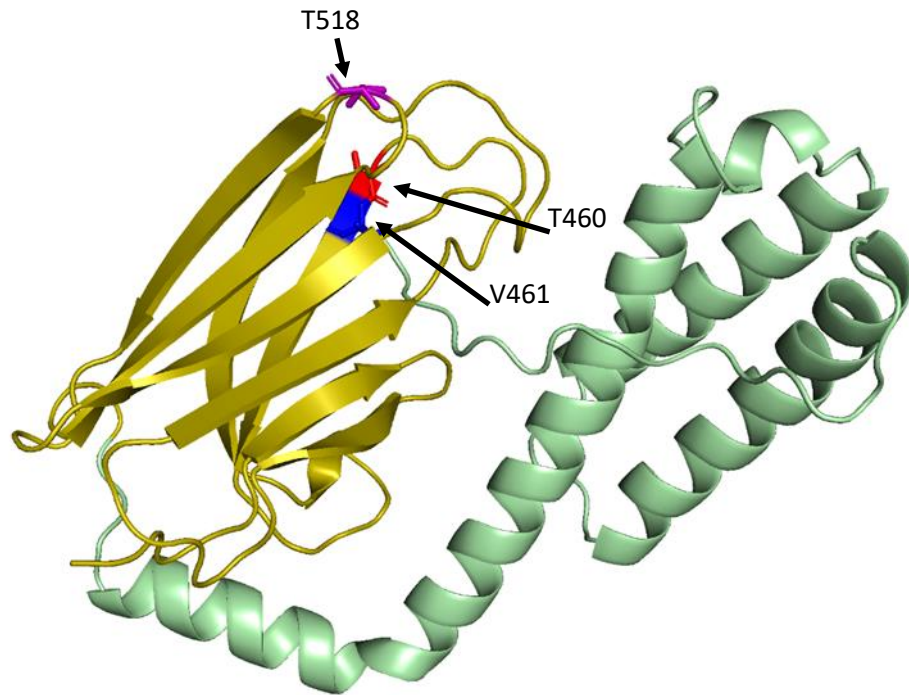


**Figure 51: V461F and T518 position in relation to the phosphomimetic mutation site T460D.**  
 A cartoon depicting the crystal structure (PDB code 58E5) of BiP's SBD coloured coded with SBD $\beta$  (yellow) and SBD $\alpha$  (green) with the T460 (Red), V461 (Blue) and T518 (purple) displayed as sticks.

The second phosphorylation site Y570D is located at the SBD $\alpha$  SBD $\beta$  interface. This interface is stabilized by six conserved ionic contacts (Figure 52) between the subdomains which have been identified in DnaK (212). The residue Y570 is located in the middle of this region (Figure 52) and an introduction of negative charge in this region is likely to disrupt these ionic interdomain contacts. The interactions between SBD $\alpha$  and SBD $\beta$  play a key role in the domain rearrangement, with the destabilization of SBD $\alpha$  SBD $\beta$  contacts causing the chaperone to favour domain docking, while the stabilization of the ionic contacts causes a shift in the equilibrium toward the domain undocked state (36,42,46,213). This is in full agreement with the data presented on the Y570D mutation. Moreover, similar to the T460D substitution, perturbations in the T570 site result in fine tuning of the chaperone cycle with it favouring the domain docked conformation, while the chaperone activity can be still regulated by ATP and substrate binding.

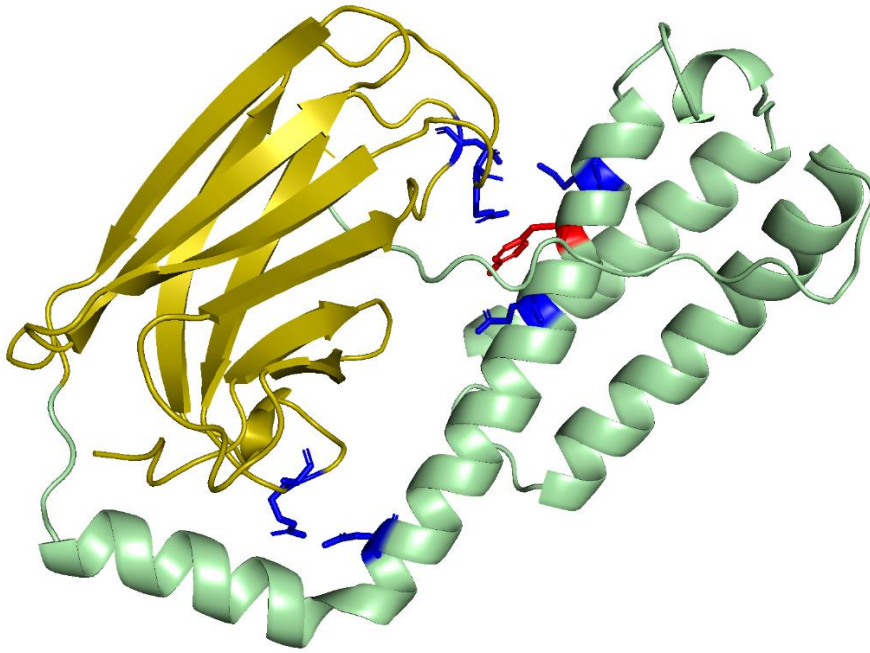


**Figure 52: Y570D location between the ionic contact point.** A cartoon depicting the crystal structure (PDB code 58E5) of BiP's SBD coloured coded with SBD $\beta$  (yellow) and SBD $\alpha$  (green) with the Y570 (Red) and residues which form the ionic contact points (Blue) displayed as sticks.

Perturbations in both phosphorylation sites not only favour the domain docked conformation, but also affect ATPase activity of the chaperone. An increase in ATPase activity of Hsp70 by perturbations in the allosteric hotspots that control interdomain interactions has been previously observed (42), in that case the increase being attributed to the population of the transient intermediate state that is structurally and functionally distinct from either domain docked and undocked conformations (42). Conformational analysis through the use of methyl-TROSY NMR of bacterial Hsp70 DnaK shows the existence of a transient intermediate state, in which the SBD is undocked from NBD but the interdomain linker (IDL) is still docked to the NBD. In this this conformation, the IDL interacts with  $\beta$  strand of subdomain IIB of NBD (42), resulting in rearrangements in the NBD conformation essential for efficient ATP hydrolysis. This transient ATPase active conformation is populated upon substrate binding (42,45,214), upon perturbations in the allosteric hotspots (interaction with J-domain proteins to raise ATPase (215) or AMPylation to decrease basal ATPase activity (148) that control domain rearrangements in Hsp70 (46) enabling decoupling of substrate binding from ATPase activation in these variants.

However, whilst both T460D and T570D substitutions results in increase in ATPase activity in the absence of substrate, substrate binding results in further activation. This effect is reminiscent to J-domain co-chaperone binding to Hsp70 (chapter 1.4.3), suggesting that both substitutions have a similar mechanism of ATPase activation. While in the absence of co-chaperone the ATPase active IDL bound conformation is only

transiently populated. This however changes when the chaperone interacts with the J-domain co-chaperones (ERdjs) where the co-chaperone stabilizes these transient interactions slightly more, resulting in the gradual and controllable fine-tuning ATPase activity (215,216). This study speculates that the T460D and T570D BiP variants have the same mechanism; they allosterically stabilize these transient IDL NBD interactions in BiP, stimulating chaperone ATPase activity. In turn, the linker NBD interaction is not only important for ATPase activity but also prerequisite for domain docking and, thus, even minor stabilization of this transient state is likely to result in increase in the population of the domain docked conformation, in agreement with experimental observations for these variants (Figure 53).

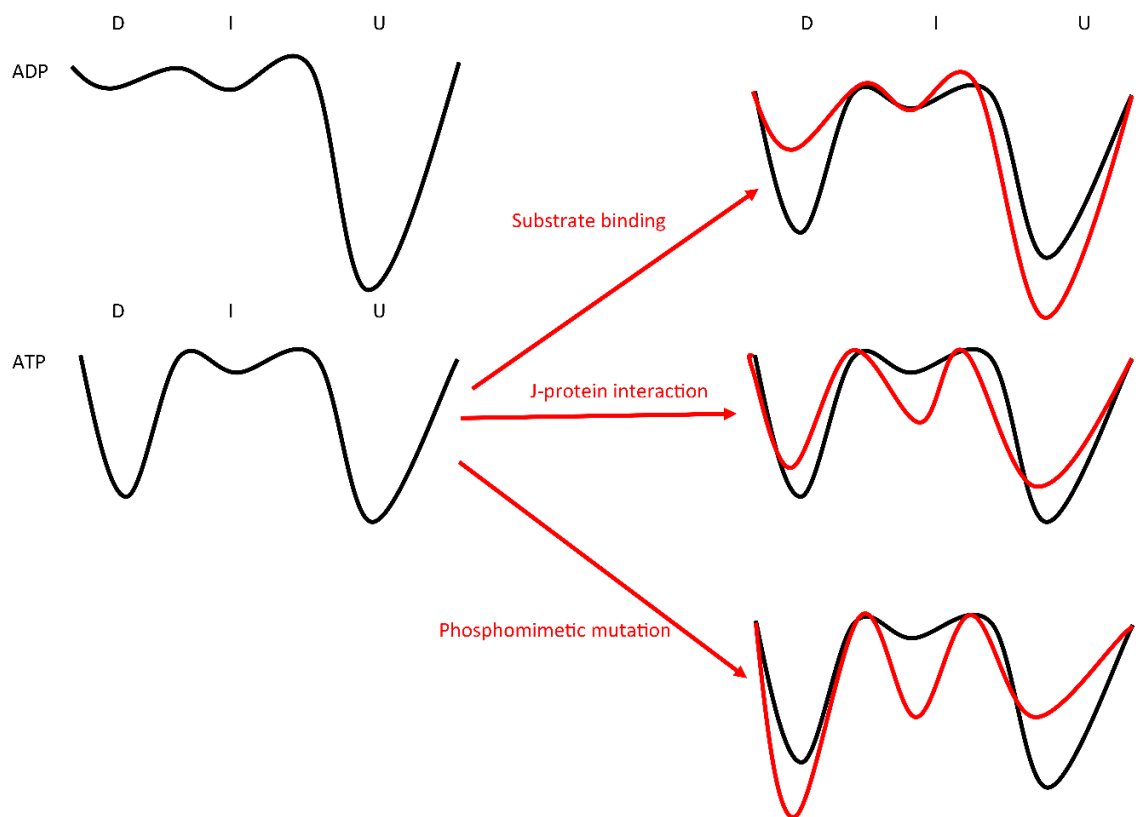


**Figure 53: stabilization of transient intermediate conformations.** The unique features of the BiP conformational landscape (domain docked (D), intermediate domain undocked linker bound (I), and domain undocked linker unbound (U)) of BiP in the presence of ATP and the shift in the conformational landscape induced by either substrate binding, J-protein interaction, or the proposed shift in Phosphomimetic mutation.

The analysis of both phosphomimetic mutants displays that both mutants have a similar allosteric mechanism by which they fine tune chaperone activity through kinetic and thermodynamic alterations in its allosteric cycle. These results suggest that the phosphomimetic mutations (and potential phosphorylation in these sites) relies on the

same (or similar) mechanism that, however, is triggered by perturbations in different allosteric hotspots that control SBD $\beta$  conformation (the T460 site) or SBD $\beta$  SBD $\alpha$  interactions (the Y570 site).

### 7.3 Functional importance of the T460 and Y570 sites

While the results discussed in the previous chapters clearly demonstrate that introduction of phosphomimetic mutations to both the phosphorylation sites enable controlling of the BiP allosteric cycle, it does not provide evidence that the effects of the perturbation are in any way physiologically significant. To address this lack of understanding of physiological significance, the study investigated the effect of perturbations in these sites on interactions between BiP and the stress sensor IRE1-LD (chapter 1.3.3). Previous results from our lab (Manuscript in preparation) suggest that IRE1-LD binds to BiP as a 'classical' chaperone substrate under control of ATP binding and hydrolysis, as an ER specific function of BiP. For these reasons, BiP induced deoligomerization of IRE1-LD has been chosen in this study as a tool to assay BiP activity *in vitro*.

While direct interactions between BiP and IRE1-LD have been suggested in a number of studies (chapter 1.3.3 (28)), the exact BiP binding site on IRE1-LD has remained elusive (111). The majority of studies have employed the use of deletion mutants to display the significance of IRE1-LD in the binding of BiP. Particularly, deletion mutations in the region 448 to 517 display a loss of BiP binding via western blot analysis (217). A more recent study from the laboratory of Professor Ron has identified the importance of the disordered regions in IRE1-LD, particularly loop structure (residues 308-357) and a C-terminal tail (residues 391-444), for IRE1-LD interactions with BiP (95); however, no precise site of this interactions has been identified. Despite being a common approach to delete regions of a protein in order to elucidate its binding sites (218), the deletion or mutation of a functionally or structurally important part of a protein might have unknown effects on the protein, such as changes in protein structure and stability that could disturb binding rather than direct perturbations of the binding site.

This study employed a divide and conquered approach to tackle this problem. First, the study used methyl NMR to identify two IRE1-LD derived peptides <sup>310</sup>GSTLPLL<sup>317</sup> and <sup>356</sup>RNYWLLI<sup>362</sup>, followed by perturbations of the identified regions in the full length IRE1-LD. Both peptides were derived from the previously suggested disordered IRE1-LD regions (95) that have been suggested to be essential for BiP binding. This allowed the study to precisely identify the two binding sites of BiP on IRE1-LD. Moreover, the perturbations of either of these sites in the full length IRE1-LD does not prevent BiP's ability to deoligomerize IRE1-LD, but only reduces it. Consequently, perturbations of either of these regions is insufficient to completely abolish BiP induced deoligomerization and can be partially compensated for by other BiP binding sites. Serving to further confirm that both sites are in fact the BiP binding sites. In addition to

this, the mere existence of two sites does raise the possibility of multiple existing sites, with this study only identifying two out of a potentially larger number of possible binding sites.

While no experimental high-resolution structure is currently available for these disordered regions (85,86,95), <sup>310</sup>GSTLPLL<sup>317</sup> and <sup>356</sup>RNYWLLI<sup>362</sup> are located closed to each other on the predicted alpha fold structure (Figure 54). This shared location of the two identified sites narrows down BiP binding to the previously identified loop structure (95) and furthermore precisely identifies the exact sections of the loop in which BiP can bind.

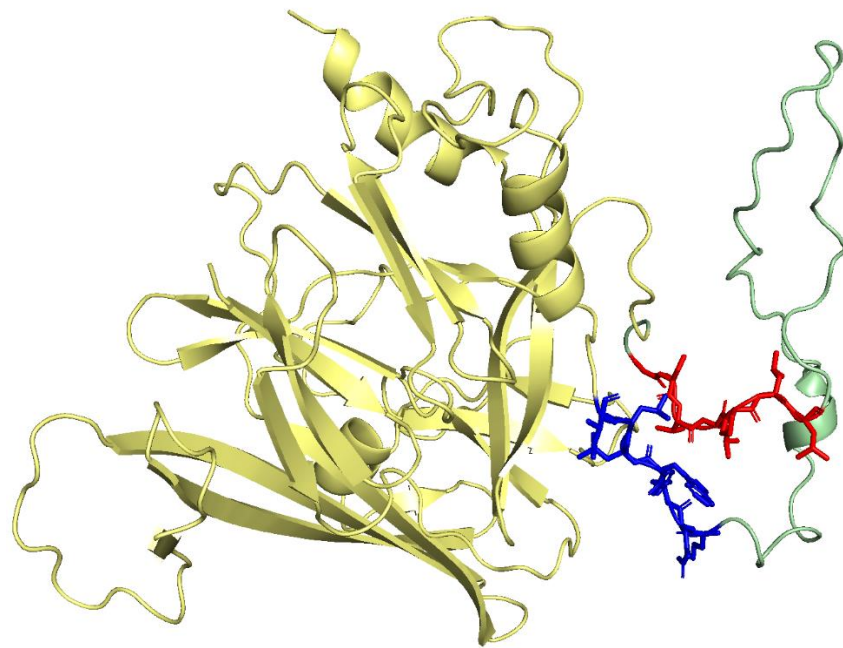


*Figure 54: Locations of two identified IRE1 binding sites. Alpha fold predicted structure of IRE1-LD (identifier AF-O75460-F1). The two identified BiP binding site <sup>310</sup>GSTLPLL<sup>317</sup> (red) <sup>356</sup>RNYWLLI<sup>362</sup> (blue) located in the disordered loop (green).*

Intriguingly, both <sup>310</sup>GSTLPLL<sup>317</sup> and <sup>356</sup>RNYWLLI<sup>362</sup> regions have previously been noted to be significant in IRE1 activation, with mutation to the <sup>312</sup>TLPL<sup>315</sup> and <sup>352</sup>LNYL<sup>356</sup> regions impairing the IRE1-ID oligomer formation and <sup>359</sup>WLLI<sup>362</sup> and <sup>352</sup>LNYL<sup>356</sup> displaying impaired XBP1 mRNA splicing in mammalian cells (102,219). This displays that this region is vital in not only BiP interactions but also IRE1-LDs ability to oligomerize (220), suggesting a possible mechanism in which BiP interferes with the IRE1 activation process. This could particularly occur during dynamic interactions between the chaperone and IRE1-LD oligomers near the oligomerization interface whereby BiP presence destabilizes IRE1s intermolecular contacts. This therefore would result in the deoligomerization of IRE1-LD oligomers, observed experimentally in this study.

The process by which BiP interacts with IRE1-LD requires ATP that drives interconversions between domain docked and domain undocked BiP conformations that, in turn, enables controllable binding to, and release from IRE1-LD oligomers. Surprisingly, despite the mutants possessing the ability to bind substrate and hydrolyse ATP, the perturbations of the kinetics and thermodynamics of the BiP chaperone cycle induced by phosphomimic mutations in T460 and Y570, interfere with BiP's ability to deoligomerize BiP. Furthermore, the results clearly demonstrate that the mutations in either site do not result in deactivation of BiP but instead result in the gradual adjustments of BiP activity. Phosphomimetic mutations do not significantly perturb IRE1-LD binding to BiP but displayed a reduced ability to deoligomerize IRE1-LD oligomers. Importantly, both phosphomimetic mutants possess higher ATPase rates compared to the WT, suggesting the "correct" timing of substrate binding and release is a critical factor for BiP activity. Increase in ATPase activity thus may not necessarily be beneficial for specific BiP functions and binding to specific substrates.

Taken together, this study provides a plausible mechanism of how two ER specific phosphorylation sites in BiP alter its activity. Both sites enable fine tuning of the BiP conformational landscape and kinetics of the chaperone cycles. Importantly, perturbations in these sites do not switch BiP off, but rather adjust its capacity to interact and deactivate IRE1. However, this relatively subtle tuning is enough to significantly interfere with IRE1-LD oligomerization process *in vitro*. Whilst many other factors such as BiP and IRE1 expression levels, the presence of co-chaperones and other protein quality control enzymes, and stress levels, inevitably further regulate the chaperone cycle *in vivo*, the findings provide new fundamental insights into the intriguing relationships between the local perturbations in BiP and more the general Hsp70 molecule, and its activity and functions. This serves to highlight the importance of post-translational modifications in the regulation of BiP activity through fine tuning of its allosteric cycle.

The current limitation of these data is that it is limited to *in vitro* assays using mutation to stimulate the effects of phosphorylation. It is unknown whether this effect is observed in actual BiP phosphorylation events. Despite this, the results still provide increased understanding of the mechanism of both the BiP allosteric cycle and BiP functions. For example, the study displayed that alteration to ATPase hydrolysis can fine tune BiP interaction with IRE1-LD. In addition, it also provides an exciting route of future research. From here the logical next step for future studies is to test the effect of specific phosphorylation events and the importance of these sites *in vivo*.

## Chapter 8: Concluding remarks.

Built upon the sequence conservation analysis of location-specific Hsp70s, the study has successfully demonstrated that post-translational modifications in the allosteric hotspots of Hsp70 are capable of gradually tuning the chaperone cycle. The study was initially able to confirm previous observations that Hsp70 activity can be regulated by perturbations in its allosteric hotspots (46), before revealing the complexity of the relationship between the thermodynamics and kinetics of the Hsp70 allosteric cycle and its specific functions. In particular, the study was able to demonstrate in the example of interactions between BiP and the stress sensor IRE1, that the increase of ATPase activity of the chaperone is not necessarily beneficial for BiP function, suggesting that fine tuning the kinetics and thermodynamics of the Hsp70 cycle is the way to control specific interactions and function, enabling precise regulation of Hsp70 activity by evolution, co-chaperones, and post-translational modifications.

The chaperone code (an environmental and condition specific combination of post-translational modification) plays a key role in precise regulation Hsp70 activity *in vivo* with growing evidence to support the existence and role of the code. Despite this, there is only a handful of examples of how PTMs can fine tune Hsp70s functions. Whilst switching chaperone activity on and off has been shown to be an efficient way to deactivate an excess of BiP in the absence of stress (such as been demonstrated by the AMPylation of BiP at T518 (148,157)), more delicate adjustments by a certain PTMs or their combinations as part of the chaperone code is still likely to be required to enable multilevel regulation of this complex chaperone system. This study has been able to provide a mechanistical understanding of how two ER specific phosphorylation sites in BiP tune its activity through fine-tuning its chaperone cycle. Despite the fact that the importance of these phosphorylation sites needs to be confirmed *in vivo*, the proposed mechanism by which these sites fine tune Hsp70 activity, is likely to be able to be applied to understanding of other PTMs of Hsp70s, opening new avenues for characterization of the Hsp70 chaperone code.

The organelle specific evolutionary rates generated by the bioinformatic analyse in this study provide information that can guide the future research that aims to address these intriguing questions. Moreover, in the long term this information can be used to target specific Hsp70s via designing small molecules that specifically interact with organelle specific PTMs or allosteric hotspots.

Finally, this project provides important insights into our understanding of how BiP interacts with the ER stress sensor IRE1, highlighting the importance of disordered regions in IRE1-LD for both interactions with BiP and IRE1-oligomerizations. The identification of two binding sites of BiP on the IRE1-LD has provided a far greater understanding on how the chaperone interacts with the stress sensor. Additionally, the disordered and unstructured nature of these regions enables multivalent interactions

with the chaperone that do not require IRE1-LD unfolding and formation of 1:1 BiP IRE1 complex, providing a beautiful example how disorder can control cellular signalling.

The study has indeed provided a greater understanding of the mechanism of regulation of the chaperone code but there are still many related puzzles about the system. Would interactions with other stress sensors (ATF6 and PERK) be affected at the same level as these or could other PTMs have a similar effect to IRE1? Would other BiP functions be activated or deactivated by these modifications? Why are these PTMs only conserved in the ER Hsp70s but not present in cytoplasmic ones? These are but a few questions that further studies could address, with this study providing a litany of potential avenues for future research.

## Chapter 9: methods

This study employed a method in which bioinformatic analysis (chapter 9.10) guided analysis of the conformational landscape and biochemical functions of BiP and its interactions with IRE1-LD (chapter 9.6 - 9.9) produced within the laboratory (chapter 9.1 – 9.5). This chapter serves to provide detail for the method employed during the study.

### 9.1 Plasmid production and sequencing

All plasmids bar the <sup>356</sup>WLLI<sup>362</sup> IRE1-LD plasmid were produced via the service of Twist bioscience. Here the desired sequences were inserted into Twist biosciences pET-29b(+) expression vector containing six histidine His-Tag and thrombin cleavage site with an additional six histidine His-Tag and a TEV cleavage site located between the desired protein and the thrombin cleavage site. The vector contains the resistance gene for kanamycin.

The human IRE1 $\alpha$ -LD <sup>356</sup>WLLI<sup>362</sup> is based on the human IRE1 $\alpha$ -LD (aa24-449, called IRE1-LD) constructs that were cloned from the full-length protein (a kind gift from David Ron, University of Cambridge) into a pET His6 TEV LIC cloning vector (1B) vector (a generous gift from Scott Gradia ((Addgene plasmid # 29653); RRID: Addgene\_29653)). These constructs were mutated to the oligomerization-deficient <sup>357</sup>WLLI<sup>361</sup>. The vector contains the resistance gene for kanamycin.

Plasmids were transformed into *E. coli* DH5 $\alpha$  cells using heat shock transformation. For this a 1:50 ratio of plasmid (80 ng/ $\mu$ l minimum concentration) to competent cells was used and incubated on ice for 20 minutes before a 45 second 42 °C heat shock was applied to the cells. These cells were incubated on ice for 5 minutes before the 20  $\mu$ l cell solution was diluted to 500  $\mu$ l through the addition of LB broth and then incubated for 1 hour with shaking at 37 °C. The cells were centrifuged, supernatant removed and resuspended in 100  $\mu$ l, before being plated on kanamycin LB agar plates. The plates were incubated overnight at 37 °C.

Plasmids replicated within DH5 $\alpha$  cells (used for plasmid replication) were produced in the laboratory, with a single colony being incubated in 5 ml of LB broth supplemented with kanamycin and grown overnight at 37 °C. The study used the PureLink® Quick Plasmid Miniprep Kit, following the manufacturer recommended method. All of the produced plasmids concentration and purity (assessed through A260/A280 ratio) was measured using a nanodrop microvolume spectrophotometer and sequenced using the source bioscience sequencing service.

## 9.2 Protein expression and purification

Plasmids were transformed into *E. coli* BL21 DE3 cells (used for expression) using heat shock transformation. For this a 1:50 ratio of plasmid (80 ng/ $\mu$ l minimum concentration) to competent cells was made and incubated on ice for 20 minutes before a 45 second 42 °C heat shock was applied to the cells. These cells were incubated on ice for 5 minutes before the 20  $\mu$ l cell solution was diluted to 500  $\mu$ l through the addition of LB broth and then incubated for 1 hour with shaking at 37 °C. The cells were centrifuged, supernatant removed and resuspended in 100  $\mu$ l, before being plated on kanamycin LB agar plates. The plates were incubated overnight at 37 °C.

An initial small-scale expression of each construct was created to ensure that the protein was capable of being expressed and was soluble. This was achieved by first incubating a single colony in 5 ml of LB broth supplemented with kanamycin and grown overnight at 37 °C. The sample was then diluted to 50 ml with additional LB broth with and incubated until OD<sub>600</sub> reached ~ 0.7. Cells were induced at this point with 1 mM final concentration of IPTG and incubated for 3-5 hours before harvesting. Samples were collected before IPTG were added and two sample were collected after the 3-5 hour incubation. The uninduced and one of the induced samples were incubated at 95°C for 5 minutes in the presence of 4x loading buffer (1M Tris-HCl pH 6.5, 200 mM DTT, 10 % SDS, bromophenol blue, 20 % glycerol) and 8M urea. The second induced sample was incubated for 20 minutes at room temperature with shaking in the presence of BugBuster, before being spun down at 21,0000 g for 5 minutes. The soluble sample supernatant was incubated at 95°C for 5 minutes in the presence of 4x loading buffer (1M Tris-HCl pH 6.5, 200 mM DTT, 10 % SDS, bromophenol blue, 20 % glycerol) and 8M urea. All samples were run on an SDS-page gel to visualize the protein.

The method for expression and purification was based on previous study (46). All non-labelled proteins constructs (Table 8) were expressed through the incubation of a single colony (BL21 DE3 cells produced in the laboratory.) in 5 ml of LB broth supplemented with kanamycin and grown overnight at 37 °C. The sample was then diluted to 500 ml with additional LB broth with kanamycin and incubated until OD<sub>600</sub> reached ~ 0.7. Samples were induced at this point with 1 mM final concentration of IPTG and incubated for 3-5 hours before harvesting. Cell pellets were resuspended in buffer 20 mM Hepes, 400 mM NaCl, pH 8 and frozen at – 80 °C.

**Table 8: Constructs used within the study.** Table depicting the protein constructs used within the study alongside the key information about the proteins. This includes which protein, the vector, key traits of the protein and why it was used.

Name	Protein	Vector	Expressible	Soluble	His-Tag cleaved	Notes	Uniprot code	Start and end
WT	BiP	pET-29b (+)	Yes	Yes	Yes	Wild type form of human BiP used in the study	P11021	V27-L654
T229G	BiP	pET-29b (+)	Yes	Yes	Yes	ATPase deficient for NMR use	P11021	V27-L654
T460D	BiP	pET-29b (+)	Yes	Yes	Yes	Phosphomimetic mutant	P11021	V27-L654
T460D T229G	BiP	pET-29b (+)	Yes	Yes	Yes	ATPase deficient for NMR use	P11021	V27-L654
Y570D	BiP	pET-29b (+)	Yes	Yes	Yes	Phosphomimetic mutant	P11021	V27-L654
Y570D T229G	BiP	pET-29b (+)	Yes	Yes	Yes	ATPase deficient for NMR use	P11021	V27-L654
WT	IRE1a-LD	pET-29b (+)	Yes	Yes	Yes	Wild type form of human IRE1-LD used in the study	O75460	S24-S450
310PL 317	IRE1a-LD	pET-29b (+)	Yes	Yes	Yes	IRE1P2 peptide-based mutant designed in study	O75460	S24-S450
356WL LI362	IRE1a-LD	a pET His6 TEV LIC cloning vector (1B)	Yes	Yes	Yes	IRE1P3 peptide-based mutant designed in study	O75460	S24-S450

Thawed cells were incubated on ice for 1 hour with 0.5 ml 50 mg/ml lysozyme and protease inhibitor cocktail. After sonication, the cells were spun down at 13,000 g for 1 hour and filtered to remove cell debris. Supernatants were loaded onto a HisTrap HP nickel column that was re-equilibrated with the binding buffer (20 mM Hepes, 400 mM NaCl, pH 8) and washed with a series of binding buffers containing 10, 20 and 30 mM imidazole for BiP and 50 mM imidazole of IRE1-LD. Proteins were eluted using binding buffer containing 500 mM imidazole and buffer, and then exchanged into final HMK buffer (20 mM Hepes, 100 mM KCl, 5 mM MgCl<sub>2</sub>, pH 7.6). All protein concentrations were calculated using a nanodrop and a Bradford assay. The Bradford assay used BSA as the standard curve from 0.2 – 1.0 mg/ml. The sample purity was assessed with an SDS-PAGE gel and by measuring the A260/A280 ratio to ensure minimal bound nucleotides. All samples were stored at – 80 °C.

### 9.3 NMR labelled protein expression and purification

Plasmids were transformed into *E. coli* BL21 DE3 cells (used for expression) using heat shock transformation. For this a 1:50 ratio of plasmid (80 ng/μl minimum concentration) to competent cells was made and incubated on ice for 20 minutes before a 45 second 42 °C heat shock was applied to the cells. These cells were incubated on ice for 5 minutes before the 20 μl cell solution was diluted to 500 μl through the addition of LB broth and then incubated for 1 hour with shaking at 37 °C. The cells were centrifuged, supernatant removed and resuspended in 100 μl, before being plated on kanamycin LB agar plates. The plates were incubated overnight at 37 °C.

Expression and purification was based on the previous study (46), in order to produce the <sup>2</sup>H, <sup>15</sup>N, Ileδ1-[<sup>13</sup>CH<sub>3</sub>] Labelled protein used within this NMR portion of this study. A single colony in 5 ml of LB broth supplemented with kanamycin was incubated for 7 hours at 37°C before the cells were harvested at 4000 g. The cell pellet was resuspended in M9 minimum NMR Medium (containing Deuterated D-glucose (CIL, 1,2,3,4,5,6,6-D7, 98% DLM-2062), <sup>15</sup>N-labeled ammonium chloride (<sup>15</sup>NH<sub>4</sub>Cl), 10% of deuterated Celvivo Complete Medium (CIL, CGM-1040-D) and D<sub>2</sub>O, pH 7.6) and grown overnight at 37°C. The cells were diluted to 500 ml with the NMR media and grown to ~ 0.7 OD, before 5 ml of methyl-<sup>13</sup>C-labeled alpha-ketobutyric acid (CLM-6820) solution (14 mg/ml in D<sub>2</sub>O, pH 10.0) was added and the cells were incubated for a further hour. The sample was induced with 1 mM final IPTG and incubated for 7-8 hours before harvesting.

The purification of labelled protein used the same method as unlabelled protein. Thawed cells were incubated on ice for 1 hour with 0.5 ml 50 mg/ml lysozyme and protease inhibitor cocktail. After sonication, cells were spun down at 13,000 g for 1 hour and filtered to remove cell debris. Supernatants were loaded onto a HisTrap HP nickel column that was re-equilibrated with the binding buffer (20 mM Hepes, 400 mM

NaCl, pH 8) and washed with a series of binding buffers containing 10, 20 and 30 mM imidazole. The proteins were eluted using binding buffer containing 500 mM imidazole and buffer, and then exchanged into final HMK buffer (20 mM Hepes, 100 mM KCl, 5 mM MgCl<sub>2</sub>, pH 7.6). All protein concentrations were calculated using a nanodrop and a Bradford assay. The Bradford assay used BSA as the standard curve from 0.2 – 1.0 mg/ml. The sample purity was assessed with an SDS-PAGE gel and by measuring the A260/A280 ratio to ensure minimal bound nucleotides. All samples were stored at – 80 °C.

#### 9.4 TEV cleavage

TEV used in this study was produced within the laboratory within *E. coli* Rosetta gold cells. The method of transformation, expression and purification (chapter 9.1 and 9.2) that was used for TEV production was the same as the method used for IRE1-LD production, with the only variation being the *E. coli* used for expression. TEV was transformed into BL21 DE3 cells (used for expression) using heat shock transformation. For this a 1:50 ratio of plasmid (80 ng/μl minimum concentration) to competent cells was made and incubated on ice for 20 minutes before a 45 second 42 °C heat shock was applied to the cells. These cells were incubated on ice for 5 minutes before the 20 μl cell solution was diluted to 500 μl through the addition of LB broth and then incubated for 1 hour with shaking at 37 °C. The cells were centrifuged, supernatant removed and resuspended in 100 μl, before being plated on kanamycin LB agar plates. The plates were incubated overnight at 37 °C.

TEV were expressed through the incubation of a single colony (BL21 DE3 cells produced in the laboratory.) in 5 ml of LB broth supplemented with ampicillin and grown overnight at 37 °C. The sample was then diluted to 500 ml with additional LB broth with ampicillin and incubated until OD<sub>600</sub> reached ~ 0.7. Samples were induced at this point with 1 mM final concentration of IPTG and incubated for 3-5 hours before harvesting. Cell pellets were resuspended in buffer 20 mM Hepes, 400 mM NaCl, pH 8 and frozen at – 80 °C.

The thawed cells were incubated on ice for 1 hour with 0.5 ml 50 mg/ml lysozyme and protease inhibitor cocktail. After sonication, cells were spun down at 13,000 g for 1 hour and filtered to remove cell debris. Supernatants were loaded onto a HisTrap HP nickel column that was re-equilibrated with the binding buffer (20 mM Hepes, 400 mM NaCl, pH 8) and washed with the binding buffers containing 50 mM imidazole. Proteins were eluted using binding buffer containing 500 mM imidazole and buffer, and then exchanged into final HMK buffer (20 mM Hepes, 100 mM KCl, 5 mM MgCl<sub>2</sub>, pH 7.6). All protein concentrations were calculated using a nanodrop and a Bradford assay. The Bradford assay used BSA as the standard curve from 0.2 – 1.0 mg/ml. The sample purity was assessed with an SDS-PAGE gel and by measuring the A260/A280 ratio to ensure minimal bound nucleotides. All samples were stored at – 80 °C.

BiP and IRE1-LD were incubated with TEV at a ratio of 10:1 for either 1 hour at room temperature (IRE1-LD) or 4 °C overnight (BiP). The cleaved His-Tags were removed from solution via being passed through a nickel column, where the sample was loaded onto the column that was re-equilibrated with the binding buffer (20 mM Hepes, 400 mM NaCl, pH 8) and the column was washed with the same buffer. The sample flow through (after being loaded) and the wash fraction were collected as it contained cleaved proteins. All protein concentrations were calculated using a nanodrop and a Bradford assay. The Bradford assay used a BSA as the standard curve from 0.2 – 1.0 mg/ml. Cleaved sample was stored at – 80 °C.

## 9.5 Peptide stock and addition to samples

All peptides were purchased from BioMatik. The peptides were centrifuged for 1 minute at 1000 g, before being resuspended in HMK buffer or DMSO, at either 100 mM (for CP2 and IRE1 peptides) or 2 mM (dESP) (details in table 9). All peptides were purchased from BioMatik. The peptides were centrifuged for 1 minute at 1000 g, before being resuspended in HMK buffer or DMSO, at either 100 mM (for CP2 and IRE1 peptides) or 2 mM (dESP) (details in table 9).

*Table 9: summary of Peptides used in the study. A table summarizing the peptides used throughout out study, including information about sequences, stock concentration and the buffer in which the peptide were dissolved in (98,123).*

Peptide	Sequence	Stock concentration (mM)	Buffer
Control peptide 2 (CP2)	HTFPAVL	100	HMK or DMSO
IRE1 <sup>P1</sup>	<sup>305</sup> AVVPRGS <sup>311</sup>	100	DMSO
IRE1 <sup>P2</sup>	<sup>310</sup> GSTLPLL <sup>317</sup>	100	DMSO
IRE1 <sup>P3</sup>	<sup>356</sup> RNYWLLI <sup>362</sup>	100	DMSO
IRE1 <sup>P4</sup>	<sup>385</sup> KHRENVJ <sup>391</sup>	100	DMSO
IRE1 <sup>P5</sup>	<sup>388</sup> ENVIPADS <sup>395</sup>	100	DMSO
IRE1 <sup>P6</sup>	<sup>442</sup> KDMATIIL <sup>449</sup>	100	DMSO
dESP	MKKHKRILALCFLGLLQSSYSAAK	2	HMK

## 9.6 Mass spectrometry analysis

All samples were subject to mass spectrometry for intact protein mass measurements in order to ensure the expected size of the construct was achieved for both labelled and unlabelled samples, in addition to confirming the cleavage of His-Tag via TEV cleavage.

The study used Liquid chromatography mass spectrometry (LC-MS) system (Waters MClass UPLC and the Waters Xevo G2-XS QTOF mass spectrometer). Samples were all in HMK buffer (20 mM Hepes, 100 mM KCl, 5 mM MgCl<sub>2</sub>, pH 7.6). Samples were at 1 μM with 0.1% Trifluoroacetic acid (TFA). 1 μl sample was loaded on Acquity UPLC Protein BEH C4 column Acquity with an Acquity UPLC Protein BEH VanGuard Pre-Column. The system flowrate was a constant 50 μl/min, loading sample onto trap column in 20% acetonitrile/0.1% formic acid and washed for 5 minutes. After this, the bound protein was eluted by a gradient of 20-95% solvent B (0.1% formic acid in water) in buffer A (0.1% formic acid in water) over 10 minutes. The column was subsequently washed with 95 % solvent B in A (0.1% formic acid in water) for 5 min before re-equilibration at 20% solvent B in A ready for the next injection. The mass spectrometer was calibrated using a separate injection of glu-fibrinopeptide. Data were processed using MassLynx 4.2.

## 9.7 NMR experiments and data analysis

All BiP sample were ~ 50 μM in concentration and prepared in the NMR buffer (20 mM Hepes, 100 mM KCl, 5 mM MgCl<sub>2</sub>, 5 mM DTT, 0.02% NaN<sub>3</sub>; PH 7.6) in the presence of 5 mM ADP (Adenosine 5'-triphosphate dipotassium salt hydrate) or 40 mM ATP (Adenosine-5'-diphosphate monopotassium salt dihydrate) and with a concentration of 2 % D<sub>2</sub>O. An important note is the use of potassium nucleotide salt and not sodium nucleotide salt.

All NMR experiments were based upon a previous study (46). A 2D <sup>1</sup>H-<sup>13</sup>C SOFAST-HMQC was employed to record all methyl NMR spectra. All measurements were recorded at either 5, 25 or 37 °C at 750 MHz Bruker spectrometer equipped with a Bruker TCI triple-resonance cryogenically cooled probes. The data was processed with NMRPipe (221). In required cases, peptide stock was added from a 100 mM DMSO stock to a final concentration of either 1 mM or 50 μM. A high concentration stock was used to ensure DMSO concentration was not higher than 1 % for any sample.

Analysis of the NMR spectra was performed using CCPN (222,223). Here, the peak relative intensity was measured for each of the doublet peaks. The relative intensity of each peak of the doublet is proportional to the relative population of ATP.U and ATP.D, allowing the relative population of each conformation to be calculated by comparing the intensity value. The assignment of the peaks to ATP.U or ATP.D was done in a previous

study (46). An average population of ATP.U and ATP.D was then calculated based upon the calculated population of the three peak doublets used in this study.

### 9.8 Malachite Green ATPase assay

All assays were based on previous experiments and industrial supplied kits (224,225). 30  $\mu$ l of 0.5  $\mu$ M BiP in HMK buffer (20 mM Hepes, 100 mM KCl, 5 mM  $MgCl_2$ , pH 7.6) incubated for 15 minutes at 37 °C. 4 mM ATP (total reaction volume 40  $\mu$ l) was added to the sample before incubating for 1 hour at 37 °C. After this incubation step, 200  $\mu$ l of malachite green reagent is added and the sample is incubated for 30 minutes incubation at room temperature. The samples were then measure at 620 nM.

When using the ATPase assay to assess the binding of peptides. For this peptides were added at the same time as the ATP. 100 mM peptide DMSO solution is added to a final concentration of 1 mM peptide and 1 % DMSO. A 1 % DMSO control sample was used to verify that the low concentration of the solvent did not alter ATPase activity of the chaperone.

A standard curve was generated for the assay using phosphate standard of 0 – 37.5  $\mu$ M with the addition of 4 mM ATP. The standard curve samples all contained ATP to remove the additional background effect of the phosphate that was within the ATP solution initially. Data analysis was achieved by plotting  $OD_{620\text{ nm}}$  vs phosphate standard to create the standard curve, which was used to determine the total free phosphate produced. This was converted to phosphate produced per hour per  $\mu$ M.

### 9.9 IRE1 oligomerization assay

30  $\mu$ M of IRE1-LD was spun down at 21, 000 g to ensure no higher order oligomer is in solution before the sample was allotted into 9 samples (25  $\mu$ l total volume with DTT and dESP peptide) per IRE1-LD or BiP variant being assessed. The samples is then incubated with 5 mM DTT and 100 – 400  $\mu$ M dESP peptide for 2 hours at room temperature. This stage serves to allow the formation of higher order insoluble oligomers which will be visible in solution, appearing as white cotton like strands.

The incubated IRE1-LD has either of 3  $\mu$ M BiP + 40 mM ATP, 3  $\mu$ M BiP and HMK buffer or HMK buffer (3 conditions each with 3 repeats). Each condition needs to be equal in volume, with the HMK buffer serving to ensure the volume was the same. A further 2-hour incubation at room temperature was done before the sample was spun down at 21,000 g for five minutes. The supernatant was removed and mixed with 2 X SDS loading buffer. The pellet was resuspended in equal HMK buffer volume as the supernatant and mixed 2 X SDS loading buffer. Both samples were heated at 100 °C for 5 minutes and run on SDS-PAGE gel.

The percentage of the sample in either the soluble or insoluble fraction was calculated based on band intensity which was calculated using ImageJ (226). The study employed their recommended approach to measuring pixel density and compared the two scores of soluble and insoluble to calculate the percentage based on the value. Each sample was repeated at least twice to use an average of band intensity to calculate an average portion of sample in either the soluble or insoluble fraction, using standard error.

### 9.10 Conservation of amino acids analysis

The initial stage of the conservational analysis was the selection of model organisms. The study selected organism which have been previously characterised to a high degree of detail which possesses multiple sequenced Hsp70s with at least one located in both the ER and the cytoplasm and aimed to select organisms from all known kingdoms. The model organism selected were human, *Drosophila melanogaster*, *Caenorhabditis elegans*, *Arabidopsis thaliana*, *Saccharomyces cerevisiae* and *Dictyostelium discoideum*. Sequences of all known Hsp70s of each organism were sourced from the Uniprot database (11) (table 10). The sequence identity of each Hsp70 was compared to every other Hsp70s within the same organism through the use of EMBOSS Stretcher (BLOSUM62 matrix, GAP open 12 and GAP extend 2) (227).

*Table 10: Sequences used in the study. A table displaying all sequences used in the study, along with their gene code, organism of origin, subcellular location and Uniprot code.*

<b>Protein name</b>	<b>Code name</b>	<b>Organism</b>	<b>Location</b>	<b>Uniprot code</b>
BiP	HspA5	Human	ER	P11021
Heat shock 70 kDa protein 1A	HspA1A	Human	cytoplasm	P0DMV8
Heat shock 70 kDa protein 1B	HspA1B	Human	cytoplasm	P0DMV9
Heat shock 70 kDa protein 1-like	HspA1L	Human	cytoplasm	P34931
Heat shock related 70 kDa protein 2	HspA2	Human	cytoplasm	P54652
Heat shock cognate 71 kDa protein	Hsc70	Human	cytoplasm	P11142
Heat shock 70 kDa protein 6	HspA6	Human	cytoplasm	P17066

Heat shock 70 kDa protein 8	HspA8	Human	cytoplasm	P0DMV9
GRP75	HspA9	Human	Mitochondria	P38646
Heat shock 70 kDa protein 12a	HspA12A	Human	cytoplasm/Nucleus	O43301
Heat shock 70 kDa protein 12b	HspA12B	Human	Endothelial cells	Q96MM6
Heat shock 70 kDa protein 13	HspA13	Human	microsome	P48723
Heat shock 70 kDa protein 14	HspA14	Human	cytoplasm	Q0VDF9
Putative heat shock 70 kDa protein	HspA7	Human	cytoplasm	P48741
Heat shock 70 kDa protein BIP1	BIP1_ARATH	<i>Arabidopsis thaliana</i>	ER	Q9LKR3
Heat shock 70 kDa protein BIP2	BIP2_ARATH	<i>Arabidopsis thaliana</i>	ER	Q39043
BIP3_ARATH Heat shock 70 kDa protein BIP3	BIP3_ARATH	<i>Arabidopsis thaliana</i>	ER	Q8H1B3
Heat shock 70 kDa protein 1	HS701_ARATH	<i>Arabidopsis thaliana</i>	cytoplasm	P22953
Heat shock 70 kDa protein 2	HS702_ARATH	<i>Arabidopsis thaliana</i>	cytoplasm	P22954
Heat shock 70 kDa protein 3	HSP7C_ARATH	<i>Arabidopsis thaliana</i>	cytoplasm	O65719
Heat shock 70 kDa protein 4	HS704_ARATH	<i>Arabidopsis thaliana</i>	cytoplasm	Q9LHA8
Heat shock 70 kDa protein 5	HSP7E_ARATH	<i>Arabidopsis thaliana</i>	cytoplasm	Q9S9N1
Heat shock 70 kDa protein 6	HSP7F_ARATH	<i>Arabidopsis thaliana</i>	chloroplast	Q9STW6

Heat shock 70 kDa protein 7	HSP7G_ARATH	<i>Arabidopsis thaliana</i>	chloroplast	Q9LTX9
Heat shock 70 kDa protein 8	HSP7H_ARATH	<i>Arabidopsis thaliana</i>	cytoplasm	Q9SKY8
Heat shock 70 kDa protein 9	HSP7I_ARATH	<i>Arabidopsis thaliana</i>	cytoplasm	Q8GUM2
Heat shock 70 kDa protein 10	HSP7J_ARATH	<i>Arabidopsis thaliana</i>	Mitochondria	Q9LDZ0
Heat shock 70 kDa protein 15	HSP7P_ARATH	<i>Arabidopsis thaliana</i>	cytoplasm	F4HQD4
Heat shock 70 kDa protein 17	HSP7R_ARATH	<i>Arabidopsis thaliana</i>	ER lumen	F4JMJ1
Heat shock 70 kDa protein 18	HSP7N_ARATH	<i>Arabidopsis thaliana</i>	cytoplasm	Q9C7X7
Heat shock 70 kDa protein A	HSP7A_CAEEL	<i>Caenorhabditis elegans</i>	cytoplasm	P09446
Heat shock 70 kDa protein C	HSP7C_CAEEL	<i>Caenorhabditis elegans</i>	ER	P27420
Endoplasmic reticulum chaperone BiP homolog	BIBH_CAEEL	<i>Caenorhabditis elegans</i>	ER	P20163
Heat shock 70 kDa protein F, mitochondrial	HSP7F_CAEEL	<i>Caenorhabditis elegans</i>	Mitochondria	P11141
Heat shock 70 kDa protein cognate 1	HSP7A_DROME	<i>Drosophila melanogaster</i>	cytoplasm	P29843
Heat shock 70 kDa protein cognate 2	HSP7B_DROME	<i>Drosophila melanogaster</i>	cytoplasm	P11146
Major heat shock 70 kDa protein Aa	HSP70_DROME	<i>Drosophila melanogaster</i>	cytoplasm	P82910

Major heat shock 70 kDa protein Ba	HSP72_DROME	<i>Drosophila melanogaster</i>	cytoplasm	Q8INI8
Major heat shock 70 kDa protein Bbb	HSP74_DROME	<i>Drosophila melanogaster</i>	cytoplasm	Q9VG58
Endoplasmic reticulum chaperone BiP	BIP_DROME	<i>Drosophila melanogaster</i>	ER	P29844
Heat shock 70 kDa protein cognate 4	HSP7D_DROME	<i>Drosophila melanogaster</i>	cytoplasm	P11147
Heat shock 70 kDa protein cognate 5	HSP7E_DROME	<i>Drosophila melanogaster</i>	Mitochondria	P29845
Luminal-binding protein 1	BIP1_DICDI	<i>Dictyostelium discoideum</i>	ER	Q556U6
Luminal-binding protein 2	BIP2_DICDI	<i>Dictyostelium discoideum</i>	ER	Q8T869
Heat shock 70 kDa protein, mitochondrial	HSP7M_DICDI	<i>Dictyostelium discoideum</i>	Mitochondria	Q8I0H7
Heat shock cognate 70 kDa protein 1	HS7C1_DICDI	<i>Dictyostelium discoideum</i>	cytoplasm	P36415
Heat shock cognate 70 kDa protein 2	HS7C2_DICDI	<i>Dictyostelium discoideum</i>	cytoplasm	Q557E0
Heat shock cognate 70 kDa protein 3	HS7C3_DICDI	<i>Dictyostelium discoideum</i>	cytoplasm	Q54BE0
Heat shock cognate 70 kDa protein 4	HS7C4_DICDI	<i>Dictyostelium discoideum</i>	cytoplasm	Q54BD8
Ribosome-associated molecular chaperone SSB1	SSB1_YEAST	<i>Saccharomyces cerevisiae</i>	cytoplasm	P11484
Ribosome-associated	SSB2_YEAST	<i>Saccharomyces cerevisiae</i>	cytoplasm	P40150

molecular chaperone SSB2				
Heat shock protein SSQ1, mitochondrial	HSP7Q_YEAST	<i>Saccharomyces cerevisiae</i>	Mitochondria	Q05931
Heat shock protein SSC1	HSP77_YEAST	<i>Saccharomyces cerevisiae</i>	Mitochondria	P0CS90
Heat shock protein SSA1	HSP71_YEAST	<i>Saccharomyces cerevisiae</i>	cytoplasm	P10591
Endoplasmic reticulum chaperone BiP	BIP_YEAST	<i>Saccharomyces cerevisiae</i>	ER	P16474
Heat shock protein homolog SSE1	HSP7F_YEAST	<i>Saccharomyces cerevisiae</i>	cytoplasm	P32589
Heat shock protein 70 homolog LHS1	LHS1_YEAST	<i>Saccharomyces cerevisiae</i>	ER lumen	P36016
Heat shock protein SSA2	HSP72_YEAST	<i>Saccharomyces cerevisiae</i>	cytoplasm	P10592
Heat shock protein 78, mitochondrial	HSP78_YEAST	<i>Saccharomyces cerevisiae</i>	mitochondria	P33416
Heat shock protein SSA3	HSP73_YEAST	<i>Saccharomyces cerevisiae</i>	cytoplasm	P09435
Heat shock protein SSA4	HSP74_YEAST	<i>Saccharomyces cerevisiae</i>	cytoplasm	P22202

A mean average identity between cytoplasmic located Hsp70 and ER located Hsp70 was calculated for each organism. This is in addition to the mean average for all ER located Hsp70 for all organisms. When plotted on a bar chart, it allowed the identification of the percentage window in which ER located Hsp70 are on average likely to be identical to other ER located Hsp70s but not cytoplasmic Hsp70s. These values formed the paralogue/orthologue cut-off point of 58% by taking the average sequence identity of all Hsp70 within the same organism sub-cellular location, though, the study opted for 65% to minimise the chance of an incorrect Hsp70 being sorted into either group.

ConSurf (171–173) running a Homolog search algorithm HMMER (1 iteration with an E-value cut-off of 0.0001) was used to generate a set of unique sequences that were 65 – 90 % identical to all ER and cytoplasmic Hsp70 of all “classical” Hsp70s, in order to generate multiple sets of similar sequences. The study employed a maximum of 90 % identity to remove organisms with near identical Hsp70s (such as hamster and human

Hsp70s who only possess two different amino acids) to avoid the additional bias. The multiple sets were combined into ER and cytoplasmic sets, removing any duplicates. The two sequence sets were manually checked to ensure the proteins were located in the correct sub-cellular location, not 20 % larger or smaller than BiP, and possessing the highly conserved binding sites of Hsp70 family. This formed the sequence sets used within this study.

Clustal omega (227) was used to generate multiple sequence alignments (MSA) and phylogenetic trees for both sequence sets. The MSA were then used in both Consurf (171–173) and Weblogo (174,228) to generate conservation patterns of the two sequence sets, forming the basis for conservation analysis. The phylogenetic trees served to display the evolutionary difference between Hsp70 located within ER or cytoplasm.

The sequences of human BiP (ER located Hsp70s) and human HspA1A (cytoplasmic located Hsp70) were aligned for the final stage of analysis. Here each residue was scored as either conserved in either both sets, ER set, cytoplasmic set, conserved in both but different residues or neither sets. A residue was considered conserved if it scored 7 or higher out of 9 for the Consurf datum or 2.5 out of 4 for the weblogo datum.

### 9.11 Source of reagents used throughout the study

*Table 11: Reagents source. Tabel depicting the reagents used throughout the study and location they were sourced from.*

<b>Reagents</b>	<b>Source</b>	<b>Item code / catalogue number</b>
The PureLink® Quick Plasmid Miniprep Kit	Thermo Fisher Scientific	K210010
2x High-Fidelity Q5 polymerase master mix	New England Biolabs	M0492S
primers	Integrated DNA Technologies	N/A
LB Broth (Lennox)	SIGMA-ALDRICH	L3022
Kanamycin monosulphate	VWR International	J61272.09
Tris buffer	Fisher Scientific Ltd	11448361
DTT (dithiothreitol)	VWR International	BC99
SDS (Sodium dodecyl sulfate)	Fisher Scientific Ltd	11431652

Bromophenol blue	VWR International	A18469.18
Glycerol	SLS (Scientific Laboratory Supplies)	356350-500ML
Urea	Promega UK Ltd	V3171
BugBuster® Master Mix	MILLIPORE	71456-3
7.5% MP TGX Gel	Bio-Rad Laboratories	4561026
Imidazole	VWR International	1747.0100
Hepes	Fluorochem Limited	F047861-500G
KCl	VWR International	7447-40-7
MgCl <sub>2</sub>	VWR International	ACRO223210010
Bradford assay	Bio-Rad Laboratories	5000205
Deuterium oxide (D <sub>2</sub> O)	Goss scientific	DLM-6-1000
10% of deuterated Celtone Complete Medium	Goss scientific	CIL, CGM-1040-D
Deuterated D-glucose (CIL, 1,2,3,4,5,6-D <sub>7</sub> , 98%)	Goss scientific	DLM-2062
<sup>15</sup> N-labeled ammonium chloride ( <sup>15</sup> NH <sub>4</sub> Cl)	Goss scientific	NLM-467-1
Alpha-Ketobutyric acid	Goss scientific	CLM-6820
IPTG	VWR International	10021-2
DMSO (Dimethyl sulfoxide)	VWR International	BKC-17
Adenosine 5'-triphosphate dipotassium salt hydrate	SIGMA-ALDRICH	A8937-1G
Adenosine-5'-diphosphate monopotassium salt dihydrate	Thermo Scientific Alfa Aesar	15420147
ATP Solution (100 mM)	Thermo Fisher Scientific	R0441
ATPase/GTPase Activity Assay Kit	SIGMA-ALDRICH	MAK113-1KT

## References

1. Rosenzweig R, Nillegoda NB, Mayer MP, Bukau B. *The Hsp70 chaperone network*. *Nature Reviews Molecular Cell Biology*. 2019. p. 665–680. <https://doi.org/10.1038/s41580-019-0133-3>.
2. Mayer MP. The Hsp70-Chaperone Machines in Bacteria. *Frontiers in Molecular Biosciences*. 2021;8. <https://doi.org/10.3389/fmolb.2021.694012>.
3. Radons J. *The human HSP70 family of chaperones: where do we stand?*. *Cell Stress and Chaperones*. 2016. p. 379–404. <https://doi.org/10.1007/s12192-016-0676-6>.
4. Finka A, Sood V, Quadroni M, Rios PDL, Goloubinoff P. Quantitative proteomics of heat-treated human cells show an across-the-board mild depletion of housekeeping proteins to massively accumulate few HSPs. *Cell Stress and Chaperones*. 2015;20(4): 605–620. <https://doi.org/10.1007/s12192-015-0583-2>.
5. Kohler V, Andréasson C. Hsp70-mediated quality control: should I stay or should I go? *Biological Chemistry*. 2020;401(11): 1233–1248. <https://doi.org/10.1515/hsz-2020-0187>.
6. Shiber A, Döring K, Friedrich U, Klann K, Merker D, Zedan M, et al. Cotranslational assembly of protein complexes in eukaryotes revealed by ribosome profiling. *Nature*. 2018;561(7722): 268–272. <https://doi.org/10.1038/s41586-018-0462-y>.
7. Craig EA. Hsp70 at the membrane: driving protein translocation. *BMC Biology*. 2018;16(1): 11. <https://doi.org/10.1186/s12915-017-0474-3>.
8. Lüders J, Demand J, Höhfeld J. The Ubiquitin-related BAG-1 Provides a Link between the Molecular Chaperones Hsc70/Hsp70 and the Proteasome. *Journal of Biological Chemistry*. 2000;275(7): 4613–4617. <https://doi.org/10.1074/jbc.275.7.4613>.
9. Gamerding M, Kaya AM, Wolfrum U, Clement AM, Behl C. BAG3 mediates chaperone-based aggresome-targeting and selective autophagy of misfolded proteins. *EMBO reports*. 2011;12(2): 149–156. <https://doi.org/10.1038/embor.2010.203>.
10. Madeira F, Pearce M, Tivey ARN, Basutkar P, Lee J, Edbali O, et al. Search and sequence analysis tools services from EMBL-EBI in 2022. *Nucleic Acids Research*. 2022;50(W1): W276–W279. <https://doi.org/10.1093/nar/gkac240>.

11. *UniProt*.
12. Hetz C. The unfolded protein response: controlling cell fate decisions under ER stress and beyond. *Nature Reviews Molecular Cell Biology*. 2012;13(2): 89–102. <https://doi.org/10.1038/nrm3270>.
13. Araki K, Nagata K. Protein folding and quality control in the ER. *Cold Spring Harbor perspectives in biology*. 2011;3(11): a007526. <https://doi.org/10.1101/cshperspect.a007526>.
14. Vincenz-Donnelly L, Hipp MS. The endoplasmic reticulum: A hub of protein quality control in health and disease. *Free Radical Biology and Medicine*. 2017;108: 383–393. <https://doi.org/10.1016/j.freeradbiomed.2017.03.031>.
15. Schwarz DS, Blower MD. The endoplasmic reticulum: structure, function and response to cellular signaling. *Cellular and Molecular Life Sciences*. 2016;73(1): 79–94. <https://doi.org/10.1007/s00018-015-2052-6>.
16. Walter P, Ibrahim I, Blobel G. Translocation of proteins across the endoplasmic reticulum. I. Signal recognition protein (SRP) binds to in-vitro-assembled polysomes synthesizing secretory protein. *The Journal of cell biology*. 1981;91(2): 545–550. <https://doi.org/10.1083/jcb.91.2.545>.
17. Walter P, Blobel G. Translocation of proteins across the endoplasmic reticulum. II. Signal recognition protein (SRP) mediates the selective binding to microsomal membranes of in-vitro-assembled polysomes synthesizing secretory protein. *The Journal of cell biology*. 1981;91(2): 551–556. <https://doi.org/10.1083/jcb.91.2.551>.
18. Rapoport TA. Protein translocation across the eukaryotic endoplasmic reticulum and bacterial plasma membranes. *Nature*. 2007;450(7170): 663–669. <https://doi.org/10.1038/nature06384>.
19. Meyer DI, Krause E, Dobberstein B. Secretory protein translocation across membranes—the role of the ‘docking protein’. *Nature*. 1982;297(5868): 647–650. <https://doi.org/10.1038/297647a0>.
20. Gilmore R, Blobel G, Walter P. Protein translocation across the endoplasmic reticulum. I. Detection in the microsomal membrane of a receptor for the signal recognition particle. *The Journal of cell biology*. 1982;95(2): 463–469. <https://doi.org/10.1083/jcb.95.2.463>.

21. Braakman I, Hebert DN. Protein Folding in the Endoplasmic Reticulum. *Cold Spring Harbor Perspectives in Biology*. 2013;5(5): a013201–a013201. <https://doi.org/10.1101/cshperspect.a013201>.
22. Fagone P, Jackowski S. Membrane phospholipid synthesis and endoplasmic reticulum function. *Journal of Lipid Research*. 2009;50: S311–S316. <https://doi.org/10.1194/jlr.R800049-JLR200>.
23. Clapham DE. Calcium Signaling. *Cell*. 2007;131(6): 1047–1058. <https://doi.org/10.1016/j.cell.2007.11.028>.
24. Samtleben S, Jaepel J, Fecher C, Andreska T, Rehberg M, Blum R. Direct imaging of ER calcium with targeted-esterase induced dye loading (TED). *Journal of visualized experiments : JoVE*. 2013;(75): e50317. <https://doi.org/10.3791/50317>.
25. Oslowski CM, Urano F. Measuring ER Stress and the Unfolded Protein Response Using Mammalian Tissue Culture System. In: 2011. p. 71–92. <https://doi.org/10.1016/B978-0-12-385114-7.00004-0>.
26. Lin JH, Walter P, Yen TSB. Endoplasmic Reticulum Stress in Disease Pathogenesis. *Annual Review of Pathology: Mechanisms of Disease*. 2008;3(1): 399–425. <https://doi.org/10.1146/annurev.pathmechdis.3.121806.151434>.
27. Gardner BM, Pincus D, Gotthardt K, Gallagher CM, Walter P. Endoplasmic Reticulum Stress Sensing in the Unfolded Protein Response. *Cold Spring Harbor Perspectives in Biology*. 2013;5(3): a013169–a013169. <https://doi.org/10.1101/cshperspect.a013169>.
28. Adams CJ, Kopp MC, Larburu N, Nowak PR, Ali MMU. Structure and molecular mechanism of ER stress signaling by the unfolded protein response signal activator IRE1. *Frontiers in Molecular Biosciences*. 2019;6(MAR). <https://doi.org/10.3389/fmolb.2019.00011>.
29. Wang J, Lee J, Liem D, Ping P. *HSPA5 Gene encoding Hsp70 chaperone BiP in the endoplasmic reticulum*. *Gene*. 2017. p. 14–23. <https://doi.org/10.1016/j.gene.2017.03.005>.
30. Feige MJ, Hendershot LM. Quality control of integral membrane proteins by assembly-dependent membrane integration. *Molecular cell*. 2013;51(3): 297–309. <https://doi.org/10.1016/j.molcel.2013.07.013>.

31. Yang J, Nune M, Zong Y, Zhou L, Liu Q. Close and Allosteric Opening of the Polypeptide-Binding Site in a Human Hsp70 Chaperone BiP. *Structure*. 2015;23(12): 2191–2203. <https://doi.org/10.1016/j.str.2015.10.012>.
32. Mayer MP, Bukau B. Hsp70 chaperones: Cellular functions and molecular mechanism. *Cellular and Molecular Life Sciences*. 2005;62(6): 670–684. <https://doi.org/10.1007/s00018-004-4464-6>.
33. Sarkar NK, Kundnani P, Grover A. Functional analysis of Hsp70 superfamily proteins of rice (*Oryza sativa*). *Cell Stress and Chaperones*. 2013;18(4): 427–437. <https://doi.org/10.1007/s12192-012-0395-6>.
34. Flaherty KM, DeLuca-Flaherty C, McKay DB. Three-dimensional structure of the ATPase fragment of a 70K heat-shock cognate protein. *Nature*. 1990;346(6285): 623–628. <https://doi.org/10.1038/346623a0>.
35. Liebscher M, Roujeinikova A. Allosteric Coupling between the Lid and Interdomain Linker in DnaK Revealed by Inhibitor Binding Studies. *Journal of Bacteriology*. 2009;191(5): 1456–1462. <https://doi.org/10.1128/JB.01131-08>.
36. Zhuravleva A, Gierasch LM. Substrate-binding domain conformational dynamics mediate Hsp70 allostery. *Proceedings of the National Academy of Sciences of the United States of America*. 2015;112(22): E2865–E2873. <https://doi.org/10.1073/pnas.1506692112>.
37. Yan Y, Rato C, Rohland L, Preissler S, Ron D. MANF antagonizes nucleotide exchange by the endoplasmic reticulum chaperone BiP. *Nature Communications*. 2019;10(1): 541. <https://doi.org/10.1038/s41467-019-08450-4>.
38. Mayer MP, Schuck S, Ernst R, Ali MMU, Adams CJ, Kopp MC, et al. Structure and Molecular Mechanism of ER Stress Signaling by the Unfolded Protein Response Signal Activator IRE1. *Frontiers in Molecular Biosciences* | [www.frontiersin.org](http://www.frontiersin.org). 2019;6: 11. <https://doi.org/10.3389/fmolb.2019.00011>.
39. Zhu X, Zhao X, Burkholder WF, Gragerov A, Ogata CM, Gottesman ME, et al. Structural Analysis of Substrate Binding by the Molecular Chaperone DnaK. *Science*. 1996;272(5268): 1606–1614.
40. Zuiderweg ERP, Bertelsen EB, Rousaki A, Mayer MP, Gestwicki JE, Ahmad A. Allostery in the Hsp70 Chaperone Proteins. *Topics in Current Chemistry*. 2012; 99–153. [https://doi.org/10.1007/128\\_2012\\_323](https://doi.org/10.1007/128_2012_323).

41. Mayer MP. Hsp70 chaperone dynamics and molecular mechanism. *Trends in Biochemical Sciences*. 2013;38(10): 507–514. <https://doi.org/10.1016/J.TIBS.2013.08.001>.
42. Zhuravleva A, Clerico EM, Gierasch LM. An interdomain energetic tug-of-war creates the allosterically active state in Hsp70 molecular chaperones. *Cell*. 2012;151(6): 1296–1307. <https://doi.org/10.1016/j.cell.2012.11.002>.
43. Meng W, Clerico EM, McArthur N, Gierasch LM. Allosteric landscapes of eukaryotic cytoplasmic Hsp70s are shaped by evolutionary tuning of key interfaces. *Proceedings of the National Academy of Sciences of the United States of America*. 2018;115(47): 11970–11975. <https://doi.org/10.1073/pnas.1811105115>.
44. Bertelsen EB, Chang L, Gestwicki JE, Zuiderweg ERP. Solution conformation of wild-type E. coli Hsp70 (DnaK) chaperone complexed with ADP and substrate. *Proceedings of the National Academy of Sciences*. 2009;106(21): 8471–8476. <https://doi.org/10.1073/pnas.0903503106>.
45. Swain JF, Dinler G, Sivendran R, Montgomery DL, Stotz M, Gierasch LM. Hsp70 Chaperone Ligands Control Domain Association via an Allosteric Mechanism Mediated by the Interdomain Linker. *Molecular Cell*. 2007;26(1): 27–39. <https://doi.org/10.1016/j.molcel.2007.02.020>.
46. Wieteska L, Shahidi S, Zhuravleva A. Allosteric fine-tuning of the conformational equilibrium poises the chaperone BiP for post-translational regulation. *eLife*. 2017;6(e29430.). <https://doi.org/10.7554/eLife.29430.001>.
47. Kityk R, Kopp J, Sinning I, Mayer MP. Structure and Dynamics of the ATP-Bound Open Conformation of Hsp70 Chaperones. *Molecular Cell*. 2012;48(6): 863–874. <https://doi.org/10.1016/j.molcel.2012.09.023>.
48. Qi R, Sarbeng EB, Liu Q, Le KQ, Xu X, Xu H, et al. Allosteric opening of the polypeptide-binding site when an Hsp70 binds ATP. *Nature Structural and Molecular Biology*. 2013;20(7): 900–907. <https://doi.org/10.1038/nsmb.2583>.
49. Kumar DP, Vorvis C, Sarbeng EB, Cabra Ledesma VC, Willis JE, Liu Q. The Four Hydrophobic Residues on the Hsp70 Inter-Domain Linker Have Two Distinct Roles. *Journal of Molecular Biology*. 2011;411(5): 1099–1113. <https://doi.org/10.1016/j.jmb.2011.07.001>.

50. Mayer MP, Bukau B, Schröder H, Rüdiger S, Paal K, Laufen T. Multistep mechanism of substrate binding determines chaperone activity of Hsp70. *Nature Structural Biology*. 2000;7(7): 586–593. <https://doi.org/10.1038/76819>.
51. Fenton AW. Allostery: an illustrated definition for the ‘second secret of life’. *Trends in Biochemical Sciences*. 2008;33(9): 420–425. <https://doi.org/10.1016/j.tibs.2008.05.009>.
52. Kityk R, Vogel M, Schlecht R, Bukau B, Mayer MP. Pathways of allosteric regulation in Hsp70 chaperones. *Nature Communications*. 2015;6(1): 8308. <https://doi.org/10.1038/ncomms9308>.
53. Pobre KFR, Poet GJ, Hendershot LM. The endoplasmic reticulum (ER) chaperone BiP is a master regulator of ER functions: Getting by with a little help from ERdj friends. *Journal of Biological Chemistry*. 2019;294(6): 2098–2108. <https://doi.org/10.1074/jbc.REV118.002804>.
54. Easton DP, Kaneko Y, Subject JR. The Hsp110 and Grp170 stress proteins: newly recognized relatives of the Hsp70s. *Cell Stress & Chaperones*. 2000;5(4): 276–290.
55. Behnke J, Feige MJ, Hendershot LM. BiP and Its Nucleotide Exchange Factors Grp170 and Sil1: Mechanisms of Action and Biological Functions. *Journal of Molecular Biology*. 2015;427(7): 1589–1608. <https://doi.org/10.1016/j.jmb.2015.02.011>.
56. Mayer MP, Rüdiger S, Bukau B. Molecular Basis for Interactions of the DnaK Chaperone with Substrates. *Biological Chemistry*. 2000;381(9–10). <https://doi.org/10.1515/BC.2000.109>.
57. Buczynski G, Slepnev S V., Sehorn MG, Witt SN. Characterization of a Lidless Form of the Molecular Chaperone DnaK. *Journal of Biological Chemistry*. 2001;276(29): 27231–27236. <https://doi.org/10.1074/jbc.M100237200>.
58. Petrova K, Oyadomari S, Hendershot LM, Ron D. Regulated association of misfolded endoplasmic reticulum luminal proteins with P58/DNAJc3. *EMBO Journal*. 2008;27(21): 2862–2872. <https://doi.org/10.1038/emboj.2008.199>.
59. Rüdiger S, Germeroth L, Schneider-Mergener J, Bukau B. Substrate specificity of the DnaK chaperone determined by screening cellulose-bound peptide libraries. *The EMBO journal*. 1997;16(7): 1501–1507. <https://doi.org/10.1093/emboj/16.7.1501>.

60. Stevens SY, Cai S, Pellicchia M, Zuiderweg ERP. The solution structure of the bacterial HSP70 chaperone protein domain DnaK(393-507) in complex with the peptide NRLLLTG. *Protein Science*. 2009;12(11): 2588–2596. <https://doi.org/10.1110/ps.03269103>.
61. Cupp-Vickery JR, Peterson JC, Ta DT, Vickery LE. Crystal structure of the molecular chaperone HscA substrate binding domain complexed with the IscU recognition peptide ELPPVKIHC. *Journal of molecular biology*. 2004;342(4): 1265–1278. <https://doi.org/10.1016/j.jmb.2004.07.025>.
62. Jiang J, Prasad K, Lafer EM, Sousa R. Structural basis of interdomain communication in the Hsc70 chaperone. *Molecular cell*. 2005;20(4): 513–524. <https://doi.org/10.1016/j.molcel.2005.09.028>.
63. Pellicchia M, Montgomery DL, Stevens SY, Vander Kooi CW, Feng HP, Gierasch LM, et al. Structural insights into substrate binding by the molecular chaperone DnaK. *Nature structural biology*. 2000;7(4): 298–303. <https://doi.org/10.1038/74062>.
64. Morshauer RC, Hu W, Wang H, Pang Y, Flynn GC, Zuiderweg ERP. High-resolution solution structure of the 18 kDa substrate-binding domain of the mammalian chaperone protein Hsc70 1 1 Edited by P. E. Wright. *Journal of Molecular Biology*. 1999;289(5): 1387–1403. <https://doi.org/10.1006/jmbi.1999.2776>.
65. Simons JF, Ferro-Novick S, Rose MD, Helenius A. BiP/Kar2p serves as a molecular chaperone during carboxypeptidase Y folding in yeast. *The Journal of cell biology*. 1995;130(1): 41–49. <https://doi.org/10.1083/jcb.130.1.41>.
66. Plemper RK, Böhmeler S, Bordallo J, Sommer T, Wolf DH. Mutant analysis links the translocon and BiP to retrograde protein transport for ER degradation. *Nature*. 1997;388(6645): 891–895. <https://doi.org/10.1038/42276>.
67. Stolz A, Wolf DH. Endoplasmic reticulum associated protein degradation: A chaperone assisted journey to hell. *Biochimica et Biophysica Acta (BBA) - Molecular Cell Research*. 2010;1803(6): 694–705. <https://doi.org/10.1016/j.bbamcr.2010.02.005>.
68. Lièvremont JP, Rizzuto R, Hendershot L, Meldolesi J. BiP, a Major Chaperone Protein of the Endoplasmic Reticulum Lumen, Plays a Direct and Important Role in the Storage of the Rapidly Exchanging Pool of Ca<sup>2+</sup>. *Journal of Biological Chemistry*. 1997;272(49): 30873–30879. <https://doi.org/10.1074/jbc.272.49.30873>.

69. Mekahli D, Bultynck G, Parys JB, De Smedt H, Missiaen L. Endoplasmic-Reticulum Calcium Depletion and Disease. *Cold Spring Harbor Perspectives in Biology*. 2011;3(6): a004317–a004317. <https://doi.org/10.1101/cshperspect.a004317>.
70. Zhang Y, Liu R, Ni M, Gill P, Lee AS. Cell Surface Relocalization of the Endoplasmic Reticulum Chaperone and Unfolded Protein Response Regulator GRP78/BiP. *Journal of Biological Chemistry*. 2010;285(20): 15065–15075. <https://doi.org/10.1074/jbc.M109.087445>.
71. Arap MA, Lahdenranta J, Mintz PJ, Hajitou A, Sarkis AS, Arap W, et al. Cell surface expression of the stress response chaperone GRP78 enables tumor targeting by circulating ligands. *Cancer Cell*. 2004;6(3): 275–284. <https://doi.org/10.1016/j.ccr.2004.08.018>.
72. Tsai YL, Zhang Y, Tseng CC, Stanciuskas R, Pinaud F, Lee AS. Characterization and Mechanism of Stress-induced Translocation of 78-Kilodalton Glucose-regulated Protein (GRP78) to the Cell Surface. *Journal of Biological Chemistry*. 2015;290(13): 8049–8064. <https://doi.org/10.1074/jbc.M114.618736>.
73. Kelber JA, Panopoulos AD, Shani G, Booker EC, Belmonte JC, Vale WW, et al. Blockade of Cripto binding to cell surface GRP78 inhibits oncogenic Cripto signaling via MAPK/PI3K and Smad2/3 pathways. *Oncogene*. 2009;28(24): 2324–2336. <https://doi.org/10.1038/onc.2009.97>.
74. Shani G, Fischer WH, Justice NJ, Kelber JA, Vale W, Gray PC. GRP78 and Cripto Form a Complex at the Cell Surface and Collaborate To Inhibit Transforming Growth Factor  $\beta$  Signaling and Enhance Cell Growth. *Molecular and Cellular Biology*. 2008;28(2): 666–677. <https://doi.org/10.1128/MCB.01716-07>.
75. Misra UK, Deedwania R, Pizzo SV. Activation and Cross-talk between Akt, NF- $\kappa$ B, and Unfolded Protein Response Signaling in 1-LN Prostate Cancer Cells Consequent to Ligation of Cell Surface-associated GRP78. *Journal of Biological Chemistry*. 2006;281(19): 13694–13707. <https://doi.org/10.1074/jbc.M511694200>.
76. Ren H, Zhai W, Lu X, Wang G. The Cross-Links of Endoplasmic Reticulum Stress, Autophagy, and Neurodegeneration in Parkinson's Disease. *Frontiers in Aging Neuroscience*. 2021;13(691881). <https://doi.org/10.3389/fnagi.2021.691881>.
77. Bhattarai KR, Chaudhary M, Kim HR, Chae HJ. Endoplasmic Reticulum (ER) Stress Response Failure in Diseases. *Trends in Cell Biology*. 2020;30(9): 672–675. <https://doi.org/10.1016/j.tcb.2020.05.004>.

78. Hetz C, Zhang K, Kaufman RJ. Mechanisms, regulation and functions of the unfolded protein response. <https://doi.org/10.1038/s41580-020-0250-z>.
79. Kaufman RJ. Orchestrating the unfolded protein response in health and disease. *Journal of Clinical Investigation*. 2002;110(10): 1389–1398. <https://doi.org/10.1172/JCI16886>.
80. Ron D, Walter P. Signal integration in the endoplasmic reticulum unfolded protein response. *Nature Reviews Molecular Cell Biology*. 2007;8(7): 519–529. <https://doi.org/10.1038/nrm2199>.
81. Read A, Schröder M. The Unfolded Protein Response: An Overview. *Biology*. 2021;10(5): 384. <https://doi.org/10.3390/biology10050384>.
82. Yoshida H, Matsui T, Yamamoto A, Okada T, Mori K. XBP1 mRNA Is Induced by ATF6 and Spliced by IRE1 in Response to ER Stress to Produce a Highly Active Transcription Factor. *Cell*. 2001;107(7): 881–891. [https://doi.org/10.1016/S0092-8674\(01\)00611-0](https://doi.org/10.1016/S0092-8674(01)00611-0).
83. Shen J, Chen X, Hendershot L, Prywes R. ER Stress Regulation of ATF6 Localization by Dissociation of BiP/GRP78 Binding and Unmasking of Golgi Localization Signals. *Developmental Cell*. 2002;3(1): 99–111. [https://doi.org/10.1016/S1534-5807\(02\)00203-4](https://doi.org/10.1016/S1534-5807(02)00203-4).
84. Haze K, Yoshida H, Yanagi H, Yura T, Mori K. Mammalian Transcription Factor ATF6 Is Synthesized as a Transmembrane Protein and Activated by Proteolysis in Response to Endoplasmic Reticulum Stress. *Molecular Biology of the Cell*. 1999;10(11): 3787–3799. <https://doi.org/10.1091/mbc.10.11.3787>.
85. Zhou J, Liu CY, Back SH, Clark RL, Peisach D, Xu Z, et al. The crystal structure of human IRE1 luminal domain reveals a conserved dimerization interface required for activation of the unfolded protein response. *Proceedings of the National Academy of Sciences*. 2006;103(39): 14343–14348. <https://doi.org/10.1073/pnas.0606480103>.
86. Carrara M, Prischi F, Nowak PR, Ali MM. Crystal structures reveal transient PERK luminal domain tetramerization in endoplasmic reticulum stress signaling. *The EMBO Journal*. 2015;34(11): 1589–1600. <https://doi.org/10.15252/emj.201489183>.

87. Shamu CE, Walter P. Oligomerization and phosphorylation of the Ire1p kinase during intracellular signaling from the endoplasmic reticulum to the nucleus. *The EMBO journal*. 1996;15(12): 3028–3039.
88. Tirasophon W, Welihinda AA, Kaufman RJ. A stress response pathway from the endoplasmic reticulum to the nucleus requires a novel bifunctional protein kinase/endoribonuclease (Ire1p) in mammalian cells. *Genes & Development*. 1998;12(12): 1812–1824. <https://doi.org/10.1101/gad.12.12.1812>.
89. Harding HP, Zhang Y, Ron D. Protein translation and folding are coupled by an endoplasmic-reticulum-resident kinase. *Nature*. 1999;397(6716): 271–274. <https://doi.org/10.1038/16729>.
90. Prischi F, Nowak PR, Carrara M, Ali MMU. Phosphoregulation of Ire1 RNase splicing activity. *Nature Communications*. 2014;5(1): 3554. <https://doi.org/10.1038/ncomms4554>.
91. Vattem KM, Wek RC. Reinitiation involving upstream ORFs regulates ATF4 mRNA translation in mammalian cells. *Proceedings of the National Academy of Sciences*. 2004;101(31): 11269–11274. <https://doi.org/10.1073/pnas.0400541101>.
92. Calfon M, Zeng H, Urano F, Till JH, Hubbard SR, Harding HP, et al. IRE1 couples endoplasmic reticulum load to secretory capacity by processing the XBP-1 mRNA. *Nature*. 2002;415(6867): 92–96. <https://doi.org/10.1038/415092a>.
93. Cox JS, Walter P. A Novel Mechanism for Regulating Activity of a Transcription Factor That Controls the Unfolded Protein Response. *Cell*. 1996;87(3): 391–404. [https://doi.org/10.1016/S0092-8674\(00\)81360-4](https://doi.org/10.1016/S0092-8674(00)81360-4).
94. Hollien J, Weissman JS. Decay of Endoplasmic Reticulum-Localized mRNAs During the Unfolded Protein Response. *Science*. 2006;313(5783): 104–107. <https://doi.org/10.1126/science.1129631>.
95. Amin-Wetzel N, Neidhardt L, Yan Y, Mayer MP, Ron D. Unstructured regions in IRE1 $\alpha$  specify BiP-mediated destabilisation of the luminal domain dimer and repression of the UPR. *eLife*. 2019;8. <https://doi.org/10.7554/eLife.50793>.
96. Promlek T, Ishiwata-Kimata Y, Shido M, Sakuramoto M, Kohno K, Kimata Y. Membrane aberrancy and unfolded proteins activate the endoplasmic reticulum stress sensor Ire1 in different ways. *Molecular Biology of the Cell*. 2011;22(18): 3520–3532. <https://doi.org/10.1091/mbc.e11-04-0295>.

97. Karagöz GE, Acosta-Alvear D, Nguyen HT, Lee CP, Chu F, Walter P. An unfolded protein-induced conformational switch activates mammalian IRE1. *eLife*. 2017;6(e30700). <https://doi.org/10.7554/eLife.30700>.
98. Gardner BM, Walter P. Unfolded Proteins Are Ire1-Activating Ligands That Directly Induce the Unfolded Protein Response. *Science*. 2011;333(6051): 1891–1894. <https://doi.org/10.1126/science.1209126>.
99. Kimata Y, Ishiwata-Kimata Y, Ito T, Hirata A, Suzuki T, Oikawa D, et al. Two regulatory steps of ER-stress sensor Ire1 involving its cluster formation and interaction with unfolded proteins. *The Journal of Cell Biology*. 2007;179(1): 75–86. <https://doi.org/10.1083/jcb.200704166>.
100. Credle JJ, Finer-Moore JS, Papa FR, Stroud RM, Walter P. On the mechanism of sensing unfolded protein in the endoplasmic reticulum. *Proceedings of the National Academy of Sciences*. 2005;102(52): 18773–18784. <https://doi.org/10.1073/pnas.0509487102>.
101. Karagöz GE, Acosta-Alvear D, Walter P. The Unfolded Protein Response: Detecting and Responding to Fluctuations in the Protein-Folding Capacity of the Endoplasmic Reticulum. *Cold Spring Harbor Perspectives in Biology*. 2019;11(9): a033886. <https://doi.org/10.1101/cshperspect.a033886>.
102. Karagöz GE, Acosta-Alvear D, Nguyen HT, Lee CP, Chu F, Walter P. An unfolded protein-induced conformational switch activates mammalian IRE1. *eLife*. 2017; <https://doi.org/10.7554/eLife.30700.001>.
103. Oikawa D, Kimata Y, Kohno K, Iwawaki T. Activation of mammalian IRE1 $\alpha$  upon ER stress depends on dissociation of BiP rather than on direct interaction with unfolded proteins. *Experimental Cell Research*. 2009;315(15): 2496–2504. <https://doi.org/10.1016/j.yexcr.2009.06.009>.
104. Preissler S, Ron D. Early Events in the Endoplasmic Reticulum Unfolded Protein Response. *Cold Spring Harbor Perspectives in Biology*. 2019;11(4): a033894. <https://doi.org/10.1101/cshperspect.a033894>.
105. Amin-Wetzel N, Saunders RA, Kamphuis MJ, Rato C, Preissler S, Harding HP, et al. A J-Protein Co-chaperone Recruits BiP to Monomerize IRE1 and Repress the Unfolded Protein Response. *Cell*. 2017;171(7): 1625–1637.e13. <https://doi.org/10.1016/j.cell.2017.10.040>.

106. Ma K, Vattem KM, Wek RC. Dimerization and Release of Molecular Chaperone Inhibition Facilitate Activation of Eukaryotic Initiation Factor-2 Kinase in Response to Endoplasmic Reticulum Stress. *Journal of Biological Chemistry*. 2002;277(21): 18728–18735. <https://doi.org/10.1074/jbc.M200903200>.
107. Okamura K, Kimata Y, Higashio H, Tsuru A, Kohno K. Dissociation of Kar2p/BiP from an ER Sensory Molecule, Ire1p, Triggers the Unfolded Protein Response in Yeast. *Biochemical and Biophysical Research Communications*. 2000;279(2): 445–450. <https://doi.org/10.1006/bbrc.2000.3987>.
108. Bertolotti A, Zhang Y, Hendershot LM, Harding HP, Ron D. Dynamic interaction of BiP and ER stress transducers in the unfolded-protein response. *Nature Cell Biology*. 2000;2(6): 326–332. <https://doi.org/10.1038/35014014>.
109. Sepulveda D, Rojas-Rivera D, Rodríguez DA, Groenendyk J, Köhler A, Lebeaupin C, et al. Interactome Screening Identifies the ER Luminal Chaperone Hsp47 as a Regulator of the Unfolded Protein Response Transducer IRE1 $\alpha$ . *Molecular Cell*. 2018;69(2): 238-252.e7. <https://doi.org/10.1016/j.molcel.2017.12.028>.
110. Carrara M, Prischi F, Nowak PR, Kopp MC, Ali MM. Noncanonical binding of BiP ATPase domain to Ire1 and Perk is dissociated by unfolded protein CH1 to initiate ER stress signaling. *eLife*. 2015;4. <https://doi.org/10.7554/eLife.03522>.
111. Kopp MC, Nowak PR, Larburu N, Adams CJ, Ali MM. In vitro FRET analysis of IRE1 and BiP association and dissociation upon endoplasmic reticulum stress. *eLife*. 2018;7(e30257). <https://doi.org/10.7554/eLife.30257>.
112. Carrara M, Prischi F, Nowak PR, Kopp MC, Ali MM. Noncanonical binding of BiP ATPase domain to Ire1 and Perk is dissociated by unfolded protein CH1 to initiate ER stress signaling. *eLife*. 2015;4(e03522). <https://doi.org/10.7554/eLife.03522>.
113. Todd-Corlett A, Jones E, Seghers C, Gething MJ. Lobe IB of the ATPase Domain of Kar2p/BiP Interacts with Ire1p to Negatively Regulate the Unfolded Protein Response in *Saccharomyces cerevisiae*. *Journal of Molecular Biology*. 2007;367(3): 770–787. <https://doi.org/10.1016/j.jmb.2007.01.009>.
114. Kopp MC, Larburu N, Durairaj V, Adams CJ, Ali MMU. UPR proteins IRE1 and PERK switch BiP from chaperone to ER stress sensor. *Nature Structural and Molecular Biology*. 2019;26(11): 1053–1062. <https://doi.org/10.1038/s41594-019-0324-9>.

115. Sou SN, Ilieva KM, Polizzi KM. Binding of human BiP to the ER stress transducers IRE1 and PERK requires ATP. *Biochemical and Biophysical Research Communications*. 2012;420(2): 473–478. <https://doi.org/10.1016/j.bbrc.2012.03.030>.
116. Griffith AA, Holmes W. Fine Tuning: Effects of Post-Translational Modification on Hsp70 Chaperones. *International Journal of Molecular Sciences*. 2019;20(17): 4207. <https://doi.org/10.3390/ijms20174207>.
117. Silver JT, Noble EG. Regulation of survival gene hsp70. *Cell stress & chaperones*. 2012;17(1): 1–9. <https://doi.org/10.1007/s12192-011-0290-6>.
118. Alagar Boopathy LR, Jacob-Tomas S, Alecki C, Vera M. Mechanisms tailoring the expression of heat shock proteins to proteostasis challenges. *Journal of Biological Chemistry*. 2022;298(5): 101796. <https://doi.org/10.1016/j.jbc.2022.101796>.
119. Anckar J, Sistonen L. Regulation of HSF1 function in the heat stress response: implications in aging and disease. *Annual Review of Biochemistry*. 2011;80(1): 1089–1115. <https://doi.org/10.1146/annurev-biochem-060809-095203>.
120. Vihervaara A, Sistonen L. HSF1 at a glance. *Journal of Cell Science*. 2014;127(2): 261–266. <https://doi.org/10.1242/jcs.132605>.
121. Yu E meng, Yoshinaga T, Jalufka FL, Ehsan H, Mark Welch DB, Kaneko G. The complex evolution of the metazoan HSP70 gene family. *Scientific Reports*. 2021;11(1): 17794. <https://doi.org/10.1038/s41598-021-97192-9>.
122. Marcinowski M, Rosam M, Seitz C, Elferich J, Behnke J, Bello C, et al. Conformational selection in substrate recognition by Hsp70 chaperones. *Journal of Molecular Biology*. 2013;425(3): 466–474. <https://doi.org/10.1016/j.jmb.2012.11.030>.
123. Marcinowski M, Höller M, Feige MJ, Baerend D, Lamb DC, Buchner J. Substrate discrimination of the chaperone BiP by autonomous and cochaperone-regulated conformational transitions. *Nature Publishing Group*. 2011; <https://doi.org/10.1038/nsmb.1970>.
124. Behnke J, Hendershot LM. The large Hsp70 Grp170 binds to unfolded protein substrates in vivo with a regulation distinct from conventional Hsp70s. *Journal of Biological Chemistry*. 2014;289(5): 2899–2907. <https://doi.org/10.1074/jbc.M113.507491>.

125. Haßdenteufel S, Johnson N, Paton AW, Paton JC, High S, Zimmermann R. Chaperone-Mediated Sec61 Channel Gating during ER Import of Small Precursor Proteins Overcomes Sec61 Inhibitor-Reinforced Energy Barrier. *Cell reports*. 2018;23(5): 1373–1386. <https://doi.org/10.1016/j.celrep.2018.03.122>.
126. Brodsky JL, Schekman R. A Sec63p-BiP complex from yeast is required for protein translocation in a reconstituted proteoliposome. *The Journal of cell biology*. 1993;123(6 Pt 1): 1355–1363. <https://doi.org/10.1083/jcb.123.6.1355>.
127. Blau M, Mullapudi S, Becker T, Dudek J, Zimmermann R, Penczek PA, et al. ERj1p uses a universal ribosomal adaptor site to coordinate the 80S ribosome at the membrane. *Nature Structural & Molecular Biology*. 2005;12(11): 1015–1016. <https://doi.org/10.1038/nsmb998>.
128. Dudek J, Greiner M, Müller A, Hendershot LM, Kopsch K, Nastainczyk W, et al. ERj1p has a basic role in protein biogenesis at the endoplasmic reticulum. *Nature Structural & Molecular Biology*. 2005;12(11): 1008–1014. <https://doi.org/10.1038/nsmb1007>.
129. Shen Y, Hendershot LM. ERdj3, a stress-inducible endoplasmic reticulum DnaJ homologue, serves as a cofactor for BiP's interactions with unfolded substrates. *Molecular biology of the cell*. 2005;16(1): 40–50. <https://doi.org/10.1091/mbc.e04-05-0434>.
130. Jin Y, Awad W, Petrova K, Hendershot LM. Regulated release of ERdj3 from unfolded proteins by BiP. *The EMBO journal*. 2008;27(21): 2873–2882. <https://doi.org/10.1038/emboj.2008.207>.
131. Jin Y, Zhuang M, Hendershot LM. ERdj3, a luminal ER DnaJ homologue, binds directly to unfolded proteins in the mammalian ER: identification of critical residues. *Biochemistry*. 2009;48(1): 41–49. <https://doi.org/10.1021/bi8015923>.
132. Weitzmann A, Baldes C, Dudek J, Zimmermann R. The heat shock protein 70 molecular chaperone network in the pancreatic endoplasmic reticulum – a quantitative approach. *FEBS Journal*. 2007;274(19): 5175–5187. <https://doi.org/10.1111/j.1742-4658.2007.06039.x>.
133. Shen Y, Meunier L, Hendershot LM. Identification and Characterization of a Novel Endoplasmic Reticulum (ER) DnaJ Homologue, Which Stimulates ATPase Activity of BiP in Vitro and Is Induced by ER Stress. *Journal of Biological Chemistry*. 2002;277(18): 15947–15956. <https://doi.org/10.1074/jbc.M112214200>.

134. Fritz JM, Dong M, Apsley KS, Martin EP, Na CL, Sitaraman S, et al. Deficiency of the BiP cochaperone ERdj4 causes constitutive endoplasmic reticulum stress and metabolic defects. *Molecular Biology of the Cell*. 2014;25(4): 431–440. <https://doi.org/10.1091/mbc.e13-06-0319>.
135. Maegawa K ichi, Watanabe S, Noi K, Okumura M, Amagai Y, Inoue M, et al. The Highly Dynamic Nature of ERdj5 Is Key to Efficient Elimination of Aberrant Protein Oligomers through ER-Associated Degradation. *Structure*. 2017;25(6): 846-857.e4. <https://doi.org/10.1016/j.str.2017.04.001>.
136. Puig A, Lyles MM, Noiva R, Gilbert HF. The role of the thiol/disulfide centers and peptide binding site in the chaperone and anti-chaperone activities of protein disulfide isomerase. *Journal of Biological Chemistry*. 1994;269(29): 19128–19135. [https://doi.org/10.1016/S0021-9258\(17\)32284-6](https://doi.org/10.1016/S0021-9258(17)32284-6).
137. Behnke J, Mann MJ, Scruggs FL, Feige MJ, Hendershot LM. Members of the Hsp70 Family Recognize Distinct Types of Sequences to Execute ER Quality Control. *Molecular Cell*. 2016;63(5): 739–752. <https://doi.org/10.1016/j.molcel.2016.07.012>.
138. Tao J, Petrova K, Ron D, Sha B. Crystal structure of P58(IPK) TPR fragment reveals the mechanism for its molecular chaperone activity in UPR. *Journal of molecular biology*. 2010;397(5): 1307–1315. <https://doi.org/10.1016/j.jmb.2010.02.028>.
139. Ohta M, Takaiwa F. Emerging features of ER resident J-proteins in plants. *Plant signaling & behavior*. 2014;9(3): e28194. <https://doi.org/10.4161/psb.28194>.
140. Schorr S, Klein MC, Gamayun I, Melnyk A, Jung M, Schäuble N, et al. Co-chaperone Specificity in Gating of the Polypeptide Conducting Channel in the Membrane of the Human Endoplasmic Reticulum. *The Journal of biological chemistry*. 2015;290(30): 18621–18635. <https://doi.org/10.1074/jbc.M115.636639>.
141. Bracher A, Verghese J. GrpE, Hsp110/Grp170, HspBP1/Sil1 and BAG Domain Proteins: Nucleotide Exchange Factors for Hsp70 Molecular Chaperones. *Subcellular Biochemistry*. 2015;78: 1–33. [https://doi.org/10.1007/978-3-319-11731-7\\_1](https://doi.org/10.1007/978-3-319-11731-7_1).
142. Bukau B, Weissman J, Horwich A. Molecular Chaperones and Protein Quality Control. *Cell*. 2006;125(3): 443–451. <https://doi.org/10.1016/j.cell.2006.04.014>.

143. Porter AW, Nguyen DN, Clayton DR, Ruiz WG, Mutchler SM, Ray EC, et al. The molecular chaperone GRP170 protects against ER stress and acute kidney injury in mice. *JCI insight*. 2022;7(5). <https://doi.org/10.1172/jci.insight.151869>.
144. Truman AW, Bourbouli D, Mollapour M. Decrypting the chaperone code. *Journal of Biological Chemistry*. 2021;296: 100293. <https://doi.org/10.1016/j.jbc.2021.100293>.
145. Nitika, Porter CM, Truman AW, Truttmann MC. *Post-translational modifications of Hsp70 family proteins: Expanding the chaperone code*. *Journal of Biological Chemistry*. 2020. p. 10689–10708. <https://doi.org/10.1074/jbc.REV120.011666>.
146. Callis J. The ubiquitination machinery of the ubiquitin system. *The arabidopsis book*. 2014;12: e0174. <https://doi.org/10.1199/tab.0174>.
147. Freiden PJ, Gaut JR, Hendershot LM. Interconversion of three differentially modified and assembled forms of BiP. *EMBO Journal*. 1992;11(1): 63–70. <https://doi.org/10.1002/j.1460-2075.1992.tb05028.x>.
148. Preissler S, Rato C, Chen R, Antrobus R, Ding S, Fearnley IM, et al. AMPylation matches BiP activity to client protein load in the endoplasmic reticulum. *eLife*. 2015;4(e12621). <https://doi.org/10.7554/eLife.12621>.
149. Preissler S, Rato C, Chen Ru, Antrobus R, Shujing Ding, Fearnley IM, et al. AMPylation matches BiP activity to clientprotein load in the endoplasmic reticulum. *Elife*. 2015;
150. Chambers JE, Petrova K, Tomba G, Vendruscolo M, Ron D. ADP ribosylation adapts an ER chaperone response to short-term fluctuations in unfolded protein load. *Journal of Cell Biology*. 2012;198(3): 371–385. <https://doi.org/10.1083/jcb.201202005>.
151. Staddon JM, Bouzyk MM, Rozengurt E. Interconversion of GRP78/BiP. A novel event in the action of Pasteurella multocida toxin, bombesin, and platelet-derived growth factor. *The Journal of biological chemistry*. 1992;267(35): 25239–25245.
152. Hendershot LM, Ting J, Lee AS. Identity of the immunoglobulin heavy-chain-binding protein with the 78,000-dalton glucose-regulated protein and the role of posttranslational modifications in its binding function. *Molecular and Cellular Biology*. 1988;8(10): 4250–4256. <https://doi.org/10.1128/MCB.8.10.4250>.

153. Xu L, Nitika, Hasin N, Cuskelly DD, Wolfgeher D, Doyle S, et al. Rapid deacetylation of yeast Hsp70 mediates the cellular response to heat stress. *Scientific Reports*. 2019;9(1): 16260. <https://doi.org/10.1038/s41598-019-52545-3>.
154. Sanyal A, Zbornik EA, Watson BG, Christoffer C, Ma J, Kihara D, et al. Kinetic and structural parameters governing Fic-mediated adenylylation/AMPylation of the Hsp70 chaperone, BiP/GRP78. *Cell Stress and Chaperones*. 2021;26(4): 639–656. <https://doi.org/10.1007/s12192-021-01208-2>.
155. Sanyal A, Chen AJ, Nakayasu ES, Lazar CS, Zbornik EA, Worby CA, et al. A Novel Link between Fic (Filamentation Induced by cAMP)-mediated Adenylylation/AMPylation and the Unfolded Protein Response. *Journal of Biological Chemistry*. 2015;290(13): 8482–8499. <https://doi.org/10.1074/jbc.M114.618348>.
156. Gao W wei, Xiao R quan, Peng B ling, Xu H teng, Shen H feng, Huang M feng, et al. Arginine methylation of HSP70 regulates retinoid acid-mediated RAR $\beta$ 2 gene activation. *Proceedings of the National Academy of Sciences*. 2015;112(26). <https://doi.org/10.1073/pnas.1509658112>.
157. Preissler S, Rohland L, Yan Y, Chen R, Read RJ, Ron D. AMPylation targets the rate-limiting step of BiP's ATPase cycle for its functional inactivation. *eLife*. 2017;6(e29428). <https://doi.org/10.7554/eLife.29428.001>.
158. Dorner AJ, Wasley LC, Kaufman RJ. Overexpression of GRP78 mitigates stress induction of glucose regulated proteins and blocks secretion of selective proteins in Chinese hamster ovary cells. *The EMBO Journal*. 1992;11(4): 1563–1571. <https://doi.org/10.1002/j.1460-2075.1992.tb05201.x>.
159. Hendershot LM, Wei JY, Gaut JR, Lawson B, Freiden PJ, Murti KG. In vivo expression of mammalian BiP ATPase mutants causes disruption of the endoplasmic reticulum. *Molecular Biology of the Cell*. 1995;6(3): 283–296. <https://doi.org/10.1091/mbc.6.3.283>.
160. *GRP78 (human)*.
161. Bordoli MR, Yum J, Breitkopf SB, Thon JN, Italiano JE, Xiao J, et al. A Secreted Tyrosine Kinase Acts in the Extracellular Environment. *Cell*. 2014;158(5): 1033–1044. <https://doi.org/10.1016/j.cell.2014.06.048>.

162. Casado P, Alcolea MP, Iorio F, Rodríguez-Prados JC, Vanhaesebroeck B, Saez-Rodríguez J, et al. Phosphoproteomics data classify hematological cancer cell lines according to tumor type and sensitivity to kinase inhibitors. *Genome Biology*. 2013;14(4): R37. <https://doi.org/10.1186/gb-2013-14-4-r37>.
163. Tsai CF, Wang YT, Yen HY, Tsou CC, Ku WC, Lin PY, et al. Large-scale determination of absolute phosphorylation stoichiometries in human cells by motif-targeting quantitative proteomics. *Nature Communications*. 2015;6(1): 6622. <https://doi.org/10.1038/ncomms7622>.
164. Gaut JR, Hendershot LM. Mutations within the nucleotide binding site of immunoglobulin-binding protein inhibit ATPase activity and interfere with release of immunoglobulin heavy chain. *The Journal of biological chemistry*. 1993;268(10): 7248–7255.
165. Preissler S, Chambers JE, Crespillo-Casado A, Avezov E, Miranda E, Perez J, et al. Physiological modulation of BiP activity by trans-protomer engagement of the interdomain linker. *eLife*. 2015;4(e08961). <https://doi.org/10.7554/eLife.08961.001>.
166. Satoh M, Nakai A, Sokawa Y, Hirayoshi K, Nagata K. Modulation of the Phosphorylation of Glucose-Regulated Protein, GRP78, by Transformation and Inhibition of Glycosylation. *Experimental Cell Research*. 1993;205(1): 76–83. <https://doi.org/10.1006/excr.1993.1060>.
167. Ballinger CA, Connell P, Wu Y, Hu Z, Thompson LJ, Yin LY, et al. Identification of CHIP, a Novel Tetratricopeptide Repeat-Containing Protein That Interacts with Heat Shock Proteins and Negatively Regulates Chaperone Functions. *Molecular and Cellular Biology*. 1999;19(6): 4535–4545. <https://doi.org/10.1128/MCB.19.6.4535>.
168. Muller P, Ruckova E, Halada P, Coates PJ, Hrstka R, Lane DP, et al. C-terminal phosphorylation of Hsp70 and Hsp90 regulates alternate binding to co-chaperones CHIP and HOP to determine cellular protein folding/degradation balances. *Oncogene*. 2013;32(25): 3101–3110. <https://doi.org/10.1038/onc.2012.314>.
169. Verghese J, Abrams J, Wang Y, Morano KA. Biology of the Heat Shock Response and Protein Chaperones: Budding Yeast (*Saccharomyces cerevisiae*) as a Model System. *Microbiology and Molecular Biology Reviews*. 2012;76(2): 115–158. <https://doi.org/10.1128/MMBR.05018-11>.

170. Carugo O, Pongor S. A normalized root-mean-square distance for comparing protein three-dimensional structures. *Protein Science*. 2001;10(7): 1470–1473. <https://doi.org/10.1110/ps.690101>.
171. Ashkenazy H, Abadi S, Martz E, Chay O, Mayrose I, Pupko T, et al. ConSurf 2016: an improved methodology to estimate and visualize evolutionary conservation in macromolecules. *Nucleic Acids Research*. 2016;44(W1): W344–W350. <https://doi.org/10.1093/NAR/GKW408>.
172. Ashkenazy H, Erez E, Martz E, Pupko T, Ben-Tal N. ConSurf 2010: Calculating evolutionary conservation in sequence and structure of proteins and nucleic acids. *Nucleic Acids Research*. 2010;38(SUPPL. 2). <https://doi.org/10.1093/nar/gkq399>.
173. Celniker G, Nimrod G, Ashkenazy H, Glaser F, Martz E, Mayrose I, et al. ConSurf: Using evolutionary data to raise testable hypotheses about protein function. *Israel Journal of Chemistry*. 2013;53(3–4): 199–206. <https://doi.org/10.1002/ijch.201200096>.
174. Crooks GE, Hon G, Chandonia JM, Brenner SE. WebLogo: A Sequence Logo Generator: Figure 1. *Genome Research*. 2004;14(6): 1188–1190. <https://doi.org/10.1101/gr.849004>.
175. Moro F, Fernández-Sáiz V, Muga A. The Lid Subdomain of DnaK Is Required for the Stabilization of the Substrate-binding Site. *Journal of Biological Chemistry*. 2004;279(19): 19600–19606. <https://doi.org/10.1074/jbc.M400921200>.
176. Mayer MP, Schröder H, Rüdiger S, Paal K, Laufen T, Bukau B. Multistep mechanism of substrate binding determines chaperone activity of Hsp70. *Nature Structural & Molecular Biology*. 2000;7(7): 586–593.
177. Macias AT, Williamson DS, Allen N, Borgognoni J, Clay A, Daniels Z, et al. Adenosine-Derived Inhibitors of 78 kDa Glucose Regulated Protein (Grp78) ATPase: Insights into Isoform Selectivity. *Journal of Medicinal Chemistry*. 2011;54(12): 4034–4041. <https://doi.org/10.1021/jm101625x>.
178. Zhuravleva A, Gierasch LM. Allosteric signal transmission in the nucleotide-binding domain of 70-kDa heat shock protein (Hsp70) molecular chaperones. *BIOPHYSICS AND COMPUTATIONAL BIOLOGY*. 2011;108(17): 6987–6992. <https://doi.org/10.1073/pnas.1014448108/-/DCSupplemental>.

179. Lee KPK, Dey M, Neculai D, Cao C, Dever TE, Sicheri F. Structure of the Dual Enzyme Ire1 Reveals the Basis for Catalysis and Regulation in Nonconventional RNA Splicing. *Cell*. 2008;132(1): 89–100. <https://doi.org/10.1016/j.cell.2007.10.057>.
180. Westerhuis WHJ, Sturgis JN, Niederman RA. Reevaluation of the Electrophoretic Migration Behavior of Soluble Globular Proteins in the Native and Detergent-Denatured States in Polyacrylamide Gels. *Analytical Biochemistry*. 2000;284(1): 143–152. <https://doi.org/10.1006/abio.2000.4684>.
181. Linda Hendershot RM, Jue-yang Wei ft, Gaut JR, Lawson B, Freiden PJ, Gopal Murti K. In Vivo Expression of Mammalian BiP ATPase Mutants Causes Disruption of the Endoplasmic. *Molecular Biology of the Cell*. 1995;6: 283–296.
182. Bandla S, Diaz S, Nasheuer HP, FitzGerald U. ATPase activity of human binding immunoglobulin protein (BiP) variants is enhanced by signal sequence and physiological concentrations of Mn<sup>2+</sup>. *FEBS Open Bio*. 2019;9(8): 1355–1369. <https://doi.org/10.1002/2211-5463.12645>.
183. Baxter NJ, Williamson MP. Temperature dependence of <sup>1</sup>H chemical shifts in proteins . *Journal of Biomolecular NMR*. 1997;9(4): 359–369. <https://doi.org/10.1023/A:1018334207887>.
184. Schneider M, Rosam M, Glaser M, Patronov A, Shah H, Back KC, et al. BiPPred: Combined sequence- and structure-based prediction of peptide binding to the Hsp70 chaperone BiP. *Proteins: Structure, Function, and Bioinformatics*. 2016;84(10): 1390–1407. <https://doi.org/10.1002/prot.25084>.
185. Belyy V, Zuazo-Gaztelu I, Alamban A, Ashkenaz A, Walter P. Endoplasmic reticulum stress activates human IRE1 $\alpha$  through reversible assembly of inactive dimers into small oligomers. *eLife*. 2022;11(e74342).
186. Thakur AK, Meng W, Gierasch LM. Local and non-local topological information in the denatured state ensemble of a  $\beta$ -barrel protein. *Protein Science*. 2018;27(12): 2062–2072. <https://doi.org/10.1002/pro.3516>.
187. Kathuria S V., Kayatekin C, Barrea R, Kondrashkina E, Graceffa R, Guo L, et al. Microsecond barrier-limited chain collapse observed by time-resolved FRET and SAXS. *Journal of Molecular Biology*. 2014;426(9): 1980–1994. <https://doi.org/10.1016/j.jmb.2014.02.020>.

188. Amin-Wetzel N, Saunders RA, Kamphuis MJ, Rato C, Preissler S, Harding HP, et al. A J-Protein Co-chaperone Recruits BiP to Monomerize IRE1 and Repress the Unfolded Protein Response. *Cell*. 2017;171(7): 1625-1637.e13. <https://doi.org/10.1016/j.cell.2017.10.040>.
189. Chakafana G, Zininga T, Shonhai A. Comparative structure-function features of Hsp70s of Plasmodium falciparum and human origins. *Biophysical Reviews*. 2019;11(4): 591–602. <https://doi.org/10.1007/s12551-019-00563-w>.
190. Mayer MP. Gymnastics of Molecular Chaperones. *Molecular Cell*. 2010;39(3): 321–331. <https://doi.org/10.1016/j.molcel.2010.07.012>.
191. Evans CG, Chang L, Gestwicki JE. Heat shock protein 70 (Hsp70) as an emerging drug target. *Journal of Medicinal Chemistry*. 2010;53(12): 4585–4602. <https://doi.org/10.1021/jm100054f>.
192. Barth J, Schach T, Przyborski JM. HSP70 and their co-chaperones in the human malaria parasite P. falciparum and their potential as drug targets. *Frontiers in Molecular Biosciences*. 2022;9(968248). <https://doi.org/10.3389/fmolb.2022.968248>.
193. Assimon VA, Gilies AT, Rauch JN, Gestwicki JE. Hsp70 Protein Complexes as Drug Targets. *Current Pharmaceutical Design*. 2013;19(3): 404–427.
194. Nitzsche B, Höpfner M, Biersack B. Synthetic Small Molecule Modulators of Hsp70 and Hsp40 Chaperones as Promising Anticancer Agents. *International Journal of Molecular Sciences*. 2023;24(4). <https://doi.org/10.3390/ijms24044083>.
195. Lazarev VF, Sverchinsky D V., Mikhaylova ER, Semenyuk PI, Komarova EY, Niskanen SA, et al. Sensitizing tumor cells to conventional drugs: HSP70 chaperone inhibitors, their selection and application in cancer models. *Cell Death and Disease*. 2018;9(2). <https://doi.org/10.1038/s41419-017-0160-y>.
196. Abd El-Fattah EE, Zakaria AY. Targeting HSP47 and HSP70: promising therapeutic approaches in liver fibrosis management. *Journal of Translational Medicine*. 2022;20(1). <https://doi.org/10.1186/s12967-022-03759-z>.
197. Mouawad N, Capasso G, Ruggeri E, Martinello L, Severin F, Visentin A, et al. Is It Still Possible to Think about HSP70 as a Therapeutic Target in Onco-Hematological Diseases? *Biomolecules*. 2023;13(4). <https://doi.org/10.3390/biom13040604>.

198. Albakova Z, Mangasarova Y, Albakov A, Gorenkova L. HSP70 and HSP90 in Cancer: Cytosolic, Endoplasmic Reticulum and Mitochondrial Chaperones of Tumorigenesis. *Frontiers in Oncology*. 2022;12. <https://doi.org/10.3389/fonc.2022.829520>.
199. Rai R, Kennedy AL, Isingizwe ZR, Javadian P, Benbrook DM, Kabakov AE. Similarities and Differences of Hsp70, hsc70, Grp78 and Mortalin as Cancer Biomarkers and Drug Targets. *Cells*. 2021;10(11). <https://doi.org/10.3390/cells>.
200. Shao H, Taguwa S, Gilbert L, Shkedi A, Sannino S, Guerriero CJ, et al. A campaign targeting a conserved Hsp70 binding site uncovers how subcellular localization is linked to distinct biological activities. *Cell Chemical Biology*. 2022;29(8): 1303-1316.e3. <https://doi.org/10.1016/j.chembiol.2022.06.006>.
201. Chen L, Fan Z, Chang J, Yang R, Hou H, Guo H, et al. Sequence-based drug design as a concept in computational drug design. *Nature communications*. 2023;14(1): 4217. <https://doi.org/10.1038/s41467-023-39856-w>.
202. Anderson AC. The Process of Structure-Based Drug Design. *Chemistry & Biology*. 2003;10(9): 787–797. <https://doi.org/10.1016/j.chembiol.2003.09.002>.
203. Capra JA, Singh M. Predicting functionally important residues from sequence conservation. *Bioinformatics*. 2007;23(15): 1875–1882. <https://doi.org/10.1093/bioinformatics/btm270>.
204. Chen Y, Wang Z, Wang L, Wang J, Li P, Cao D, et al. Deep generative model for drug design from protein target sequence. *Journal of Cheminformatics*. 2023;15(1): 38. <https://doi.org/10.1186/s13321-023-00702-2>.
205. Verbruggen B, Gunnarsson L, Kristiansson E, Österlund T, Owen SF, Snape JR, et al. ECOdrug: A database connecting drugs and conservation of their targets across species. *Nucleic Acids Research*. 2018;46(D1): D930–D936. <https://doi.org/10.1093/nar/gkx1024>.
206. Rudikoff S, Giusti AM, Cook WD, Scharff MD. Single amino acid substitution altering antigen-binding specificity. *Proceedings of the National Academy of Sciences of the United States of America*. 1982;79(6): 1979–1983. <https://doi.org/10.1073/pnas.79.6.1979>.

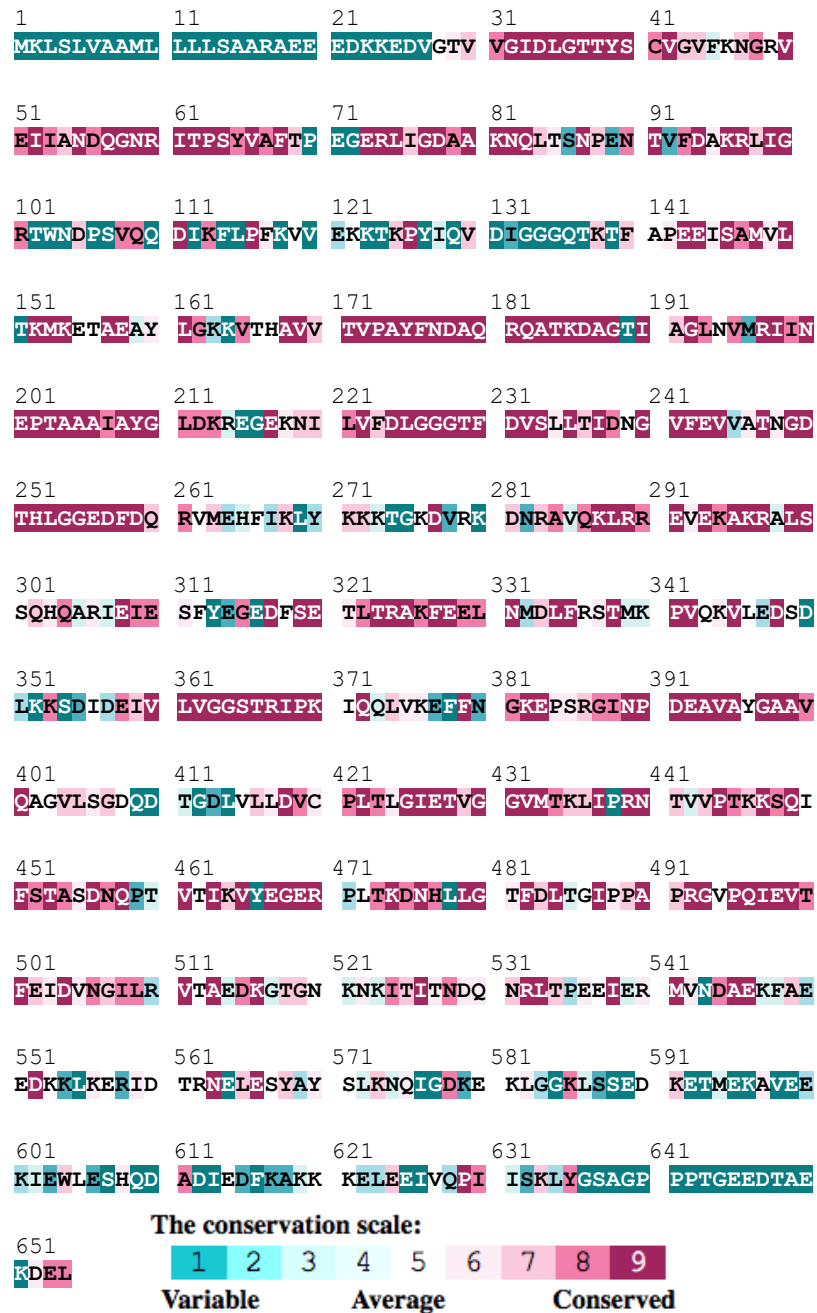
207. Ammar A, Cavill R, Evelo C, Willighagen E. P\_SnpBind-ML: predicting the effect of binding site mutations on protein-ligand binding affinity. *Journal of Cheminformatics*. 2023;15(1): 31. <https://doi.org/10.1186/s13321-023-00701-3>.
208. Zdraljjevic S, Strand C, Seidel HS, Cook DE, Doench JG, Andersen EC. Natural variation in a single amino acid substitution underlies physiological responses to topoisomerase II poisons. *PLOS Genetics*. 2017;13(7): e1006891. <https://doi.org/10.1371/journal.pgen.1006891>.
209. Doyle SM, Hoskins JR, Kravats AN, Heffner AL, Garikapati S, Wickner S. Intermolecular Interactions between Hsp90 and Hsp70. *Journal of Molecular Biology*. 2019;431(15): 2729–2746. <https://doi.org/10.1016/j.jmb.2019.05.026>.
210. Mukherjee M, Sabir S, O'Regan L, Sampson J, Richards MW, Huguenin-Dezot N, et al. Mitotic phosphorylation regulates Hsp72 spindle localization by uncoupling ATP binding from substrate release. *Science Signaling*. 2018;11(543). <https://doi.org/10.1126/scisignal.aao2464>.
211. Laufen T, Mayer MP, Beisel C, Klostermeier D, Mogk A, Reinstein J, et al. Mechanism of regulation of Hsp70 chaperones by DnaJ cochaperones. *Proceedings of the National Academy of Sciences*. 1999;96(10): 5452–5457. <https://doi.org/10.1073/pnas.96.10.5452>.
212. Fernández-Sáiz V, Moro F, Arizmendi JM, Acebrón SP, Muga A. Ionic Contacts at DnaK Substrate Binding Domain Involved in the Allosteric Regulation of Lid Dynamics. *Journal of Biological Chemistry*. 2006;281(11): 7479–7488. <https://doi.org/10.1074/jbc.M512744200>.
213. Umehara K, Hoshikawa M, Tochio N, Tate SI. Substrate Binding Switches the Conformation at the Lynchpin Site in the Substrate-Binding Domain of Human Hsp70 to Enable Allosteric Interdomain Communication. *Molecules (Basel, Switzerland)*. 2018;23(3). <https://doi.org/10.3390/molecules23030528>.
214. Vogel M, Mayer MP, Bukau B. Allosteric regulation of Hsp70 chaperones involves a conserved interdomain linker. *Journal of Biological Chemistry*. 2006;281(50): 38705–38711. <https://doi.org/10.1074/jbc.M609020200>.
215. Liberek K, Marszalek J, Ang D, Georgopoulos C, Zylicz M. Escherichia coli DnaJ and GrpE heat shock proteins jointly stimulate ATPase activity of DnaK. *Proceedings of the National Academy of Sciences*. 1991;88(7): 2874–2878. <https://doi.org/10.1073/pnas.88.7.2874>.

216. Kampinga HH, Craig EA. The HSP70 chaperone machinery: J proteins as drivers of functional specificity. *Nature Reviews Molecular Cell Biology*. 2010;11(8): 579–592. <https://doi.org/10.1038/nrm2941>.
217. Kimata Y, Oikawa D, Shimizu Y, Ishiwata-Kimata Y, Kohno K. A role for BiP as an adjustor for the endoplasmic reticulum stress-sensing protein Ire1. *Journal of Cell Biology*. 2004;167(3): 445–456. <https://doi.org/10.1083/jcb.200405153>.
218. Høie MH, Cagiada M, Beck Frederiksen AH, Stein A, Lindorff-Larsen K. Predicting and interpreting large-scale mutagenesis data using analyses of protein stability and conservation. *Cell Reports*. 2022;38(2): 110207. <https://doi.org/10.1016/j.celrep.2021.110207>.
219. Kettel P, Marosits L, Spinetti E, Rechberger M, Niedermoser I, Fischer I, et al. Stress-induced clustering of the UPR sensor IRE1 $\alpha$  is driven by disordered 1 regions within its ER luminal domain. *Cold Spring Harbor Laboratory* . 2023; <https://doi.org/10.1101/2023.03.30.534746>.
220. Fu F, Doroudgar S. IRE1/XBP1 and endoplasmic reticulum signaling — from basic to translational research for cardiovascular disease. *Current Opinion in Physiology*. 2022;28: 100552. <https://doi.org/10.1016/j.cophys.2022.100552>.
221. Delaglio F, Grzesiek S, Vuister GeertenW, Zhu G, Pfeifer J, Bax A. NMRPipe: A multidimensional spectral processing system based on UNIX pipes. *Journal of Biomolecular NMR*. 1995;6(3). <https://doi.org/10.1007/BF00197809>.
222. Skinner SP, Fogh RH, Boucher W, Ragan TJ, Mureddu LG, Vuister GW. CcpNmr AnalysisAssign: a flexible platform for integrated NMR analysis. *Journal of Biomolecular NMR*. 2016;66(2): 111–124. <https://doi.org/10.1007/s10858-016-0060-y>.
223. Vranken WF, Boucher W, Stevens TJ, Fogh RH, Pajon A, Llinas M, et al. The CCPN data model for NMR spectroscopy: Development of a software pipeline. *Proteins: Structure, Function, and Bioinformatics*. 2005;59(4): 687–696. <https://doi.org/10.1002/prot.20449>.
224. Carter SG, Karl DW. Inorganic phosphate assay with malachite green: An improvement and evaluation. *Journal of Biochemical and Biophysical Methods*. 1982;7(1): 7–13. [https://doi.org/10.1016/0165-022X\(82\)90031-8](https://doi.org/10.1016/0165-022X(82)90031-8).

225. Chang L, Bertelsen EB, Wisén S, Larsen EM, Zuiderweg ERP, Gestwicki JE. High-throughput screen for small molecules that modulate the ATPase activity of the molecular chaperone DnaK. *Analytical Biochemistry*. 2008;372(2): 167–176. <https://doi.org/10.1016/j.ab.2007.08.020>.
226. Schneider CA, Rasband WS, Eliceiri KW. NIH Image to ImageJ: 25 years of image analysis. *Nature Methods*. 2012;9(7): 671–675. <https://doi.org/10.1038/nmeth.2089>.
227. Madeira F, Pearce M, Tivey ARN, Basutkar P, Lee J, Edbali O, et al. Search and sequence analysis tools services from EMBL-EBI in 2022. *Nucleic Acids Research*. 2022;50(W1): W276–W279. <https://doi.org/10.1093/nar/gkac240>.
228. Schneider TD, Stephens RM. Sequence logos: a new way to display consensus sequences. *Nucleic acids research*. 1990;18(20): 6097–6100. <https://doi.org/10.1093/nar/18.20.6097>.

## Appendix figures

### Appendix.1 Conservational analysis additional data

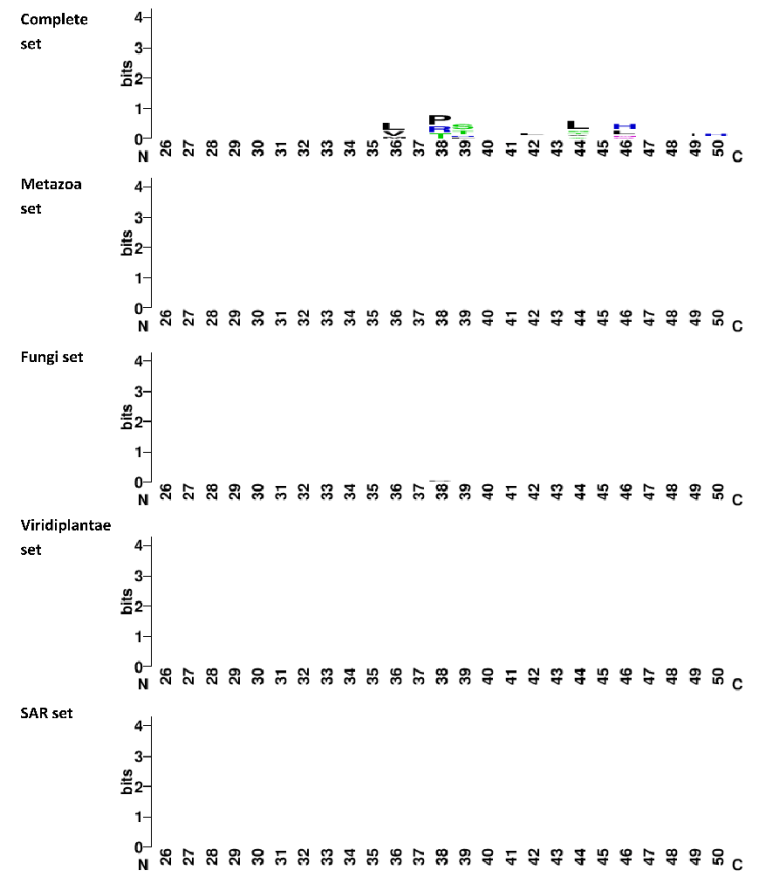
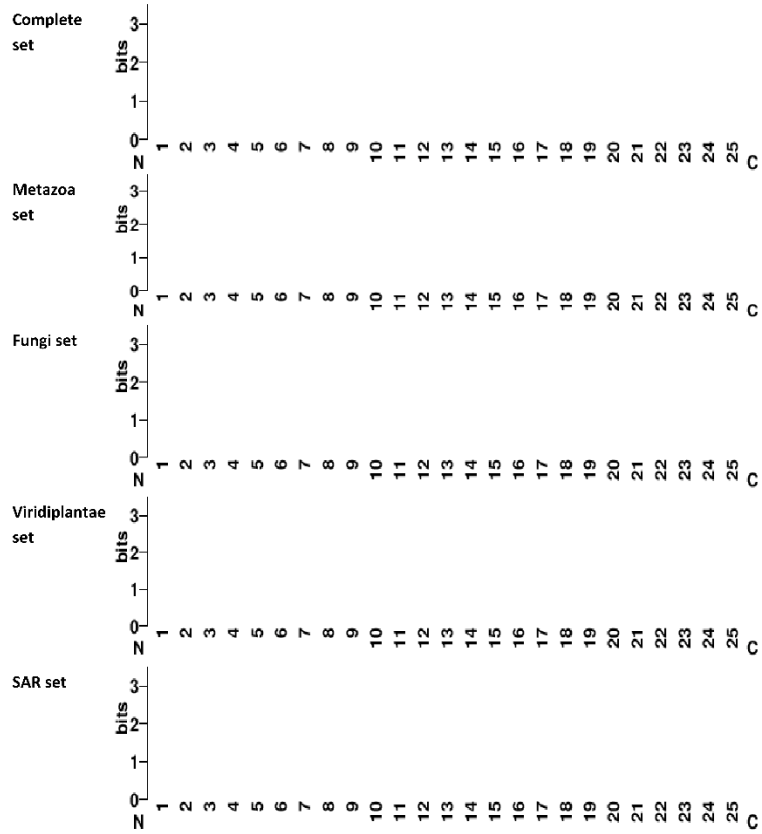


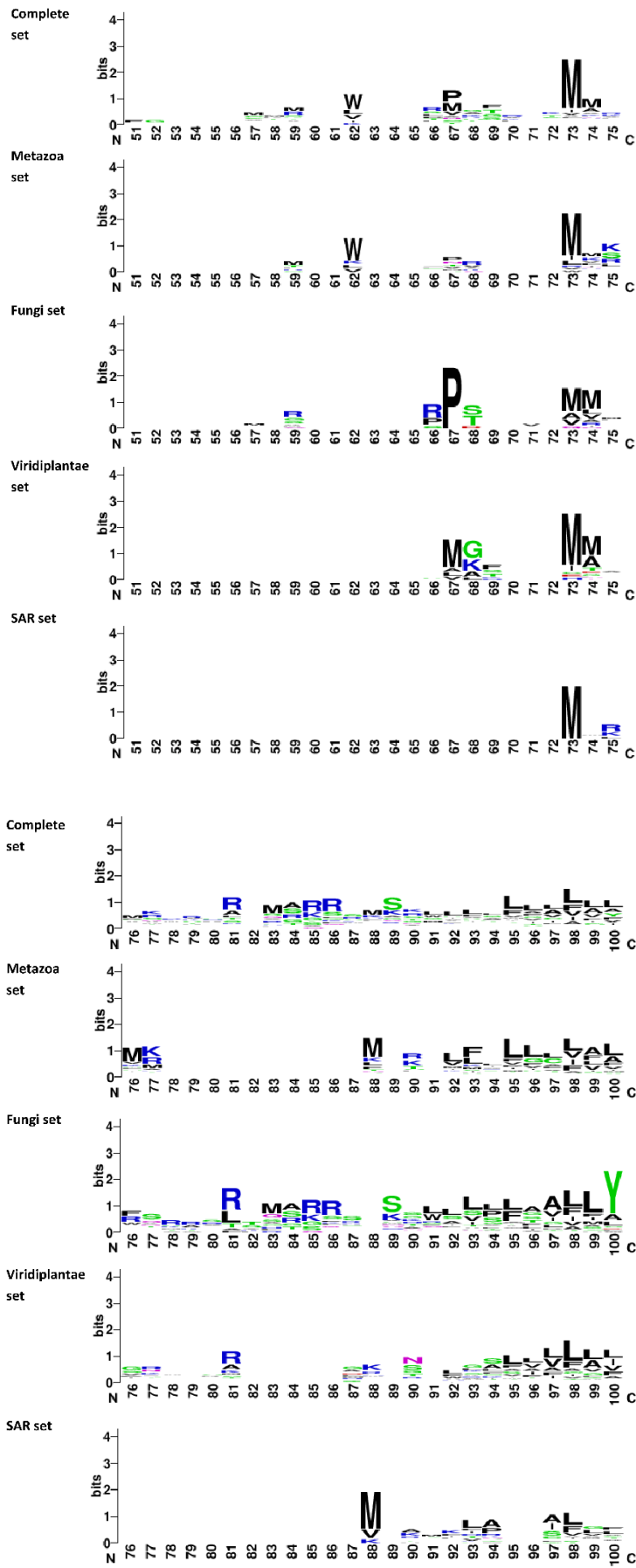
**Appendix Figure 1: Conservation of ER Hsp70.** BiP sequence colour coded using the ConSurf conservation generated pattern (171–173) based on the ER located Hsp70 data set.

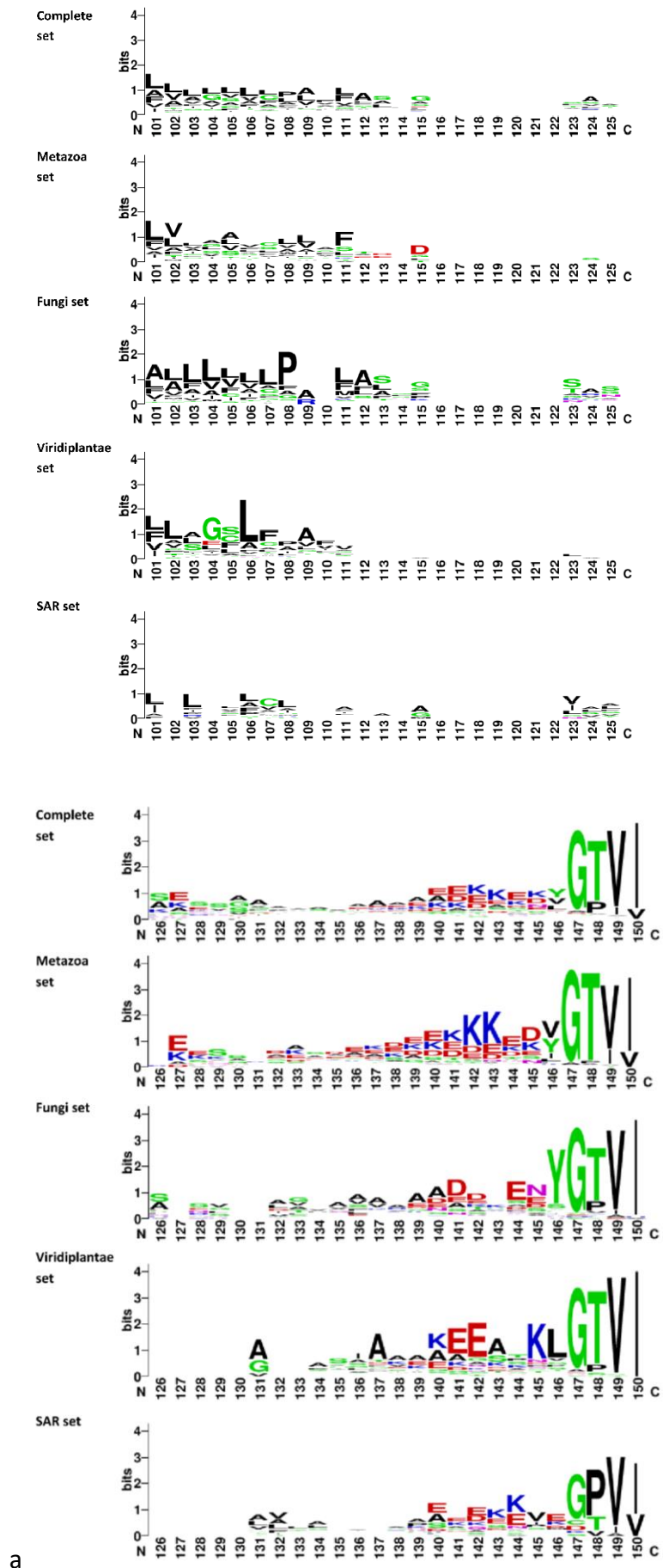
1                    11                    21                    31                    41  
 MAKAAAIKID LGTTYSCVGV FQHGKVEIIA NDOGNRTTPS YVAFDTDFRL  
  
 51                    61                    71                    81                    91  
 IGDAAKNOVA LNPQNTVFDA KRLIGRKEGD PVVQSDMKHW PFQVINDGDK  
  
 101                    111                    121                    131                    141  
 PKVQVSYKGE TKAFYPEEIS SMVLTMKKEI AEAYLGYEVT NAVITVPAYF  
  
 151                    161                    171                    181                    191  
 NDSQRQATKD AGVIAGLNVL RIINEPTAAA IAYGLDRTGK GERNVLIFDL  
  
 201                    211                    221                    231                    241  
 GGGTFDVSIL TIDDGI FEVK ATAGDTHLGG EDFDNRLVNH FVEEKRKHK  
  
 251                    261                    271                    281                    291  
 KDISQNKRAV RRLRTACEFA KRTLSSSTQA SLEIDSLIEG IDFYTSITRA  
  
 301                    311                    321                    331                    341  
 RFEELCSDLF RSTLEPVEKA LRDAKIDKAQ IHDLVLVGGG TRIPKVQKLL  
  
 351                    361                    371                    381                    391  
 QDFENGRDLN KSINPDEAVA YGAAVQAAIL MGDKSENVQD LLLLDVAPLS  
  
 401                    411                    421                    431                    441  
 LGLETAGGVM TALIKRNSTI PTKQTOIETT YSDNQPCVLI QVYEGERAMT  
  
 451                    461                    471                    481                    491  
 KDNNLLGRFE LSGIPPAPRG VPQIEVTFDI DANGILNVTA IDKSTGKANK  
  
 501                    511                    521                    531                    541  
 ITITNDKGRIL SKEETERMVQ EAEKYKAEDE VQREVSANK ALESYAFNMK  
  
 551                    561                    571                    581                    591  
 SAVEDEGLKG KISEADKKV LDKCQEVISW LDANTLAEKD EFEHKRKELE  
  
 601                    611                    621                    631                    641  
 QVCNPIISGL YQGAGGPGPG GFQAQGPKGG SGSGPTIEEV D

**The conservation scale:**  
 1 2 3 4 5 6 7 8 9  
 Variable                    Average                    Conserved

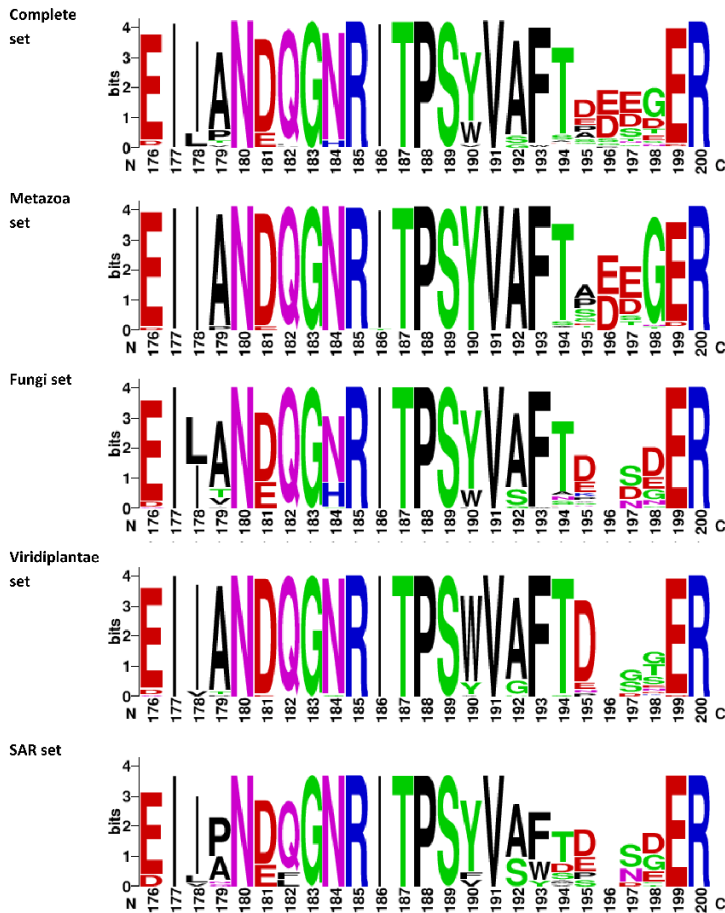
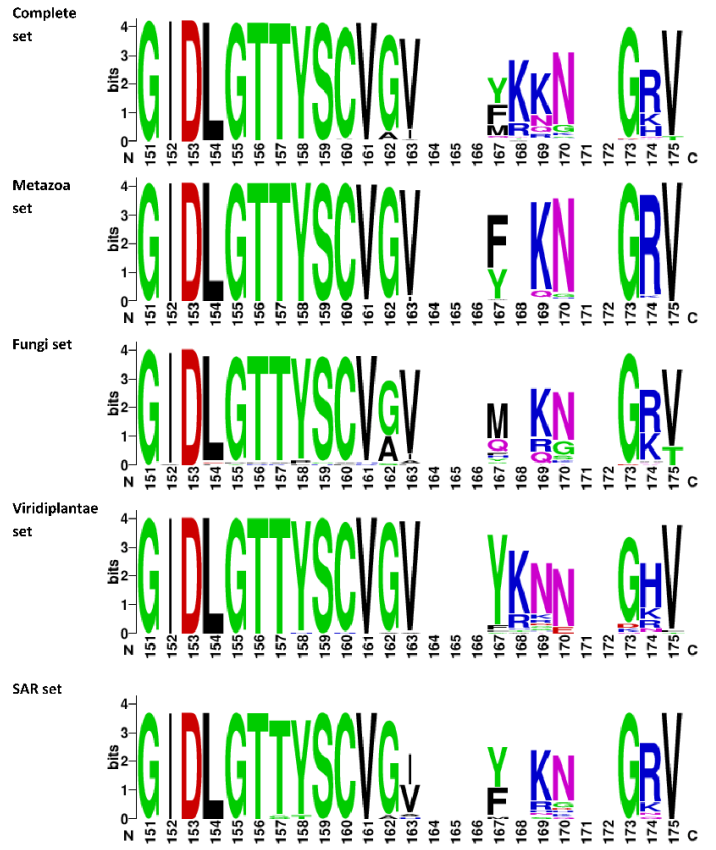
**Appendix Figure 2: Conservation of cytoplasmic Hsp70.** HspA1A sequence colour coded using the ConSurf conservation generated pattern (171–173) based on the cytoplasmic located Hsp70 data set.

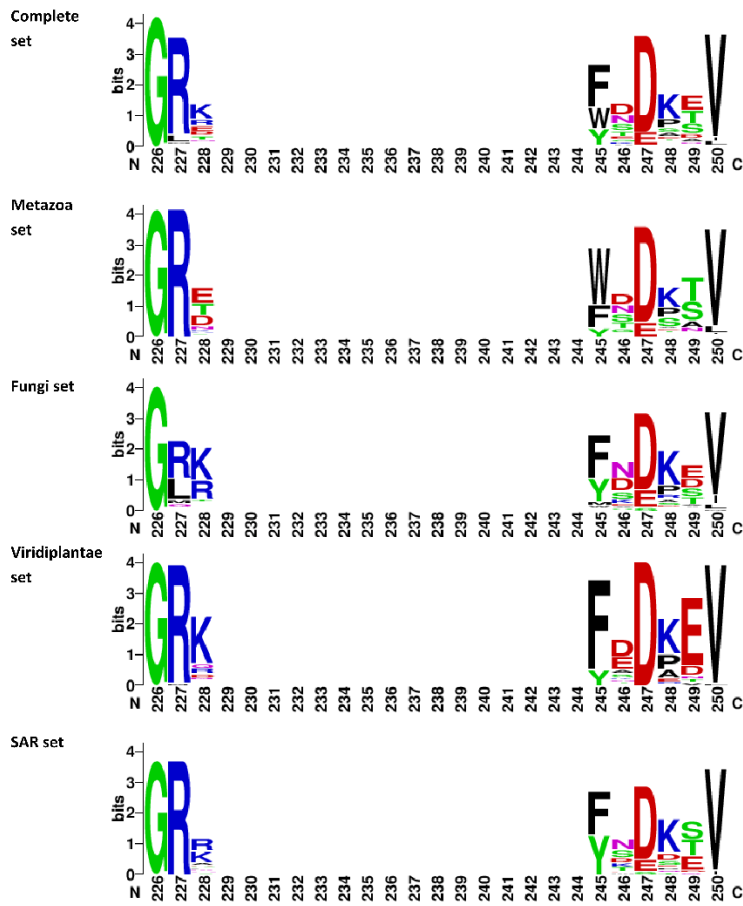
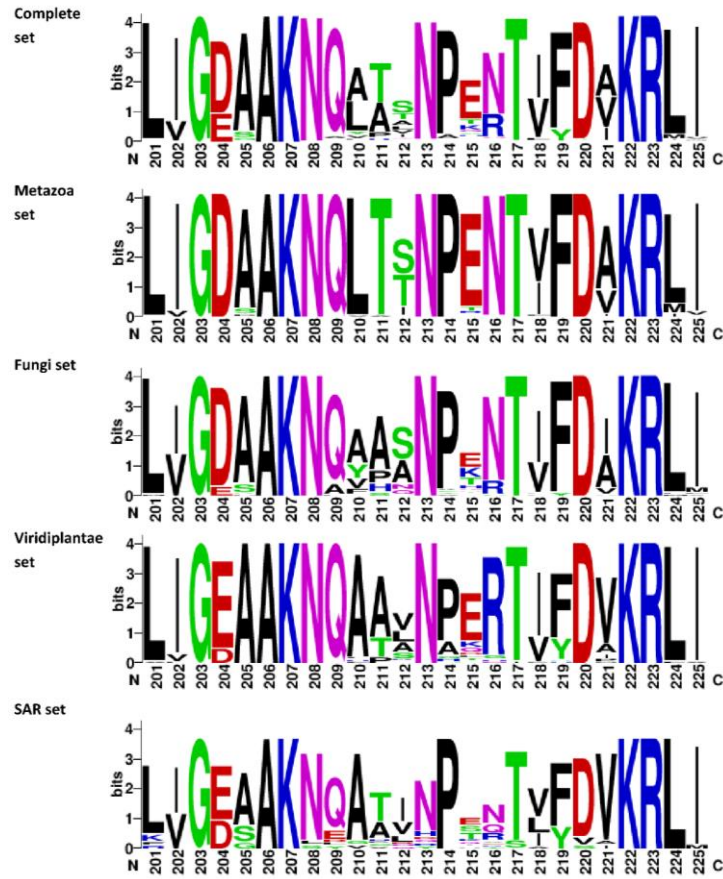


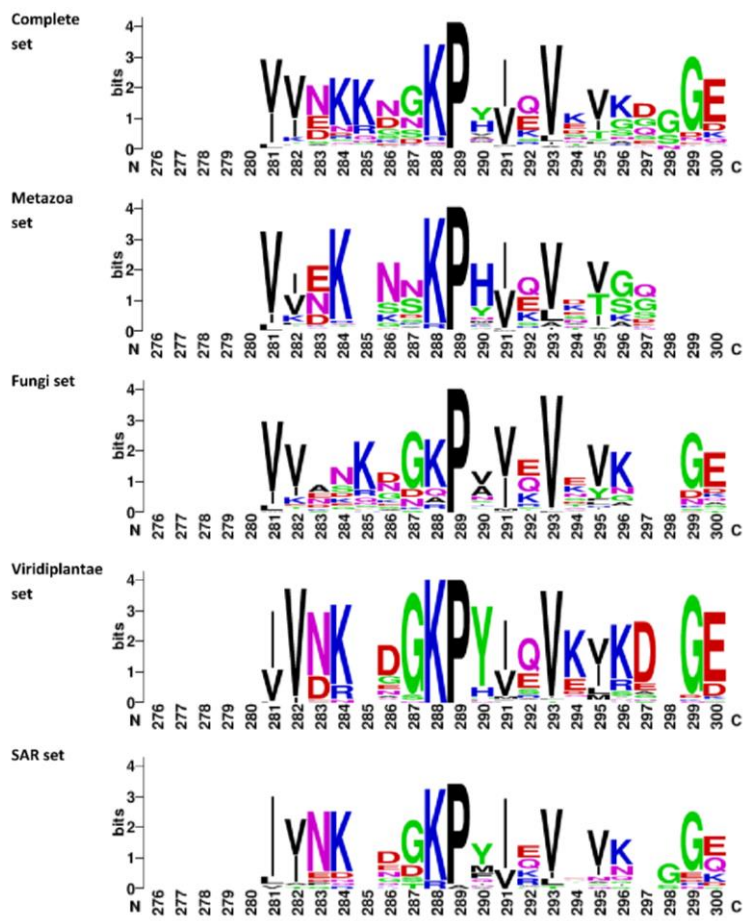
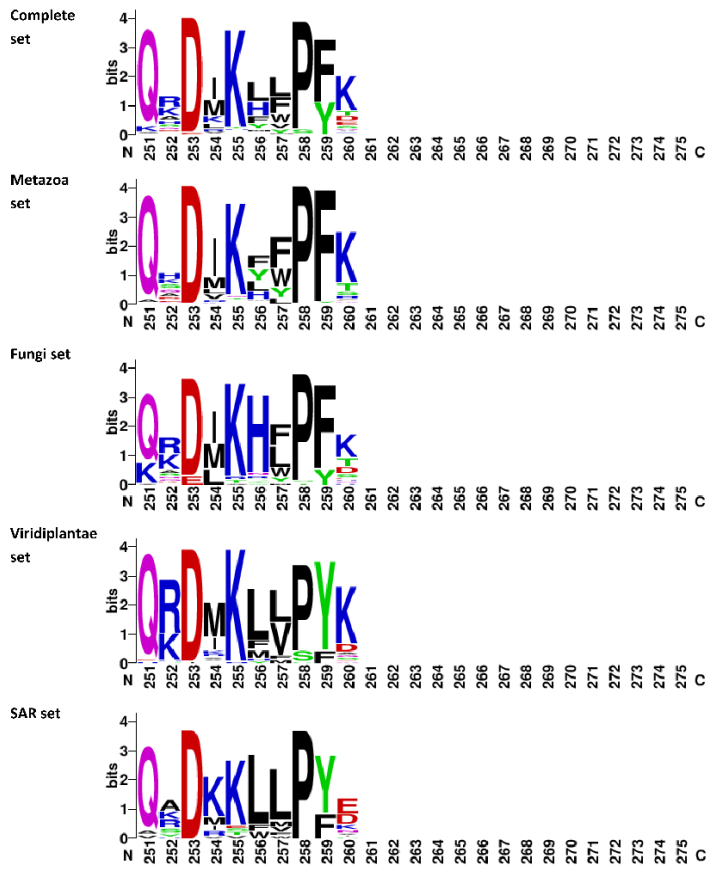


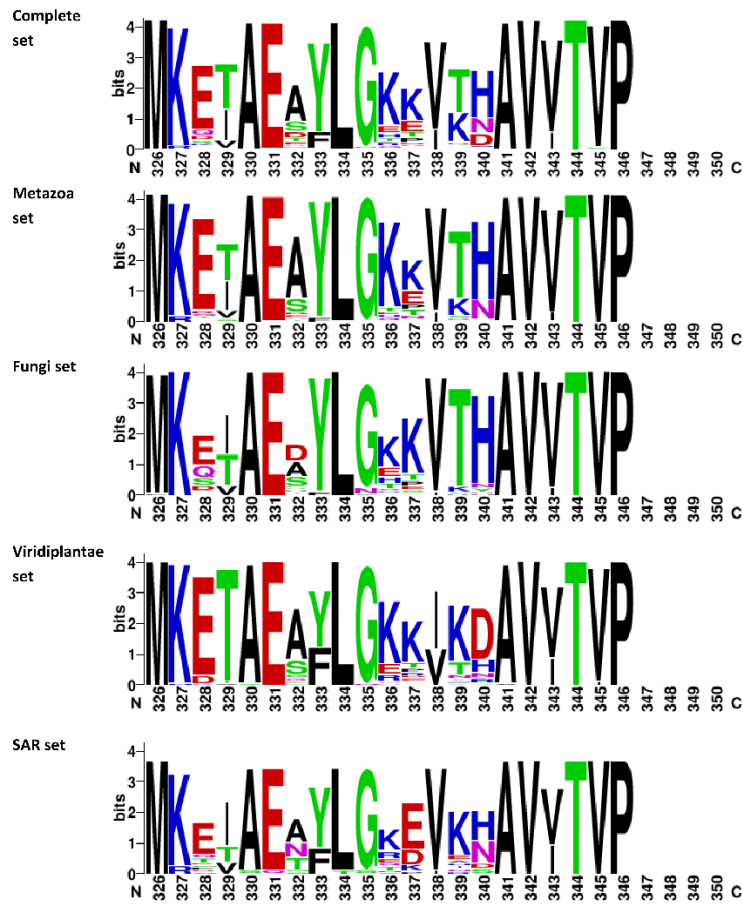
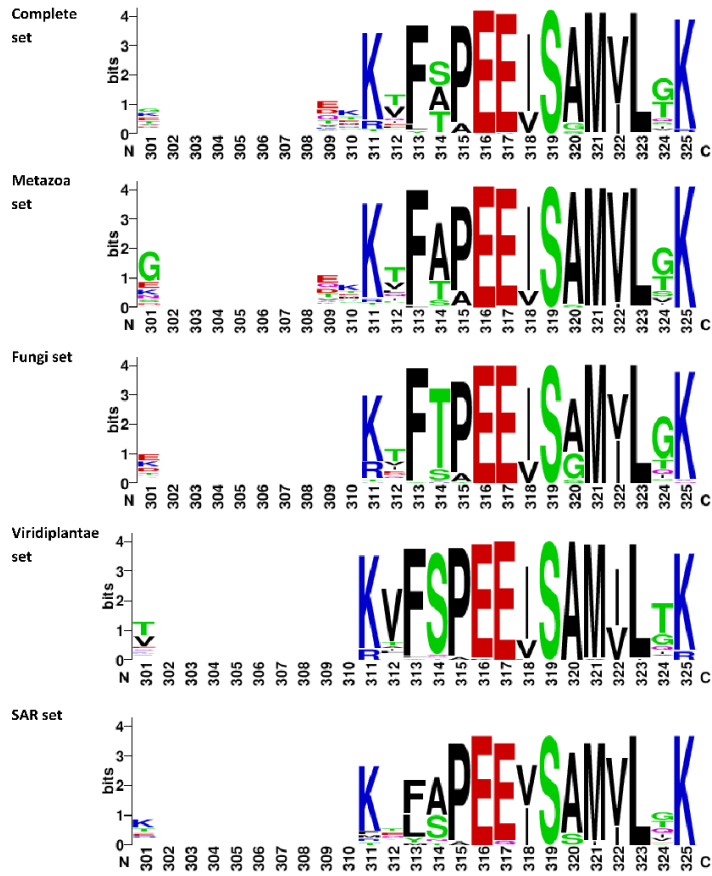


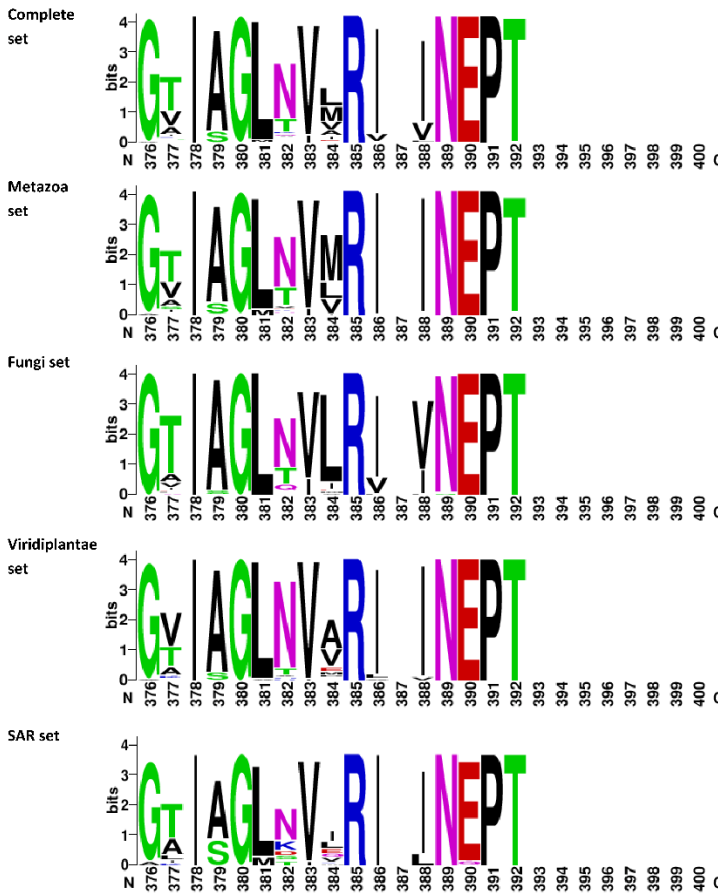
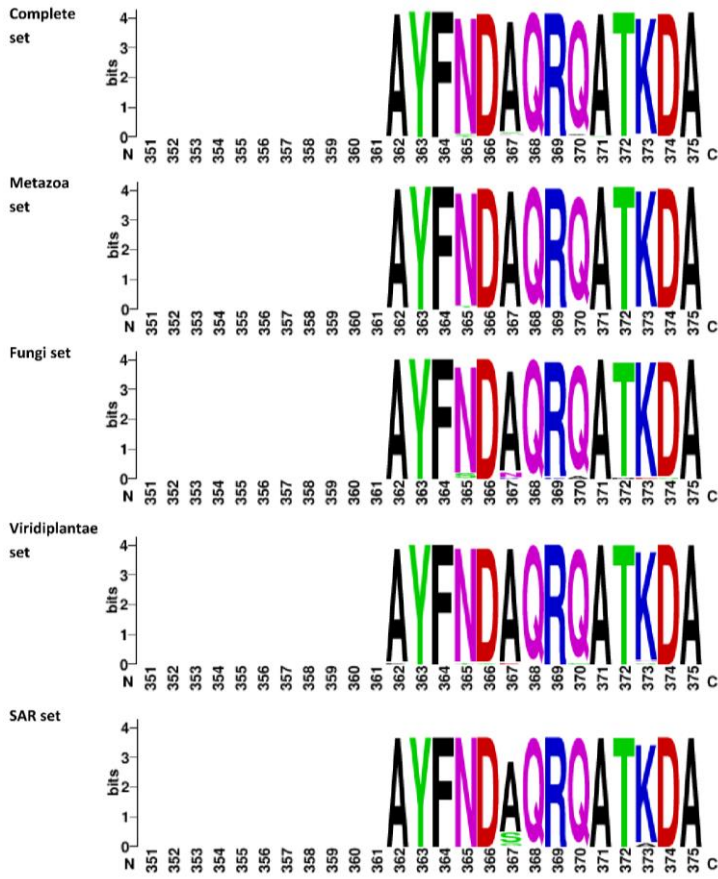
a

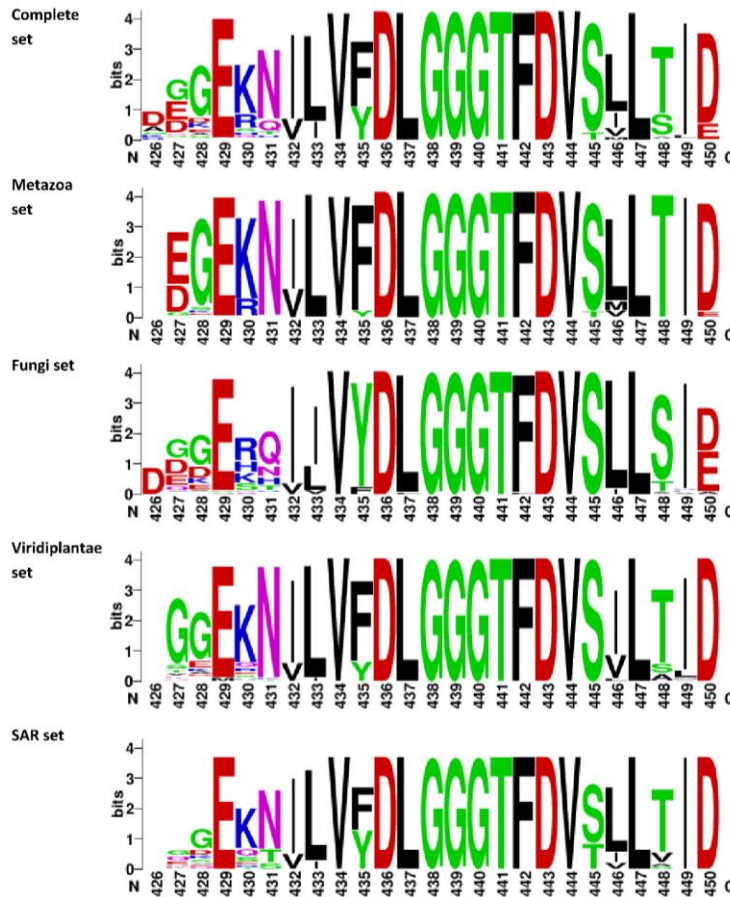
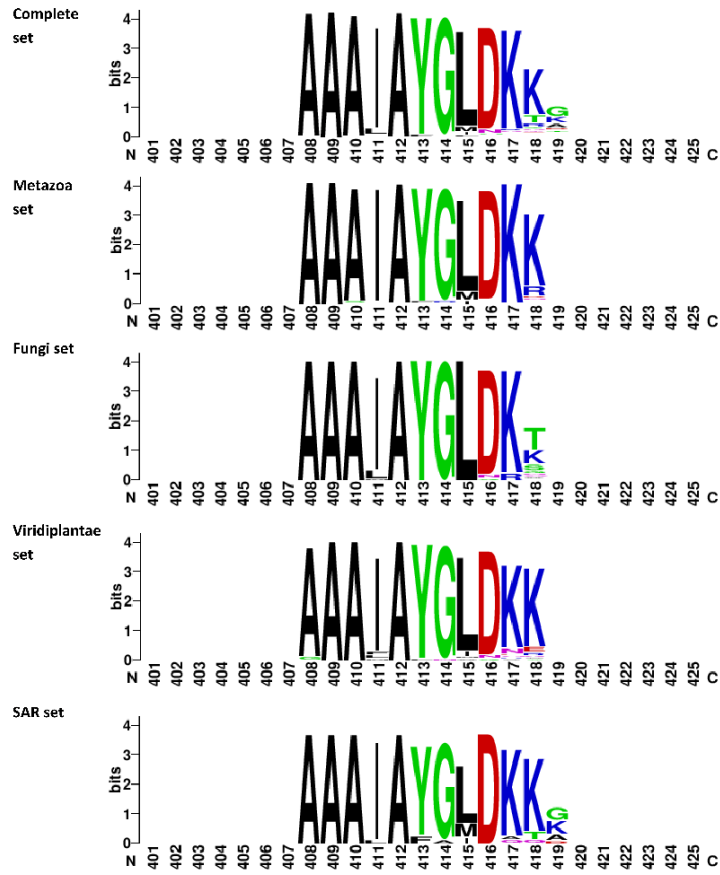


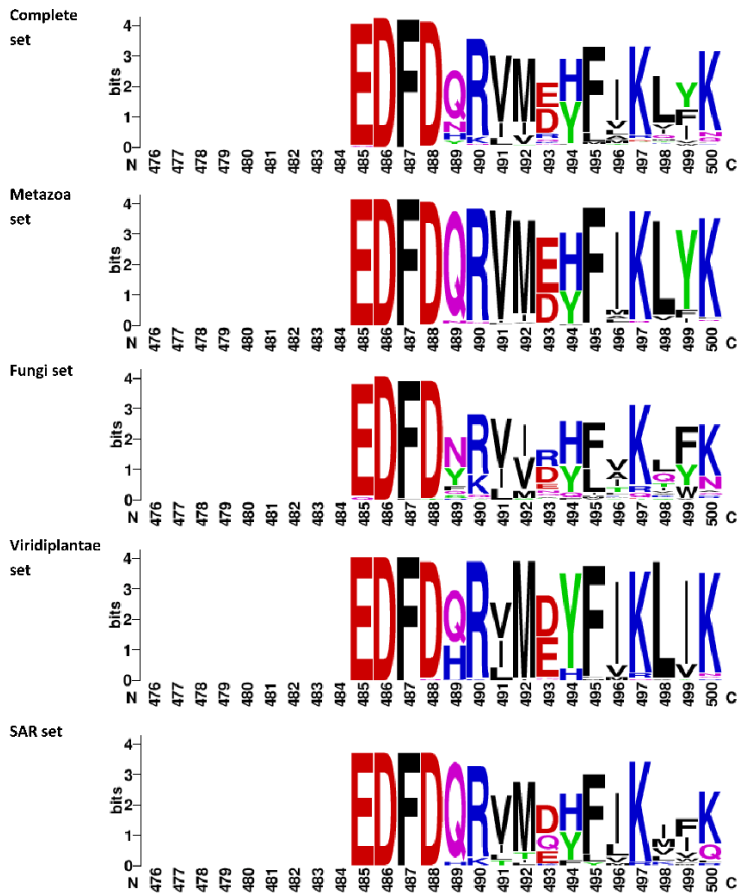
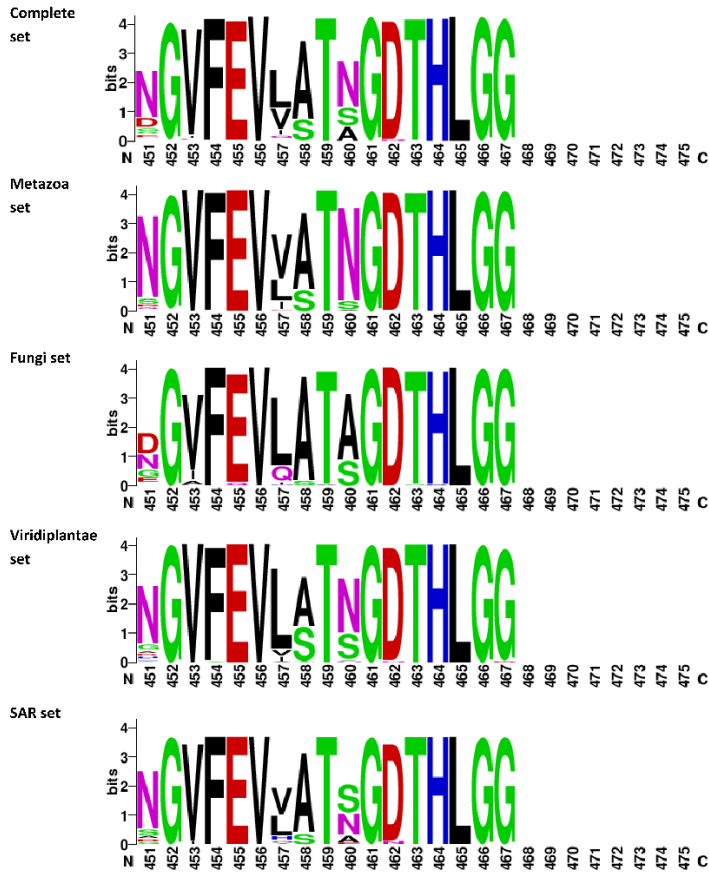


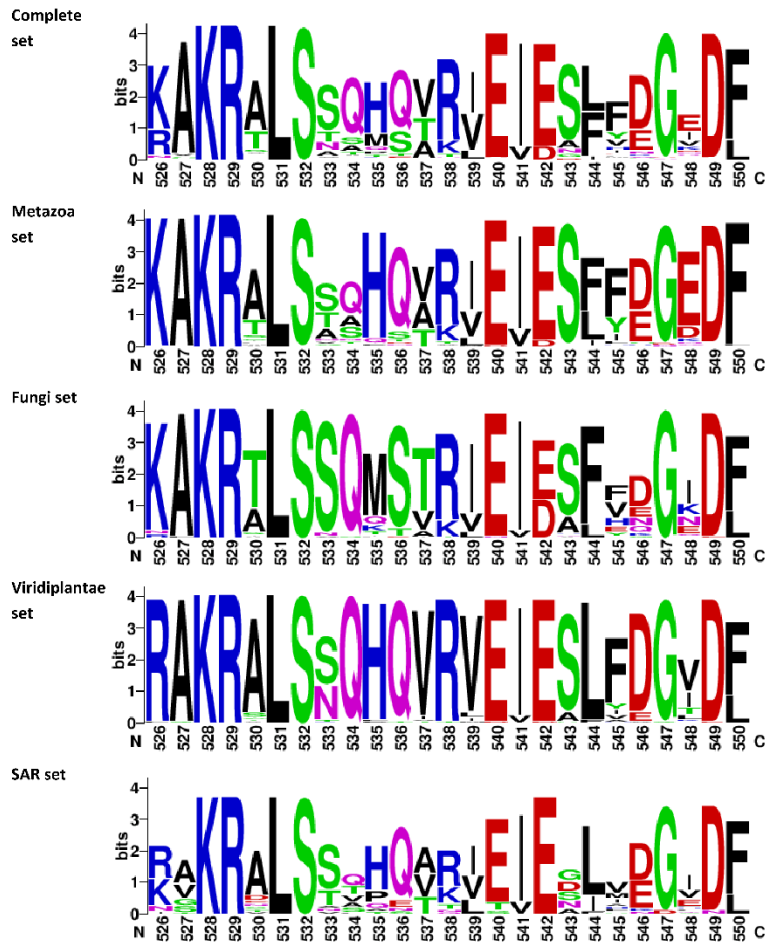
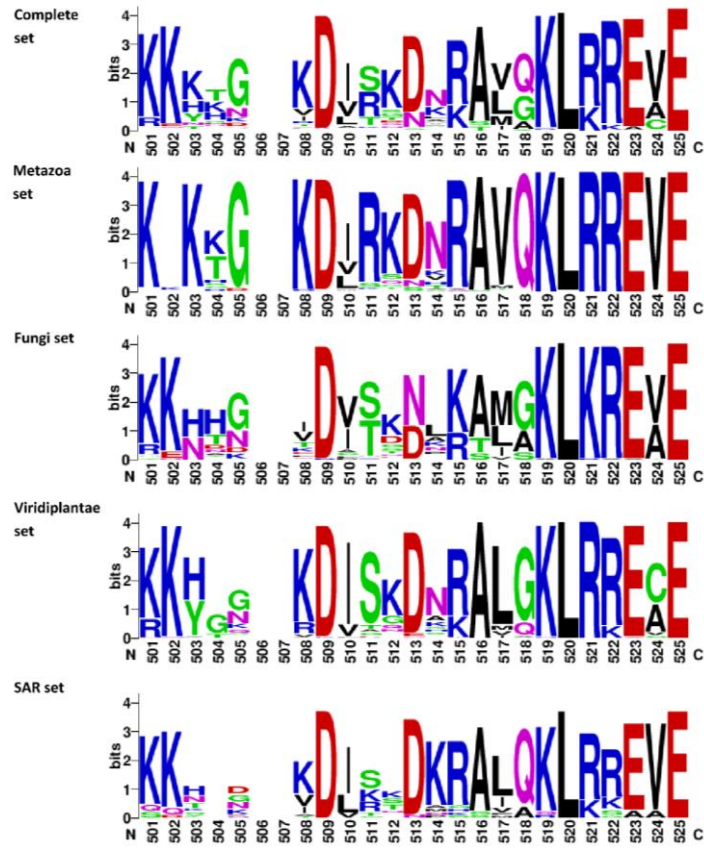


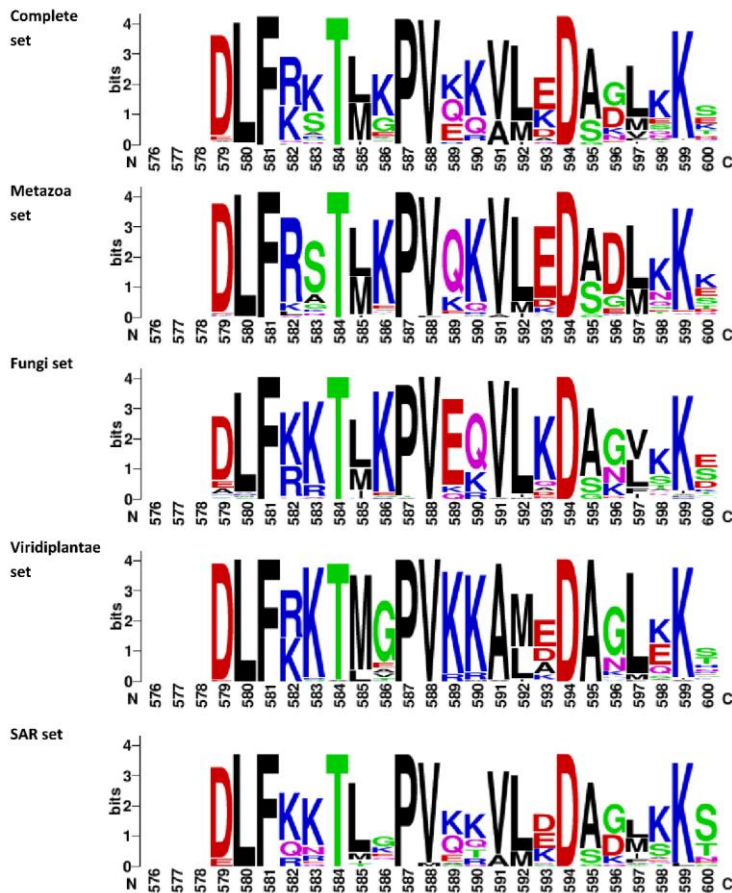
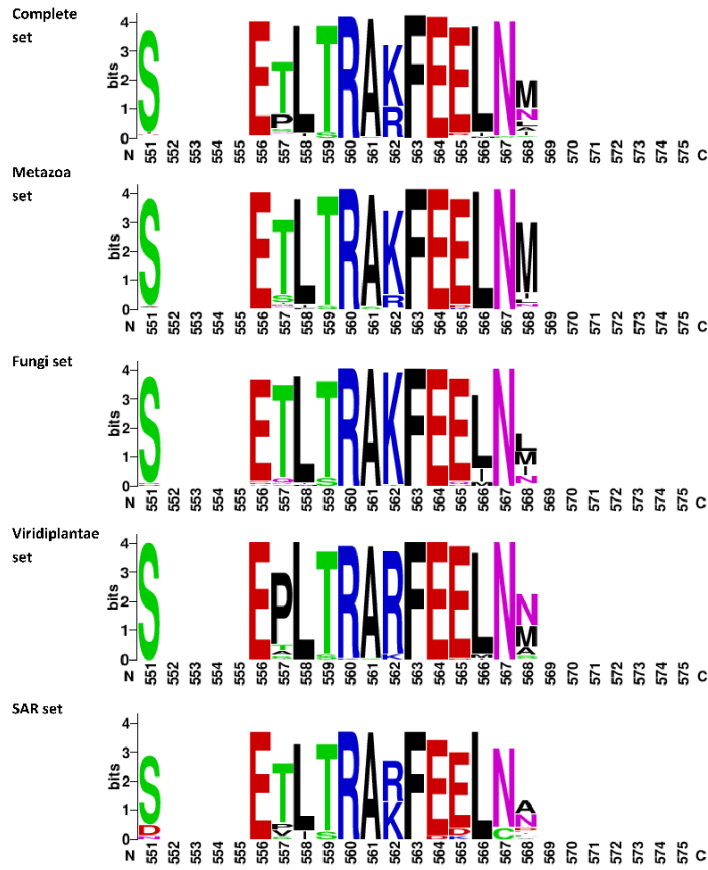


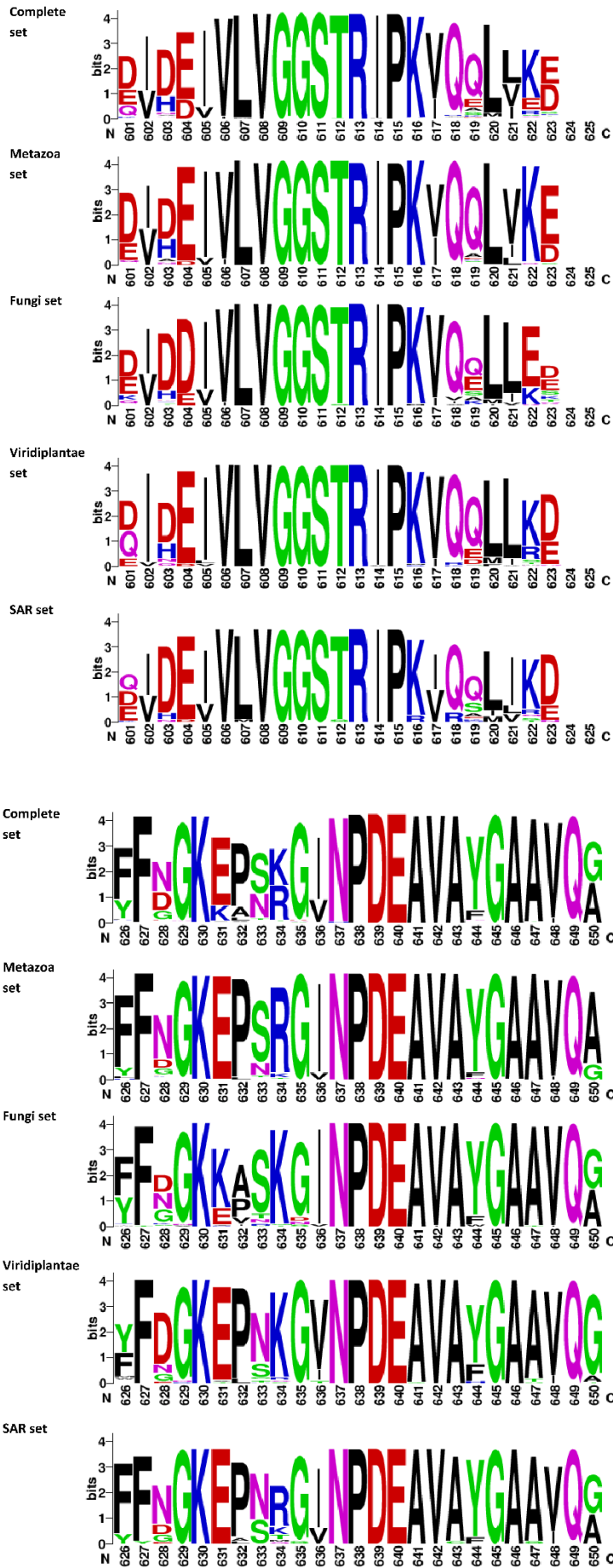


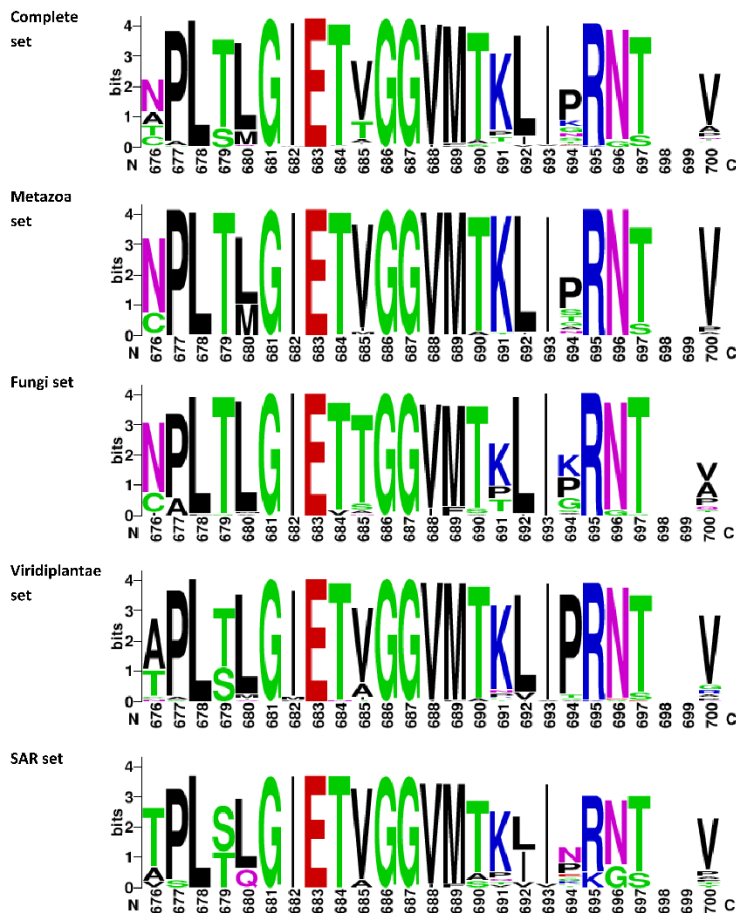
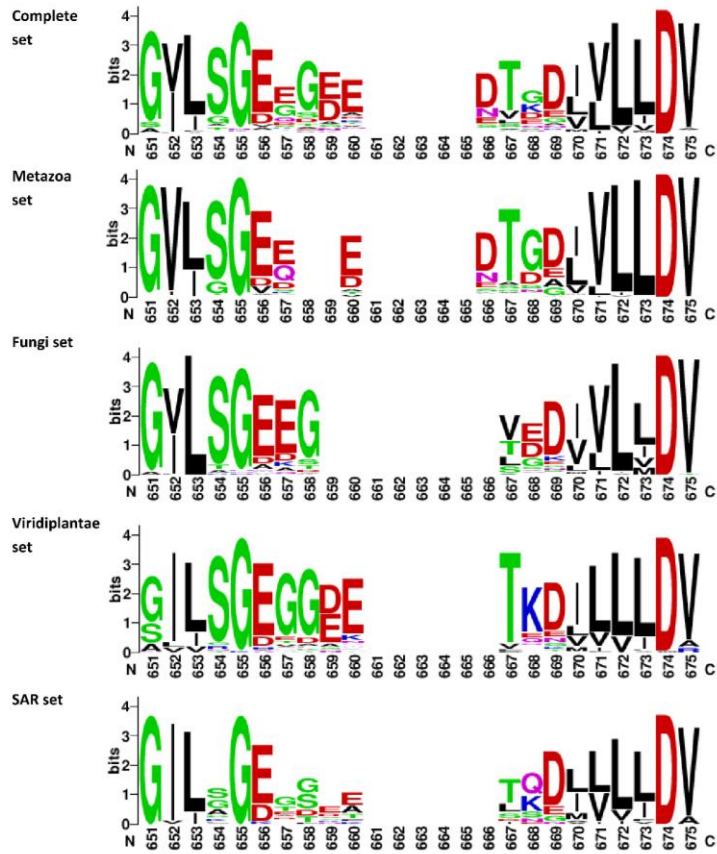


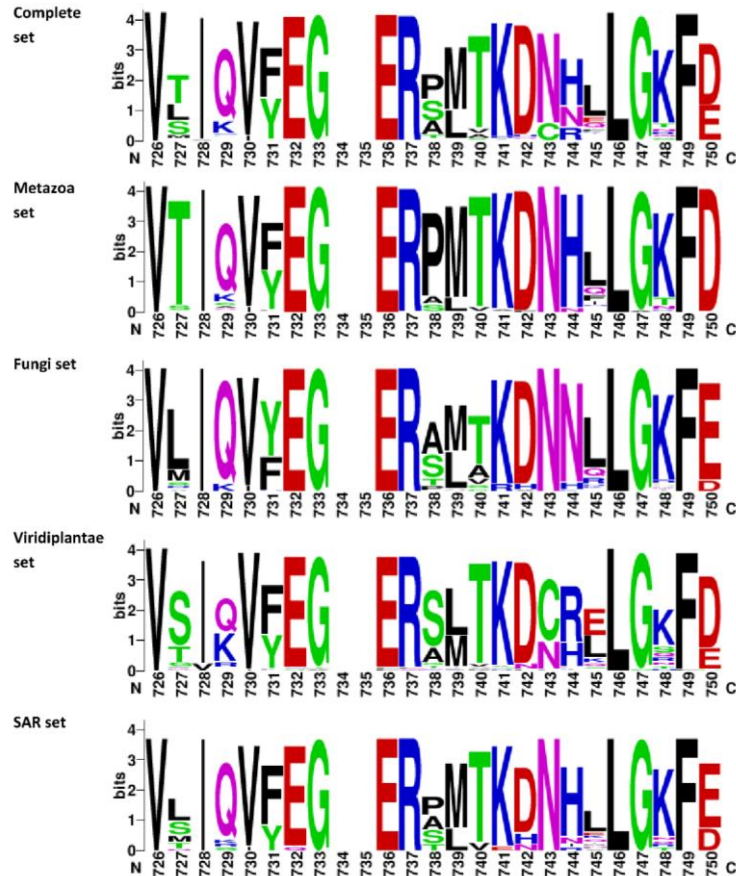
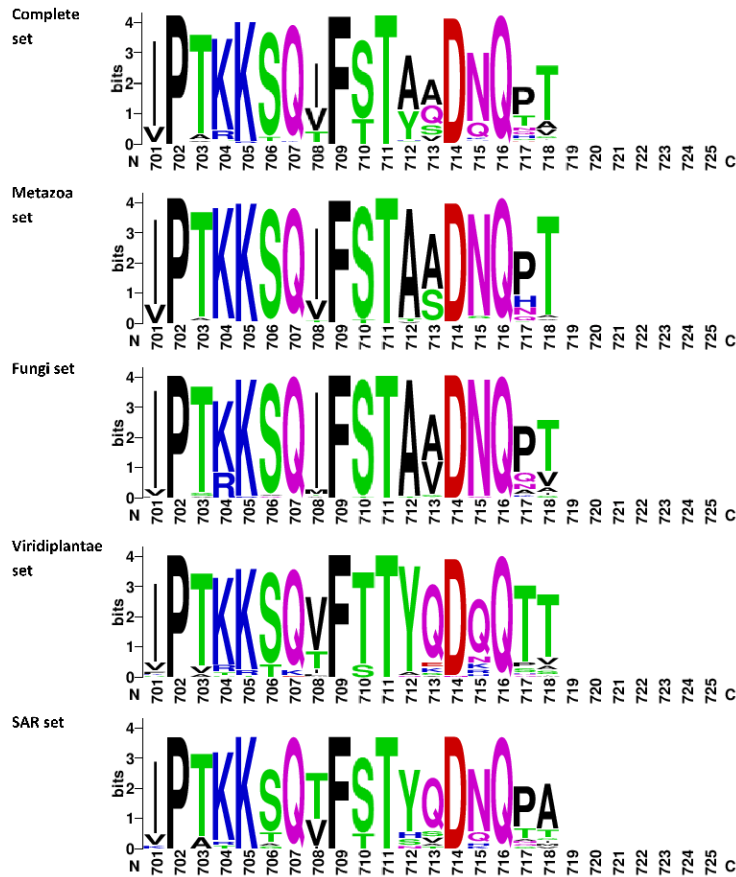


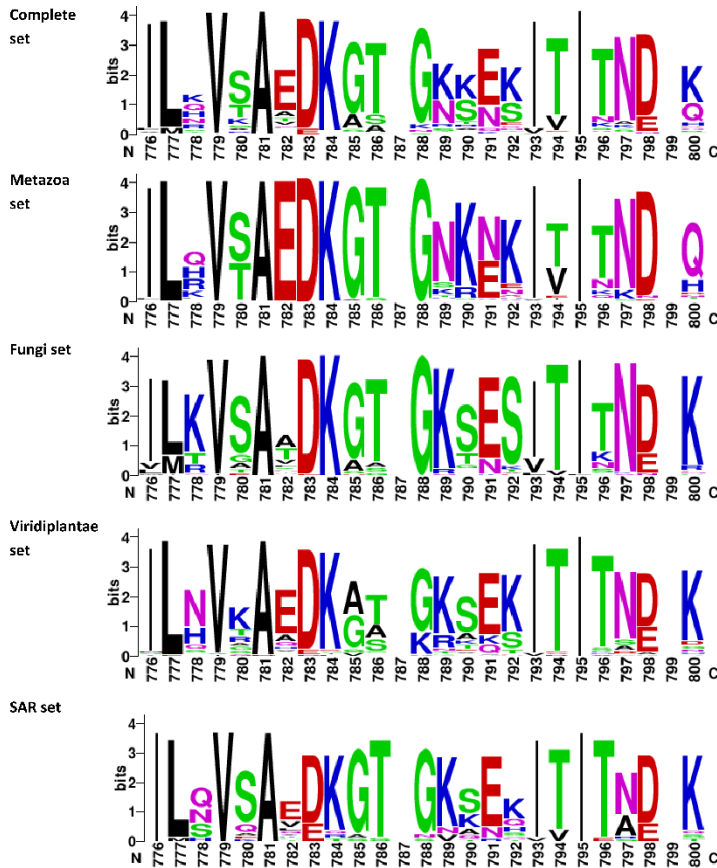
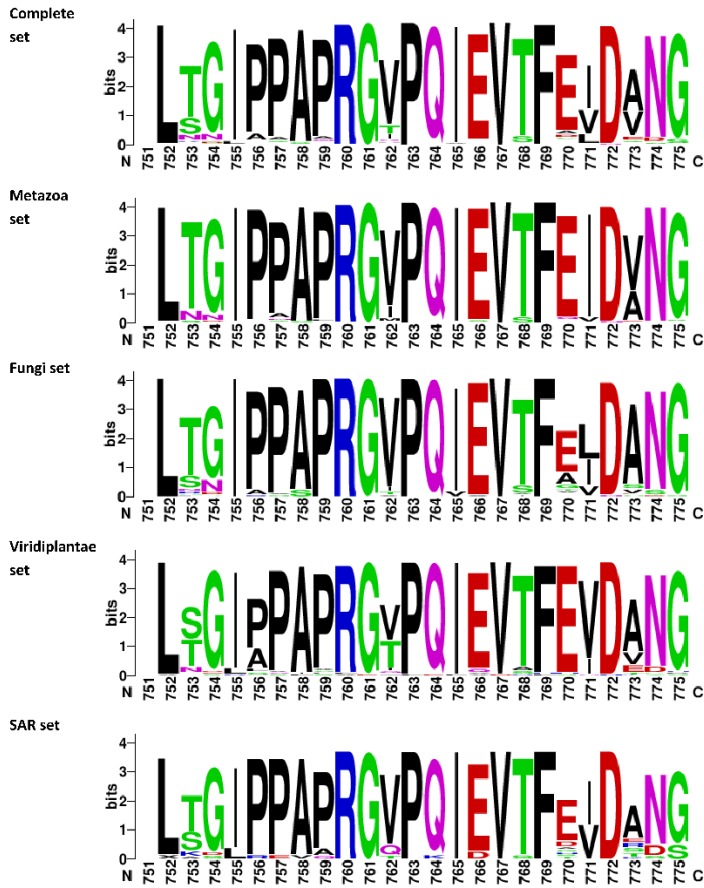


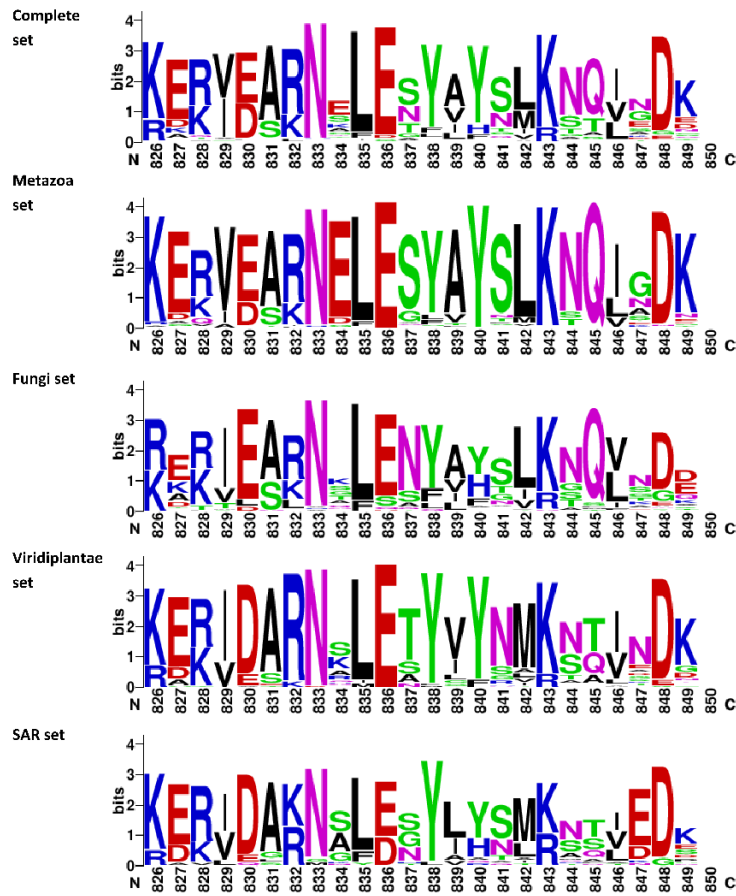
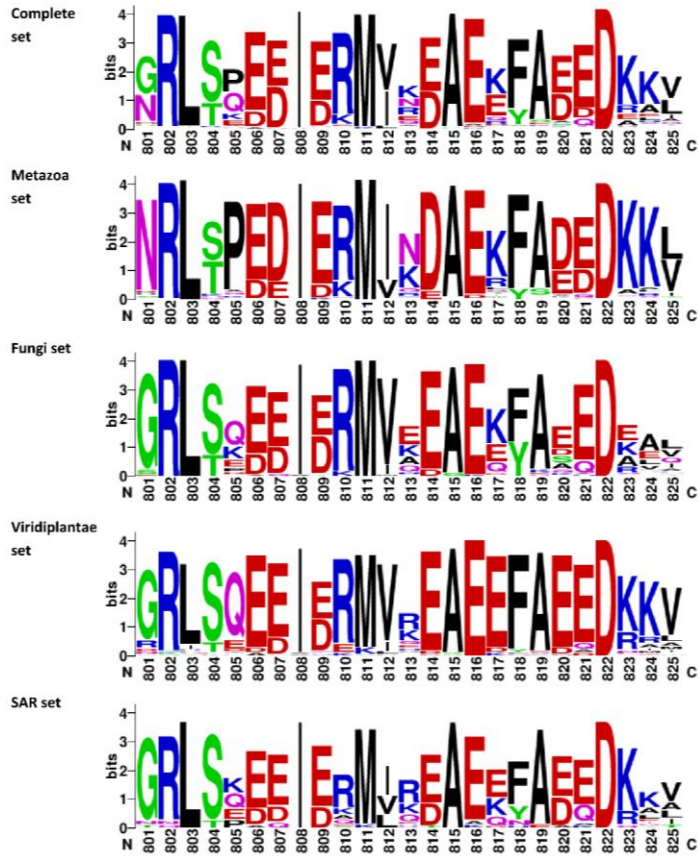


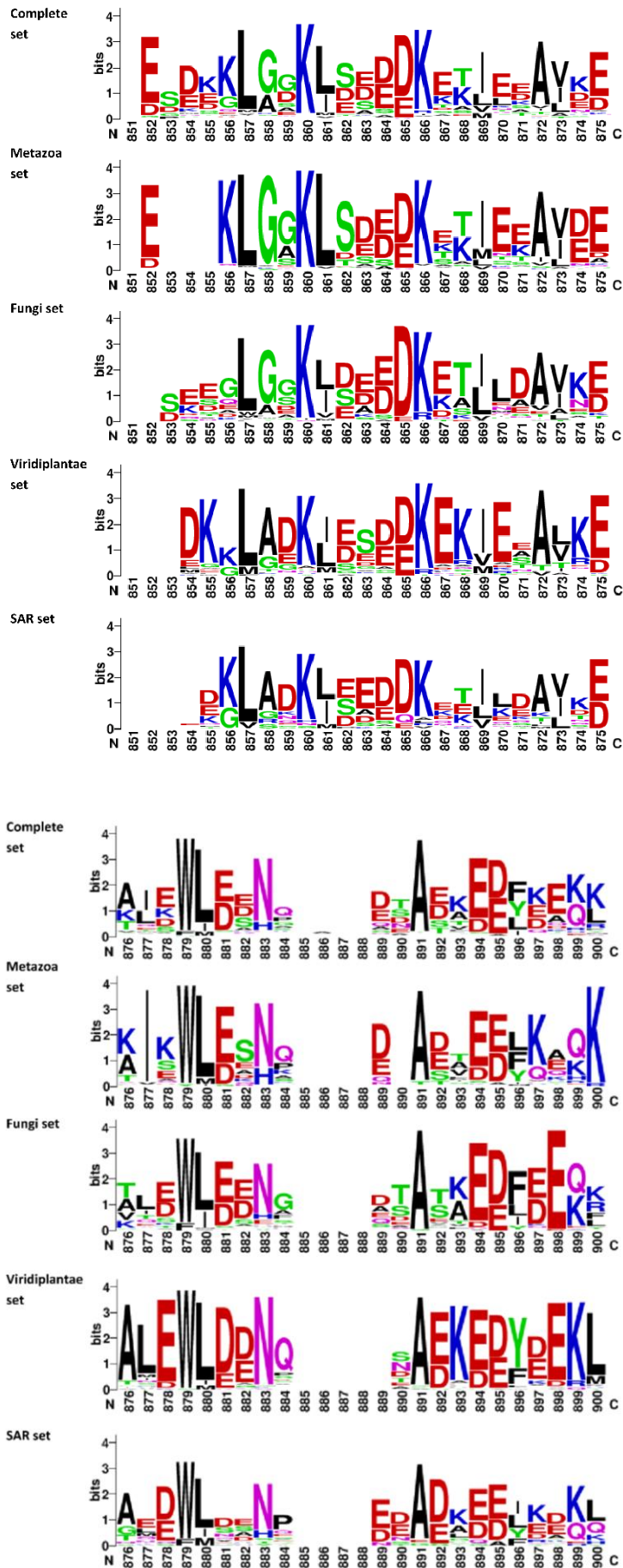


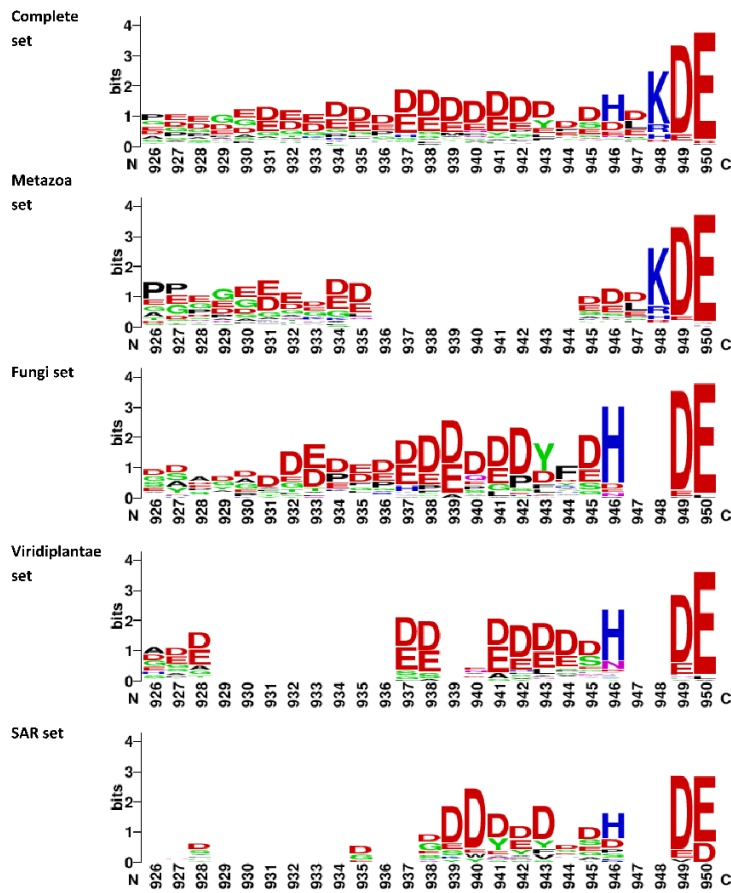
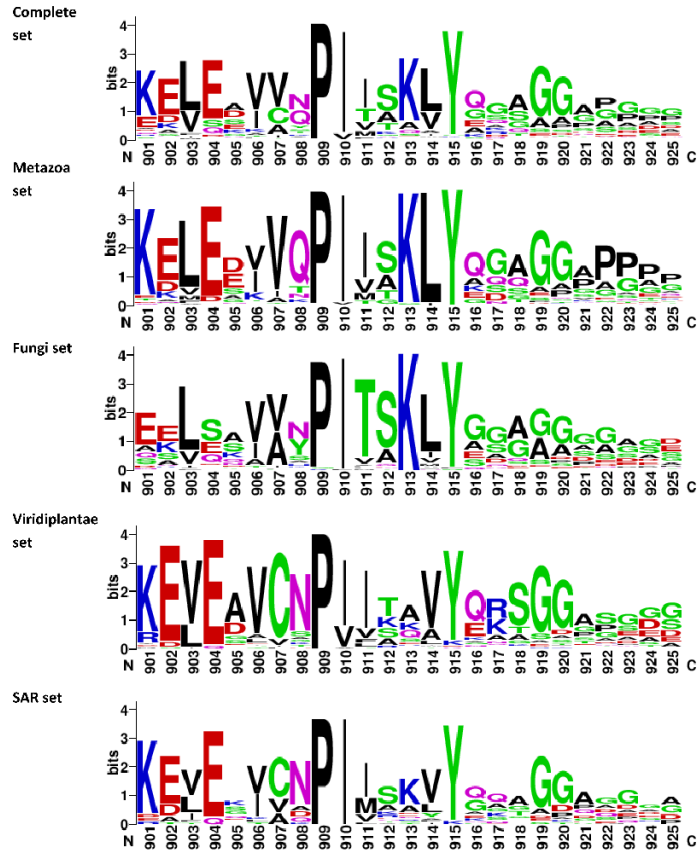


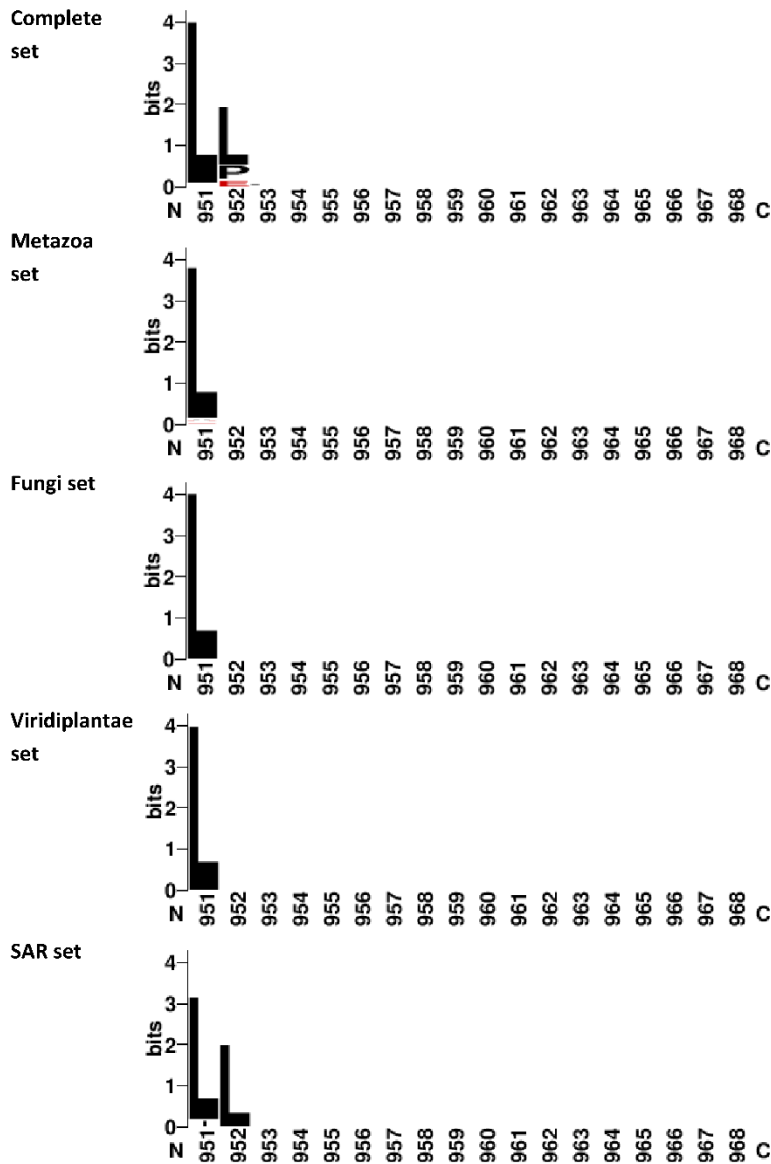




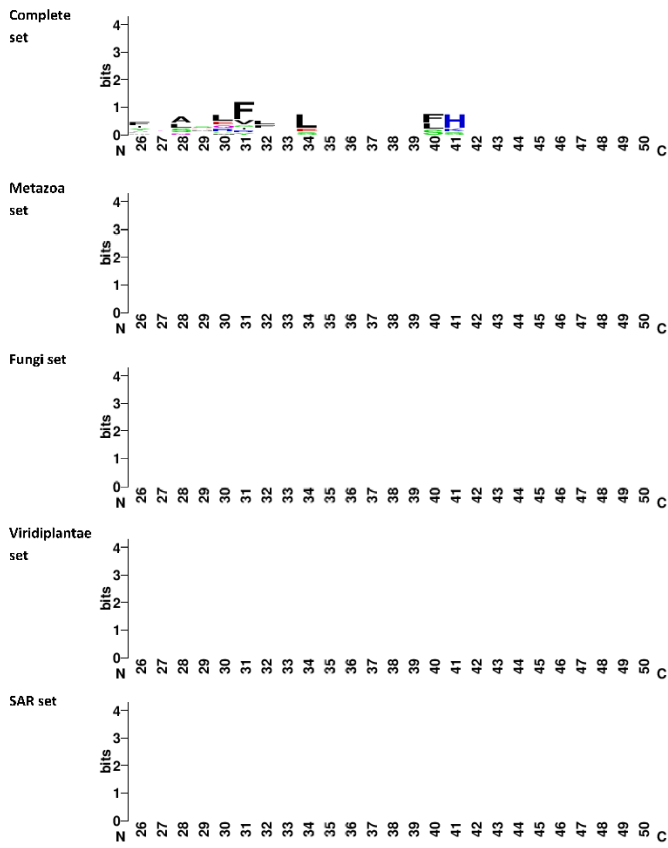
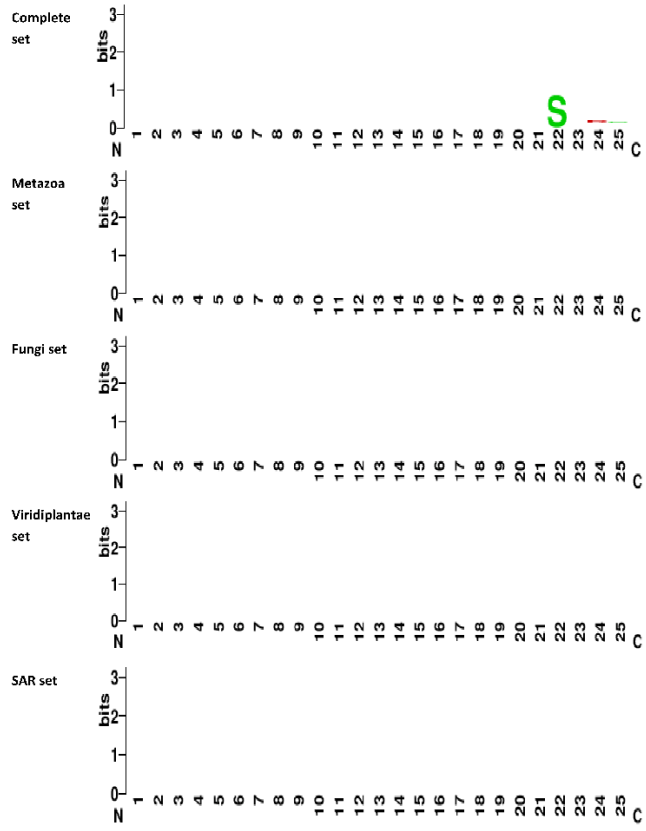


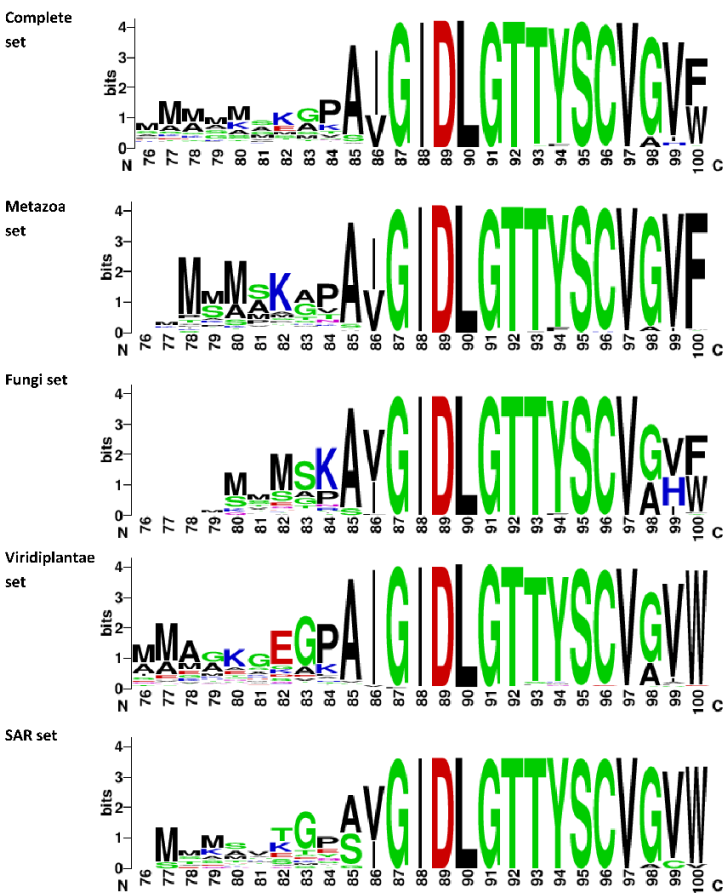
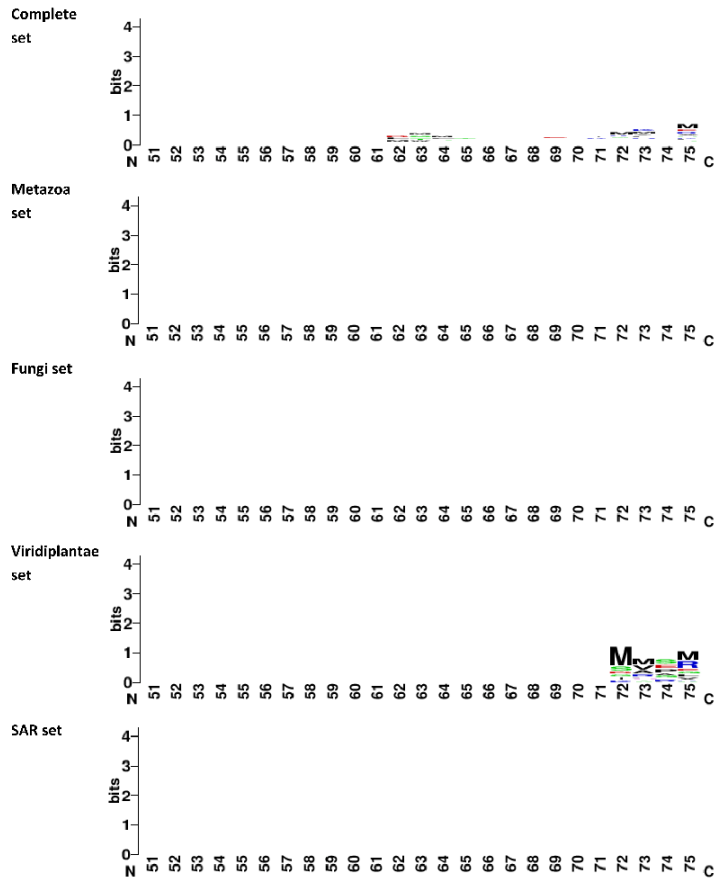


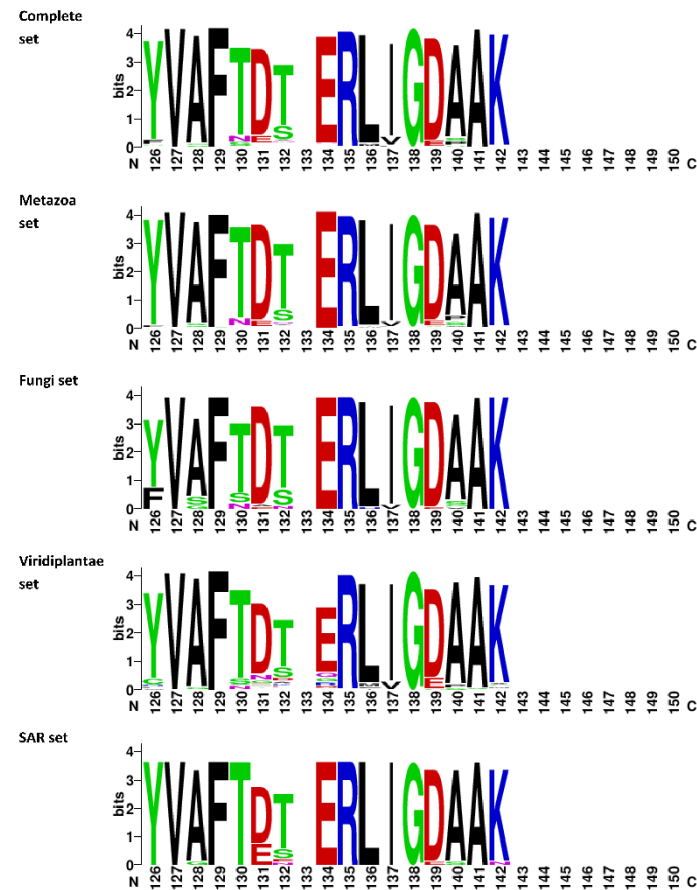
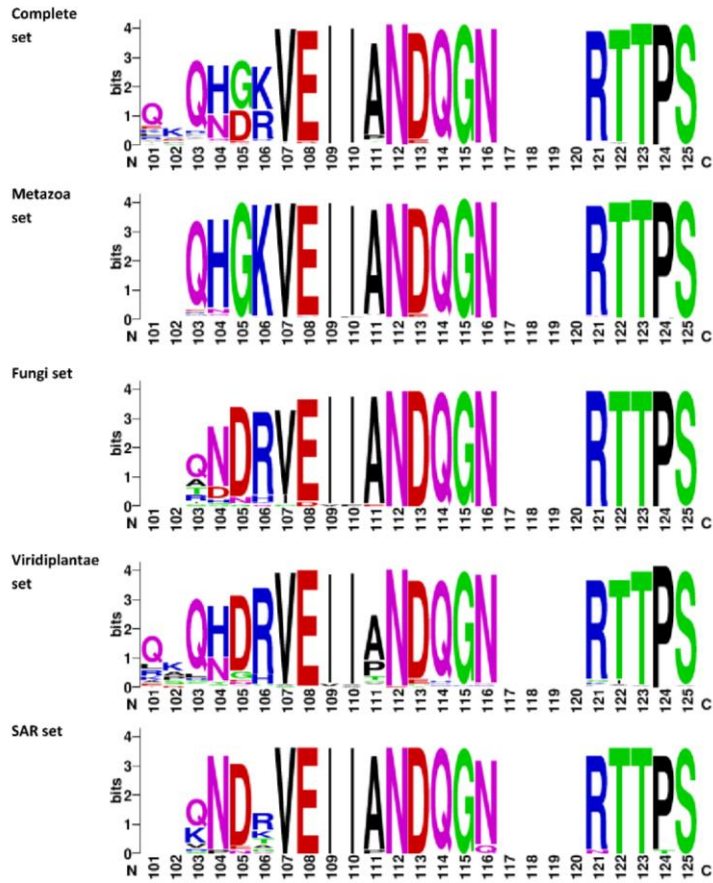


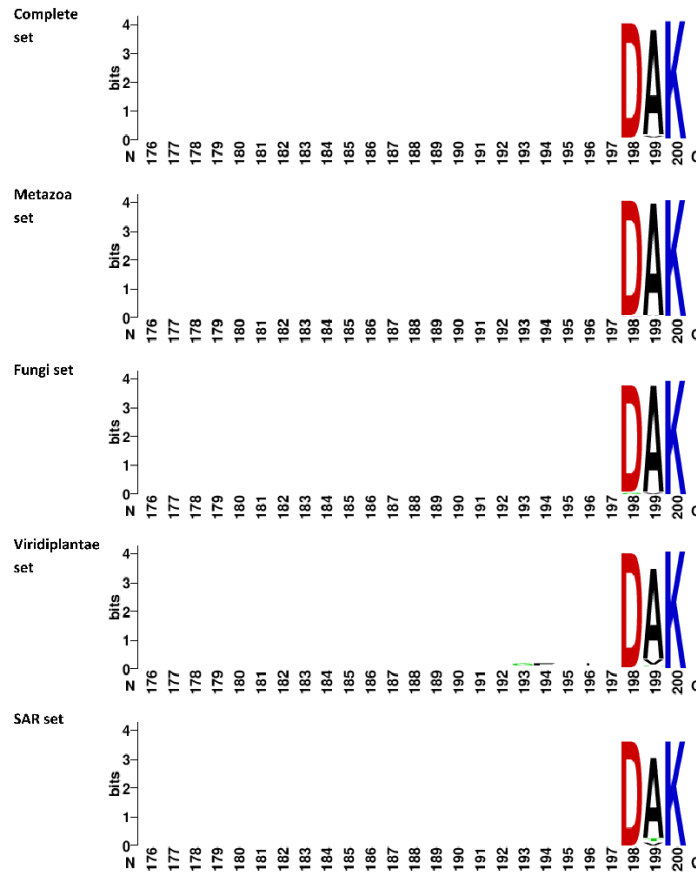
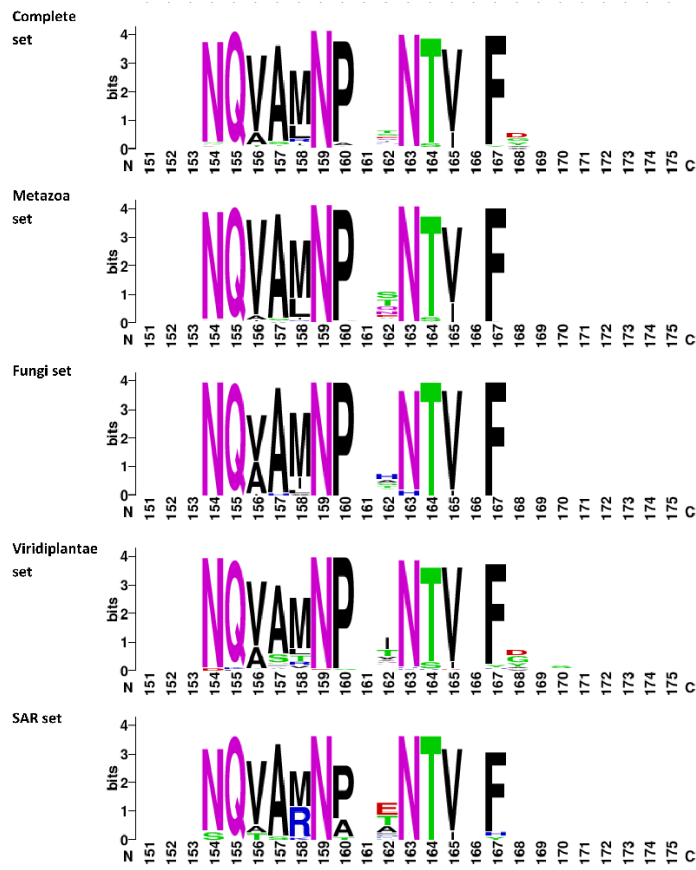


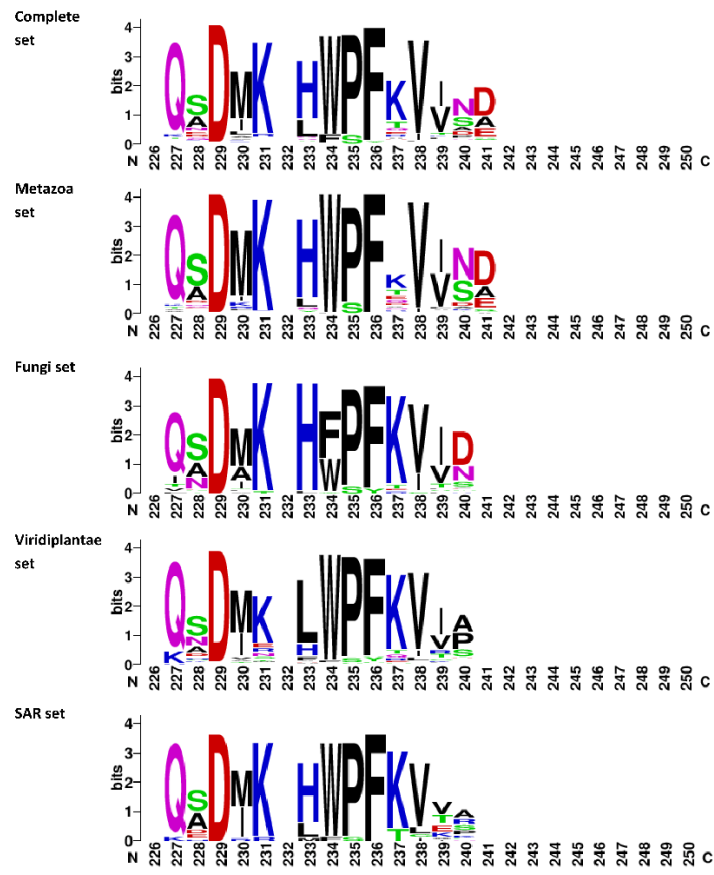
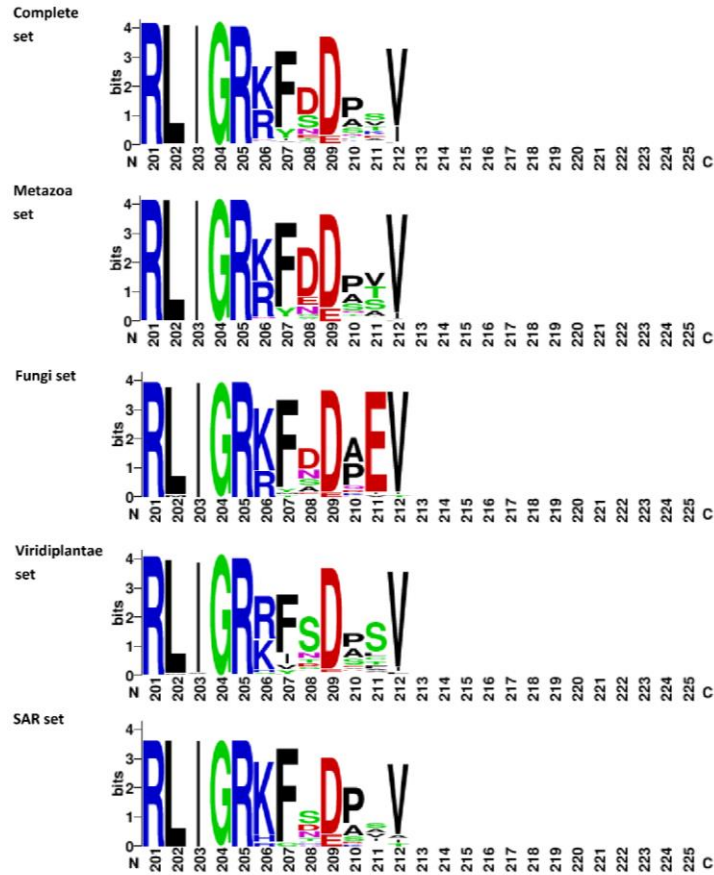
**Appendix Figure 3: ER Weblogo.** The complete Weblogo (174) generated pattern of ER located Hsp70 sequence set. Residues of 2.5 or higher out of 4 are considered conserved. Gaps found in sequences arose due to fasta format used in the generation of the multiple sequence alignment and are not found in the actual protein.

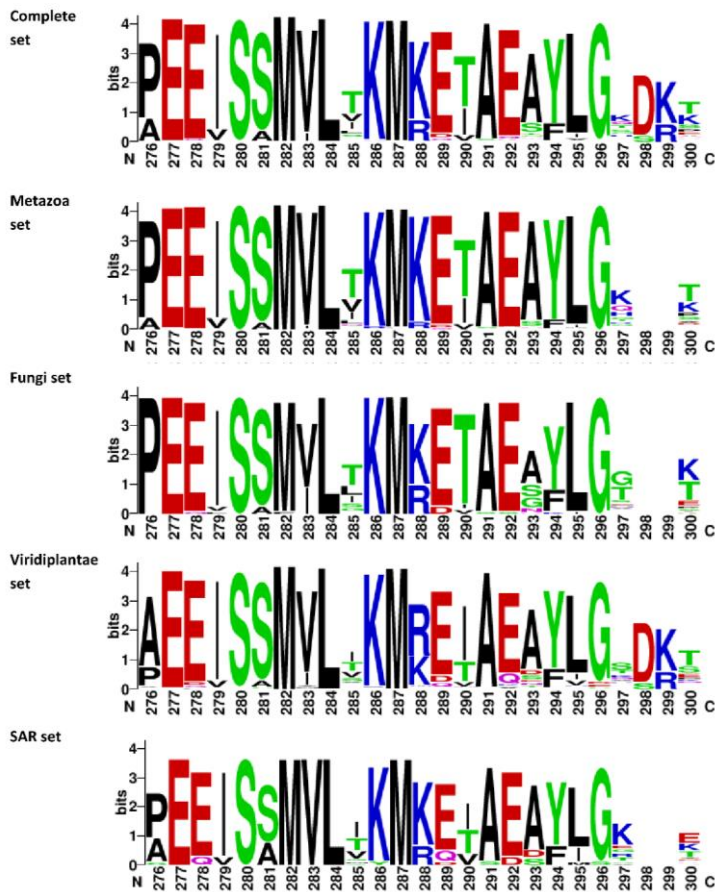
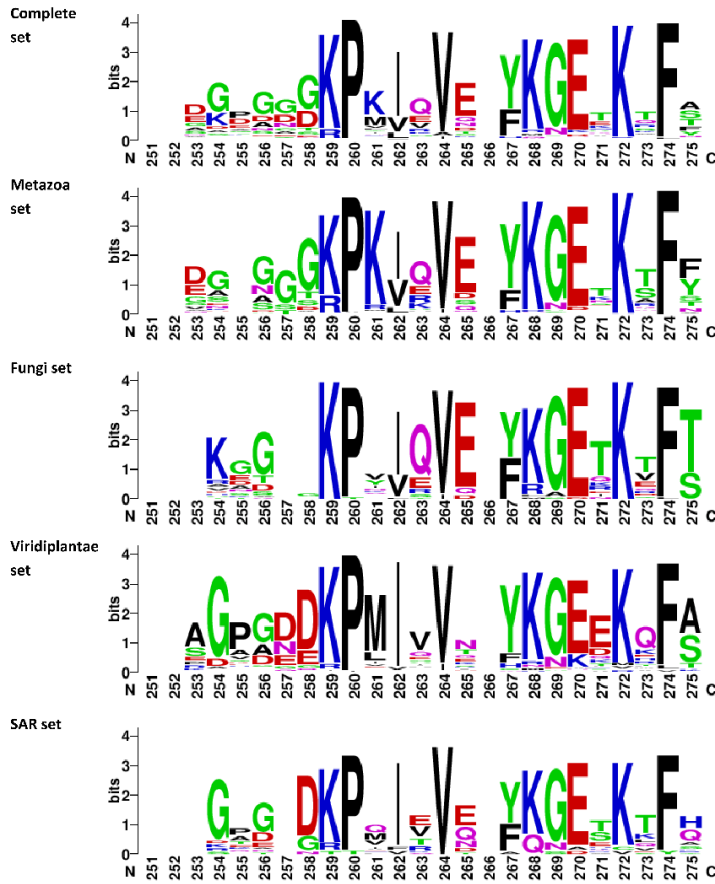


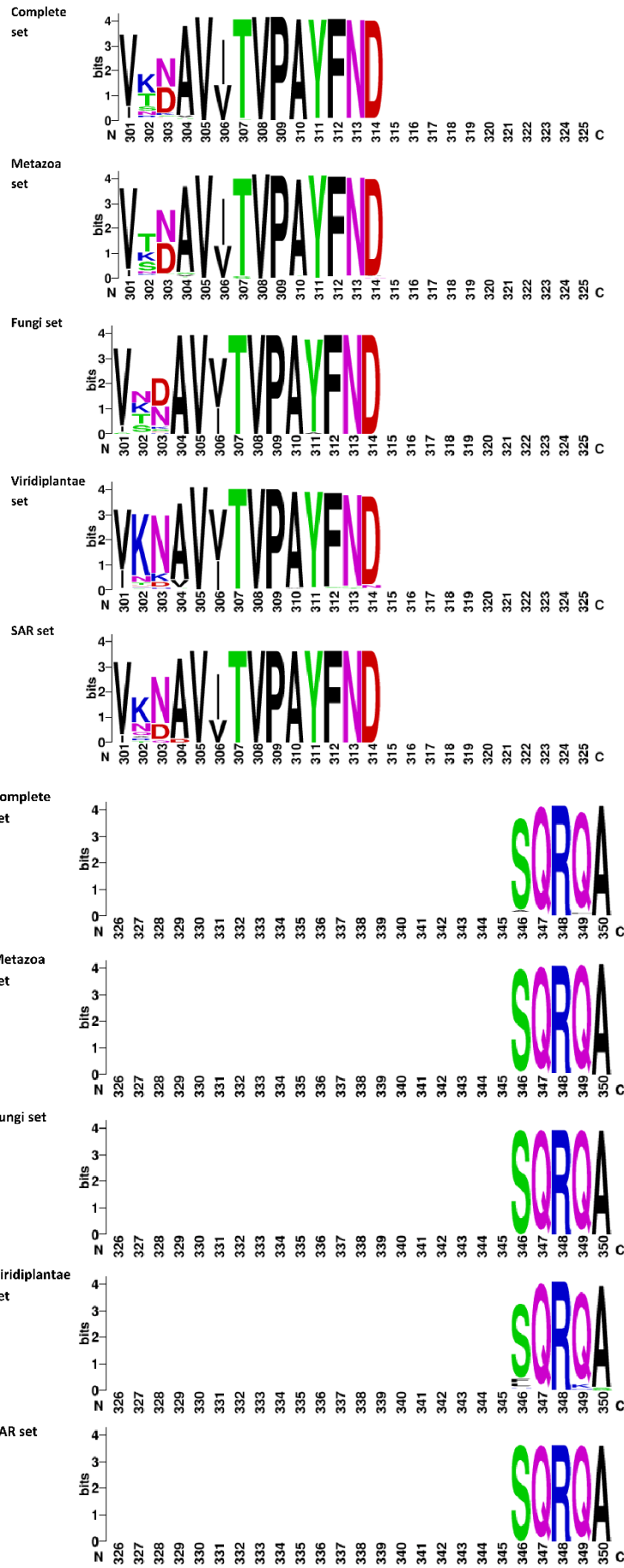


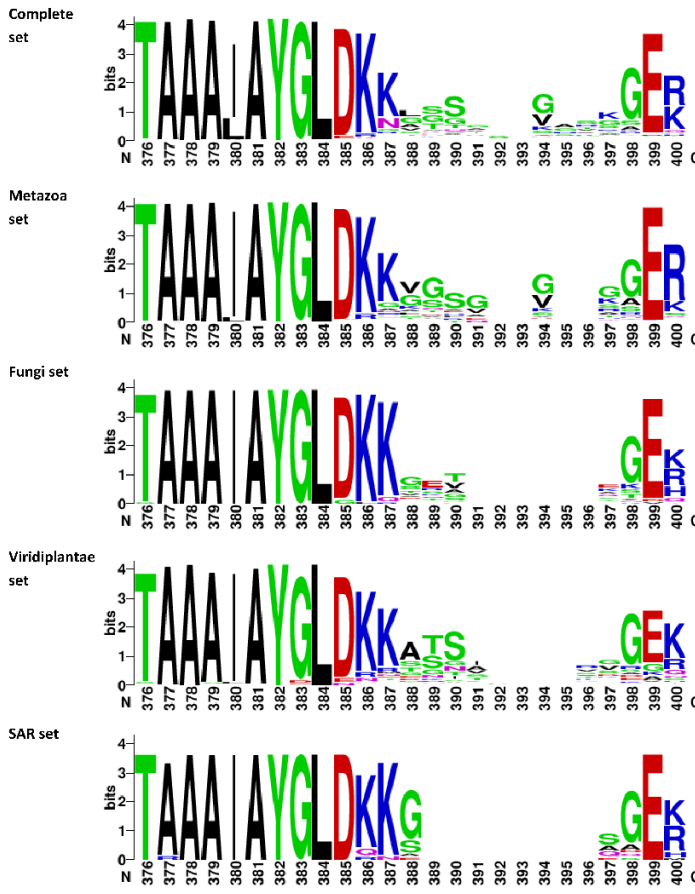
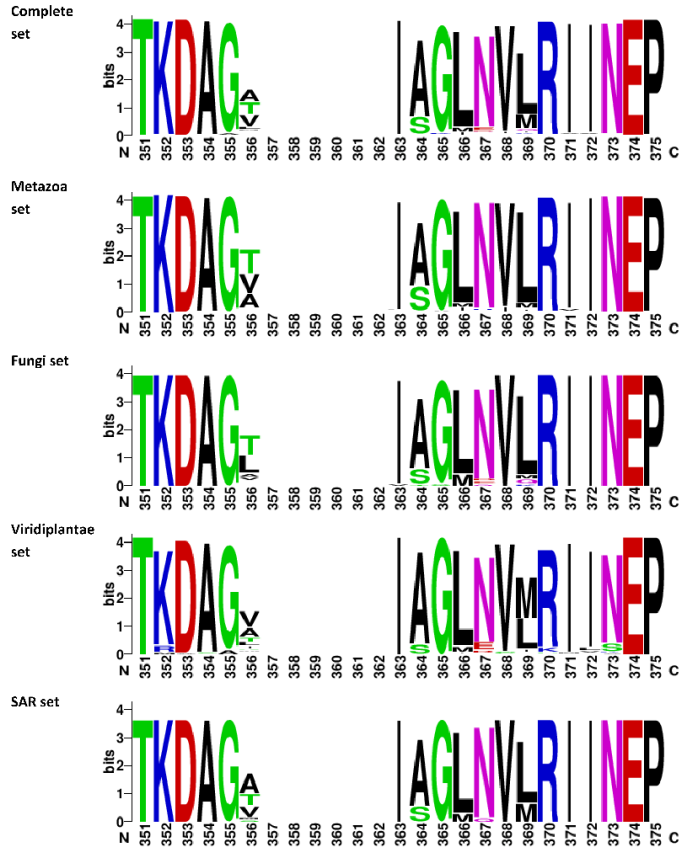


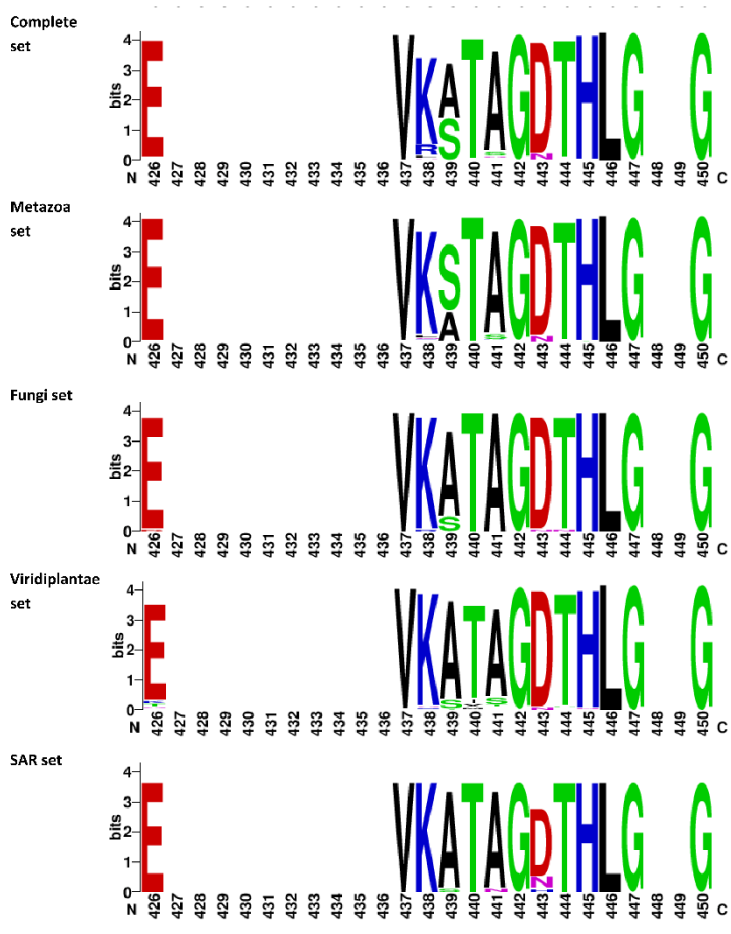
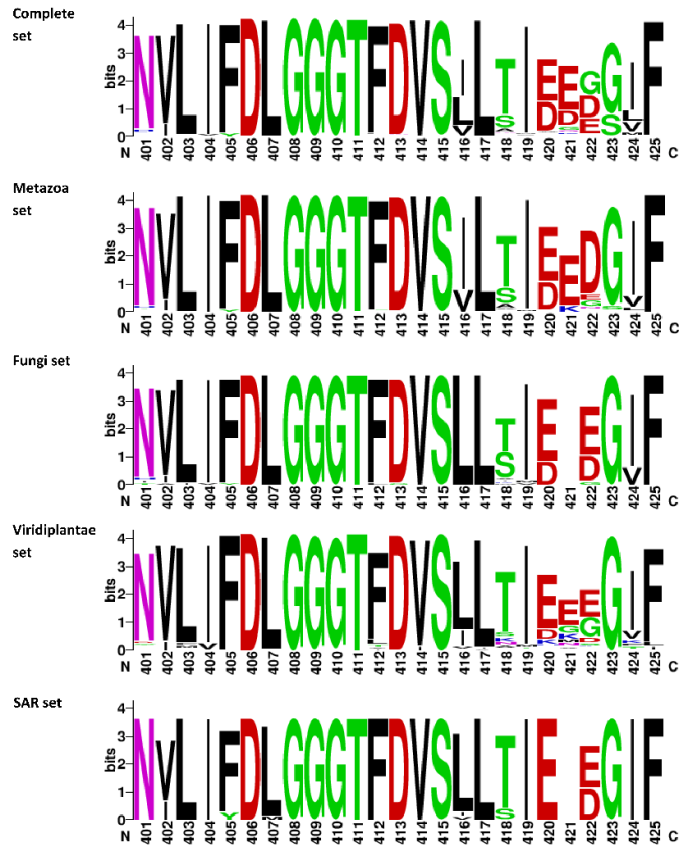


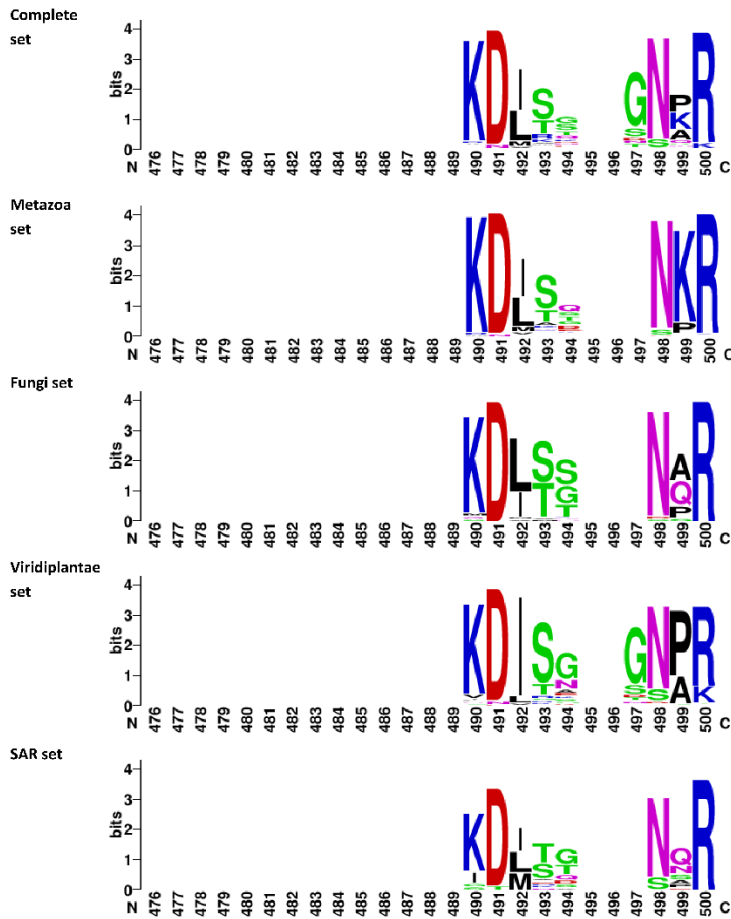
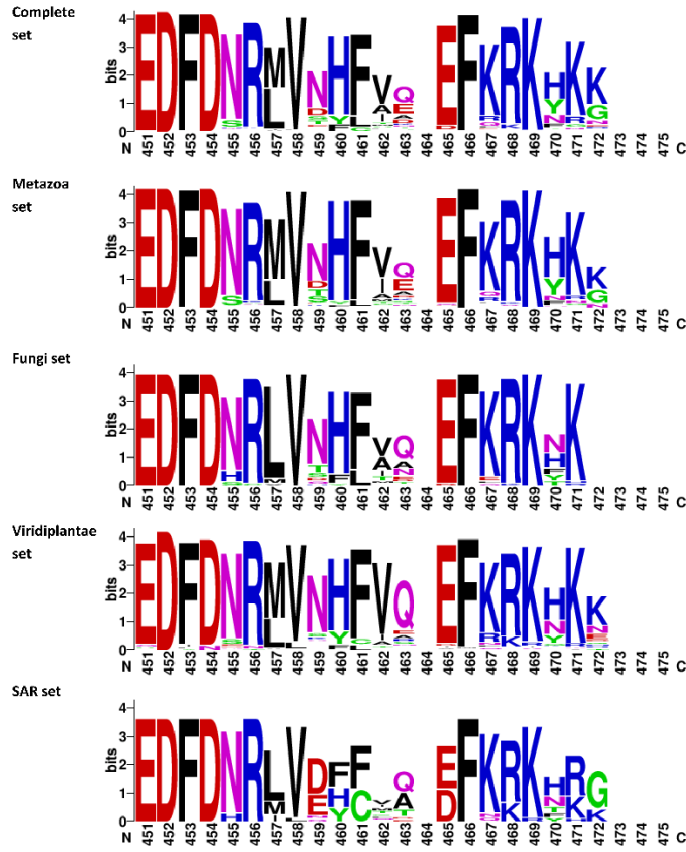


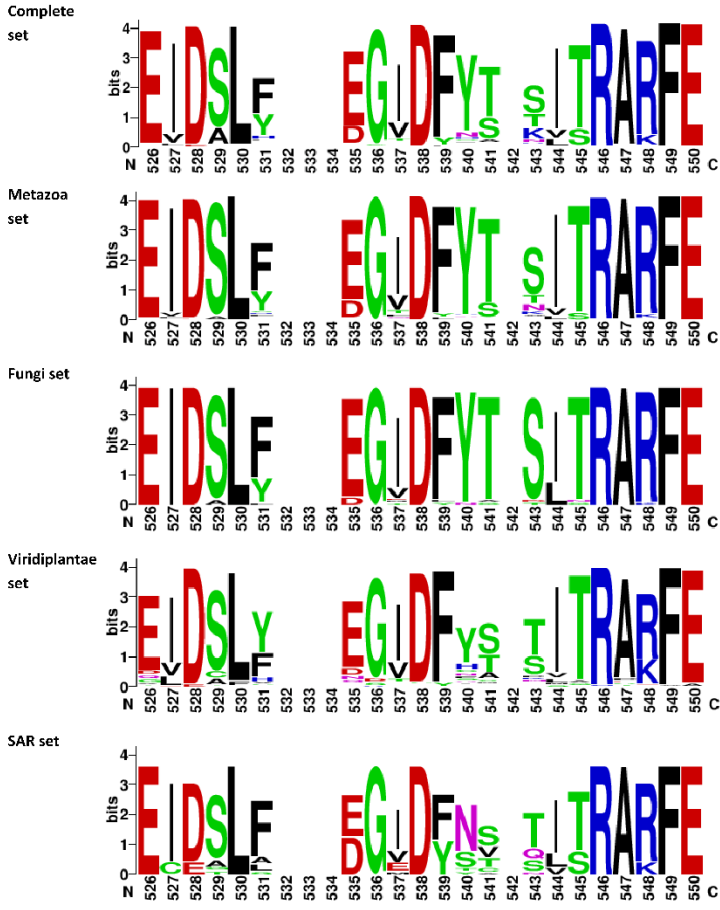
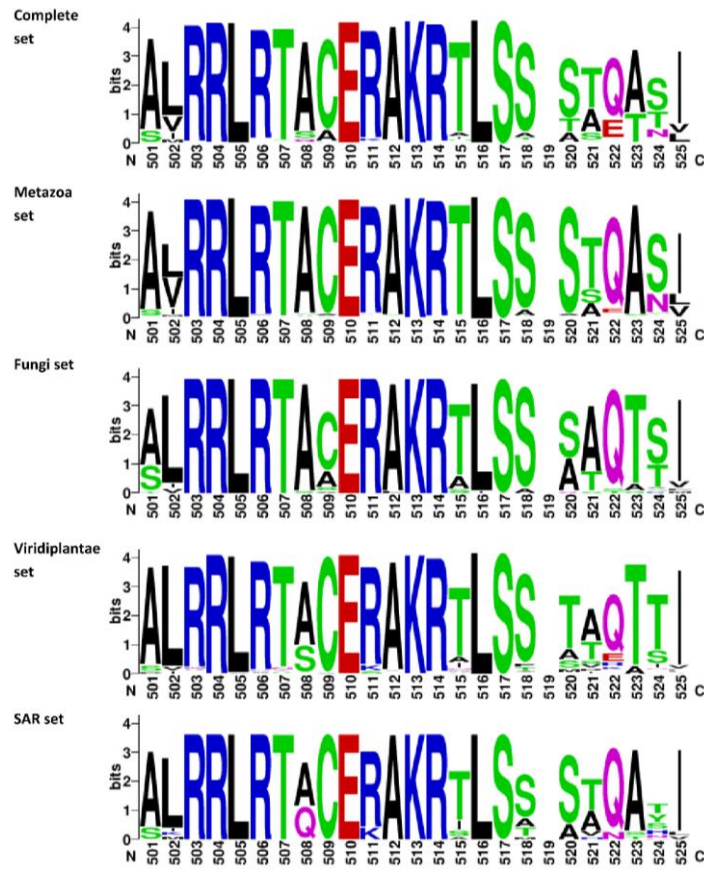


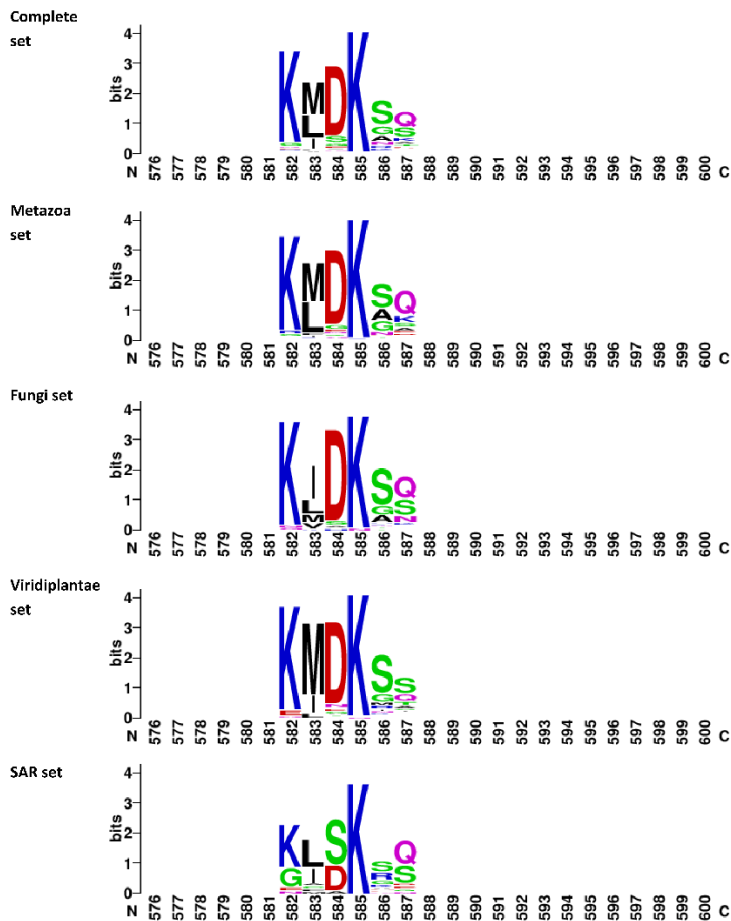
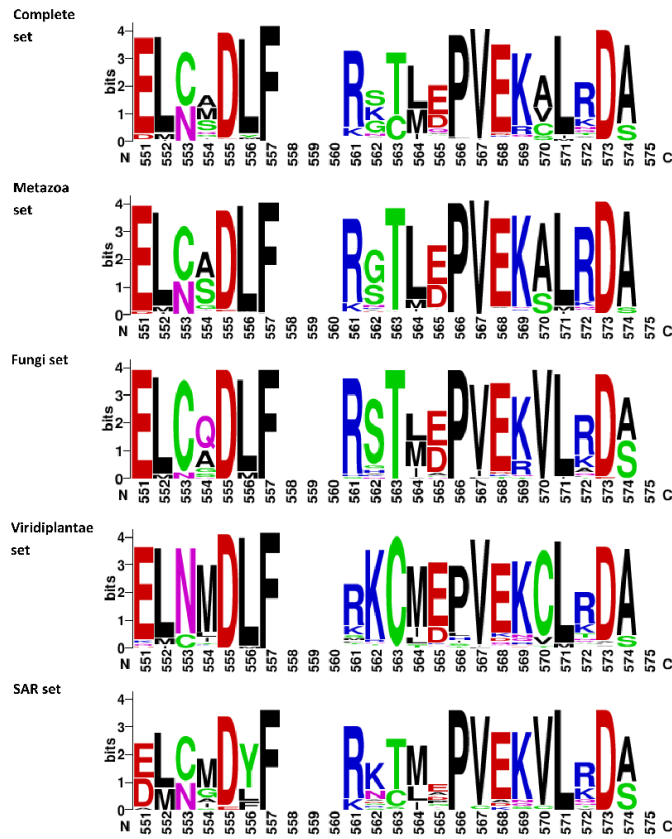


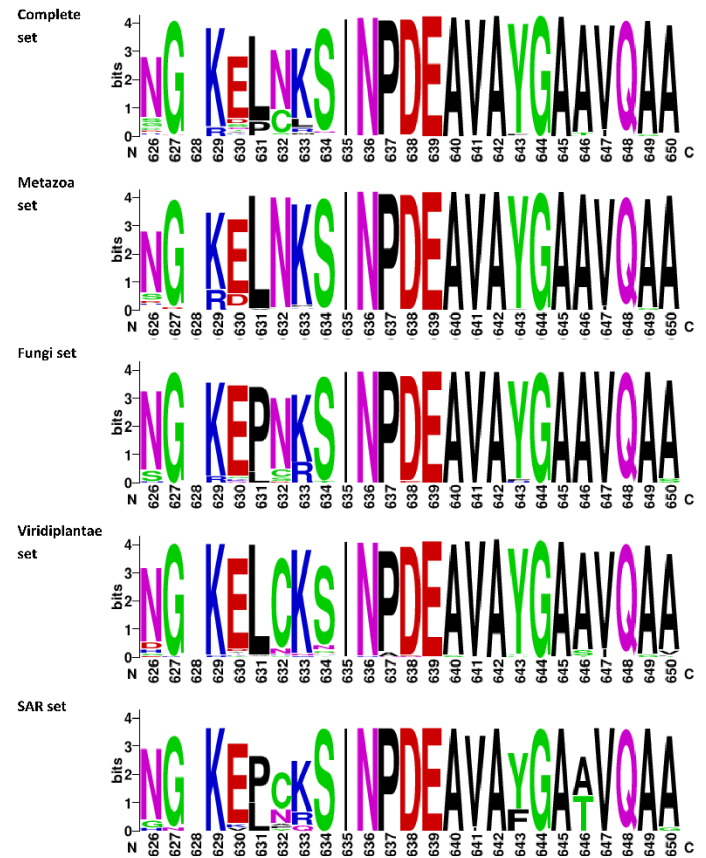
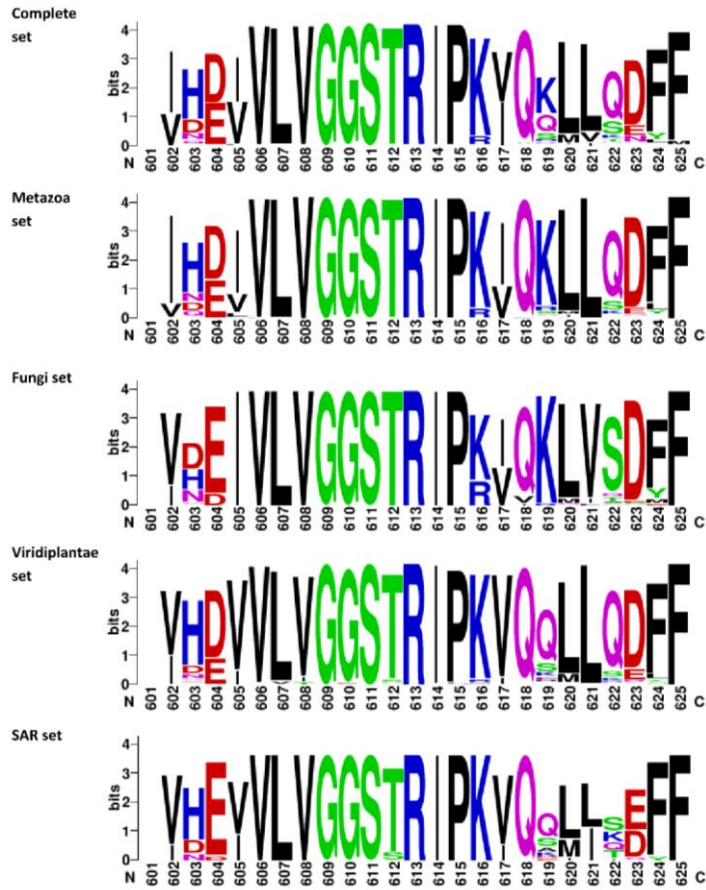


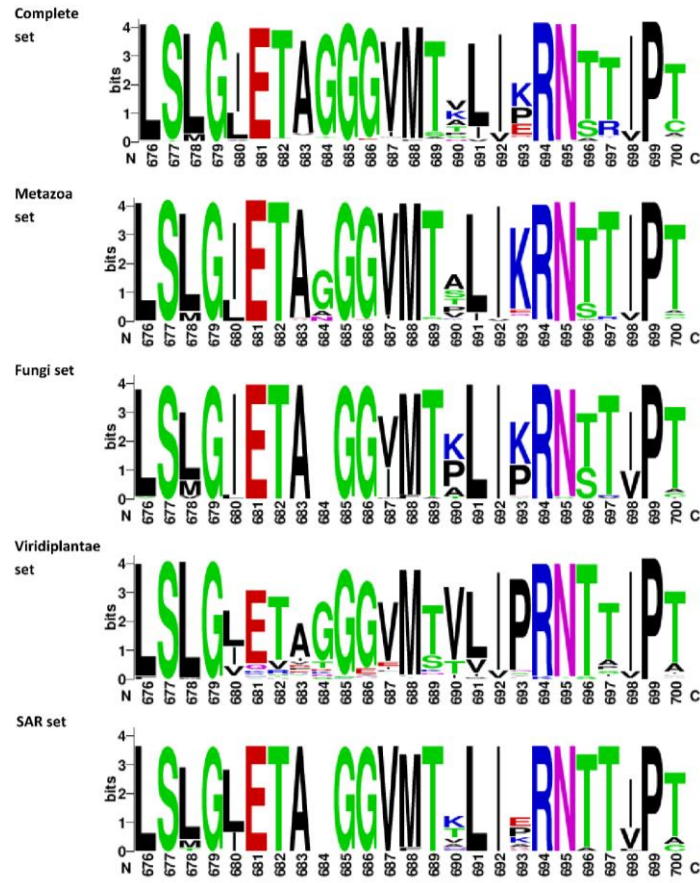
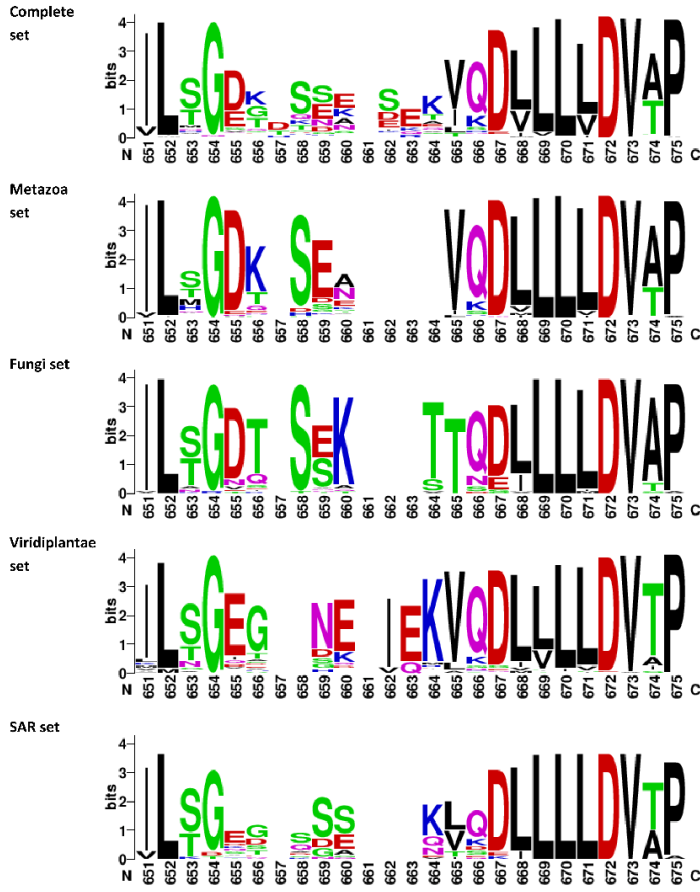


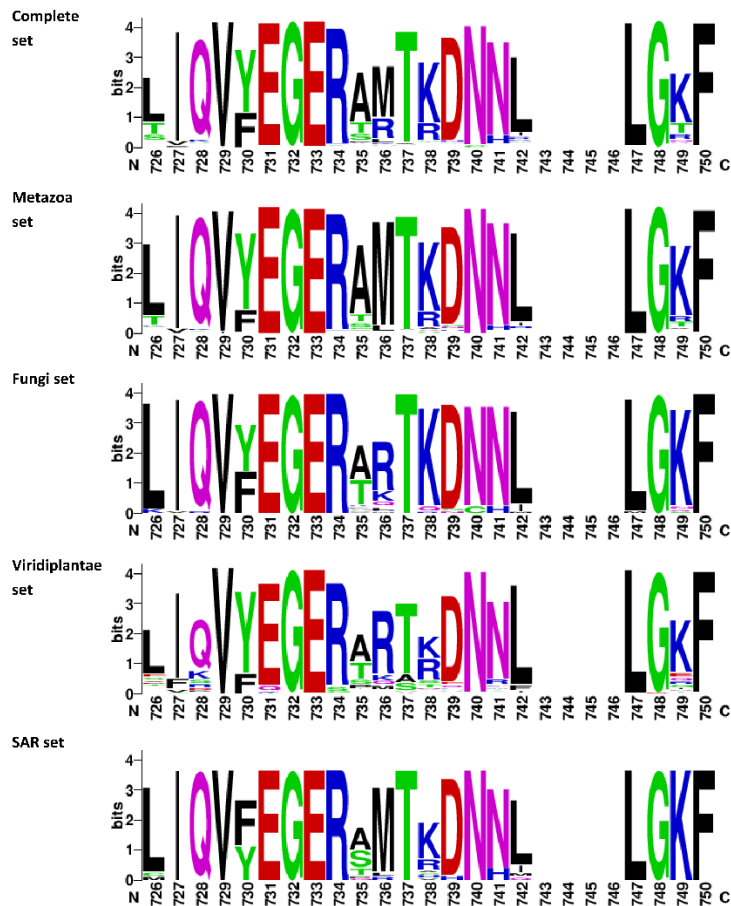
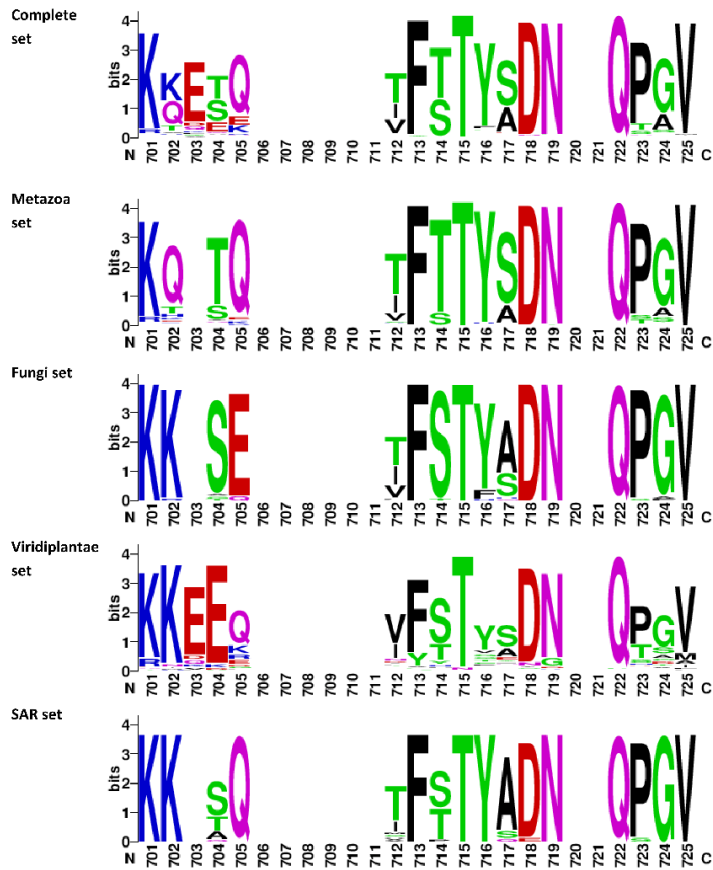


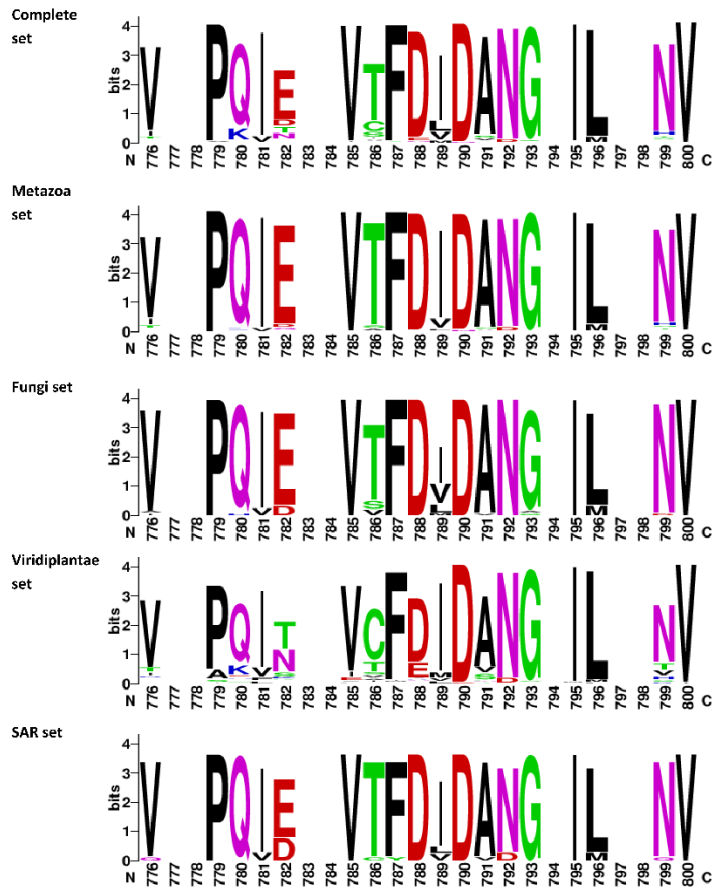
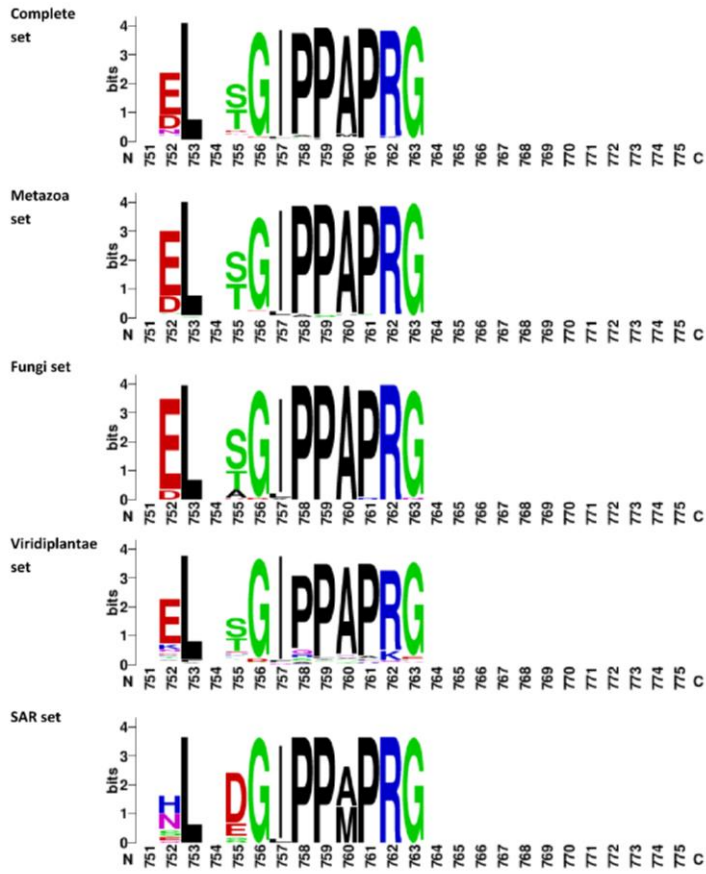


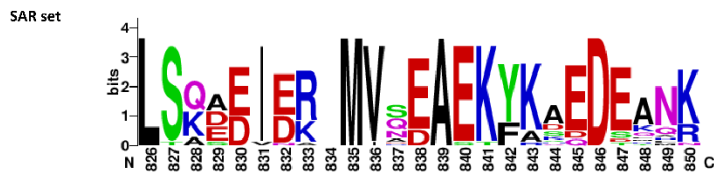
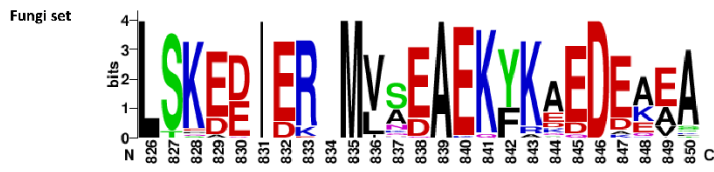
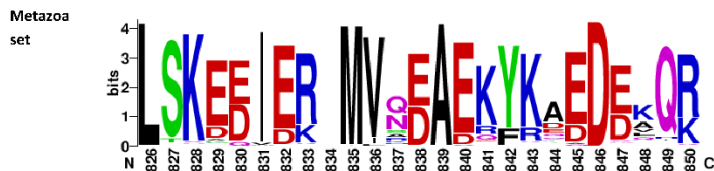
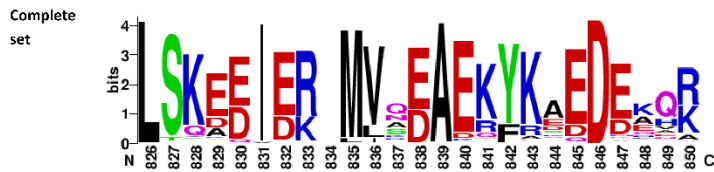
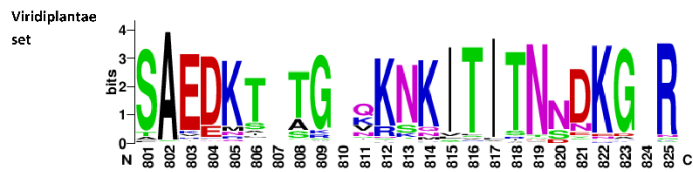
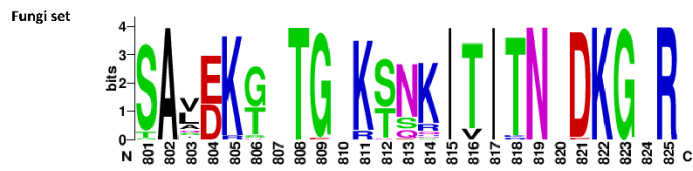
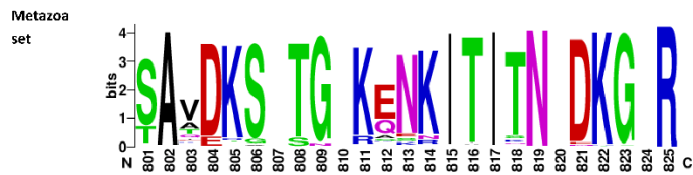
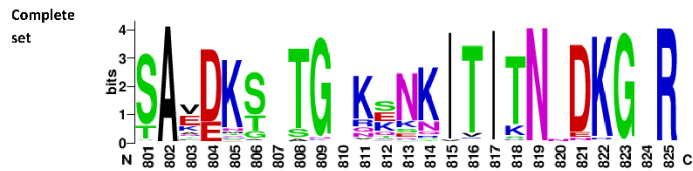


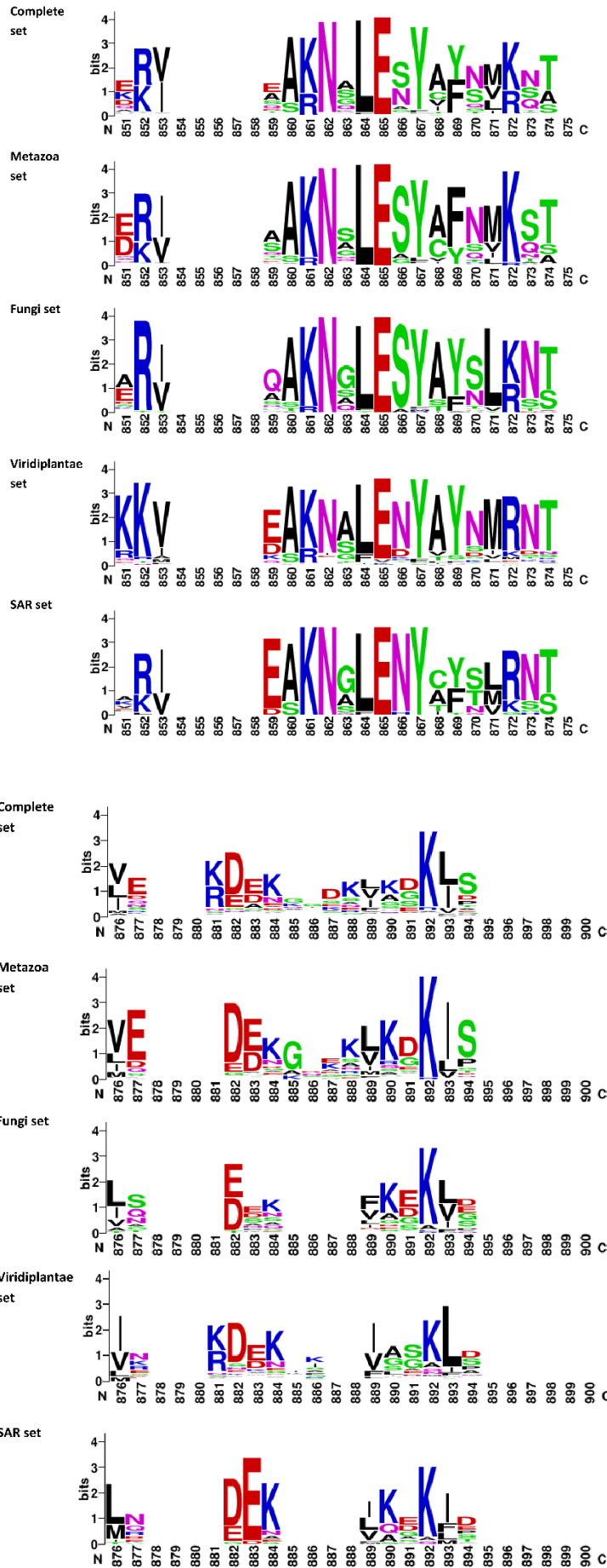


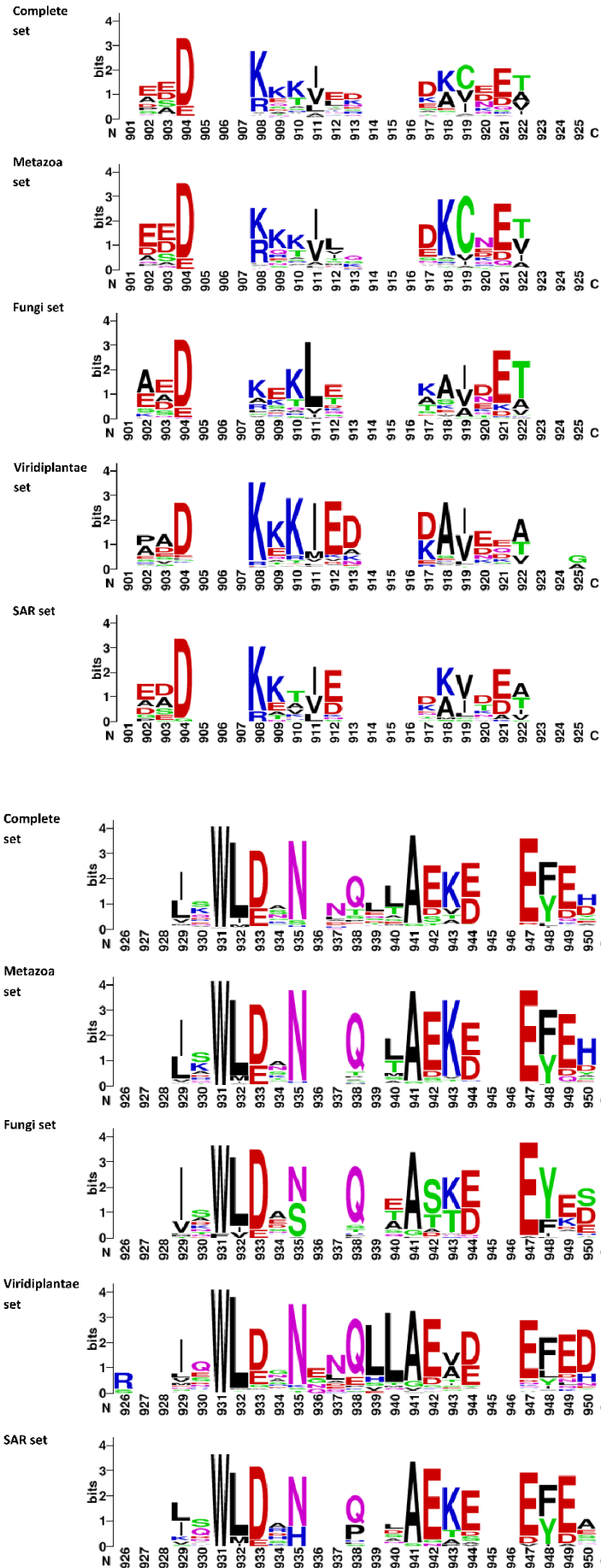


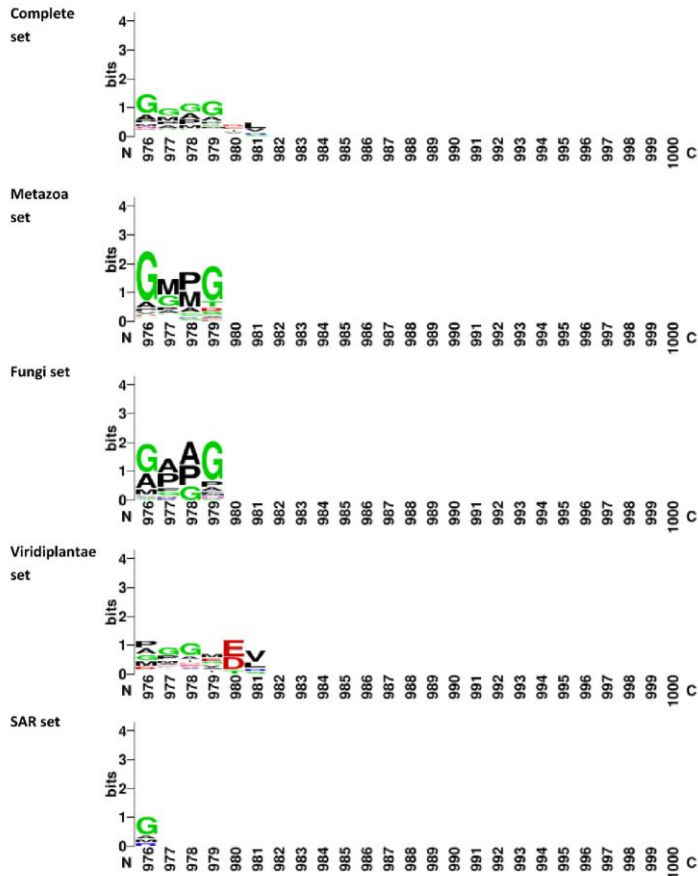
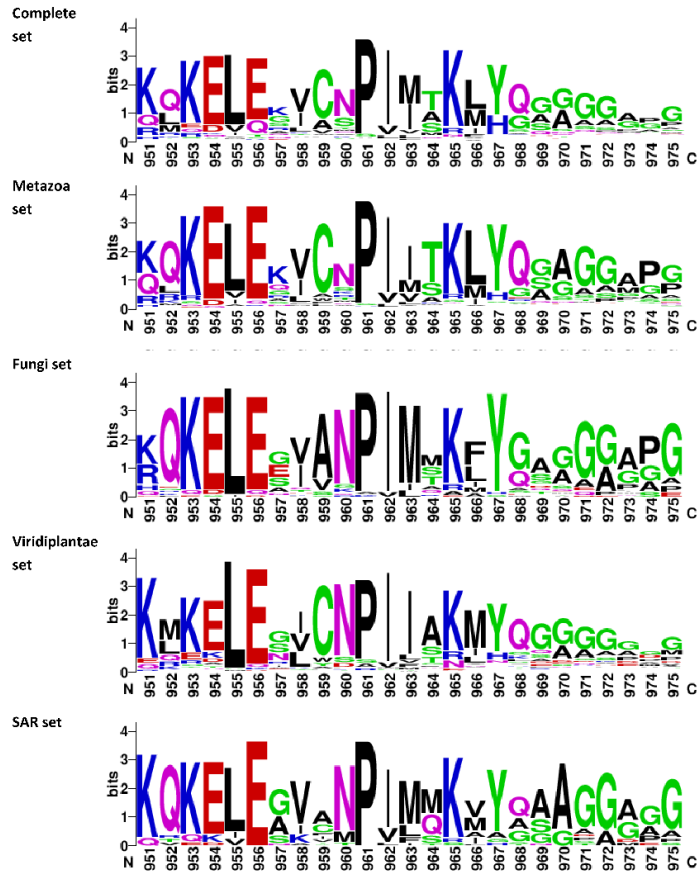


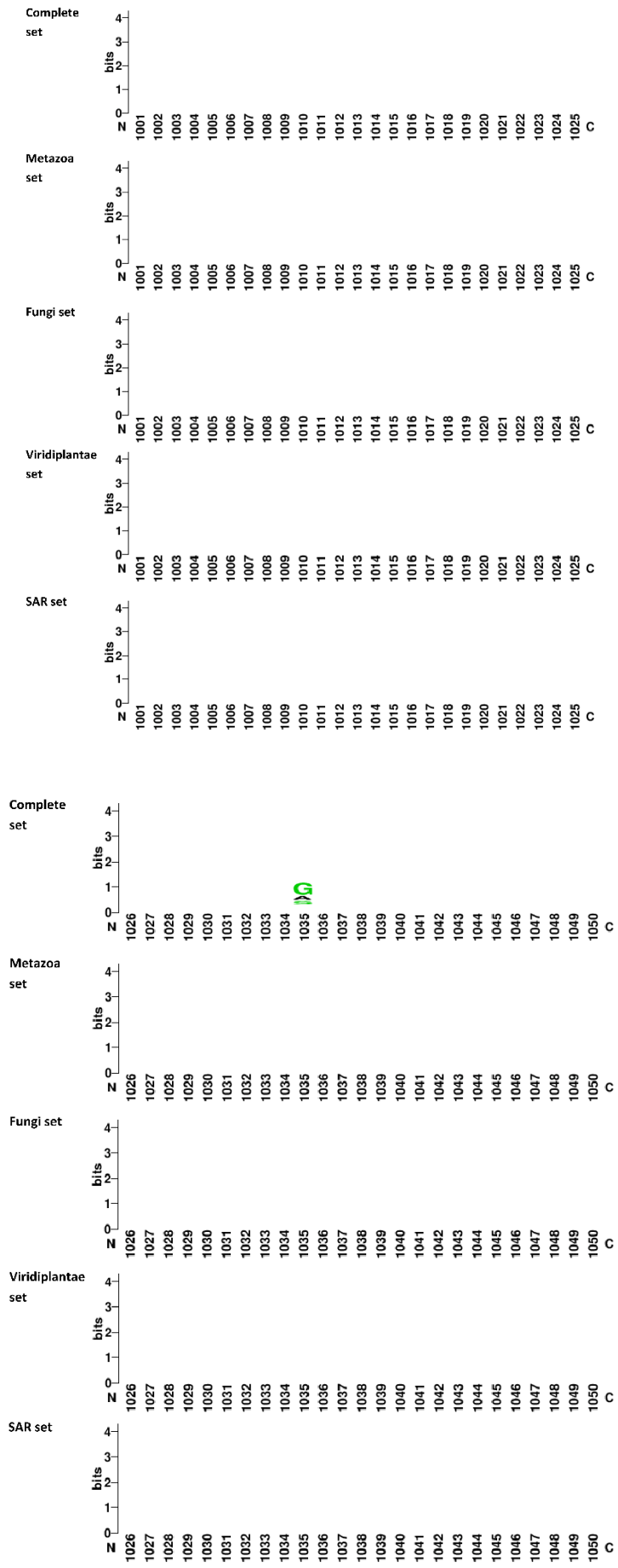


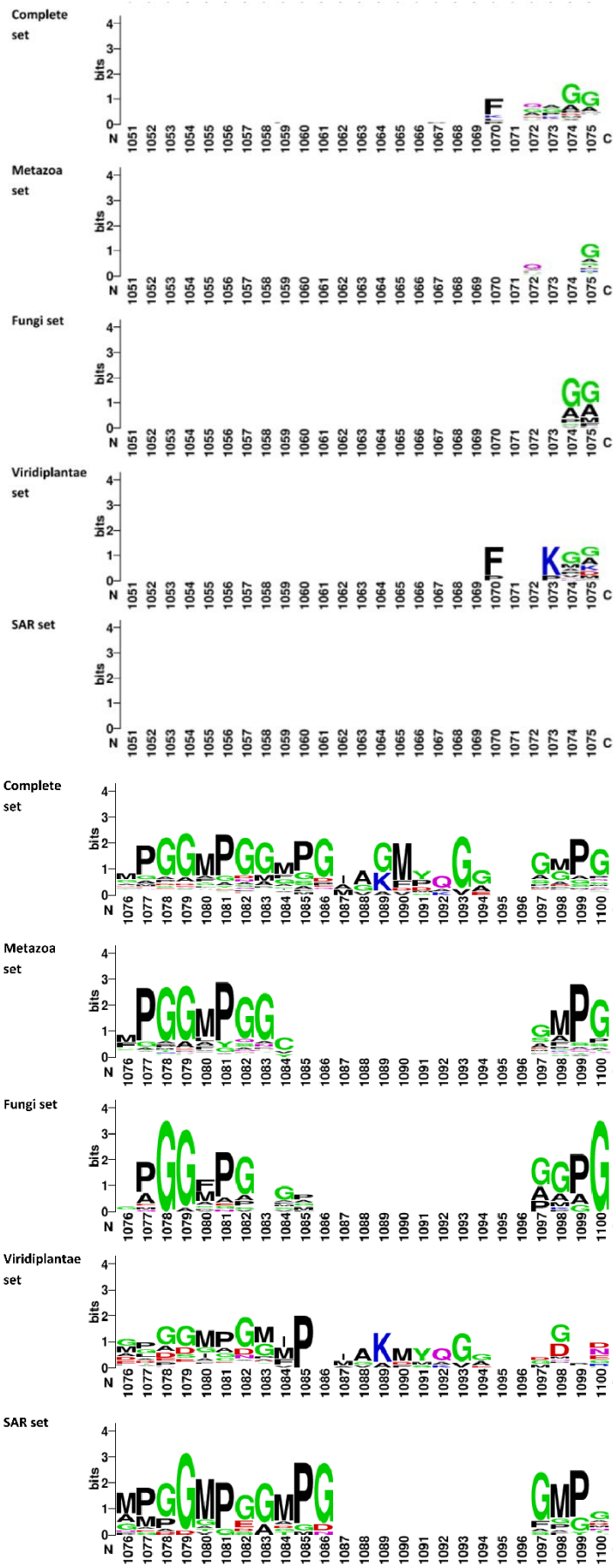


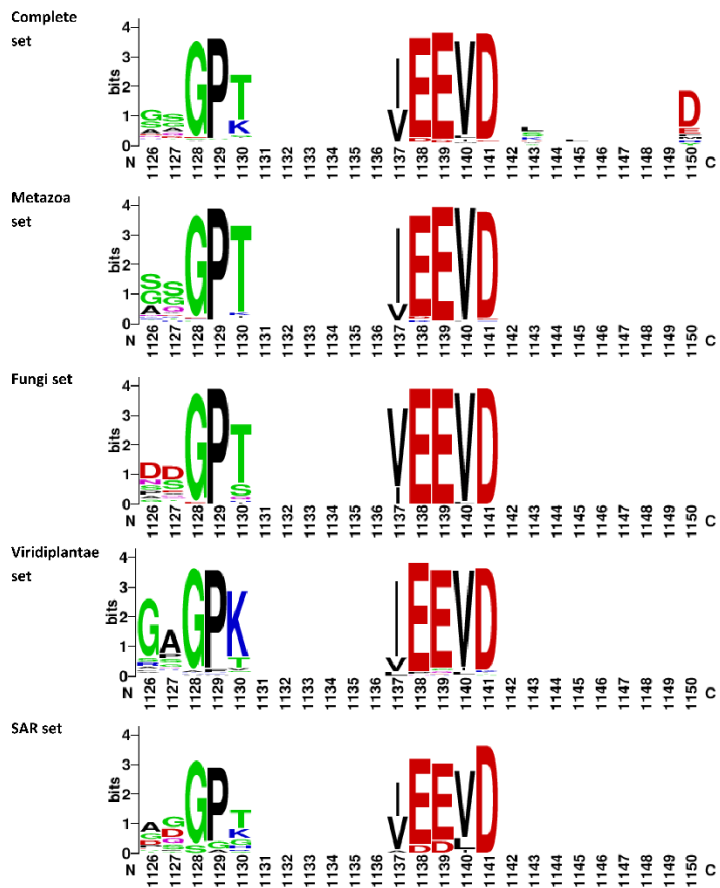
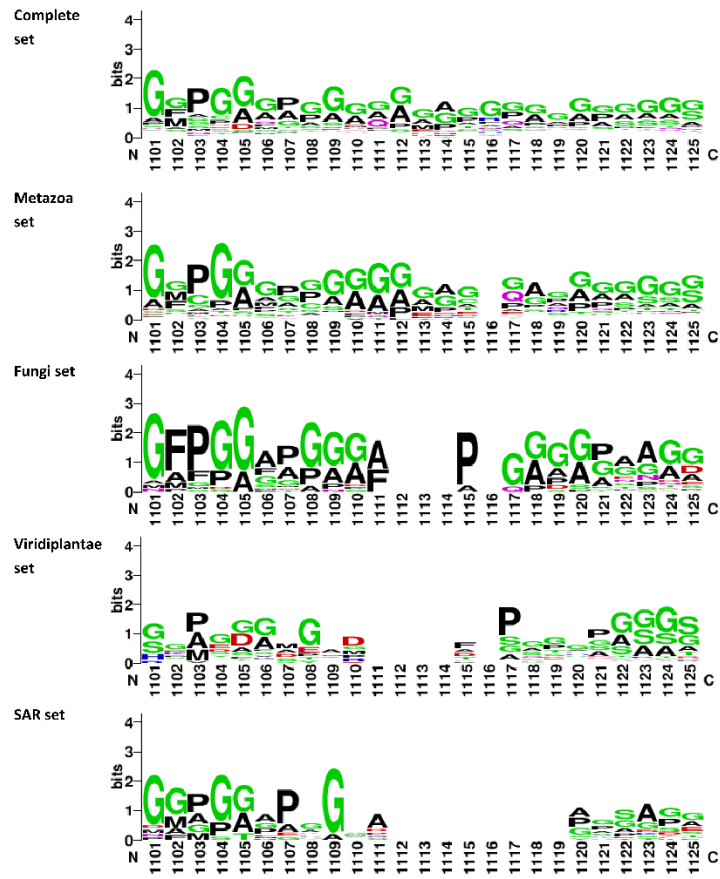


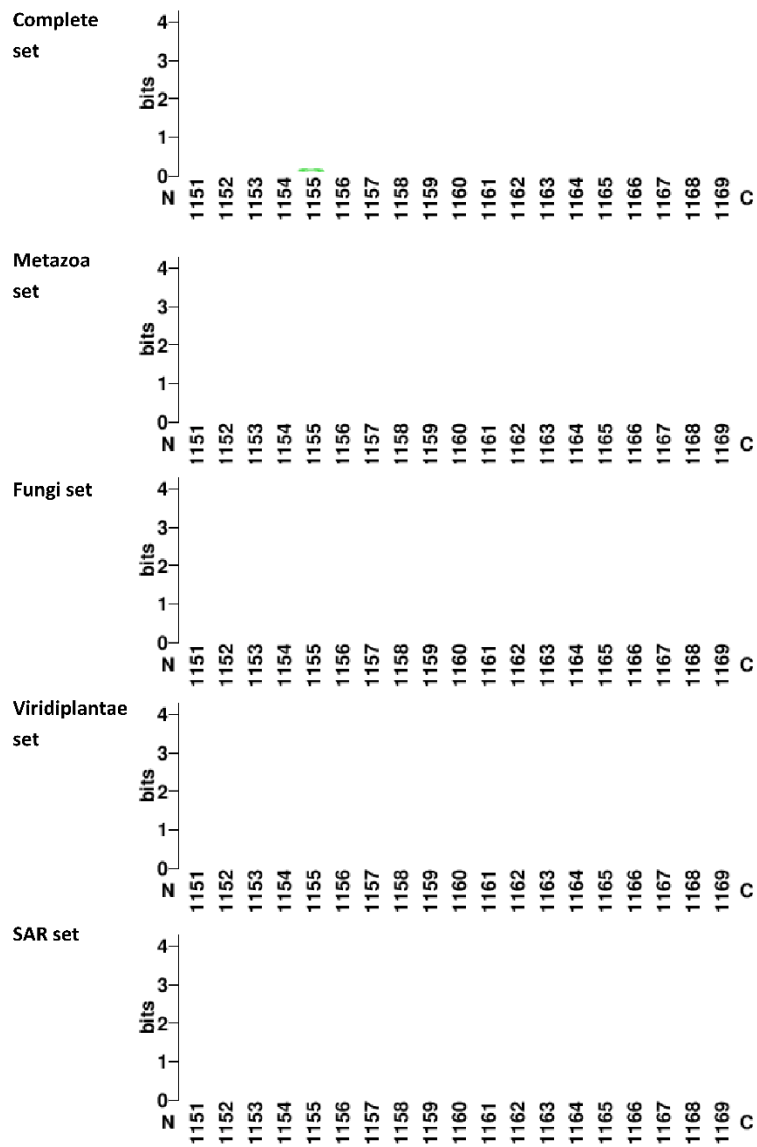




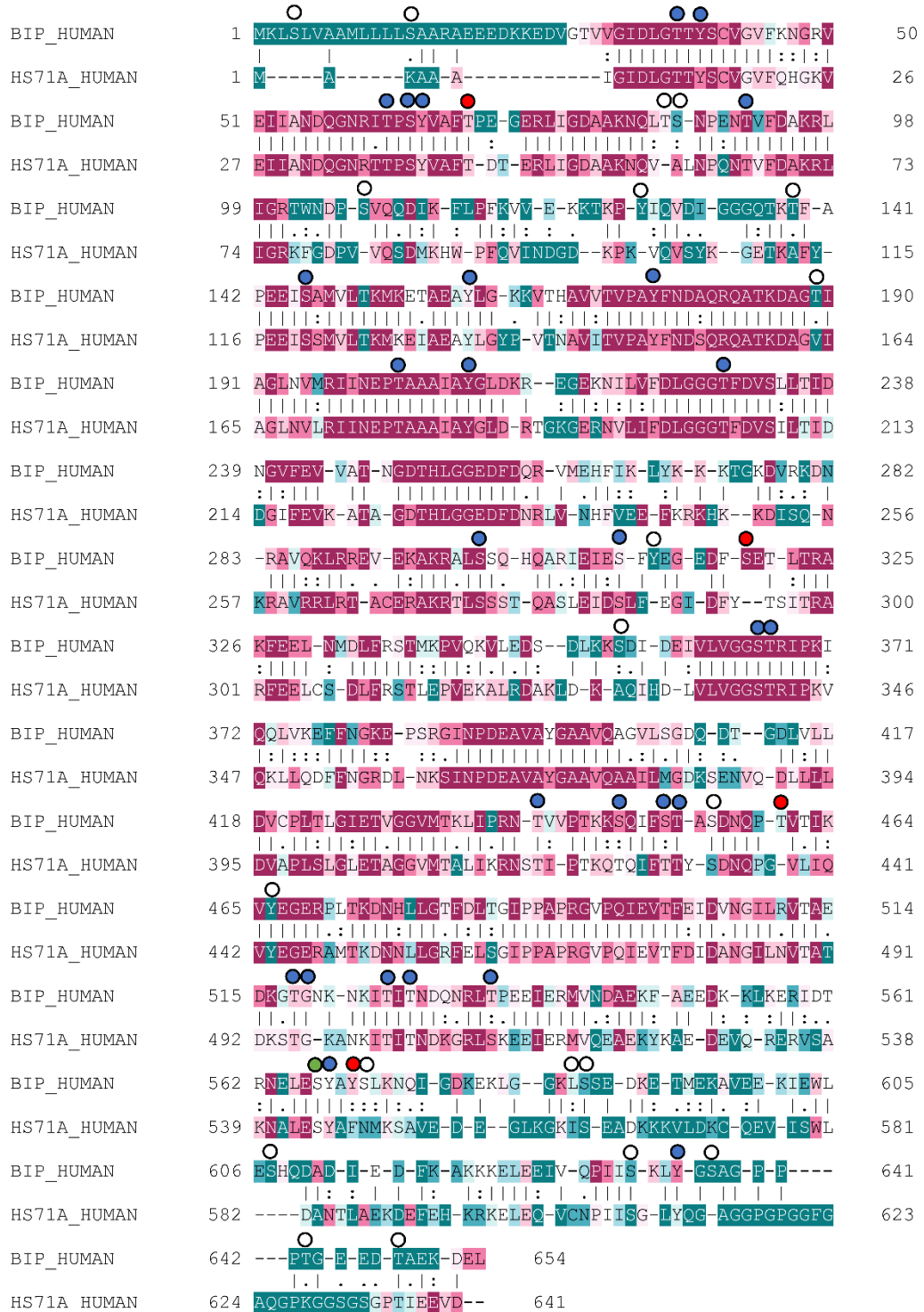








**Appendix Figure 4: Cytoplasmic Weblogo.** The complete Weblogo (174) generated pattern of cytoplasmic located Hsp70 sequence set. Residues of 2.5 or higher out of 4 are considered conserved. Gaps found in sequences arose due to fasta format used in the generation of the multiple sequence alignment and are not found in the actual protein.

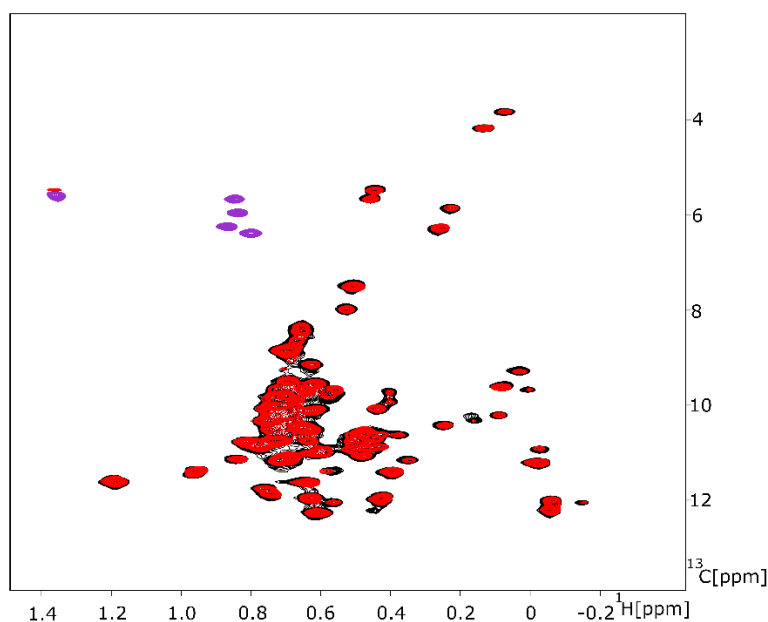


**The conservation scale:**

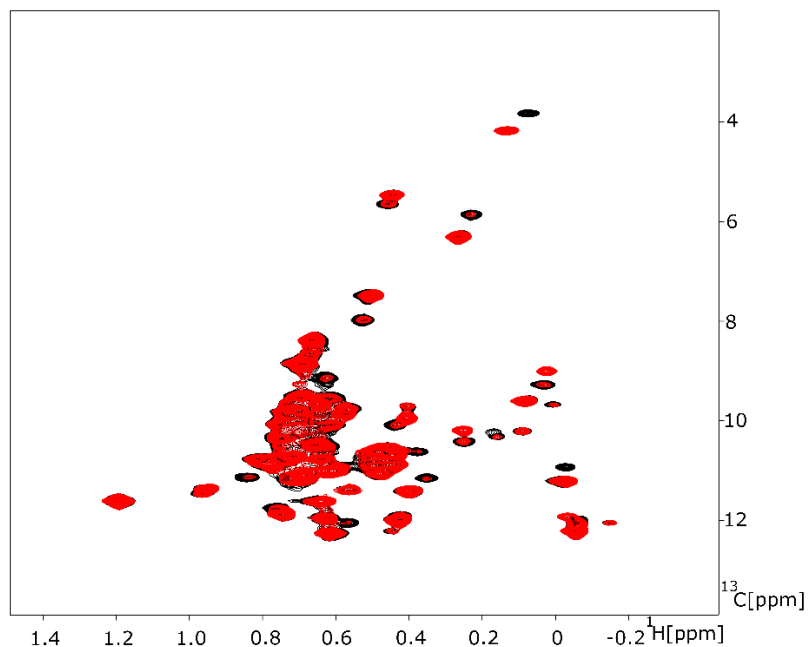


**Appendix Figure 5: conservation patterns of phosphorylation sites.** Sequence of BIP and coloured with ConSurf (171–173) with spheres (coloured coded for conserved in either ER (Red), cytoplasmic (green), all hsp70 (blue) or none (white)) displaying phosphorylation sites.

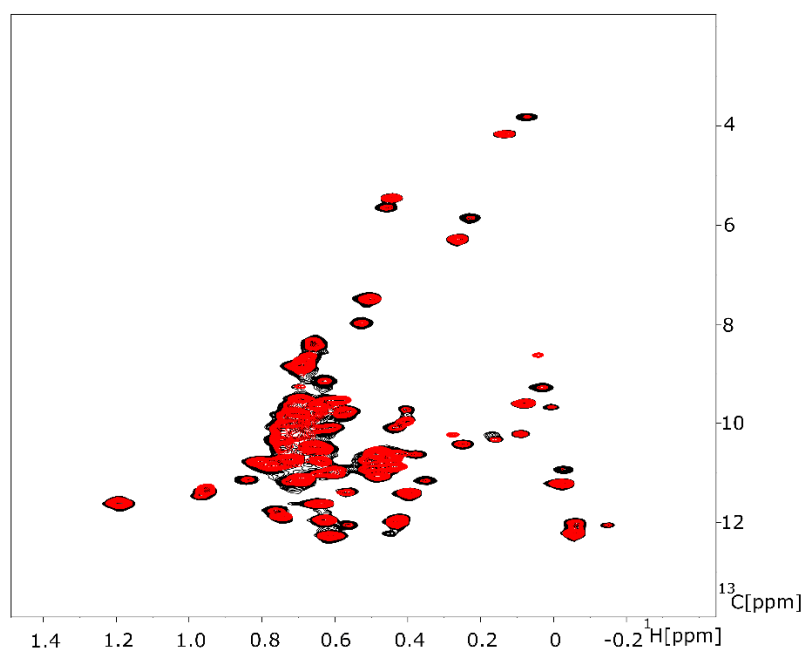
## Appendix. 2 Additional NMR spectra



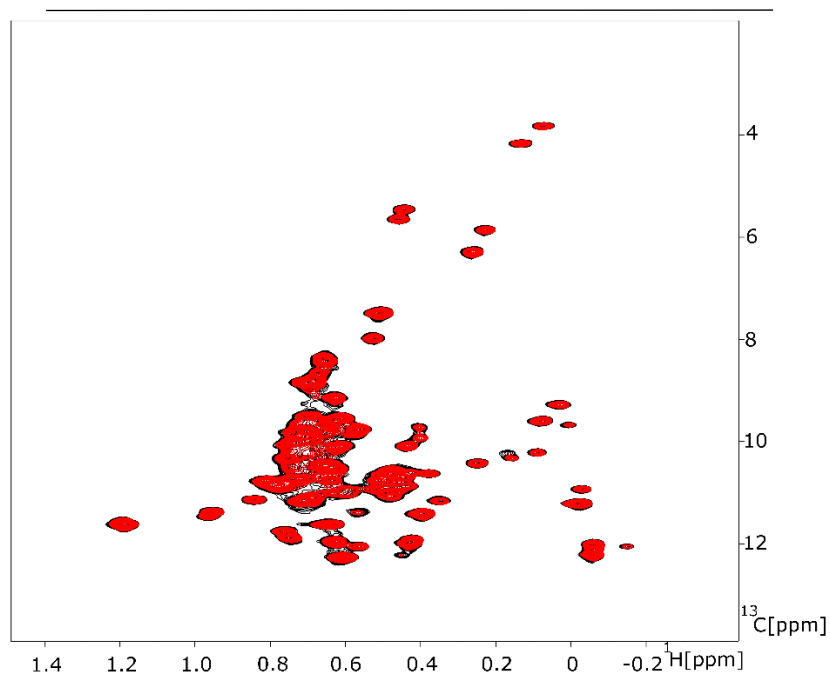
**Appendix Figure 6: Full spectra of T229G BiP in the presence of IRE1<sup>P1</sup>.** Overlay of the isoleucine region of methyl-TROSY spectra of full length human BiP T229G in the presence of 40 mM ATP (Black) and full length human BiP T229G in the presence of 40 mM ATP and 1 mM IRE1<sup>P1</sup> (Red) recorded at 25 °C on a 750 MHz Bruker spectrometer.



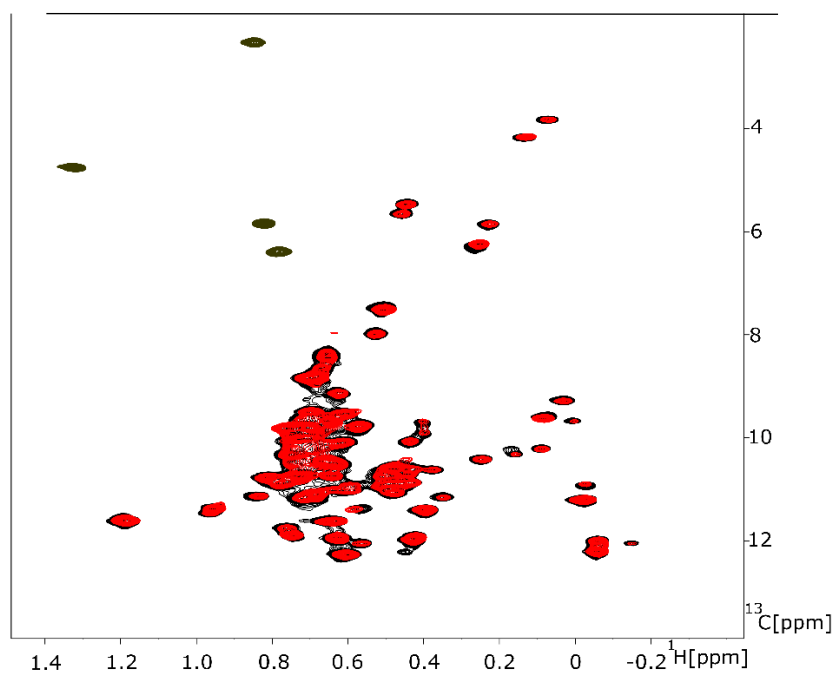
**Appendix Figure 7: Full spectra of T229G BiP in the presence of IRE1<sup>P2</sup>.** Overlay of the isoleucine region of methyl-TROSY spectra of full length human BiP T229G in the presence of 40 mM ATP (Black) and full length human BiP T229G in the presence of 40 mM ATP and 50  $\mu$ M IRE1<sup>P2</sup> (Red) recorded at 25 °C on a 750 MHz Bruker spectrometer.



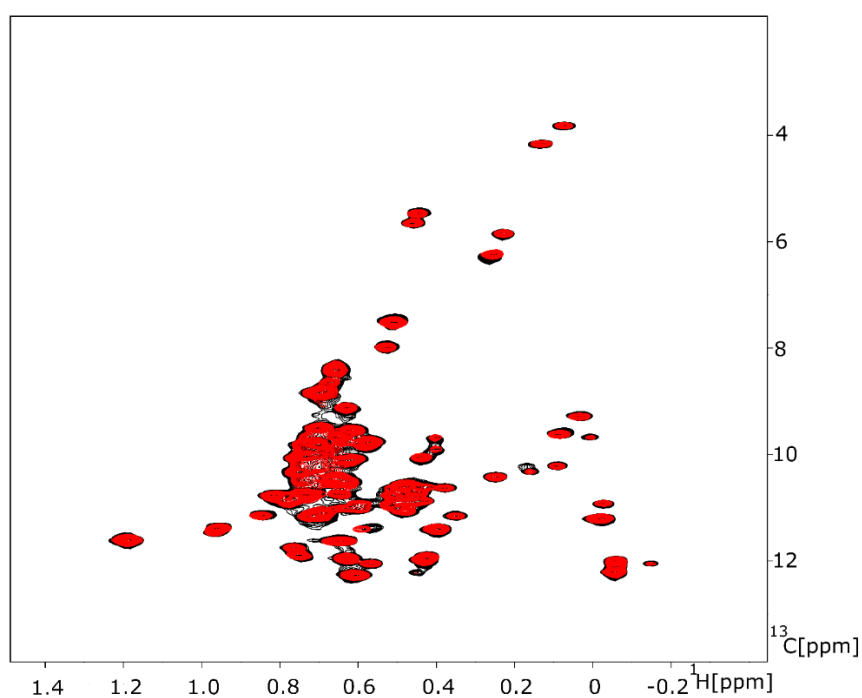
**Appendix Figure 8: Full spectra of T229G BiP in the presence of IRE1<sup>P3</sup>.** Overlay of the isoleucine region of methyl-TROSY spectra of full length human BiP T229G in the presence of 40 mM ATP (Black) and full length human BiP T229G in the presence of 40 mM ATP and 50 μM IRE1<sup>P3</sup> (Red) recorded at 25 °C on a 750 MHz Bruker spectrometer.



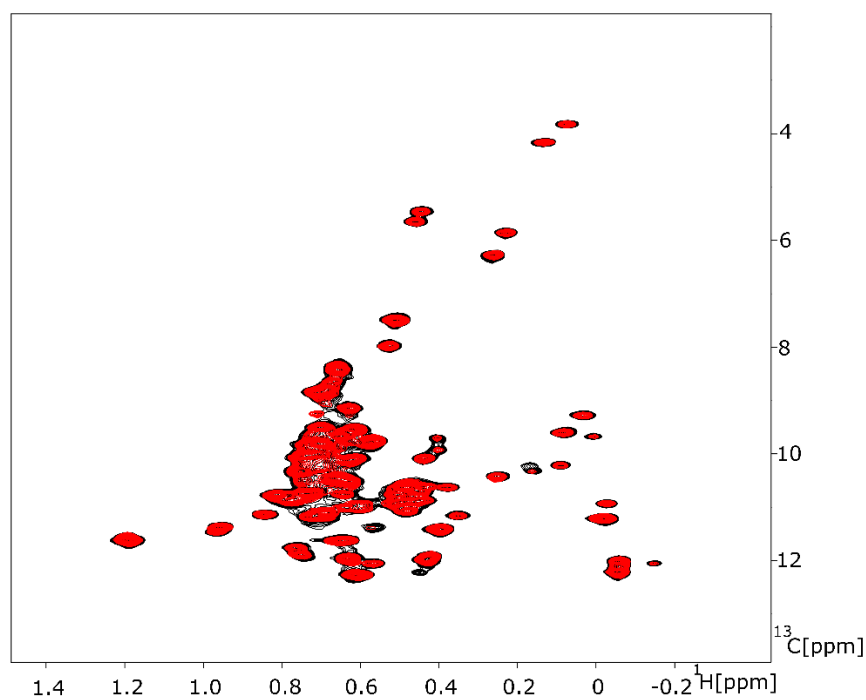
**Appendix Figure 9: Full spectra of T229G BiP in the presence of IRE1<sup>P4</sup>.** Overlay of the isoleucine region of methyl-TROSY spectra of full length human BiP T229G in the presence of 40 mM ATP (Black) and full length human BiP T229G in the presence of 40 mM ATP and 1 mM IRE1<sup>P4</sup> (Red) recorded at 25 °C on a 750 MHz Bruker spectrometer.



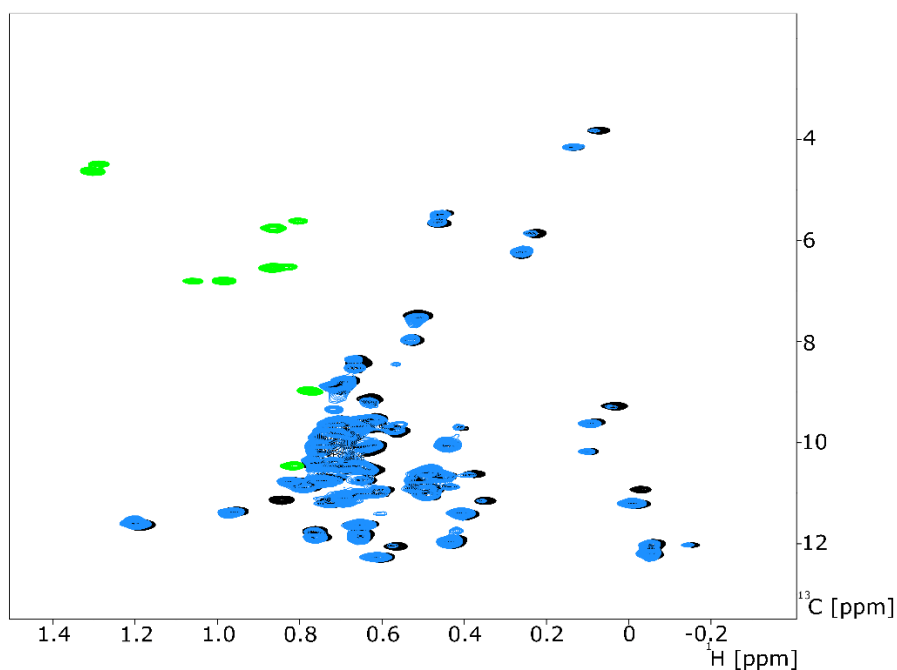
**Appendix Figure 10: Full spectra of T229G BiP in the presence of IRE1<sup>P5</sup>.** Overlay of the isoleucine region of methyl-TROSY spectra of full length human BiP T229G in the presence of 40 mM ATP (Black) and full length human BiP T229G in the presence of 40 mM ATP and 1 mM IRE1<sup>P5</sup> (Red) recorded at 25 °C on a 750 MHz Bruker spectrometer.



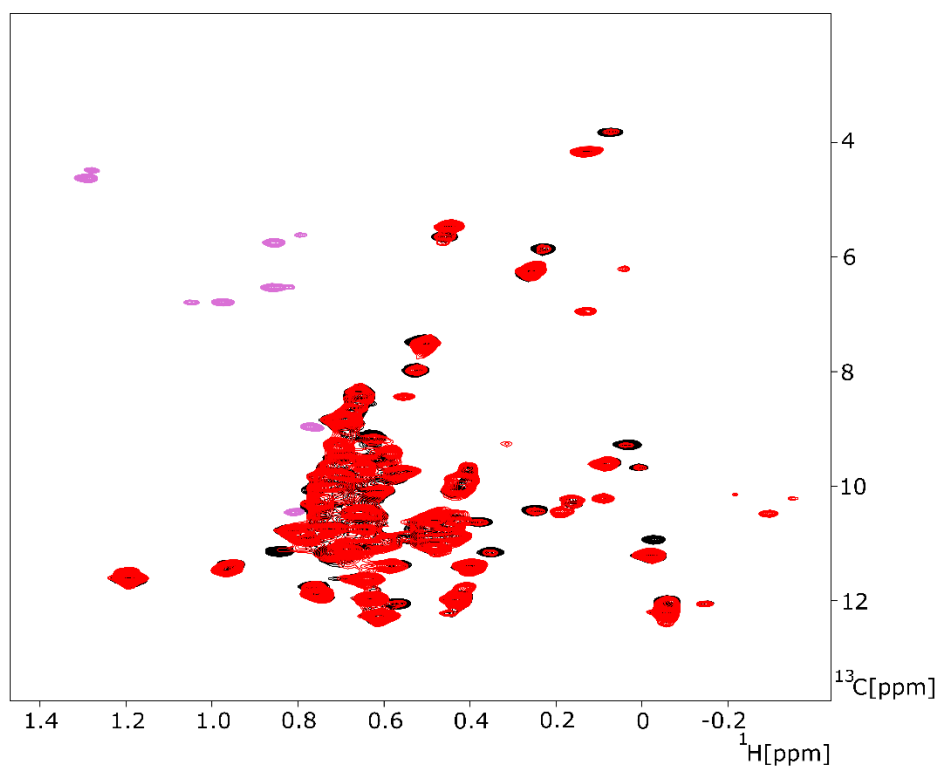
**Appendix Figure 11: Full spectra of T229G BiP in the presence of IRE1<sup>P6</sup>.** Overlay of the isoleucine region of methyl-TROSY spectra of full length human BiP T229G in the presence of 40 mM ATP (Black) and full length human BiP T229G in the presence of 40 mM ATP and 1 mM IRE1<sup>P6</sup> (Red) recorded at 25 °C on a 750 MHz Bruker spectrometer.



**Appendix Figure 12: Full spectra of T229G BiP in the presence of 50  $\mu\text{M}$  CP2.** Overlay of the isoleucine region of methyl-TROSY spectra of full length human BiP T229G in the presence of 40 mM ATP (Black) and full length human BiP T229G in the presence of 40 mM ATP and 50  $\mu\text{M}$  CP2 (Red) recorded at 25  $^{\circ}\text{C}$  on a 750 MHz Bruker spectrometer.

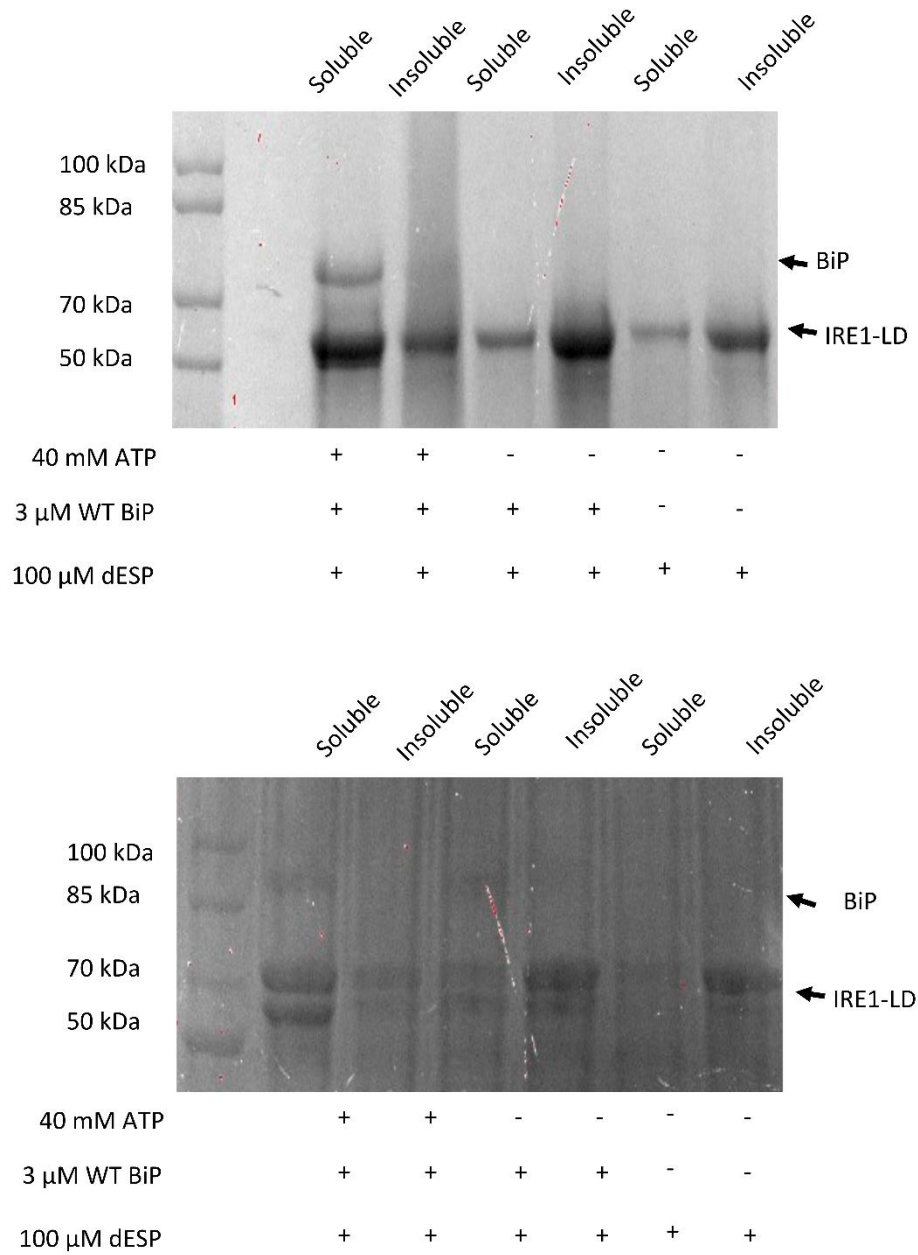


**Appendix Figure 13: Full spectra of T229G Y570D BiP in the presence of 50  $\mu\text{M}$  IRE1<sup>P3</sup>.** Overlay of the isoleucine region of methyl-TROSY spectra of full length human BiP Y570D T229G in the presence of 40 mM ATP (Blue) and full length human BiP Y570D T229G in the presence of 40 mM ATP and 50  $\mu\text{M}$  IRE1<sup>P3</sup> (Black) recorded at 25  $^{\circ}\text{C}$  on a 750 MHz Bruker spectrometer.

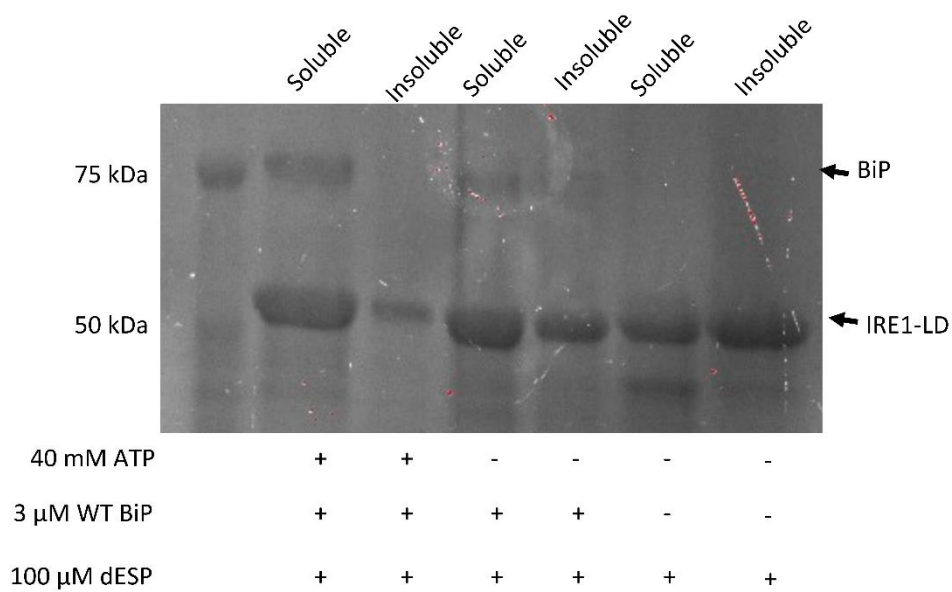


**Appendix Figure 14:** Full spectra of T229G BiP in the presence of 1 mM CP2. Overlay of the isoleucine region of methyl-TROSY spectra of full length human BiP T229G in the presence of 40 mM ATP (black) and full length human BiP T229G in the presence of 40 mM ATP and 1 mM CP2 (red) recorded at 25 °C on a 750 MHz Bruker spectrometer.

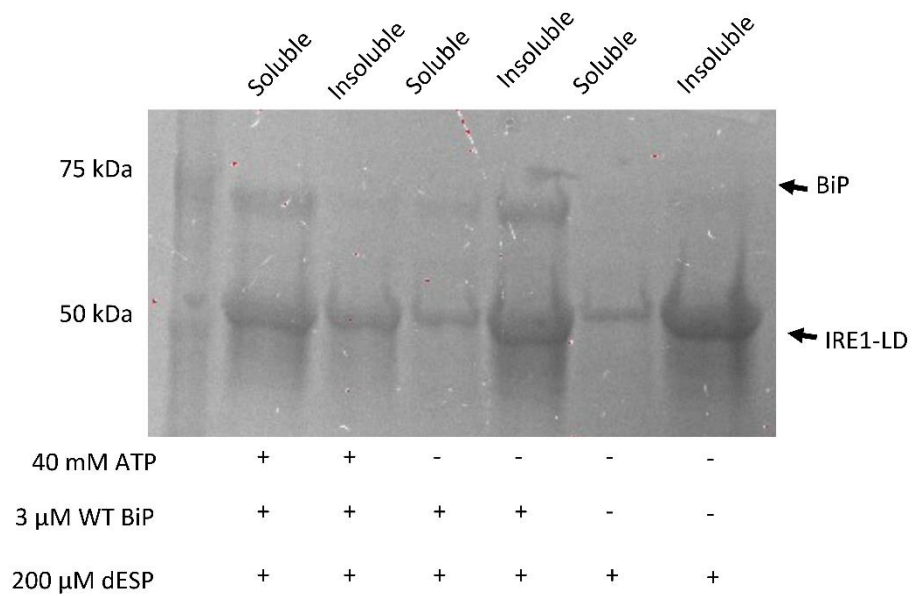
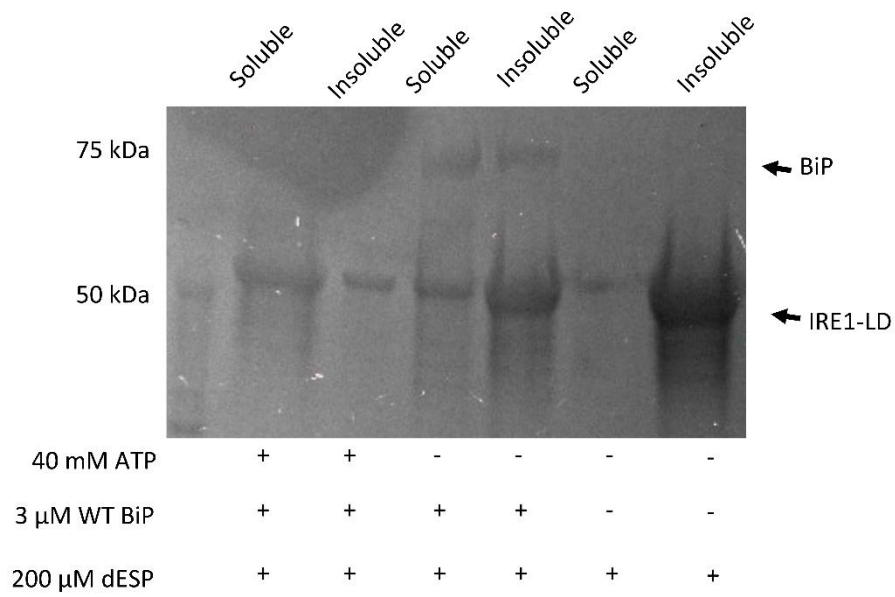
Appendix. 3 Additional IRE1-LD oligomerization gels



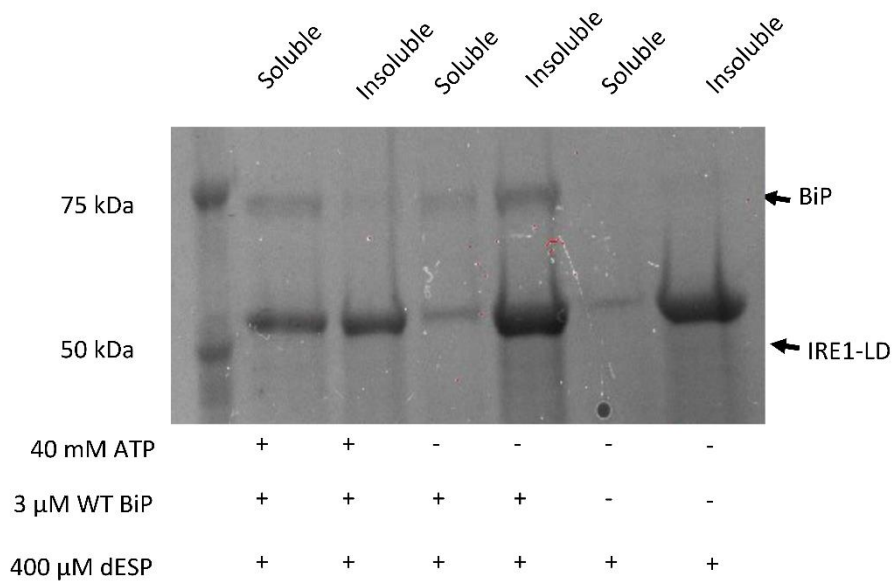
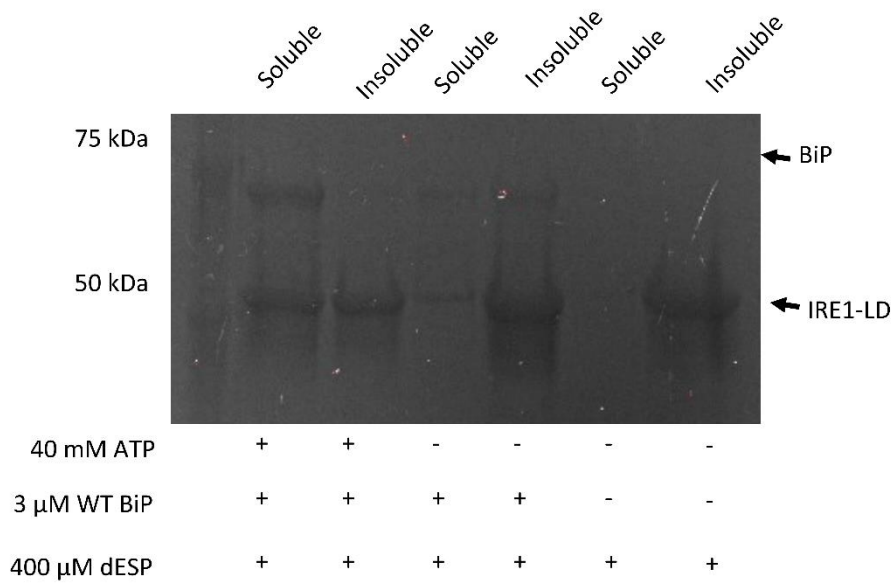
**Appendix Figure 15: 100 WT ire1 uncleaved with WT BiP.** SDS-PAGE gels depicting the soluble dimer fraction and the high order insoluble oligomers for the His-tag uncleaved WT IRE1-LD construct in the presence of 100 μM dESP peptide and either 40 mM ATP + 3 μM BiP, 3 μM BiP or HMK buffer.



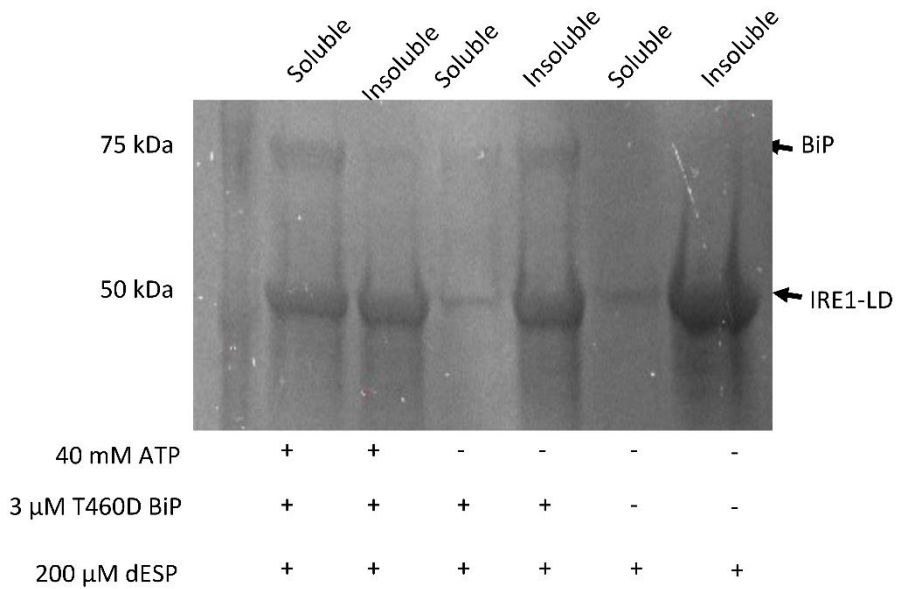
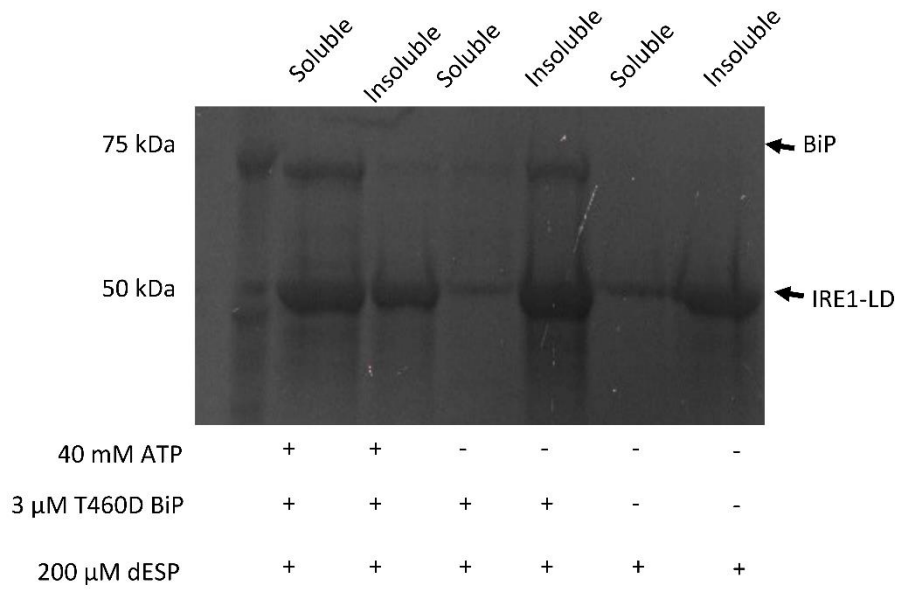
**Appendix Figure 16: 100 WT *ire1* cleaved with WT BiP.** SDS-PAGE gels depicting the soluble dimer fraction and the high order insoluble oligomers for the His-tag cleaved WT IRE1-LD construct in the presence of 100 μM dESP peptide and either 40 mM ATP + 3 μM BIP, 3 μM BIP or HMK buffer.



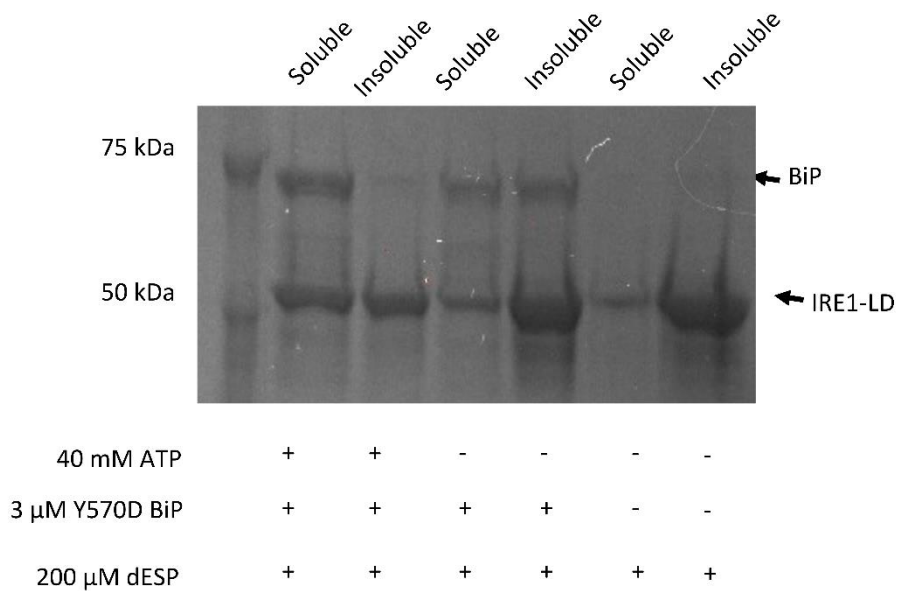
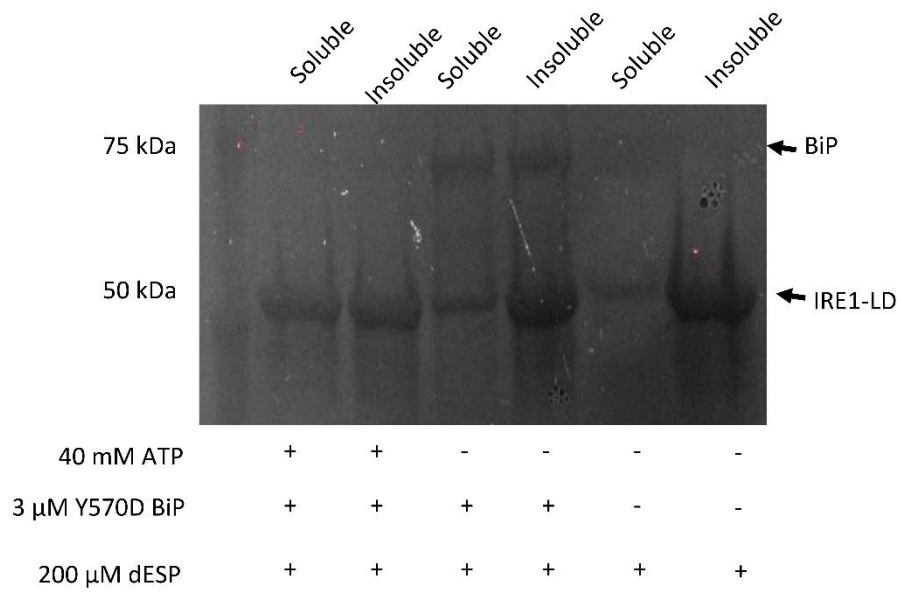
**Appendix Figure 17: 200 WT *ire1* cleaved with WT BiP.** SDS-PAGE gels depicting the soluble dimer fraction and the high order insoluble oligomers for the His-tag cleaved WT IRE1-LD construct in the presence of 200 μM dESP peptide and either 40 mM ATP + 3 μM BIP, 3 μM BIP or HMK buffer.



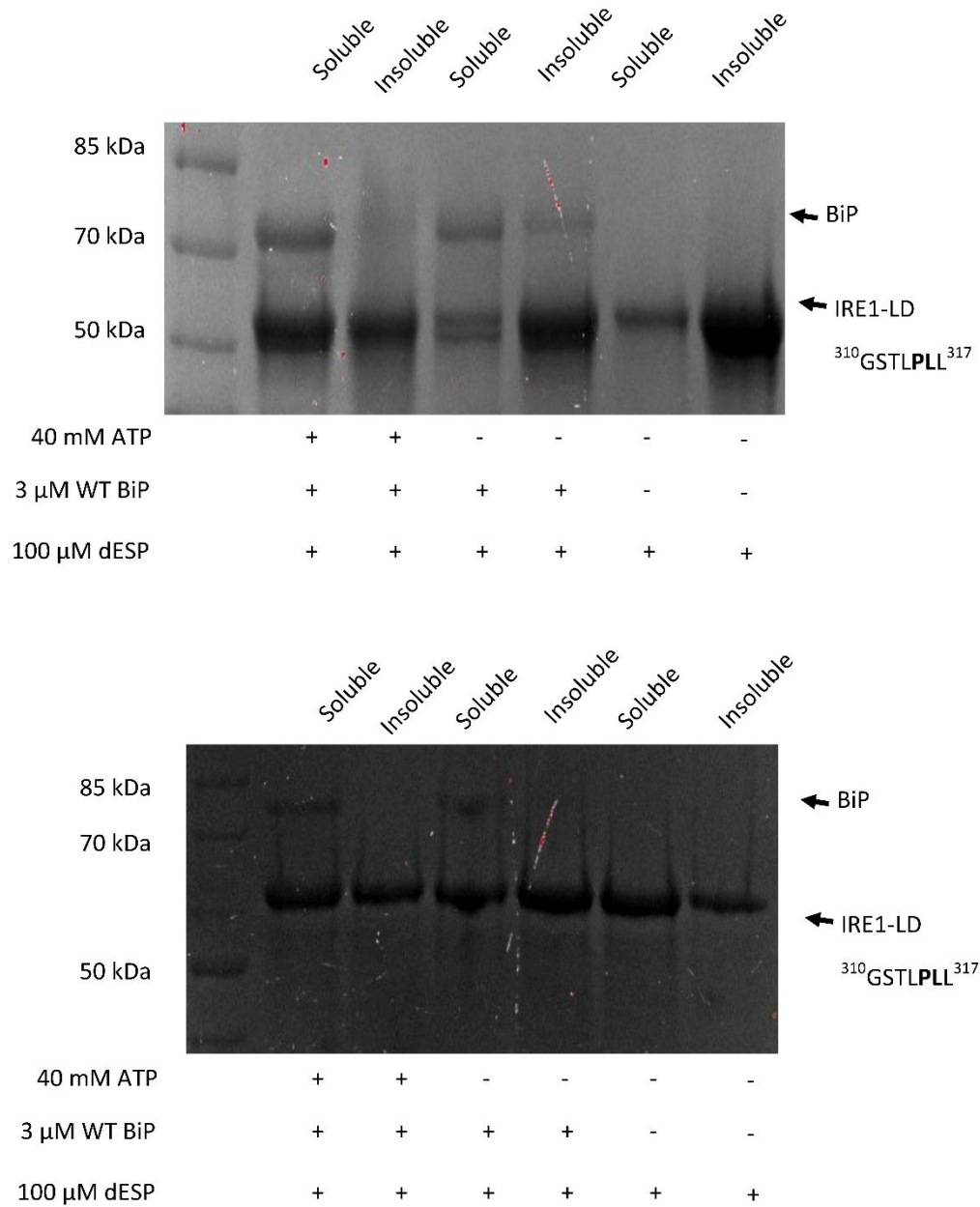
**Appendix Figure 18: 400 WT ire1 cleaved with wildtype BiP.** SDS-PAGE gels depicting the soluble dimer fraction and the high order insoluble oligomers for the His-tag cleaved WT IRE1-LD construct in the presence of 400  $\mu$ M dESP peptide and either 40 mM ATP + 3  $\mu$ M BiP, 3  $\mu$ M BiP or HMK buffer.



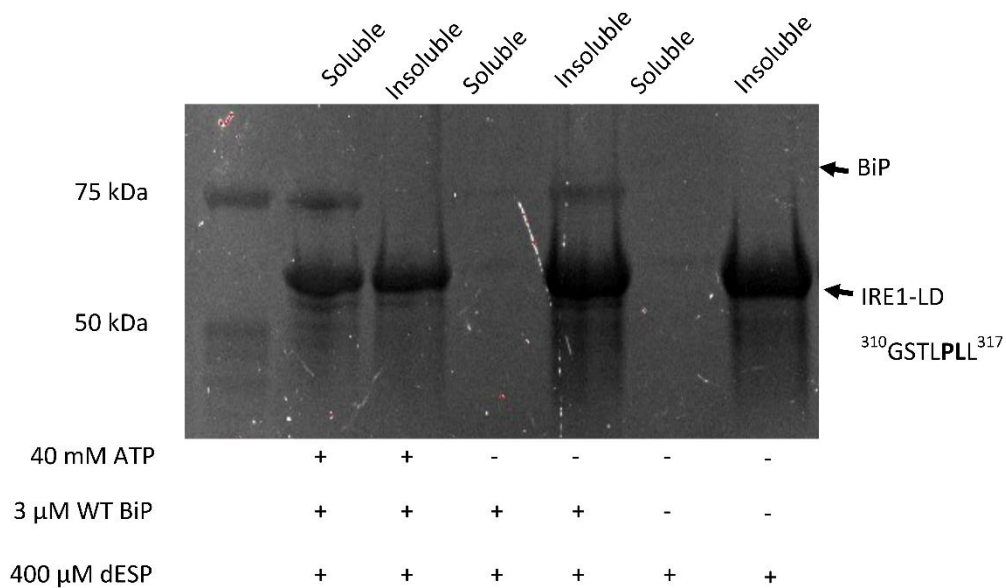
**Appendix Figure 19: 200 WT ire1 cleaved with BiP T460D.** SDS-PAGE gels depicting the soluble dimer fraction and the high order insoluble oligomers for the His-tag cleaved WT IRE1-LD construct in the presence of 200  $\mu$ M dESP peptide and either 40 mM ATP + 3  $\mu$ M T460D BiP, 3  $\mu$ M T460D BiP or HMK buffer.



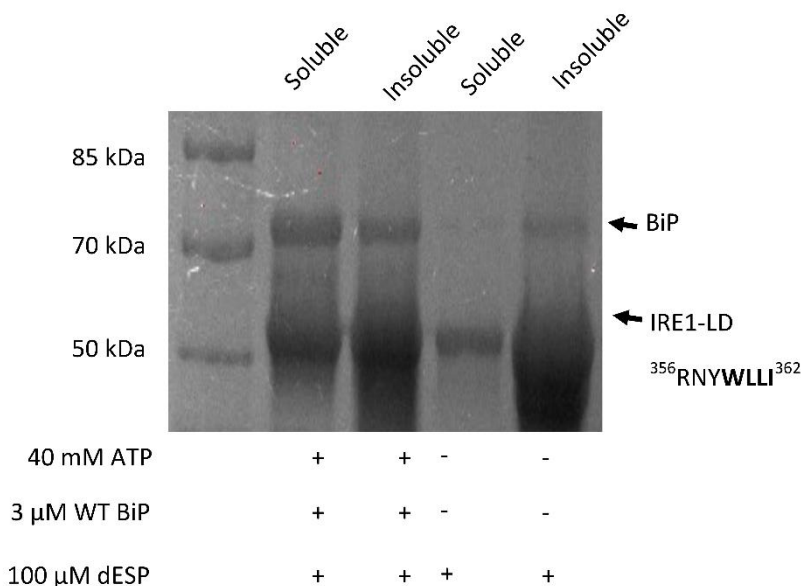
**Appendix Figure 20: 200 WT *ire1* cleaved with BiP Y570D.** SDS-PAGE gels depicting the soluble dimer fraction and the high order insoluble oligomers for the His-tag cleaved WT IRE1-LD construct in the presence of 200 μM dESP peptide and either 40 mM ATP + 3 μM Y570D BIP, 3 μM Y570D BIP or HMK buffer.



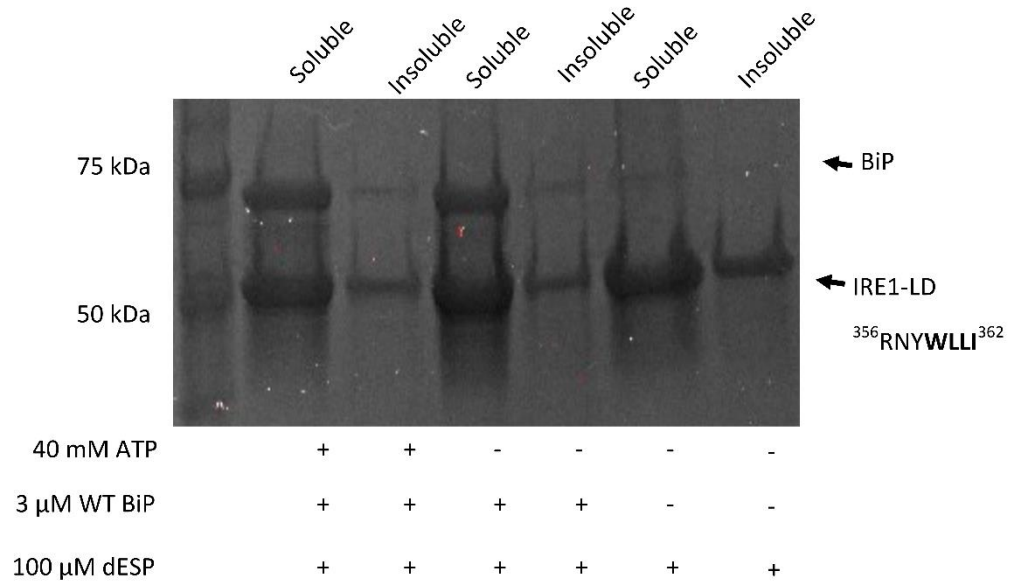
**Appendix Figure 21: 100 310GSTLPLL317 ire1 uncleaved with Wildtype BiP.** SDS-PAGE gels depicting the soluble dimer fraction and the high order insoluble oligomers for the His-tag uncleaved 310GSTLPLL317 IRE1-LD construct in the presence of either 100 μM dESP peptide and either 40 mM ATP + 3 μM BIP, 3 μM BIP or HMK buffer.



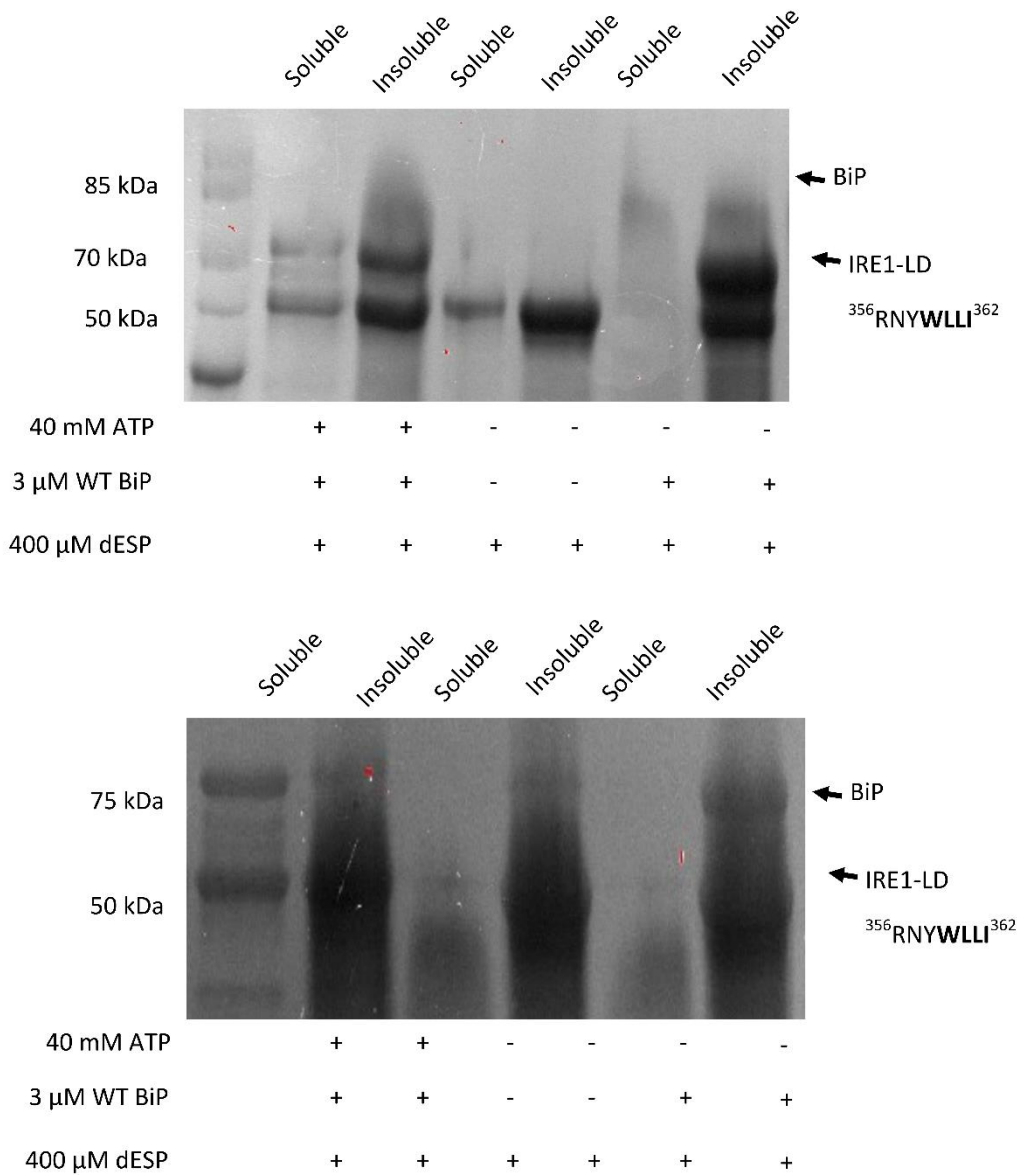
**Appendix Figure 22: 400 310GSTLPLL317 ire1 cleaved with Wildtype BiP.** SDS-PAGE gels depicting the soluble dimer fraction and the high order insoluble oligomers for the His-tag cleaved 310GSTLPLL317 IRE1-LD construct in the presence of either 400 μM dESP peptide and either 40 mM ATP + 3 μM BIP, 3 μM BIP or HMK buffer.



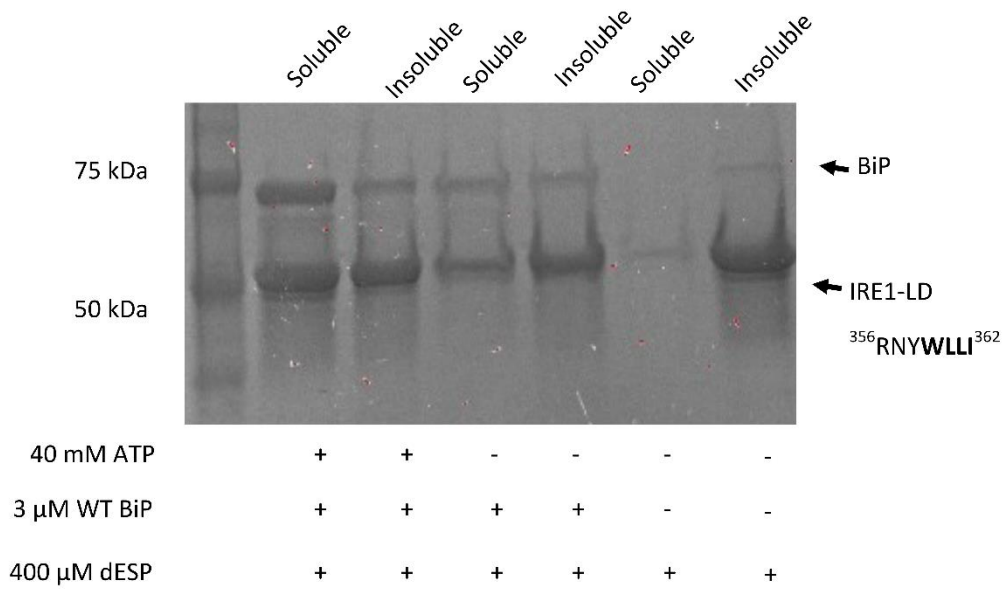
**Appendix Figure 23: 100 356RNYWLLI362 ire1 uncleaved with Wildtype BiP.** SDS-PAGE gels depicting the soluble dimer fraction and the high order insoluble oligomers for the His-tag uncleaved 356RNYWLLI362 IRE1-LD construct in the presence of either 100 μM dESP peptide and either 40 mM ATP + 3 μM BIP, 3 μM BIP or HMK buffer.



**Appendix Figure 24: 100 356RNYWLLI362 ire1 cleaved with Wildtype BiP.** SDS-PAGE gels depicting the soluble dimer fraction and the high order insoluble oligomers for the His-tag cleaved 356RNYWLLI362IRE1-LD construct in the presence of either 100 μM dESP peptide and either 40 mM ATP + 3 μM BIP, 3 μM BIP or HMK buffer.



**Appendix Figure 25: 400 356RNYWLLI362 ire1 uncleaved with Wildtype BiP.** SDS-PAGE gels depicting the soluble dimer fraction and the high order insoluble oligomers for the His-tag uncleaved 356RNYWLLI362IRE1-LD construct in the presence of either 400 μM dESP peptide and either 40 mM ATP + 3 μM BIP, 3 μM BIP or HMK buffer.



**Appendix Figure 26: 400 356RNYWLLI362 ire1 cleaved with Wildtype BiP.** SDS-PAGE gels depicting the soluble dimer fraction and the high order insoluble oligomers for the His-tag cleaved 356RNYWLLI362IRE1-LD construct in the presence of 400 μM dESP peptide and either 40 mM ATP + 3 μM BiP, 3 μM BiP or HMK buffer.